2014

Micro deep drawing of Aluminium foils AA1235

Syamsul Hadi
University of Wollongong

UNIVERSITY OF WOLLONGONG

Micro deep drawing of Aluminium foils AA1235

A thesis submitted in partial fulfillment of the requirements for the award of the degree

Doctor of Philosophy

from

UNIVERSITY OF WOLLONGONG

by

SYAMSUL HADI

School of Mechanical, Materials and Mechatronic Engineering
Faculty of Engineering and Information Sciences

2014

Declaration

I, Syamsul Hadi, declare that this thesis, submitted in partial fulfillment of the requirements for the award of Doctor of Philosophy, in the School of Mechanical, Materials and Mechatronic Engineering, University of Wollongong, Australia, is wholly my own work unless otherwise referenced or acknowledged, and has not been submitted for qualifications at any other university or academic institution.

Syamsul Hadi

August 2014

Abstract

The rapid development of product miniaturization has promoted significant research in the field of micro-forming. However wrinkles and folds in the flange and cup wall, tear in the corner radius, and earing on the cup edge were often observed in a micro deep drawing process. Results of a deep drawing process have indicated that a reduction of the cup wall thickness always appears at the cup corner radius, and the cup edge thickenning compared to the initial blank thickness made it difficult to eject a cup. Generally tear began to occur at the cup corner radius.

This thesis aims to investigate the micro deep drawing of Aluminium AA1235 of thicknesses 130 to 300 μm. The above issues of cup drawing discussed above have been considered in the experiments which are supported by a three-dimensional (3D) FEM simulation. The mechanical properties and microstructure of AA1235 have been characterized by tensile tests, EBSD/SEM and TEM for a number of processes such as fully annealed, four and six cycles accumulative roll bonding (ARB), combined asymmetric rolling (AR) with ARB and heat treatment after ARB and AR process. Under these conditions, the effects of anisotropy and grain size have been considered. Tensile tests have been carried out for annealed AA1235 as well as ARB processed sample with thicknesses from 16 to 300 microns to account for the size effect in the forming operation.

The investigation specifically focus on the issues that affect the product quality such as: wrinkling, tearing, earing, size effect, heat treatment, anisotropy, grain size, die and punch corner radii, blank thickness, and clearance.

Another focus of investigation is on the deep drawing of materials processed by conditions such as: fully annealed, four-cycle ARB process and subsequent stress relieved, combined six cycles ARB process and AR. A safe region for micro deep drawing has been mapped out, based on the forming limit diagram (FLD).

A 3D FEM simulation model, fully validated by experiment, has been set up to quantify the effects of different deep drawing variables on the quality of the products such as wrinkles. Simulation results without wrinkles have already been obtained with blank thickness of 300 μm and diameter of 14 and 15 mm. Wrinkles began to appear at the cup edge to the blank thickness of 150 μm, and the more wrinkles to the blank thickness of 70 μm.

Results from the experiment and simulation have shown that the use of a bulged punch for the first time with a profiled shape between two diameters offers advantages such as; (1) prevent the formation of wrinkles, (2) reduce the occurrence of earing, (3) increase the cup wall thickness in the area of the cup corner radius and hence less tear, and (4) reduce the cup edge thickness.

Acknowledgements

I would like to express my sincere and deep gratitude to my supervisors, Professor Anh Kiet Tieu and Associate Professor Cheng Lu. It would have been impossible to finish this thesis without their continuous guidance, constant encouragement, invaluable advice and great support over the years.

I express my gratitude to Dr. Hailiang Yu for his help in simulation programming by LS Dyna for my experiment results and Dr. Prabuono Buyung Kosasih for licenses support to the High Performance Computer (HPC/cluster). I'd like to thank Dr. Philip Whitten for his help on tensile test by Shimadzu tensile machine, to Dr. Lihong Su for her helps to obtain the EBSD images by SEM and all the valuable discussions, and also to Ika Lestari Damayanti and Jose Perez de la Cruz for proofreading the first draft of this thesis. I would also like to express my appreciation to Dr. Hongtao Zhu, Dr. Qiang Zhu, and Associate Professor Andrecj Chalka for their help and support. I wish to take the opportunity to thank Mr. Ron Marshall, Mr. Stuart Rodd, Mr. Andrew Scobie, Mr. Joe Abbott, Mr. Greg Tillman, Mr. Mick Weir, Mr. Nick Mackie, Mr. Brian Webb, Mr. Steve Selby, and Mr. Rodger Apton for their great help in my experiments, their friendship, and for servicing in the computer and internet facilities. I acknowledge the University of Wollongong, Electron Microscopy Centre for using of FEGSEM JSM 7001-F (LE0882813) funded by Australian Research Council grant(s) for scanning images by SEM with EBSD method.

I would also like to thank my fellow research students and my friends Ida Bagus Rai Widiarsa, PhD., Dianta Ginting M.Sc, Mao Liu, Khoa Duy Vo, Saud Almotairy, Bingjing Lin, Yong Sun, Bradley Davis, Wenzhen Xia, Shengnan Yang, Youyou Wu, Oyong Novareza, PhD., Pipit Wahyu Nugroho, Mochammad Rusli, Dr. Guanyu Deng, Wenxu Li, Ning Kong, Yu Xiang Long, Dr. Haina Lu and Alain Kusmoko. We shared our feelings, comfort and support each others during the PhD process. I feel very lucky to have such good friends.

I would like to express my gratitude to The Director of State Polytechnic of Malang, Indonesia for his support of my study in University of Wollongong over than 4 years. I would also like to thank The Director of Human Resources, Directorate General for Higher Education (DIKTI), Ministry of Education and Culture of Indonesian Government for the PhD scholarship for my study.

Many thank for the motivation and encouragement to pursue a PhD degree to my lecturer, Prof. Ir. R. Soekrisno, MSME, PhD in Gadjah Mada University, Jogjakarta, Indonesia; my supervisor Prof. Ir. Djati Nursuhud, MSME, in Sepuluh Nopember, Institute of Technology, Surabaya, Indonesia; the Director of the International Development Program (IDP) in Malang, Prof. Dr. Ir. Loekito Adi Soehono, MSc. Agr., and my colleague Mr. Jaswadi, PhD.

Finally, I would like to express my appreciation to my family, my wife and my daughters for their love, patience, support and encouragement.

List of publications

1. **Hadi, S.,** Tieu, A. K., Lu, C., *Flow stress of Aluminium foil AA1235/H14 in micro forming*, a **Poster** was presented in 15th International Conference on Advances in Materials and Processing Technologies, 23-26 September 2012, University of Wollongong-Novotel Hotel, Wollongong, NSW, Australia.
2. **Hadi, S.,** Yu, H.L., Tieu, K., Lu, C., *Simulation of defects in micro-deep drawing of an aluminium alloy foil.* The 11th International Conference on Numerical Methods in Industrial Forming Processes, AIP Conf. Proc., 2013. **1532**, p. **298-303,** doi: 10.1063/1.4806838.
3. **Hadi, S.,** Tieu, A. K., Lu, C., Su, L.H., Yu, H.L, *Grain refinement in the formability of Aluminium thin cup.* Materials Science Forum, 2013. **773-774**: p. **166-175**.
4. **Hadi, S.,** Tieu, A. K., Lu, C., Zhu, H.T., *A micro deep drawing of ARB processed aluminium foil AA1235.* International Journal of Materials and Product Technology, 2013. **47**(1/2/3/4): p. **175-187**.
5. **Hadi, S.,** Tieu, K., Lu, C., Yu, H.L., Caesarendra, W., Kusmoko, A., *The effect of bulged punch on wrinkles reduction in micro deep drawing*. Journal of Material Processing Technology, 2014, **submitted**.
6. Yu, H.L., **Hadi, S.,** Tieu, A.K., Lu, C., Godbole, A., Kong, C., *High strength and ductility of ultrathin laminate foils by accumulative roll bonding and asymmetric rolling*, Metallurgical and Materials Transactions A, 2014, Manuscript #E-TP-14-689-A, **accepted**.
7. Caesarendra, W., Kosasih, B., Tieu, A.K., Kong, N., **Hadi, S.**, *Early damage detection on low speed slew bearing based on vibration, wear debris, and failure analysis*, Engineering Failure Analysis, 2014, **submitted**.
8. Kusmoko, A., Dahar, R., Li, H., **Hadi, S.**, *A study surface layer and hardness produced by induction hardened S45C steel,* Journal of Applied Mechanics and Materials (TTP publisher), 2014. 664, p.43-47, doi: 10.4028/ww.scientific.net/AMM.664.43.

List of abbreviations

ρ	Density
τ	Friction shear strength
ν	Poisson ratio
ε	True strain
ΔR	Planar anisotropy
AA	Aluminium alloys
AFM	Atomic force microscopy
AR	Asymmetric rolling
ARB	Accumulative roll bonding
ARB4c-SR	ARB 4 cycles subsequent SR
As-R	As-received
BP	Bulged punch
c	Cycle
CG	Coarse-grained
cl	Clearance
CLP	Closed lubricant pockets
CR	Cryo-rolling
DB	Diameter of Blank
DD	Diagonal direction/diameter of die
DP	Diameter of punch
E	Young modulus
EBSD	Electron backscattered diffraction
EDAX	Energy dispersive X-ray
f	Friction factor
F	Friction force
FA	Full annealing
FCC	Face centered cubic
FEG	Field emission gun
FLD	Forming limit diagram
G	Grain size number
HCP	Hexagonal close packed
K	Kurtosis / material constant
N	Normal force
n	Strain hardening coefficient
NG	Nano-scale grains
NP	Normal punch
O/CLP	open/closed lubricant pockets
OLP	Open lubricant pockets
R_a or (Rq)	Root mean square
R_{avg}	Normal/average anisotropy
RCA	Real contact area
RD	Rolling direction / radius of die
RP	Radius of punch
RT	Room temperature
RTR	Room temperature rolling
SEM	Scanning electron microscopy
Sk	Skewness
SR	Stress relieving
SyR	Symmetric (conventional) rolling
TB, (t)	Thickness of blank, (thickness)
TD	Transverse direction
TEM	Transverse electron microscopy
V_{Punch}	Punch speed
Vr	Speed ratio
YS, TS	Yield strength, Tensile strength
α_{RC}	Real contact area fraction
σ	True stress

Table of contents

List of figures

List of tables

Chapter 1 Introduction

The rapid development of product miniaturization has promoted a significant research in the field of micro-forming, especially in the production of micro parts to reduce the weight and volume of the product [1].

Wrinkle and folding in the flange and cup wall [2], tearing in the corner radius, and earing on the cup edge [3] are often found in a micro deep drawing process. Earings on the cup edge have been attributed to anisotropy. Various attempts to minimize wrinkles have been made by many researchers. However results of a deep drawing process have indicated that a reduction of the cup wall thickness always appears at the cup corner radius, and the cup edge thickened compared to the initial blank thickness. Generally tears begin to occur at the punch corner radius. The current difficulty of ejecting a cup is due to the thickening of the cup edge. Reported problems ejecting the cup can be attributed to the presence of earing [4].

In this thesis, Aluminium AA1235 of thicknesses 130 to 300 μm has been used to form cups by micro deep drawing. Various issues discussed above will be considered in the experiments which are supported by a three-dimensional (3D) FEM simulation. The mechanical properties and microstructure of AA1235 have been characterized through tensile tests, EBSD/SEM and TEM for a number of processes such as full annealing, four and six cycles accumulative roll bonding (ARB), combined asymmetric rolling (AR) with ARB and heat treatment after ARB and AR process. Under these conditions, the effects of anisotropy on earing have been accounted for in the experiment, but were not considered in the simulation. Tensile tests have been carried out for annealed AA1235 as well as ARB processed sample

with thicknesses from 16 to 300 microns to account for the size effect in the forming operation. Friction in the process has been selected when the punch force from the simulation matches with the measured value.

The objectives of the micro deep drawing research are to produce that the cups product: without wrinkles, to reduce the earing, to increase the cup corner thickness, and to reduce the wall top edge thickness.

Results obtained in this study have shown that the use of a bulged punch with a profiled shape between two diameters offers advantages such as; (1) preventing the formation of wrinkles, (2) reducing the occurrence of earing, (3) increasing the cup wall thickness in an area of the punch corner radius, and (4) significantly reducing the cup edge thickness.

This thesis consists of 7 chapters; Chapter 1 outlines the overall framework of the thesis and scope of the research.

Chapter 2 presents a brief overview of the micro-forming, micro cup drawing, ARB, AR, tensile testing, anisotropy of materials, and the simulation of deep drawing process. In micro cup drawing, the discussion will specifically focus on the issues of wrinkling, tearing, earing, size effect, heat treatment, open/close lubricant pocket, effect of die and punch corner radii, blank holder pressure, blank thickness, and clearance.

Chapter 3 describes the experimental procedures and testing equipment for characterisation.

Chapter 4 presents the results of rolling processes ARB and AR. It discusses ARB processes for four cycles and six cycles, AR associated with speed ratio, anisotropy, grain size, thickness reduction, and TEM images.

Chapter 5 focuses on the results and discussion of deep drawing processes for materials on conditions such as: as-received (As-R), fully annealed, four cycles ARB process and subsequent stress relief, combined six cycles ARB process, AR and stress relief. As a result the forming limit diagram (FLD) for safe cup forming was formulated. The benefits of the bulged punch on wrinkling elimination were demonstrated.

Chapter 6 presents the 3D FEM simulation of deep drawing processes for materials prepared by different bulk forming processes. Simulation results without wrinkles have been obtained with blank thickness of 300 μm and diameter of 14 and 15 mm. Wrinkles begin to appear at the cup edge to the blank thickness of 150 μm, and the more wrinkles to the blank thickness of 70 μm. Moreover the chapter discusses (i) validation of the simulation models with experiment results, (ii) the effect of the punch corner radius, the die corner radius and the friction on punch force, and (iii) the effect of the clearance to the wrinkles. The correlation between simulation and experiment in the thesis is demonstrated in Fig. 1.1.

Chapter 7 summarizes the findings of the study obtained in this thesis, and some suggestions for further research.

A summary of the research in this thesis is shown in Fig. 1.2.

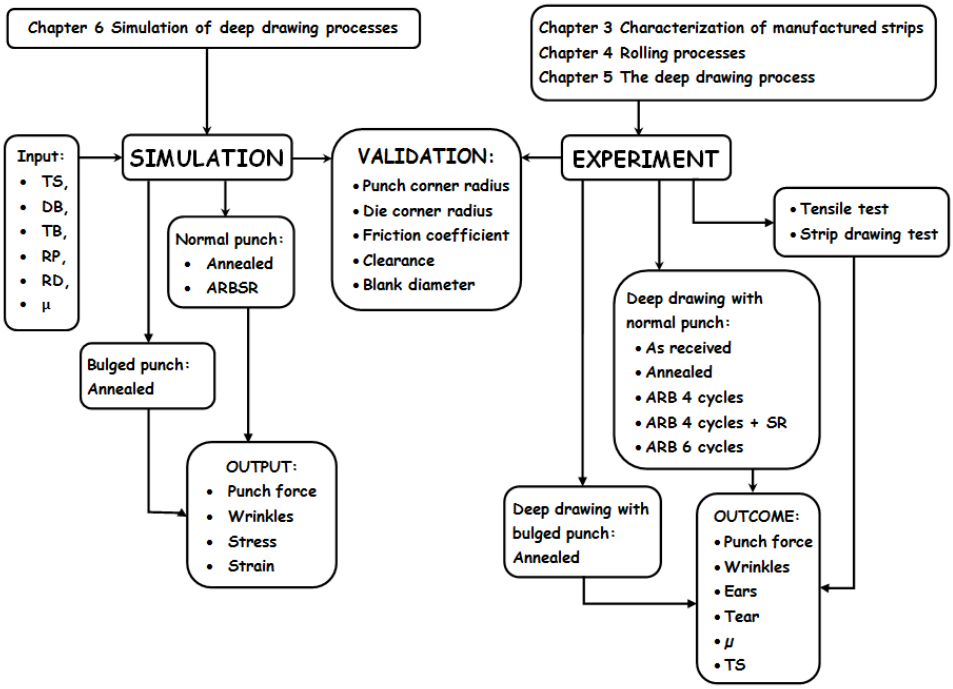

Fig. 1.1 Correlation between simulations and experiments

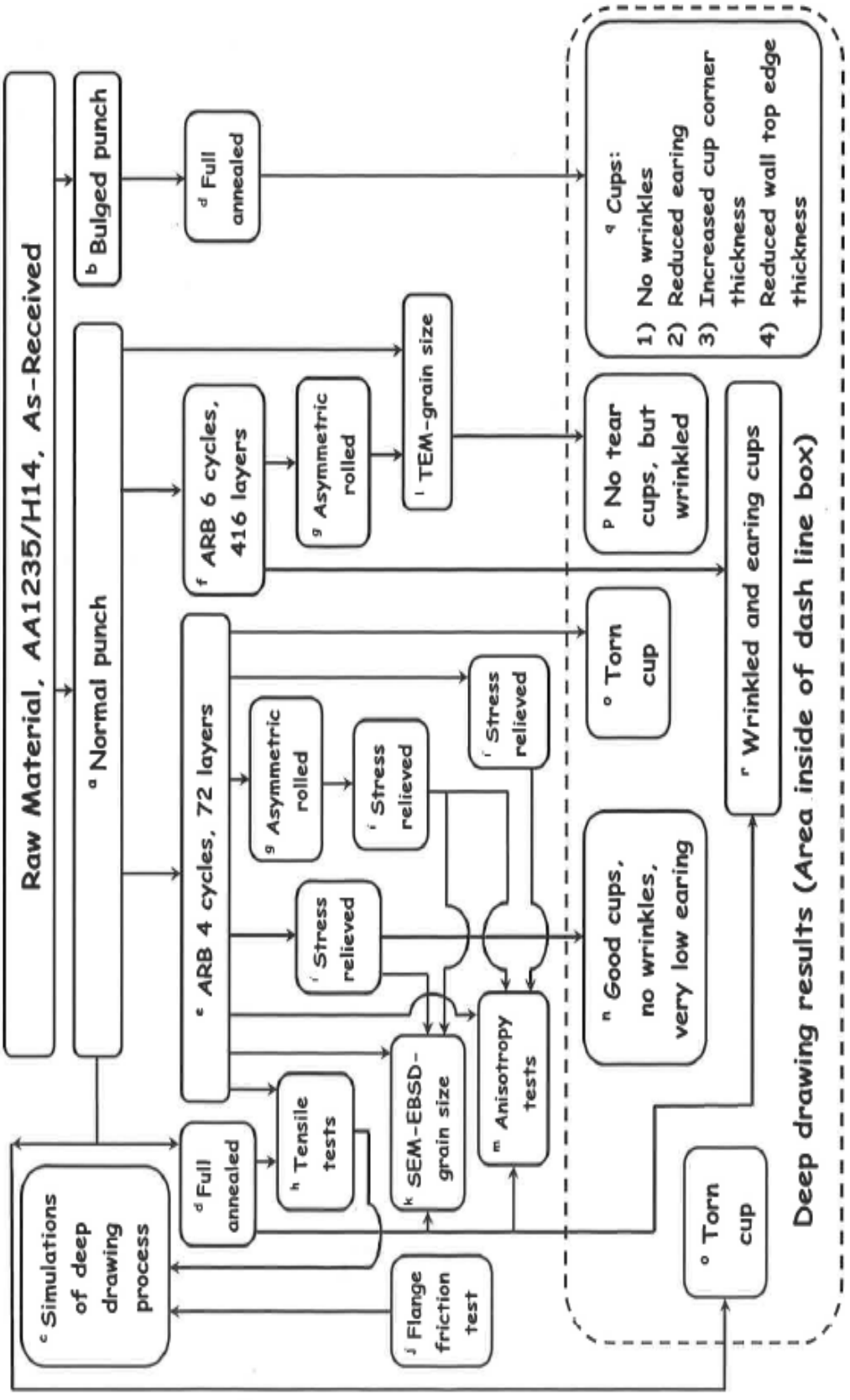

Fig. 1.2 Research outline for a micro deep drawing of AA1235 material

Chapter 2 Literatures review

2.1 Micro-forming

The rapid and recent development of miniaturised products has encouraged research in the field of micro-forming, especially in the production of micro parts, to reduce their weight and volume [1].

On this basis an analysis of the transfer of knowledge from the macro-world to the micro-world is required; as is a review of the latest basic and applied research related to the effects of size, in terms of process and forming. This research has driven the demand for new solutions, particularly manufacturing tools and machinery concepts [5]. Technology that is already established in the macro-scale cannot be directly applied to micro-size [5], because the properties of micro-size material varies significantly compared to macro-size.

Several micro-forming processes can already be carried out on many different materials, but in this thesis the process of micro-deep drawing on aluminum foil was selected. There is a difference between micro and conventional deep drawing; in micro deep drawing a cup is formed using a blank sheet of material between 0.001 and 0.300 mm thick, and a punch that is between 1 and 9 mm [6] in diameter. The definition of conventional deep-drawing is a cup that is formed from material between 0.09 and 1 mm thick, with a punch with a diameter between 100 and 1000 mm [6].

2.2 Micro cup drawing

Micro cup drawing has already been carried out on aluminium such as: Al 99.5 [7], AA1050 [8] and AA1235 [9, 10]; on copper [11]; on demagnetised mild steel

[12], and on 304 stainless steel [13, 14]. Conventional deep-drawing has already been carried out on aluminium, such as: Al-O [15], AA5754 [16], composite Al 5754, Al 5182+Mn, and Al 6111-T4 [17]. Other aluminium materials were pure Al [18], AA1050 [19], AA1200 [4], AA3003 [20], AA7075-O [3], and AZ31 [21]. Magnesium alloys such as: AZ31 [22-24], AZ31 and WE43 [25] are also included, as is SPCE-SB cold-rolled steel [26], mild steel EN10130 FeP01 [27], high formability steel-DIN 10130-99-DC05 [28], brass [29], and steel/brass composites [30].

Good quality deep drawing is characterised by a cup without wrinkles, earing, or tears. Micro-forming operations are affected by material flow stress, which is in turn influenced by the thickness of a thin material because material that is less than 300 μm thick, together with the grain size, affects its formability. The ratio (t/d) between the thickness (t) and the material grain diameter (d), known as the size-effect, is greatly affected by the results of a micro-deep drawing process. For instance, a high (t/d) ratio produce higher formability. A simple way to change the properties of a material, and thus improve its formability, is heat treatment. This means that a deep drawing process can incorporate annealing and stress relief to improve the ductility of materials. Another method is to use materials with fine grains processed by severe plastic deformation.

One aspect of micro-forming is having an open/closed lubricant pocket (O/CLP) on the flange of the deep drawing process, because a CLP can reduce the friction between the material and tool surfaces so that the force required to overcome friction in a deep drawing process is less. An O/CLP is in turn, influenced by the state of the contact surface and the presence of lubrication in the pocket.

Formability in deep drawing is affected by the geometry of the tools and process parameters such as the radii of the die, the punch, and the corners of the die and the punch; as well as blank holder pressure, the thickness of the blank, and the radial clearance between the die and the punch diameters.

2.2.1 Wrinkling

The types of failures that should be considered in a deep drawing process are wrinkling, tearing, earing [2] and folding [3].

In deep drawing, wrinkles are negative consequences resulting from changes in shape from a flat, circular blank to a cylindrical tube, especially at the edge of the cup. Wrinkles are also caused by compressive hoop stress on the flange, a stress that can be reduced by applying enough blank holder pressure (BHP), but if the pressure on the blank holder is too high, the cup will tear, but if the pressure is too low, wrinkles can occur. Wrinkles cannot always be eliminated completely; the combined clearance between the diameters of the punch and the die can cause wrinkles, but if this combined clearance is less than the thickness of the blank, the wall of the cup will become thinner. Therefore, a clearance that corresponds to the thickness of the blank can be used to determine the success of the deep-drawing process. It should be noted that some researchers have been guided by personal experiences, trying to overcome or reduce the occurrence of wrinkles.

Finite element analysis (FEA) has been carried out on each of the five stages needed to turn a circular blank into a semi-rectangular cup shape via deep drawing and ironing processes. At each stage, modifications were made to the shape and size of the punch and die, based on the FEA results [26]. These modifications included

increasing the curvature along the minor axis of the die corner radius to ensure a smooth deformation of the blank for the next stage. Increasing the angle on the die corner radius, near the minor axis, can also reduce the possibility of wrinkles. A limited drawing ratio (LDR) of 1.72 was obtained in the first stage, followed by an ironing process for the second to fifth stages. In the first stage, a 0.5 mm wall thickness was thinned down to 0.492 mm, in the form of a circular cup. A deep drawing experiment was carried out on 51.5 mm diameter blank of 0.5 mm thick cold rolled steel, from which it was concluded that with the design modification supported by a finite element, a rectangular cup with an aspect ratio (the ratio of height to the minor axis of the cup cross section) over 7.6 could be achieved without wrinkles and tears [26]. LDR is the ratio of the maximum diameter of the blank that can be drawn into a cup, over the diameter of the punch.

When warm deep drawing AZ31 material at 300^{o}C with a constant BHP, areas of wrinkles and fracture stand out; this material was 0.5 mm thick and 69.3 mm in diameter. The wrinkles were caused by a low to medium BHP with a high LDR, while the fractured area resulted from medium to high BHP and a lower LDR. Applying a variable BHP linearly from 0.21 to 3.91 MPa, with a punch stroke of 13 to 17 mm, can increase the LDR from 2.1 to 2.14 [23].

Four stages were proposed [31] to deep draw 66 mm diameter by 0.25 mm thick Cu alloy blanks. In the first stage, conventional deep drawing was carried out with a 0 to 10 mm punch stroke, and with a BHP of 1.26 MPa. In the second stage, wrinkles appeared on the flange with a 10 to 12 mm punch stroke, where the BHP had been reduced to 0.25 MPa. In the third stage, wrinkles were eliminated by the 12 mm punch stroke when the BHP was increased to 6 MPa, and the punch was in the

stopped position. The fourth stage involved correcting wrinkles at the die corner radius with a 12 to 15 mm punch stroke and the BHP reduced to 1.5 MPa. The heights of the wrinkles can be reduced to less than 50 μm via this elimination process, indeed they can be eliminated if their height is still less than 200 μm [31]. This means that a successful deep drawing process requires the correct punch stroke and BHP.

It has been proposed that an energy balance exists; the energy due to compressive hoop stress is equal to the bending energy added to the energy of the blank holder; this means the energy of the blank holder can prevent the occurrence of wrinkles. In formulating an equation that links these three energies, a cup sectioned into several regions is needed. A cup section relation includes a correlation between variations in thickness in the flange region, the number of wrinkles, and BHP. This variation in thickness is formed in five sections. The first zone is located in the flange region, the second is in the die corner radius region, zone III can be found on the cup wall, zone IV is on the punch corner radius, and the last zone (zone V) can be found near the bottom of the punch. An equation for the minimum BHP needed to prevent wrinkles was obtained from the boundary condition. The minimum BHP needed to prevent wrinkles is associated with the ratio of r_o/r_d (blank radius/inner radius of blank holder). The minimum BHP increases as a parabolic curve until it reaches a maximum value and then decreases as the punch reaches the end of its stroke. This equation was validated on 0.5 mm thick blank copper with a blank radius of 50 mm, a punch radius of 25 mm, normal anisotropy of 2.1, and a strain hardening coefficient of 0.345 [32].

A ring-shaped projection (RSP) was introduced onto the blank holder to stop the edge of the flange tearing while deep drawing AZ31 material that was 0.5 mm thick and had a blank diameter of 33.25 mm. The LDR of deep drawing AZ31 can be increased from 1.72 to 1.75 when using a blank holder with an RSP in the second stage [22]. A blank holder designed with an RSP could potentially be used to reduce tearing on the edge of the flange.

A BHP variation curve in a deep drawing process can be formulated by using the energy transformation where the bending work is equal to the release energy added to the wasting work of BHP. In this simulation a BHP curve was applied to a 0.6 mm thick AZ31 blank in three stages. In the first stage, at the beginning of the 20 mm punch stroke, the applied BHP was increased from 0.36 to 0.84 MPa. The BHP remained constant at 0.84 MPa during the second stage and then decreased to 0.48 MPa in the third stage [21]. The resulting forming limit diagram (FLD) shows that wrinkles appeared on the flange if the applied BHP was equal to 0.6 MPa. There were no wrinkles at an applied BHP of 0.2 MPa, but there was a risk of tearing. The simulation showed that a blank annealed at 100^{o}C risked a tear area greater than material annealed at 200^{o}C. There were also areas at risk of tearing when variable BHPs [21] were applied.

Simulations of the deep drawing process were carried out on blanks of AA1050 material that were 2 mm thick and 150 mm in diameter. An 84 mm diameter of punch was used and a BHP from 0.5 to 15 MPa [19] was gradually applied to the blank holder. It was concluded that a wrinkle free cup could be obtained by deep drawing if a BHP between 0.65 to 10 MPa was applied. Indeed, the simulation

showed that wrinkles occurred at a BHP of 0.4 MPa, and tearing began if the BHP exceeded 10 MPa [19].

A simulated deep drawing of a 2 mm thick AA5754-O blank was carried out with a punch that was 61x61 mm square and the BHP was between 0 and 25 MPa [33]. In this simulation, wrinkles appeared in the cup when the BHP ranged from 0 to 1.3 MPa and the cup began to tear when the BHP exceeded 18 MPa [33]. During hydro-mechanical deep drawing (HDD), the hydraulic pressure can have a remarkable effect on the wall thickness of the cup and in preventing wrinkles [34]. The researchers mentioned above considered how the BHP prevented wrinkles, while not depending on the size of the blank; indeed there is no standard procedure that can prevent wrinkles.

Samples of AA7075 aluminium that were 1.1 mm thick and 57 mm in diameter, which had been annealed at 450^{o}C produced more wrinkles during deep drawing than those samples annealed at 350 and 400^{o}C. The samples annealed at 400^{o}C had a better draw ability than those annealed at 350 and 450^{o}C because the grain growth at high temperature causes a non-uniform deformation of the sheet and reduces formability. In the low temperature range (270-350^{o}C), draw ability was poor because the micro structure was not fully recrystallised. Grains containing dislocations in the deformed state cannot be further deformed during deep drawing and can lead to early failure. At the optimum temperature (around 400^{o}C), a fully recrystallised structure can achieve the best draw ability because the recrystallised grains have formed into a set of new, fine, strain-free and equi-axed [3] grains.

Cylindrical cup drawing for cold-rolled steel was only achieved at 1.72 LDR in the first stage, and after modifications to the shape and size of the punch [26]. The

use of a constant and variable BHP on AZ31 [23] should also be tested for other materials. An application of BHP in four stages was applied to Cu alloy [31], but it cannot always be applied to other materials in the deep drawing process, especially in the micro-scale.

When simulating the deep drawing of a blank of AZ31 material 0.6 mm thick [21], a BHP of 1.2 MPa was found to be the best at avoiding tearing, albeit there was still some risks. A similar BHP should be applied when simulating other material is still needed in order to carry out the drawing process without wrinkles or tears.

A blank holder with a ring-shaped projection was intended to prevent tearing at the edge of an AZ31 [22] flange, but it may also be used to reduce wrinkles. The parabolic curve equation for the minimum BHP needed to prevent 0.5 mm thick by 100 mm diameter blank copper from wrinkling [32] should be sought and validated, as it should for other materials, to obtain a cup without wrinkles. A suitable BHP obtained by trial and error was applied to AA1050 in a number of experiments [33], and similarly, a trial and error approach by simulation is also needed for other materials. The best draw ability was obtained from samples of AA7075 that were 1.1 mm thick an 57 mm in diameter, that had been annealed at an optimum temperature of 400^{o}C [3]. It was also necessary to find the optimum temperature for other materials in order to obtain the best draw ability. Another alternative to prevent wrinkles on the wall of a cup is to use hydraulic pressure. Some researchers were still unable to apply a standard procedure that could prevent wrinkles, and that was applicable to a variety of materials.

An alternative to avoiding wrinkles is ironing, which can be done after the drawing process or directly while drawing. Ironing is a deformation process carried

out on the wall of the cup to obtain a thinner wall. If ironing is done in the second stage, then the diameter of the die should be smaller than the die used when deep drawing. When the ironing process is performed directly onto a blank, then the effective clearance becomes smaller than the thickness of the blank.

The ironing process with a reduction in thickness at 10, 25, and 40 % on a steel material (extra deep drawing/EDD) at 200, 400, and 600^{o}C was observed, and it was concluded that the best quality cup occurred with a 25 % reduction in thickness at 600^{o}C in a single stage [35, 36].

Ironing with a reduction in thickness (5-50 %), was carried out on 18/8 stainless steel with die angles of 5, 10, and 15^{o} respectively. It was concluded that the critical thickness reduction ratio was strongly influenced by the geometry of the die and the strain hardening coefficient of the material. The critical thickness reduction ratio was increased if the die angle was decreased, the length of the land was reduced, the strain hardening coefficient was increased, and the coefficients of friction between the interfaces of the cup/punch and the cup/die were increased [37].

The ironing process was carried out 1 mm thick blanks of low carbon steel [36], AA5754-O [38], and stainless steel (18/8) [37], and also on 2 mm thick blanks of steel (EDD) [35] and low carbon steel [36]. 5 mm thick blanks of hot roll mild steel (SPHE-JIS) have been used in the ironing process [39], as has 9.5 mm thick (34CrMo4) steel [40]. The die angles used during ironing ranged from 5 to 15^{o} for AA3104H19 [41], AA5754-O [38] and 18/8 stainless steel respectively [37].

When the corner of the cup became thinner while deep drawing mild steel, the cup wall reached its original thickness after 66 % of the punch stroke [39]. With a 70.8 mm diameter ironing, a 59 mm diameter punch, a 6 mm thick blank, and a clearance

of - (minus) 0.1 mm (1.67 % to the thickness of the blank), the original thickness on the edge of the area was obtained after a cup had thickened by approximately 3 %. The greater the clearance is, the thicker the cup edge will be [39].

The ironing process is influenced by the geometry of the die, especially the angle of the die and the length of its land, whereas strain hardening material also affects formability during this process. Indeed, any reduction in the thickness of the blank is limited by the material formability.

A one step process that combines deep drawing and ironing can be designed after preliminary experiments were carried out. It involves manufacturing a punch with a combination of diameters; such that the tip is a certain diameter, but then it increases in diameter where the wrinkles would form, and then increases again at the end of the punch. The transition between these two diameters is made gradually so that the overall thickness of the wall can be produced more uniformly and the expected occurrence of wrinkles can be reduced.

2.2.2 Tearing

Tears in deep drawing are usually caused by the material being unable to withstand the tensile stresses applied by the punch, or because the corner radius of the die and/or punch are too small. Tears can also occur due to frictional forces between the blank and the tools that create extra stress on the cup walls, and because the clearance between the punch and the die is too small, which thins the cup wall and causes it to tear. Simulations have been performed with 2 mm thick AA1050, and then the results were applied in an experiment with BHP's between 0.4 and 15 MPa [33]. The cup started tearing with a BHP greater than 10 MPa [33]. For 0.5 mm

thick AZ31 in a warm deep drawing process (300^{o}C), an LDR of 2.1 to 2.14 was obtained when various BHPs were applied linearly from 0.5 to 9.2 MPa. Tears occurred when the LDR was greater than 2.09 and the constant BHP was higher than 4.8 MPa [23].

Tearing usually occurs in non-uniform metal flows and irregular contact conditions between the surfaces of the blank and the tool. Tearing was avoided while deep drawing 0.5 mm thick cold rolled steel, from the circular blank into a semi-rectangular shape, through 5 stages of modifications on the curvature along the minor axis of the die corner radius. The modification effected by the ironing processes were based on FEA [26]. The reduction in thickness after the fifth stage reached 28 %, which had a high probability of tearing. Tearing can only be prevented in the second stage where the cross section of a cylindrical cup is converted into another form.

A combination of the punch and die corner radius while deep drawing pure aluminum resulted in a torn cup; this occurred in an 82 mm diameter blank where a punch with a 6 mm corner radius and die corner radii of 4, 6, and 8 mm were used. It also occurreds with a punch corner radius of 8 mm and with die corner radii of 4 and 6 mm. These experimental results have shown the limit of a deep drawing process on pure aluminum with a thickness of 1.5 mm [18].

The blank holder gap (BHG) is the gap between the top die and bottom blank holder surfaces, and it is not always the same as the thickness of the blank; indeed the best BHG is between 1-1.3 of thickness of the blank.

A larger gap of up to 1.3 of the thickness of the blank still provides a cup with a good result without tearing [42]. Tears in a cup cannot be avoided if the limitations of draw ability while deep drawing varying material thicknesses and operating

conditions are exceeded. Factors such as BHG, BHP, minimum punch corner radius, minimum die corner radius, and the minimum temperature can affect the tearing of a cup.

2.2.3 Earing

Earing is another failure in the deep drawing process that is separated from wrinkling and tearing [3]. Earing is a waste of material because a blank that is larger than necessary is needed. Earing can also make it difficult to eject the product after deep drawing is completed [4]. Earing is caused by material anisotropy, and it can be expressed in terms of normal anisotropy (R_{avg}) and planar anisotropy (ΔR) in equation (2.1) and (2.2) [2] [43]

$$R_{avg}=(R_0 + R_{90} + 2R_{45})/4 \quad (2.1)$$

$$\Delta R=(R_0 + R_{90} - 2R_{45})/2 \quad (2.2)$$

R is the ratio between the strain in the direction of the width and thickness of the tensile test specimens ($R=\varepsilon_w/\varepsilon_t$). If ΔR is equal to zero, then there is no earing [43].

Reducing the formation of ear in deep drawing can be carried out with a modified blank. The maximum punch load for the modified blank was decreased by 5.4 % compared to a circular low carbon steel blank, but it decreased by approximately 8.2 % for pure aluminum [44].

A circular blank was modified into a form almost like a normal circle, it has four arcs at 0, 90, 180, and 270^o to the rolling direction (RD) of the blank, so trimming was done. This cutting was done a certain distance from the edge of the circle, according to the results of a simulation. The results showed a significantly reduction in earing after the modified blank was drawn into a cup. The maximum cup height

before and after the blank was modified was reduced from 40 to 36 mm, while the minimum height before and after the blank was modified was reduced from 34 to 31 mm [45].

Comparisons in the experiments and simulations to four different forms of blank were carried out to make an octagonal cup. The blank was 0.8 mm thick and the punch was 175 mm in diameter. The form of the four blanks were octagonal and curved inwards, straight into the octagonal notched, octagonal straight, and circles. It was found that minimum earing when an octagonal cup was formed, was generated by a circular blank [46].

Earings on AA 5754-O and AA 2024-T4 while deep drawing 1 mm thick blanks were observed. Earing occurred at 0 and 180° for AA5754-O and at 45 and 225° for AA2024-T4. The earing of AA 2024-T4 was smaller than that of AA 5754-O [47].

Earing occurred while deep drawing 0.3 mm thick AA1235 blanks 14 mm in diameter. The experimental results of annealed material processed by accumulative roll bonding (ARB) followed by stress relief indicated that cup earing for ARB processed material followed by a stress relief was lower than the annealed material [9]. A decrease of planar anisotropy (ΔR) from 0.556 to -0.022 was responsible for reducing earing in the drawing process.

The relationship between earing and the thickness of the blanks while deep drawing 2 mm thick AA1200 blanks increased earing in the range of 0.6-0.9 mm, and decreased to the range of 1.2-1.58 mm [4].

Modifications to the radius of medium steel blanks, with a thickness of 0.9 mm and a diameter of 120 mm, reduced earing from 8.7 to 4.1 mm [48]. A simulation was carried out to optimise the modified form of circular blanks of AA2048, in order

to obtain a cup without earing forming [49]. It can be concluded from previous studies that reducing earing on a cup can be done by modifying the shape of the blank and then stress relieving it before deep drawing.

2.2.4 Size effect

Material behavior is influenced by the size and orientation of the grain, and the size of the specimen. The most common parameter used to express the behaviour of materials is flow stress because it determines the forming force. As miniaturisation increases, the flow stress varies when the size is smaller. The size factor (η) of the material is 1 for a single crystal and 0 for a poly crystal. Size/scale factor η is the ratio of the grain size and the thickness of the sheet (η=d/t), so for micro-forming the flow stress model is between the flow stress for a single crystal and poly crystal models [50]. A size factor between 0.5 and 1 was obtained after deep drawing $CuZn_{37}$ blanks that were 0.15 and 0.3 mm thick, and with diameters of 8 and 16 mm [6].

A new mathematical model was proposed to describe the behaviour of material of any thickness and grain size in micro-forming [51]. Models have been applied to C1200 copper with thicknesses (t) of 0.1, 0.2, and 0.5 mm, and grain sizes of (d) 23, 70, and 113 μm. The maximum punch loads of the new model differed by 2 % from the Swift model. The formability and flow stress for micro-forming can be expressed as a function of the t/d ratio (size effect), but the constitutive models were only suitable for t/d > 1. This model was validated with copper C1200 [52].

The results of tensile and bending tests of AAl100 and Brass-26000 concluded that where t/d > 1, the yield strength and tensile strength of the material decreased

with a lower t/d ratio, whereas when t/d <1, the yield strength increased with a decrease in the t/d ratio. Regardless of the thickness of the material, the stretch ability or formability for micro-forming worsened if the ratio t/d was reduced [53].

The simulation showed that the generated friction coefficient (μ) decreased with increasing pressure for given size effects. For the size effects (λ) 1.25, 2.5, and 6 with a range of μ values; from 0.213 to 0.052, from 0.111 to 0.036, and from 0.086 to 0.031 respectively for a normal pressure of 50 to 500 MPa [54]. When λ= A/As, A is the total contact surface and As is the outer contact surface. The total contact surface consists of RCA, OLP, and CLP. It was shown that an increase in size effects the results in a reduced friction force until it becomes a traditional lubricant friction, however, when the effect of size decreases, the friction force increases. The influence of size effects is greater in the micro-scale (λ <10) than the conventional scale (λ > 10) [54].

The friction size effect only occurred in a scaled down experiment of cylinder compression for copper alloy C3602 with soybean oil. Specimen diameters of 6, 4, 2, and 1 mm, with a height/diameter ratio of 1.5, were used in the experiment. The friction-size effect can be explained by the real contact area (RCA) under deformation, such that the higher the RCA fraction, the higher the friction [55].

2.2.5 Heat treatment

Aluminum was selected in this research into deep drawing because these materials have superior properties such as low density, good formability, corrosion resistance, and low cost.

In this thesis the micro deep drawing of AA1235/H14 aluminum foil with thicknesses of 300 and 130 μm were carried out using a set of punches with diameters 7.54 and 7.89 mm. This still met the range of micro deep drawing process that was used [6]. The heat treatment using for AA1235/H14 was annealing and stress relief. The annealing temperature was 450^{o}C for 4 hours and stress relief was at 200^{o}C for 8 hours. The purpose of annealing and stress relief was to reduce the residual stresses from the previous rolling process.

The annealing temperatures for other materials were AA6061-O at 803K (530^{o}C) for 1.5 h [56], AA1100 at 400^{o}C for 1 h [57], the Al/Al strip at 375^{o}C for 2 h [58], AA2219/5086 at 400^{o}C for 1 h [59], AA1050 at 450^{o}C for 1 h and AA6000 at 500^{o}C for 2 h [60]. While the temperatures for stress relieving AA2014 was 170^{o}C for 12 h [61], and for AA5754-O at 200^{o}C [16].

2.2.6 Open/close lubricant pocket

Comprehensive experimental work has shown that friction is increased if the size is scaled down during micro-forming. A theoretical explanation is given by the mechanical-tribological models that identify the open and closed lubricant pockets (O/CLP) and real contact area (RCA). It was shown that the common law of friction developed by Wanheim/Bay ($\tau = f\,\alpha_{RC}\,k$), can account for the scale effect [62].

When two surfaces are in contact under load, asperities deform and the lubricant trapped in the valleys can support the load [54]. The valleys of roughness that are connected to the edge of the surface cannot keep the lubricant as open lubricant pockets (OLP), whereas the oil trapped in the valleys that have not connections to the edge can support a load during forming, and are called closed lubricant pockets

(CLP). CLP can lower a normal pressure and reduce contact stress, so that the fraction of RCA is reduced. The concept of O/CLP has been observed in experimental cylinder compression for copper alloy material C3602 with four types of lubricants. The types of lubricant used include: talc powder, petroleum jelly and soybean oil. Observations were also made using no lubricant. The specimens used had diameters of 6, 4, 2, and 1 mm, and had a height/diameter ratio of $h_0/d_0 = 1.5$ [55]. It was concluded that the average friction factor increased by 0.2 from 0.11, for the annealed condition at 450^{o}C for 1 h with soybean oil [55].

Furthermore, the O/CLP can be illustrated with a surface fraction after penetration on the surface. Relative penetration between 4 and 6 μm can produce a surface fraction of OLP, CLP and RCA [62].

2.2.7 Effect of die corner radius to the cup product

The size of the tools and blanks used for deep drawing are important parameters in the success or failure of forming a cup. FEA was carried out on the deep drawing of an AZ31 blank that was 1 mm thick and had a long axis of 80 mm and a short axis of 50 mm, that was used to form an elliptic cup [63]. When the die corner radius was reduced from 6 to 4 mm, the forming load increased from 4300 to 4900 N. A BHF of 1500N, a clearance of 1.6 times the thickness of the blank and a temperature of 300^{o}C were applied in the simulation [63].

The effect of friction and spring back on the application of BH, divided into eight segments, were simulated for an Al-O blank material that was 0.5 mm thick and had diameters of 86 to 110 mm. With punch corner radii from 5 to 3 mm, the corresponding spring-back for the radius of the cup edge increased from 15.72 to

15.87 mm. When the coefficient of friction was reduced from 0.4 to 0.25, the spring-back increased from 15.55 to 15.70 mm[15].

Optimisation was done through FEA of the deep drawing process of AZ31 and WE43 blank material that was 0.5 mm thick and had a diameter of 25 mm [25]. For AZ31 the punch corner radius for 4, 3, 2, and 1 mm, produced a corresponding drawing depth of 6.7, 7.1, 7.5 and 6.4 mm. For WE4 the possible drawing depth was 4, 4.2, 4.6 and then 3.8 mm. By decreasing the forming temperatures to 400, 300, 200, and 100°C, the corresponding drawing depth increased from 2.95 to 4.1 mm, and then decreased to 3.1 and 1.5 mm [25].

A simulation was carried out to predict and minimise various sheet thicknesses while deep drawing AA1050 material with thicknesses ranging from 0.05 to 0.2 mm and diameters from 1.8 to 10.8 mm [8]. For die corner radii of 0.3, 0.25 and 0.2 mm, the corresponding cup corner thicknesses were 0.177, 0.173 and 0.168 mm. The optimum values for the die corner and blank radii respectively were 2.15 and 3.501 mm [8]. With a blank diameter of 7.02 mm and a punch diameter of 4 mm, the optimum LDR was 1.755.

Optimising the tool geometry for deep drawing was done on a blank of 1.5 mm thick pure Aluminum with a diameter of 78 mm, and it was found that by decreasing the die corner radii, the punch load decreased [18]. The die corner radius is related to the value of LDR such that the LDR decreases if the die corner radius is reduced [64].

2.2.8 Effect of punch corner radius to the cup product

In reference [8], reducing the punch corner radii in the simulations from 0.3 to 0.2 mm, increased the thicknesses of the cup corners between 0.167 and 0168 mm [8]. The radius of the punch corner and blank in the simulation were 2.99 and 3.501 mm, respectively [8]. With a blank 7.02 mm in diameter and a punch 4 mm in diameter, an optimum LDR of 1.755 was obtained. The optimum value obtained from the simulation for the punch corner radius was 2.99 mm.

In reference [22] for the blank AZ31 at 0.5 mm thick, when the punch corner radius was reduced, the LDR was lowered. Similar findings were found in reference [64].

2.2.9 Effect of the blank holder pressure to the cup product

The BHP controls the occurrence of wrinkles on the cup flange. If the BHP is greater than necessary, the cup will tear in the corner because the higher tensile stress exceeds the material strength. However, if the BHP is not great enough, there will be wrinkles in the flange and cup wall, and if the wrinkles on the sheet are significant and the existing clearance is not enough, the wall of cup will tear.

The BHP was applied gradually in a four stage strategy [31] while deep drawing 0.25 mm thick Cu alloy with blank diameter of 66 mm, during which the wrinkles were reduced to less than 50 μm high. Wrinkles can be eliminated if their height is still less than 200 μm [31], but applying BHP in four stages for setting the appropriate punch stroke and BHP.

The application of variable BHP showed that the area of wrinkle was also a region at risk of stretching [21]. The FLD for the BHP while deep drawing other materials

must be established to determine the magnitude of BHP that corresponds to areas without wrinkles. An equation of energy balance to avoid the occurrence of wrinkles has been derived [32], but a validation of the minimum BHP has not been carried out for other materials.

The simulation of a relationship between BHP and forming load to make an elliptical shaped cup with 1.0 mm thick AZ31 has already been obtained [63], with the results showing that the greater the BHP, the greater the forming load needed to form an elliptical cup; similar simulations are also needed to form a cylindrical cup.

For a BHP from 0.65 to 10 MPa, the simulation of deep drawing 2 mm thick AA1050 material with a blank diameter of 150 mm, produced a wrinkle free cup [33].

A deep drawing tool system using an adaptive BHP on a 1 mm thick low carbon steel (DC06) with a 330 x 360 mm blank [65] has been produced. A rectangular cup without any tear in the wall, with a variation in the flange thickness from 0.991 to 1.057 mm, and with an 80 mm deep punch stroke was obtained [65]. Wrinkles can be avoided with an adaptive blank holder, as indicated by the variation in the flange thickness of 68 μm, or 6.8 % of the blank thickness. An issue would arise if the system for deep drawing tools is applied to micro-forming, due the limited space available for placing a number of devices around the punch and die.

Deep drawing was carried out on a two-layer composite that consisted of 0.62 mm thick brass 0.39 mm thick steel, with blank diameters between 75 and 100 mm [30]. The flanges of three cups show various degrees of wrinkles, depending on BHP, between 0.6 to 0.12 MPa [30]. The findings indicate that so far, the appropriate BHP needed to prevent wrinkles has not yet to be determined. The method for applying

BHP better in micro deep drawing still needs to be tested, especially with regards to the space available around the punch and die. The application of adaptive BHP methods may provide a solution if the space problem around the punch and die is adequate, but that the adaptive BHP can produce no wrinkles on the cup wall if the drawing process is continued to full stroke must still be proved.

2.2.10 Effect of blank thickness to the cup product

A good cup can be produced if the thickness of the blank is combined with an appropriate clearance between the diameters of the die and the punch. If the thickness is smaller than the clearance, then wrinkles will occur, but if the thickness of the blank is greater than the designed clearance, an ironing process will occur. On a 1.2 mm thick blank of low carbon steel with a diameter of 115 mm [64], a high LDR value was achieved with an appropriate clearance of 1.15 times the thickness of the blank, so the clearance must be selected prior to the design to determine the diameters of the die and punch.

2.2.11 Effect of the clearance between the punch and die to the cup product

Deep drawing process blank material of a certain thickness requires a certain clearance in order to obtain a maximum LDR; for instance, a 0.5 mm thick blank with 0.7 mm clearance, the LDR while cold deep drawing AZ31 was reduced from 1.72 to 1.67 with respective punch corner radii of 5 and 2 mm, and it decreased from 1.72 to 1.47 when the clearance was reduced from 0.7 to 0.5 mm with a punch corner radius of 5 mm [22]. A maximum LDR of 2.238 on a clearance equal to 1.15 times the thickness of the blank was obtained while drawing a cylindrical cup from a 1.2

mm thick blank of low carbon steel with a diameter of 137 mm [64]. In this case the LDR also decreased if the clearance differed by 1.15 times the thickness of the blank. A deep drawing process rarely achieves an LDR higher than 2 [15]. Experiments were performed using a punch and die with a corner radius of 8 mm, and a solid lubricant of Zinc Sterate. The blank was a special type of material for deep drawing called EDD steel with an elongation of 45 % [45]. The LDR decreased if the clearance was 1.15 times more than the thickness of the blank [64], but if the clearance was more than 1.15 times the thickness, the wall thickened but its thickness was not uniform. However if the clearance is smaller than 1.15 times the thickness, the cup wall is ironed and becomes thinner but uniform in thickness.

Deep drawing a blank material of a certain thickness requires a certain clearance in order to obtain a maximum LDR.

2.3 Accumulative roll bonding (ARB)

A reduced flow stress from thin material due to the effects of size prompted researchers to use thin material with a smaller grain size for micro-forming because a high (t/d) ratio will produce a higher formability [66]. The accumulative roll bonding (ARB) process produces materials with smaller grains, so formability in deep drawing can be improved.

The ARB process is but one of the severe plastic deformation processes used to achieve ultra-fine grains and increase the strength of material, but with a reduced ductility. In this process the sheet thickness is reduced by 50 % or more [9], and then cut into two equal halves. The interface of the two pieces is then brushed, cleaned,

stacked, heated, and then rolled again with the same reduction. This process is repeated for several cycles and then annealed to improve ductility [57].

An ARB process was carried out on several types of materials from a group of ferrous and non-ferrous metals. The ferrous group consisted of interstitial free (IF) steel [67-70] and low carbon steel [71]. The non-ferrous group included aluminum alloy [9, 56, 57, 59, 67, 68, 70-78], copper [79, 80], Titanium [81] and composite Al-Cu, Cu-Zn-Al , and Al-Al [73, 78, 80]. The most widely used material was aluminum alloy and the least frequently tested was Titanium.

In the ARB process, one and two cycles were carried out on AA1050 and AA6061, either individually or on composite materials [78]. Four cycles were carried out on AA1235 [9, 75], five cycles on IF steel, low carbon steel, AA6061, and AA1050/AA6061 composite [56, 60, 68, 71, 73], six cycles on AA1100 and Ti-added IF steel [70], and seven cycles were carried out on Al-Mg (5083) [68], copper [79], and pure Ti [81]. Eight cycles were carried out on AA1100 [57, 68, 72, 74, 76] and composite AA2219/AA5086 [59], ten cycles were carried out on AA1100 materials [77] and IF steel [69], and fourteen cycles on sandwich Cu-Zn-Al [80]. The limitations of the ARB process were reached when the rolled edge crack was large and/or had low ductility. This was especially true when the reduction in thickness was more than 50 %.

Most ARB processes, using a reduction in thickness of 50 % [56, 57, 59, 60, 67-72, 74, 76-79, 81] and to 43 %, were carried out up to the fifth cycle on AA1100 materials [73], but it was difficult to provide an effective bond between the layers of thin sheet at 50 % reduction or less, because a reduction of more than 50 % would be needed to achieve an adequate bond. A 57 % reduction in thickness was carried out

on sandwiches of Cu-Zn-Al [80], and in this thesis, 65 % in the AA1235 material [9, 75].

Most of the material thicknesses for the ARB process were up to 1 mm [56, 57, 67, 68, 70, 73, 74, 76, 79, 80], 1.5 mm [60, 78], 2 mm [69] with the thickest being 2.5 mm [71]. Raw materials that are thinner than 1 mm, i.e. 0.5 mm, were used for AA1100, AA2219/AA5086, and Ti [59, 73, 77, 81], and the thinnest, at 0.3 mm for the AA1235 material in this thesis [9, 75] and composite sheet material of Al [80].

The grain size obtained from the ARB process ranged from 100-200 nm for IF steel, Ti, AA1050/AA6061, AA6061/AA6061 [60, 67, 69, 81]; 200-300 nm for AA1100, IF steel, AA2219/AA5086, AA1050, AA6061, AA1050/AA6061 composite [57, 59, 60, 67, 70, 76, 78, 79]. It is in the range of 300-400 nm for AA1100 material [67, 72, 74], and more than 400 nm for AA1100 Al-Mg (5083), IF steel, AA1050, AA1235 [9, 68, 75, 77, 78]. In general, the grain size obtained from the ARB process with five or more cycles was less than 500 nm.

If the ARB process is carried out below the recrystallisation temperature, then the rolled material will not be quite as ductile and the bond strength will not be strong enough [68]. To increase the bond strength, the interface of both plates can be brushed before the ARB process [68]. Samples of strips of Al/Al bonded by cold rolling and annealing carried out before ARB showed that the effect of work hardening had been eliminated [56, 58, 82]. Annealing or ageing the material after ARB can also improve its ductility and make it suitable for further processing.

The interface between materials for ARB will affect the bond because sufficient roughness and cleanliness is needed for the ARB process. For a fairly thin material, brushing can be done manually [9, 75] with a stainless steel brush, and a brush with a

wire diameters of 0.3 mm [80] for aluminum, zinc and copper, or 0.4 mm [77] for AA1100. The random surface roughness (R_a) of the results obtained by wire brushing was 1.5-1.8 μm [71]. Cleaning the interface before stacking, fastening, or welding prior to rolling can be done with Acetone. Tungsten inert gas (TIG) welding is better than riveting the front end of the samples. Edge cracks caused by high tensile stress at the edge [77] were the biggest problem from the ARB process. Edge cracks should not be ignored if the ratio between the thickness/width of the plate is less than 10 [68]. Edge cracking usually occurs for reductions in thickness of up to 50 %, and even 65 %.

2.4 Asymmetric rolling (AR)

Asymmetric rolling is rolling with a pair of rollers having a different angular velocity [83, 84]. Differences in angular velocity can be obtained using a pair of rollers of the same diameter but with different angular velocities, or by a pair of rollers of different diameters, but with the same angular velocity. AR is intended to increase the angular velocity of the top roller, while the angular velocity of the bottom roller remains constant [83, 85].

The purpose of AR is to refine and obtain a uniform microstructure across the thickness [84, 86]. It has a shear zone of constant through-thickness shear strain between the two neutral planes [84, 86, 87]. Conventional rolling (symmetric) only has two slip zones in the friction force, the forward and backward slip zone. The shear strain is non uniform, and varies from positive on one surface to negative on the other [84].

In AR, the difference in angular velocity between the upper roller and the lower roller is expressed by a speed ratio where the speed of the upper roller is faster than the roller on the bottom. Various speed ratios have been used for steel strips at 1.1, 1.2, and 1.3 [85], for low carbon steel at 1.2 [88], for IF steel at 1.2 [89], for 2205 duplex stainless steel at 1.2 and 1.4 [90], for IF steel at 1.2, 1.6, and 2 [91], IF steel with an idle roller [86, 92], AA1050 and AA6061 at 1.3 [84], Ti-grade 2 at 1.5 [87], pure Mg at 1.508 and 1.5 [93, 94], AA1050 at 1.5 and 2 [83]. AR where the speed of the lower roller was faster than the upper roller was used for steel-S355J2G3, with speed ratio of 1.01-1.15 [95], for steel-Q235 at 1.02-1.19 [96], for Si-steel at 1.125-1.5 [97], and for AA6xxx at 2 [98].

Several studies have revealed that an increased rolling speed can apply equally to the top or bottom roller. A range of speed ratios between 1.02 to 2 [96, 98] have been used, but it has been reported that the highest anisotropy value R was obtained with a speed ratio of 1.4 [90]. A high normal anisotropy value (R value) indicates that the formability of a material is also better [75].

2.5 Tensile testing

The effects of the thickness and preheating temperatures on the strength of 0.1 mm thick AA3003 aluminium annealed at 500 ^{o}C showed that the flow stress of rolled specimens had decreased and the width had reduced from 20 to 1 mm [99]. With $CuZn_{36}$ material, as the thicknesses ranged from100 to 500 μm, the material properties varied significantly during micro-forming [100], while the flow stress for brass ($CuZn_{36}$) also reduced as the thickness decreased [101]. Moreover, the strength of the material decreased when the t/d ratio (thickness/grain size) was reduced [102].

For micro-forming, the correlation between the grain size and tensile strength of the material needs further exploration.

While micro-forming copper (H3101) that had been rolled to 55 to 162 μm thick, the Holloman equation $\sigma = K\varepsilon^n$, and the strength coefficient (K) and strain hardening coefficient (n) had been influenced significantly by the thickness, as had the width of the specimen and the loading direction [100]. Another consideration in micro-forming is the accuracy of the tensile test; so when tensile tests were carried out on stainless steel (18Cr9Ni) micro-sized at 25 to 75 μm, they indicated that the eccentricity of the inserted set can affect the localisation of strain tensile specimens, and therefore it should be minimised [53]. Tensile tests were also conducted on sheets of copper (Cu 99.9 %) that ranged between 0.56 and 1.63 mm thick, to determine their strength [103].

Tensile test on Al 2S (99.0-99.5 %-DIN1747) with thicknesses of 0.17 to 2.0 mm [104] indicated that the flow stress decreased for the thinner specimens, while tensile tests of SE-Cu58 (99.95 % Cu) materials with a foil thickness ranging from 27 to 511 μm indicated that finer grains were required for micro-forming [66]. The microstructure of an IF steel sheet consists of very fine particles of ferrite particle that are responsible for higher formability while deep drawing [105].

The micro-scale tensile test of very thin specimens, 25 and 10 μm thick, was not carried out because it was difficult to prepare the specimens [106].

2.6 Anisotropy of materials

Anisotropy is the difference between the physical or mechanical properties of a material when measured in a different direction; unlike isotropy which implies identical properties in all directions.

Earing is caused by the presence of a material anisotropy which is expressed in terms of R_{avg} and ΔR is expressed by equations (2.1) and (2.2) [45] [43] [107] [108].

There are two kinds of conditions influenced by the values of R_{avg} and ΔR; if the value of R_{avg} is higher, the formability of the material will increase but if the value of ΔR is towards zero, earing will decrease, however, if the value R_{avg} has decreased, the formability of the material will be reduced and if ΔR is getting away from a zero value, then earing will be higher.

Normal anisotropy (R_{avg}) is related to formability in deep drawing and rolling, where formability has commonly been expressed in LDR or R_{avg}. Normal anisotropy has been considered in the rolling process for IF steel [92], AA6xxx-T6 [98], and duplex stainless steel (SS-2205) [90], but for deep drawing, normal anisotropy was investigated in IF steel [107], mild steel-DC06 [109], AA7075-O [2], AA2090-T3 [110], and Phosphor bronze-C5191 [108].

The R_{avg} for some materials are as follow: 2.59 at 90^o rolling direction (RD) for IF steel [107], 2.53 at 90^o RD for mild steel-DC06 [109], 0.9 at 0° RD and annealed at 400^oC for AA7075-O [2], 1.58 at 45^o RD for AA2090-T3 [110], 1.08 at 90^o RD with sheet reversal between the rolling cycles for IF steel [92], 1.2 after asymmetric rolling process (AR) for AA6xxx-T6 [98], 0.71 after the AR (speed ratio of 1.4) process and annealed at 1050^oC for stainless steel (duplex 2205) [90], and 2.45 at 0^o RD for Phosphor bronze-C5191 [108]. A high normal anisotropy indicates that the

material has high formability. IF steel has a high Lankford coefficient, mild steel is referred to as an anisotropic material, and since Phosphor bronze contains Tin which has a recrystallisation temperature below room temperature, the formability of Phosphor bronze is higher [111]. AA2090-T3 has a strong anisotropy at 1.58 on 45^{o} RD [110] and AA6xxx-T6 has a normal anisotropy increase when it is processed through a combination of strip casting and AR [98]. A normal anisotropy between 2.7 and 4.8 for pure Titanium, 1.6 mm thick was obtained [112]. The highest value of normal anisotropy belongs to pure Titanium, followed by IF steel containing Titanium, mild steels (DC06), Phosphor bronze, AA2090-T3, A6xxx-T6, AA7075-O, while stainless steel has the lowest.

Normal anisotropy increased to 1.08 and planar anisotropy was reduced to 0.07 after an IF steel was rolled in AR and the sheet direction was reversed between rolling cycles [92]. As a result, the formability of deep drawing can be improved and earing on the edge of the cup wall can be minimised. Normal anisotropy decreased to 0.78 with symmetric (conventional) rolling (SyR) and AR to 1.2 and the resulting increased planar anisotropy increased to 0.33 with SyR and 0.17 with AR [98].

2.7 Simulating the deep drawing process

Experiments based on trial and error have been conducted to obtain a particular combination of parameters that will produce a good cup, but trial and error can be time consuming. Numerical simulations have been widely used in micro-forming to obtain more information such as the punch force, and the stress/strains in the cup that lead to wrinkles and tears. It can be used to develop effective optimisation techniques

to control and optimise the process parameters. For example, FEM can be a valuable tool for assessing the performance of various blank holders [113].

A process of deep drawing a square cup from mild steel was simulated using a Vumat sub-routine of Abaqus software with 3D brick elements [114]. The effect of BHP on a wrinkle in the formation of a square cup showed that as the BHP increased, the wrinkles were reduced, and then disappeared when the blank holder pressure reached 2.03 MPa.

A model of conventional materials cannot describe material behaviour in a micro scale because of the size factor. Most of the knowledge obtained in traditional macro-forming is not suitable for micro-forming, which is why numerical simulations can provide the results of a punch force and Mises stress/strain distribution, with and without considering the size factor [115]. A simulation of micro stamping parts, by considering the size factor, showed that a von Mises stress distribution was lower than if it had not considered the size factor [54].

Determining the true stress is not entirely correct when localisation occurs, because the effective stress in the necking region has deviated from the longitudinal stress [116]. The results of a simulation which was verified by an experimental deep drawing of Cu alloys showed that wrinkles can be eliminated if their initial height is not more than 200 μm [31]. An FE simulation also showed that deep draw ability can also be improved due to a reduction of ductile damage with a blank holder control.

The BHP required to eliminate wrinkles increased rapidly when the thickness decreased; this was strongly influenced by the thickness of the blank and the coefficient of friction between the blank and tools [117]. An increase in the punch

force is needed in deep drawing if the radius of die is decreased, but if the BHP increases, the punch force required also increases [118].

The LDR can reach 2.0 on a forming temperature at 150 ^{o}C and a drawing velocity of 15 mm/s. A simulations showed that variable BHP technology can improve the LDR from 3 to 3.5, and also decrease the wall thinning ratio from 15.21 to 12.35 % [21].

Two different Al alloys were used to simulate circular cup drawing using Deform 2D. The depth of the deeper cup was obtainable at high temperatures, and a forming limit and necking location was also successfully predicted in the simulation. The optimum temperature in both blanks resulted in a uniform maximum depth of cup being obtained in the deep drawing process [119].

The FEM software Deform-3D was used to simulate the elliptical cup deep drawing of Mg alloy sheet at high temperatures. FEM was also used to investigate the effective stress and forming force in various conditions of process parameters, including the die corner radius, the clearance between the punch and the die cavity, and the BHP and temperature [63].

A pure copper flow stress behavior was determined experimentally, as were simulations that had a good agreement between the load-stroke curves in the extrusion of a micro double cup [120].

Chapter 3 Characterisation of processed strips

The experiments conducted in this study were designed to test the mechanical properties and characterise the microstructure and diffraction of AA1235/H14 foil. The mechanical properties included hardness, tensile tests, anisotropy, and a surface roughness. The microstructure was characterised by optical microscopy, the electron backscattered diffraction method (EBSD) using scanning electron microscopy (SEM), and transmission electron microscopy (TEM). A diffraction pattern was obtained by X-ray.

3.1 Mechanical properties tests

3.1.1 Hardness test

A hardness test was performed on AA1235 material from the 4-cycle ARB process to determine how the sample temperature and holding time in the furnace would affect this material after being rolled through the ARB process. The sample was cut at 15 x 10 mm, and was 0.35 mm thick, and the surface was polished with alumina powder. The samples were then heated to 150, 160, 175, 185, and 200 ^{o}C with holding times of 30 minutes, 2 hours, 5 hours, 10 hours, and 24 hours, respectively.

Some results of this chapter have already been published:
Hadi, S., Tieu, A. K., Lu, C., Zhu, H.T., *A micro deep drawing of ARB processed aluminium foil AA1235.* International Journal of Materials and Product Technology, 2013. **47**(1/2/3/4): p. **175-187**.

Hardness test were performed on the samples and tools. The hardness of the materials, as a result of the 4-cycle ARB process with 72 layers, was measured. The hardness of the tools was measured on the top and inside diameter surfaces of the die, the flat and cylindrical surfaces of the punch tip, and the lower surface of the blank holder, using an Indentec micro hardness tester with a load of 1 kg (HV_1). The loading period in the hardness measurement was 12 seconds in the Indentec hardness tester with a CCD camera and LCD line [121]. Each heat treatment was measured by 15 points 2.5 mm apart, to ensure data accuracy.

Residual stress reduction was carried out by stress relieving at 150, 165, 175, 185, and 200 ^{o}C, with holding times of 30 minutes, 1 hour, 2 hours, 4 hours, 8 hours, 10 hours, 24 hours, and 48 hours. The results of hardness tests are shown in Fig. 3.1, and indicate that the hardness had decreased significantly after holding times ranging from 0.5 to about 8 hours.

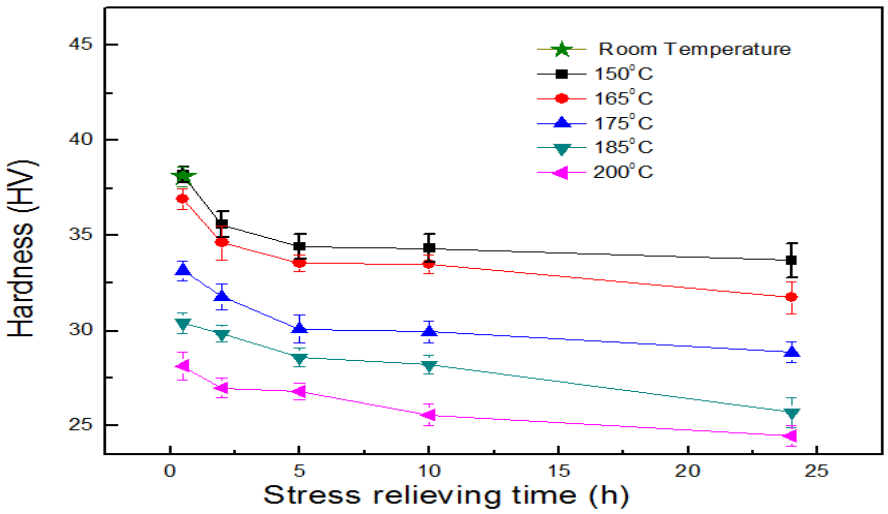

Fig. 3.1 Hardness of ARB-SR material, Hille100 rolling mill, 4 cycles, 72 layers, code: F

The average hardness on the upper surface of the die was 818.6 VHN, and the cylindrical surface hardness of the punch tip was 756.1 VHN, which was measured

within 3 mm of the flat end of the punch. The flat end of the punch had a hardness of 859.1 VHN and the bottom surface of the blank holder was 700 VHN.

Stress relieving helped to form a deeper cup without tearing from a 15 mm circular blank, and there were no wrinkles on the wall. However, the cup from the ARB processed material at 175 ^{o}C for 8 hours was torn at the corner between the bottom and the cup wall. It was found that a temperature of 200 ^{o}C and a holding time of 8 hours in an electric furnace was enough to produce a good cup.

3.1.2 Tensile test

Tensile tests were carried out on the foil with thicknesses ranging from 16, 41, 70, 130 and 300 µm. The AA1235 received from the manufacturer [122] contained the following elements: Al = 99.350 %, Fe = 0.420 %, Si = 0.100 %, Ti = 0.020 %, Zn = 0.012 %, Ni = 0.003 %, Mn = 0.002 %, Cu = 0.001 %, and others = 0.030 %. The shape and size of the tensile specimens were carried out according to Australian standards (AS1391) [123], as shown in Fig. 3.2. The tensile test specimens were annealed at 450 ^{o}C for 4 hours, and then air cooled after being taken out of the furnace.

The strain across the width and through the thickness of the tensile test specimens was measured before breakage. Withdrawal to anisotropy test was expected to be around 15 to 20 % of elongation for the first specimen [43]. An anisotropy test on aluminum alloy materials for beverage cans was carried out at a strain of 20 % [41].

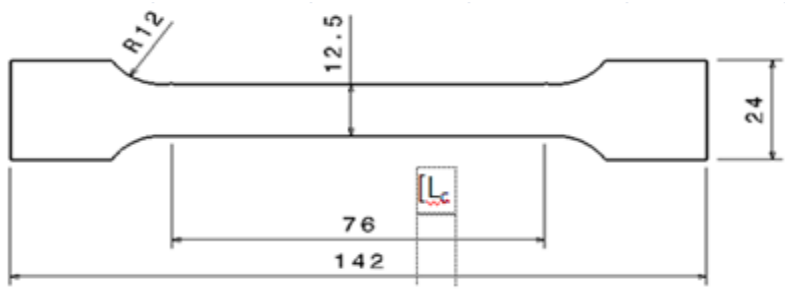

Type	Width (b)	Original gauge length (L_o)	Minimum parallel length (L_c)	Minimum transition radius (R)
1	3±0.2	12	18	3
2	6±0.3	24	36	6
3	12.5±1	50	75	12

Fig. 3.2 Size of the tensile test specimens for AA1235 [123]

To measure the surface roughness of the sample accurately means placing it in a stable holder, so the object will not move when measuring the tools (die, punch and blank holder), because they are cylindrical.

3.1.2.1 Flow stress versus thickness

Aluminium foil (AA1235/H14) with thicknesses of 16, 41, 70, 130, and 300 μm and a width of 3, 6, and 12.5 mm, prepared according to the prescribed standard [123], were annealed at 450^{o}C for 4 hours (FA), and then duplicate tensile tests were performed to ensure repeatability. Tensile testing of the first and second groups was prepared using 3 samples of each specimen thickness and width. Tensile testing was carried out by using a Shimadzu Tensile Testing Machine at a withdrawal speed of 10 mm/minute. The tensile force and displacement data were processed in order to obtain true stress-strain curves for each specimen thickness and width.

In this study the mechanical properties of Al foil related to the thickness (16-300 μm) and width of the specimen, and the grain size, were also identified. It was

necessary to carry out micro-forming as a deep forming process. The relationship between flow stress and specimen thickness for the AA1235 material is shown in Fig. 3.3. The flow stress decreases linearly with thinner specimens.

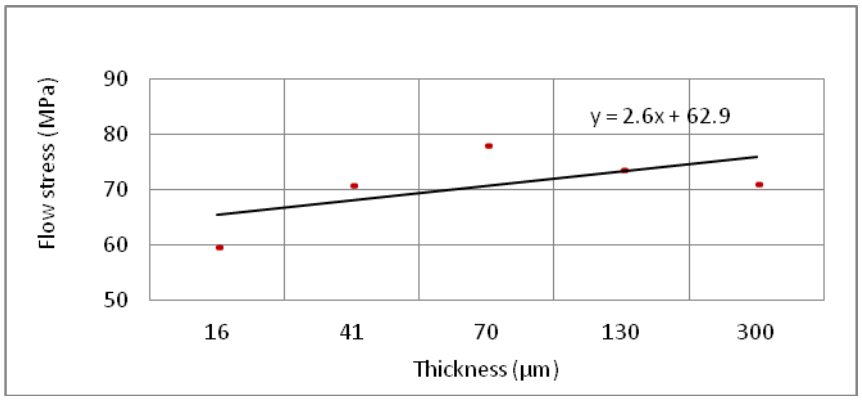

Fig. 3.3 Relationship between flow stress and specimen thickness of AA1235-FA condition

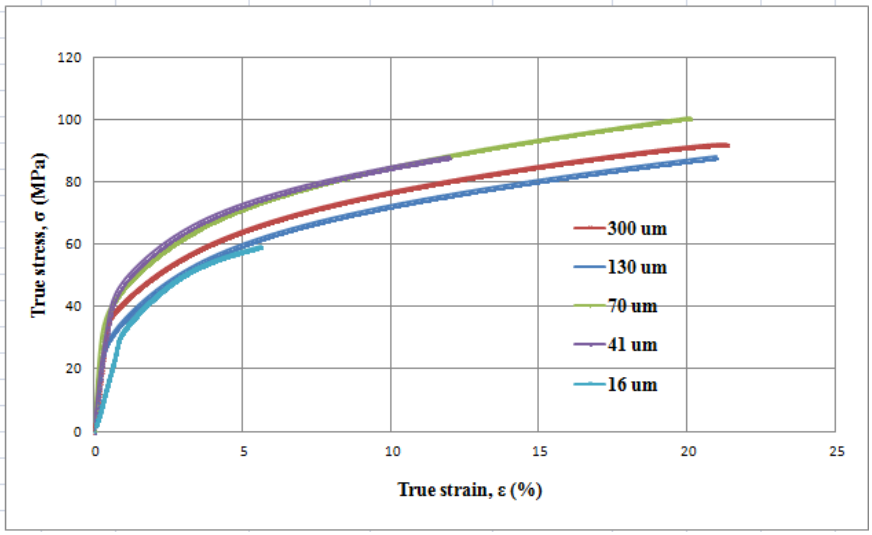

Fig. 3.4 Flow stresses of AA1235-FA condition with thicknesses of 16, 41, 70, 130, and 300 µm

The total number of tensile specimens for the first and second groups was 24 pieces, with 6 pieces each for thicknesses of 41, 70, 130, and 300 µm, all with a constant width of 12.5 mm. Each point in Fig. 3.3 was created from average of 6 tensile specimens, except for 16 µm specimen's thickness where one specimen per data point was used to the difficulties in obtaining consistent and reasonable results.

The relationship between the flow stress versus strain for five specimen thicknesses is shown in Fig. 3.4. For thicknesses of 41, 70, 130, and 300 microns, the experimental curves were the closest to the regressed trend line curves. Tensile testing of the 16 μm thick sample did not provide enough reliable data, but an example of the curve is shown for the purpose of illustration.

An equation for each group of curves representing the thickness of AA1235 material was obtained. The general equation is shown in Table 3.1 and equation (3.1).

Table 3.1 Flow stress equations of each thickness for AA1235-FA condition

No.	Thickness (μm)	Equations
1	16	$\sigma = 28.19\ \varepsilon^{0.53}$
2	41	$\sigma = 42.66\ \varepsilon^{0.26}$
3	70	$\sigma = 41.69\ \varepsilon^{0.27}$
4	130	$\sigma = 38.02\ \varepsilon^{0.30}$
5	300	$\sigma = 39.81\ \varepsilon^{0.27}$

$$\sigma = (254.1t^2 - 98.26t + 46.39)\ \varepsilon^{(-1.703\,t^2 + 0.578t + 0.249)} \quad (3.1)$$

The high exponent for 16 μm thickness reflects the difficulty and uncertainty encountered with the tensile testing a thin specimen, and because it was difficult to prepare samples, the micro-scale tensile test specimens were separated based on thickness, particularly for small values such as 25 and 10 μm [106].

A summary of the flow stresses on the 12.5 mm wide specimens with thicknesses of 16, 41, 70, 130 and 300 μm are shown in Fig. 3.5. Variations of flow stress to the width of the specimens annealed at 450 ^{o}C for 4 h, are shown in Fig. 3.5a.

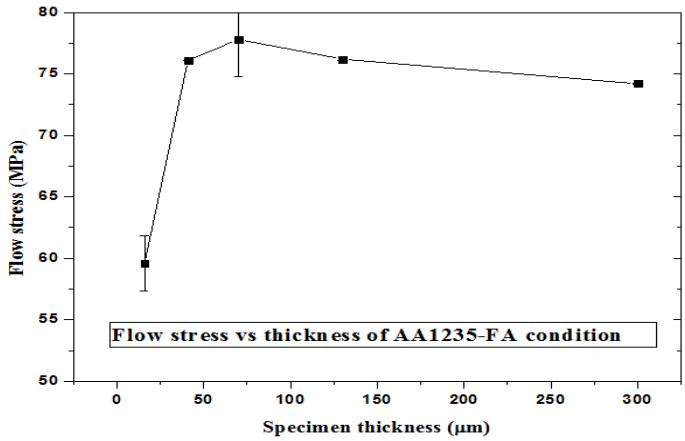

Fig. 3.5a Variation in maximum flow stress of AA1235-FA condition with thickness for specimen width of 12.5 mm

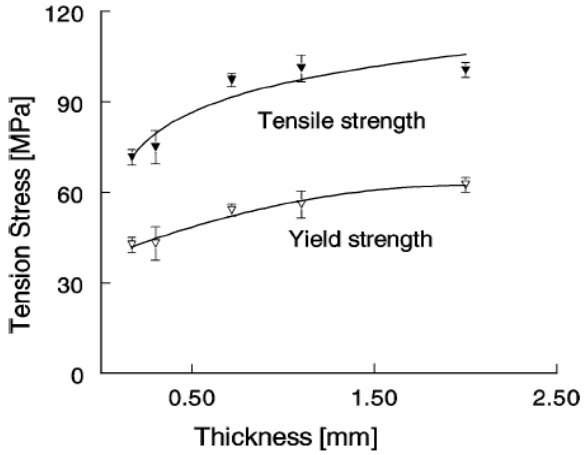

Fig. 3.5b Variation in tension stress of Al 2S with thickness [102]

Fig. 3.5a illustrates the findings obtained from the tensile tests of AA1235 that are related to specimen thickness. They showed a decrease in flow stress from a thickness of 70 to 16 μm. These findings were similar to those obtained from Al-2S (99 to 99.5 %-DIN1747) materials, which also showed decreases in thickness from 2000 to 170 μm (Fig. 3.5b) [102]. The differences between this study and other studies on Al-2S are due to differences in the series of materials, and the use of true stress and engineering stress [103].

3.1.2.2 Flow stress versus width and grain size

The variations of flow stress to the width of the specimen that was annealed at 450 ^{o}C for 4 h are shown in Fig. 3.6. With regard to the specimen width, tensile tests performed on AA1235 with a thickness of 41 and 70 μm (Fig. 3.6a) showed that the average flow stress increased by 1.93 % when the width gradually narrowed from 6 to 3 mm and then increased by 8.6 % when the width increased from 6 to 12 mm. These findings are similar to findings about the 0.1 mm thick 3003 Al foil material that had been rolled and annealed at 500 ^{o}C [100]. When the width of the specimen decreased from 6 to 3 mm, the stress also decreased gradually by about 1.1 %, and increased slightly from 6 to 10 mm. However, when the width increased from 6 to 20 mm, its value remains constant. The difference between the finding in this study and other studies on Al foil 3003 may be due to a different material series between AA1235 and AA3003, and different annealing temperatures and experimental scatter [100].

The plot of flow stress versus sample width for 70 and 41 μm thick AA1235 annealed at 450 ^{o}C for 4 h are shown in Fig. 3.7. The trend line shows that the flow stress increased for specimens of AA1235 that were 1, 3, and 6 mm wide and 41 μm thick, but it decreased at 70 μm thick (Fig. 3.7). There was more scatter for samples that were 41 μm thick.

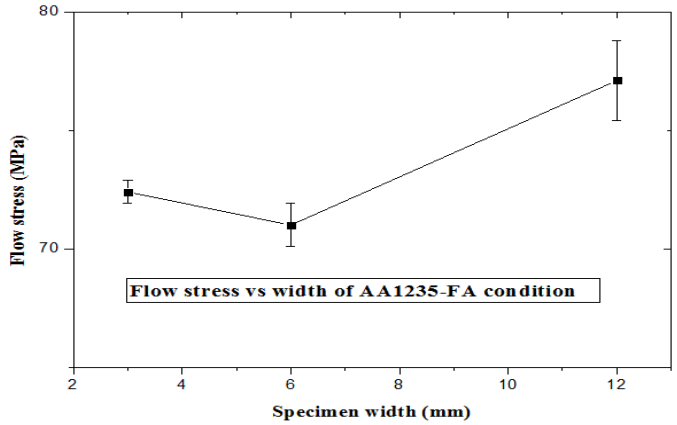

Fig. 3.6a Variation in maximum flow stress of AA1235-FA condition with specimens width

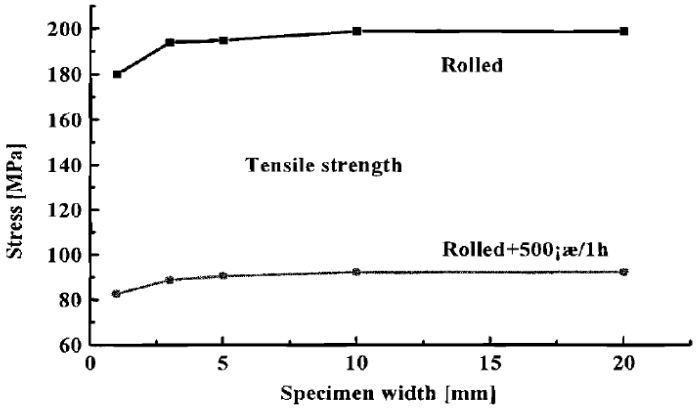

Fig. 3.6b Variation in maximum flow stress of AA3003 annealed at 500 ^{o}C for 1 h with specimens width [100]

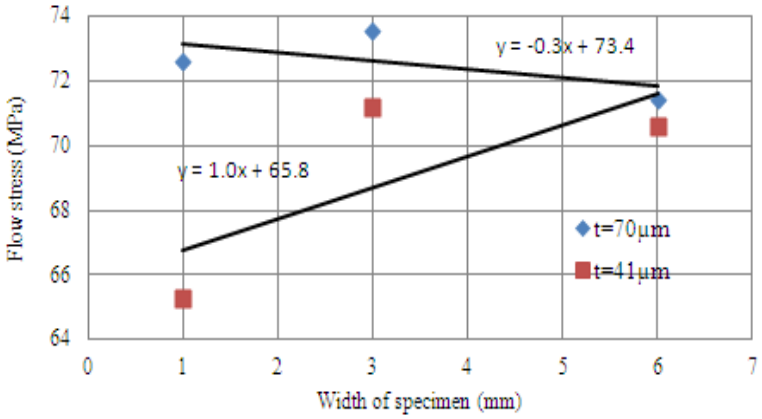

Fig. 3.7 Variation of flow stress to a specimen width of a thickness of 41 and 70 µm of AA1235-FA condition

The relationship between true stress and strain can be expressed by the Holloman equation (3.2),

$$\sigma = K\,\varepsilon^{n} \tag{3.2}$$

where σ is the true stress, ε is the true strain, K is a material constant, and n is the strain hardening coefficient [51]. The stress/strain relationship for AA1235 according to equation (3.2) can be formed as following:

$$\sigma = (254.1t^2 - 98.26t + 46.39)\varepsilon^{(-1.703t^2 - 0.578t - 0.249)} \tag{3.3}$$

where σ is the flow stress, t is the specimen thickness (μm), and ε is the strain.

The Hall-Patch equation relating the stress and grain size can be written as shown in equation (3.4) below,

$$\sigma = \sigma_{0(\varepsilon)} + k_{hp(\varepsilon)}/\sqrt{d} \tag{3.4}$$

where $\sigma_{0(\varepsilon)}$ and $k_{hp(\varepsilon)}$ are constants at a specific strain, ε, and average grain size, d, respectively.

The Hall-Patch equation indicated that the material flow stress increased with reduced grain size due to the increased number of internal grain boundaries caused by a decrease in the average grain size which prevented the dislocated grains from moving freely [51].

The correlation between specimen thickness (t) and grain size number (G) [124] of AA1235 is shown in Table 3.2. The lowest tensile stress was obtained at a thickness of 16 μm and the highest tensile stress at a thickness of 70 μm. The thickness/grain size ratio (φ=t/d) of 1.26 corresponds to a flow stress of 59.6 MPa for a thickness of 16 μm and an average grain size (d) 12.7 μm, which is 23.69 % lower than the 78.1 MPa for a thickness of 70 μm. The relationship between average grain size (d) and thickness (t) of AA1235 is presented in Fig. 3.8.

$$d = 4.395\ t^{0.387} \tag{3.5}$$

Table 3.2 Correlation between t and grain size number (G) of AA1235 foil

Thickness, t (μm)	Average grain size, d (μm)	Ratio t/d, φ	Grain size number [124] (G)	True TS*, (MPa)	YS, (MPa)
16	12.7	1.26	9	59.6	42
41	19.2	2.13	8	71.2	32
70	22.8	3.07	7.5	78.1	37
130	27.7	4.70	7	73.6	31.5
300	40.9	7.34	6	74.2	38

Note: *TS: tensile strength

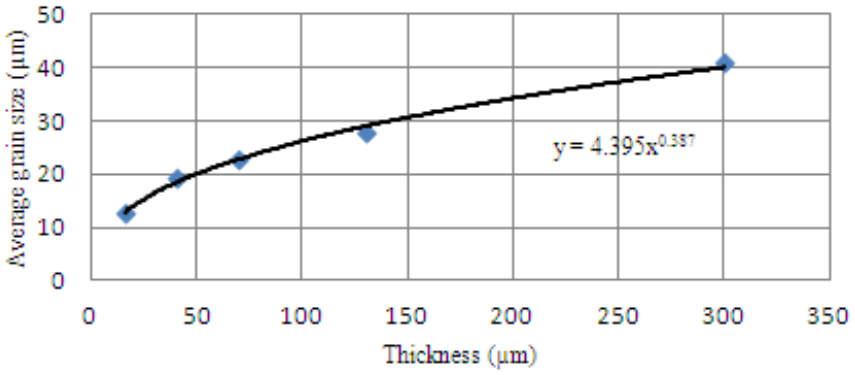

Fig. 3.8 Grain size versus thickness of AA1235

Flow stress of AA1235 in terms of the average grain size using equation (3.5) can be expressed by the following equation,

$$\sigma = (13.0d^{5.17} - 22.26d^{2.58} + 46.39)\ \varepsilon^{(-1.703t^2 - 0.578t + 0.249)} \tag{3.6}$$

where σ is the flow stress (MPa) and d is the average grain size (μm).

Grain size (d) of AA1235 for thicknesses of 16, 41, 70, 130, and 300 μm were measured by a prescribed standard [124]. The average grain sizes were 12.7, 19.2, 22.8, 27.7 and 40.9 μm, which correspond to the number of the grain sizes 9, 8, 7.5,

7, and 6 respectively. The relationship between yield strength and φ for AA1235 is shown in Fig. 3.9a.

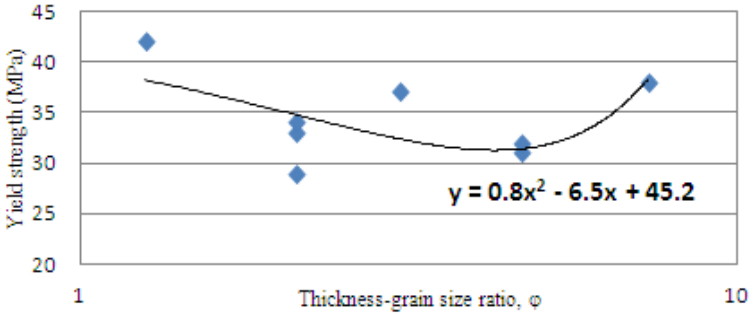

Fig. 3.9a Variation of yield strength and φ with the log scale of AA1235

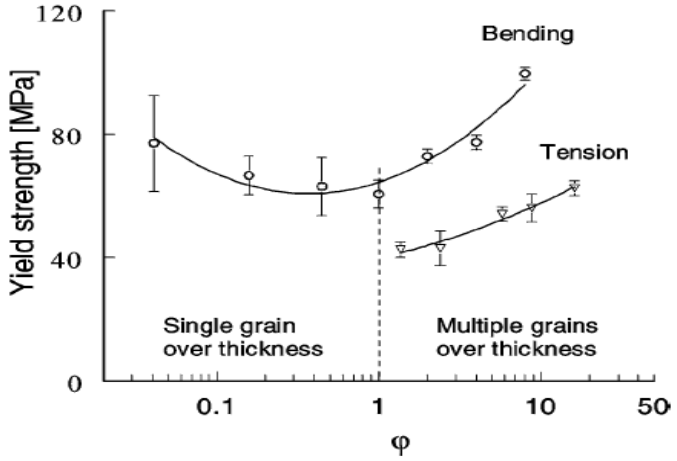

Fig. 3.9b Variation of yield strength and φ with the log scale of Al 2S [102]

Based on the φ (ratio t/d) for Al-2S, (99-99.5 % Al, DIN 1747) specimens, the yield strength increased from φ by about 1.5 to about 15 (Fig. 3.9b). While the yield strength of AA1235 decreased to a minimum value and then increased with φ. AA1235's yield strength was lower than the tensile test results of Al-2S (Fig. 3.9b) [102]. A correlation between φ and the strength of AA1235 is shown in Fig. 3.10.

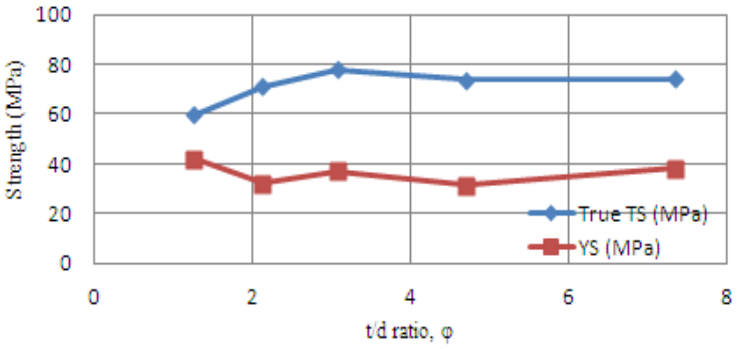

Fig. 3.10 Correlation between t/d ratio (φ) to its strength of AA1235-FA condition

3.1.3 Anisotropy test

An anisotropy test was carried out for AA1235 in FA condition. The results for other three conditions were also obtained, i.e., an ARB process, an ARB process followed by stress relieving process [75], and an ARB process followed by asymmetric rolling process. Samples were cut from the material at 0, 45 and 90^{o} to the RD into 3 pieces, and then a tensile test was carried out at a speed of 0.1 mm/minute. The test results of anisotropy were measured many times in the form of strain ratios across the width and through the thickness.

Test specimens for anisotropy had a nominal thickness of 0.300 mm, a nominal width of 3 mm, and a nominal gauge length of 19 mm for the AA1235 material under FA conditions. The nominal thickness of material for the three ARB processed samples (ARB, ARB and stress relieving, and ARB process followed by AR), were 3.1, 3.6, and 1.3 mm respectively. The nominal width was 3 mm and nominal gauge length was 19 mm, which was the same for all four materials with different treatments. To maintain accuracy, the actual thickness and width of the specimen for testing anisotropy was measured 3 times, while the gauge length was measured once before and after withdrawal.

Earing is caused by material anisotropy, which is expressed in terms of normal anisotropy R_{avg} and planar anisotropy ΔR according to equation (2.1) and (2.2) [45] [43] [108]. The formula from equations from (2.1) is $R_{avg} = (R_0 + R_{90} + 2R_{45})/4$, and from (2.2) is $\Delta R = (R_0 + R_{90} - 2R_{45})/2$. R is the strain ratio across the width and through the thickness of tensile test specimens ($R=\varepsilon_w/\varepsilon_t$). If ΔR is equal to zero, then there is no earing [43], but if the value of R_{avg} is higher, the formability of the material will increase, and if the value of ΔR moves toward zero, then earing will decrease. The anisotropy values of AA1235 with various conditions are shown in Table 3.3.

The respective R_{avg} values for different treatment conditions: FA, ARB4c, ARB4c-SR, and ARB4c-AR are 0.639, 0.594, 0.651, and 0.420. The highest value of 0.651 for R_{avg} ARB4c-SR conditions was associated with the highest LDR achieved where a cup was formed without tearing. This indicates that the greater the value of R_{avg}, the higher the formability of a material will be. Moreover, earing was also greatly reduced for ARB4c-SR material conditions compared to the FA condition.

Table 3.3 Anisotropy of AA1235 materials under various conditions

No.	Treatment	R_{avg}	ΔR	Grain Size (μm)	LDR	Remark
1	FA 450 ^oC, 4h	0.639	0.556	40.9	2.003	High earing cup & no wrinkles
2	ARB4c	0.594	0.278	1.75	1.88	Torn cup
3	ARB4c-SR 200 ^oC, 8h	0.651	-0.022	2.15	2.003	Very low earing cup & no wrinkles
4	ARB4c-AR-Vr 1:1.3	0.420	-0.040	1.655	1.88	Torn cup

Note: FA: full annealed, ARB: accumulative roll bonding, AR: asymmetric rolled, SR: stress relieved, Vr: speed ratio.

The values of R_{avg} and ΔR for the FA condition were 0.639 and 0.556 respectively. R_{avg} and ΔR of the material conditions of ARB4c-SR were 0.651 and -0.022. The value of ΔR for conditions ARB4c-SR was smaller than the FA condition, so earing was reduced. However, ARB4c material cannot be fully drawn because the material became harder after the ARB process, so to reduce its hardness meant that a stress relieving process was required.

Refining the grain size through the ARB process followed by stress relieving can lower the planar anisotropy and reduce earing. Unlike the anisotropic behaviour of AA7075 annealed between 270 to 450 ^{o}C, ΔR from 0.240 to 0.285 and R_{avg} values of 0.64 to 0.90 were produced [2]. The conditions for ARB4c-SR had a higher formability than FA or ARB4c, because of the higher value R_{avg} at 0.651 compared to 0.639 of the FA, and 0.594 for ARB4c. A high normal anisotropy R_{avg} will produce a high limiting drawing ratio (LDR) following a linear relationship [75] [125, 126].

Normal anisotropy (R_{avg}) of the 4-cycles ARB process, followed by AR with a speed ratio of 1:1.3, was 0.420. This was lower than the results of the 4 cycle ARB process only, with a value 0.594. However, the planar anisotropy (ΔR) decreased to -0.040, which was better than the results of the 4-cycles ARB process, with a value of 0.278. When this material was deep drawn it produced a cup that was torn at the corner. The relationship between R_{avg} and LDR in deep drawing of AA1235 material is shown in Fig. 3.11.

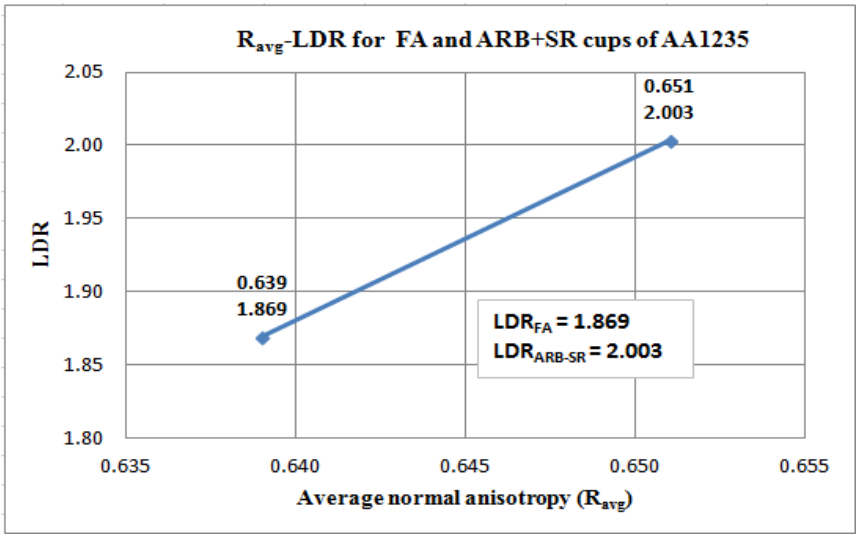

Fig. 3.11 Relationship between R_{avg} and LDR in deep drawing of AA1235

It was concluded that normal anisotropy (R_{avg}) and the coefficient of friction (μ) play an important role in influencing the LDR value, rather than the strain hardening coefficient (n) and the ratio between the thickness of the sheet to the radius of the die [125]. The LDR obviously increased with an increasing value of normal anisotropy, but it was reduced significantly as the coefficient of friction increased, then decreased slightly by the ratio between the thickness of the sheet and the radius of the die. Thus the higher the normal anisotropy of a material and the lower the μ between the materials and tools, the higher the value of LDR will be.

An LDR value of 1.98 was achieved while deep drawing AA7075-O material that was 1.1 mm thick and had been annealed at 400 ^{o}C with 0.9 normal anisotropy and planar anisotropy of -0.24 [2]. For an LDR value of 2.003, the 0.3 mm thick AA1235 material that had been annealed at 450 ^{o}C for 4 hours, the corresponding normal anisotropy and planar anisotropy were 0.639 and 0.556 respectively.

3.2 Surface roughness test

An accurate two-dimensional surface roughness measurement was obtained by placing the sample in a stable holder. Samples were placed onto a flat table to measure the two-dimensional roughness, but cylindrically shaped tools (die, punch and blank holder) were placed on a stable holder on the table to obtain surface roughness measurements.

The surface roughness of the raw material (AA1235) was observed by atomic force microscopy (AFM). Three-dimensional images of the surface profile for material that was 300 and 130 µm thick are shown in Fig. 3.12 and Fig. 3.13. Furthermore the roughness parameters of average roughness (R_a), root mean square roughness (R_q), Skewness (S_k) and Kurtosis (K) are shown in Table 3.4.

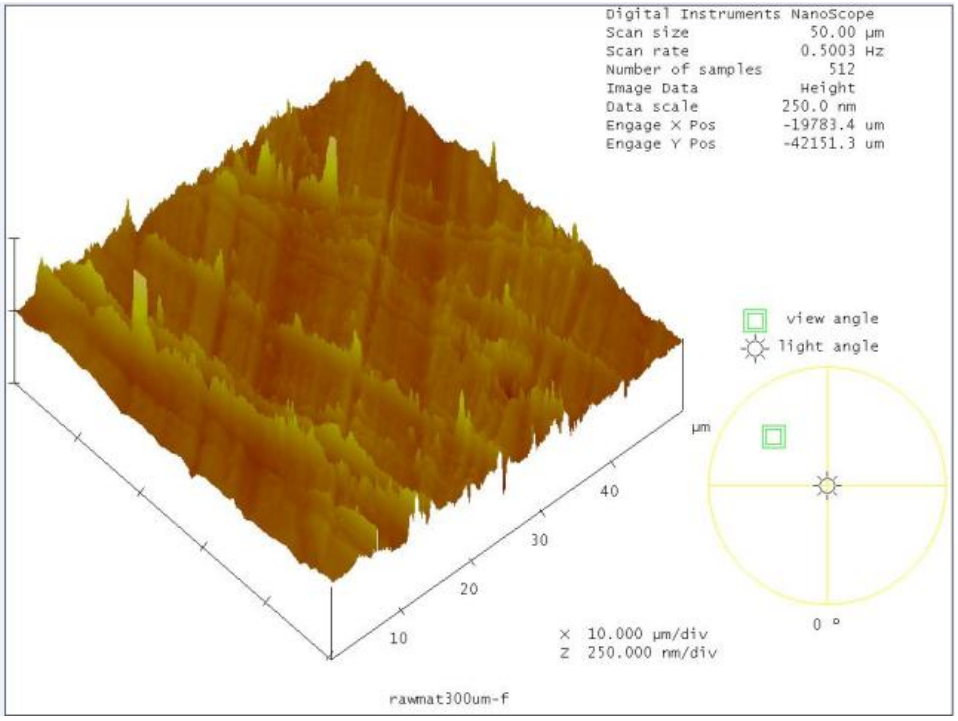

Fig. 3.12 Three dimensional surface profile of AA1235 specimen with thickness of 300 µm

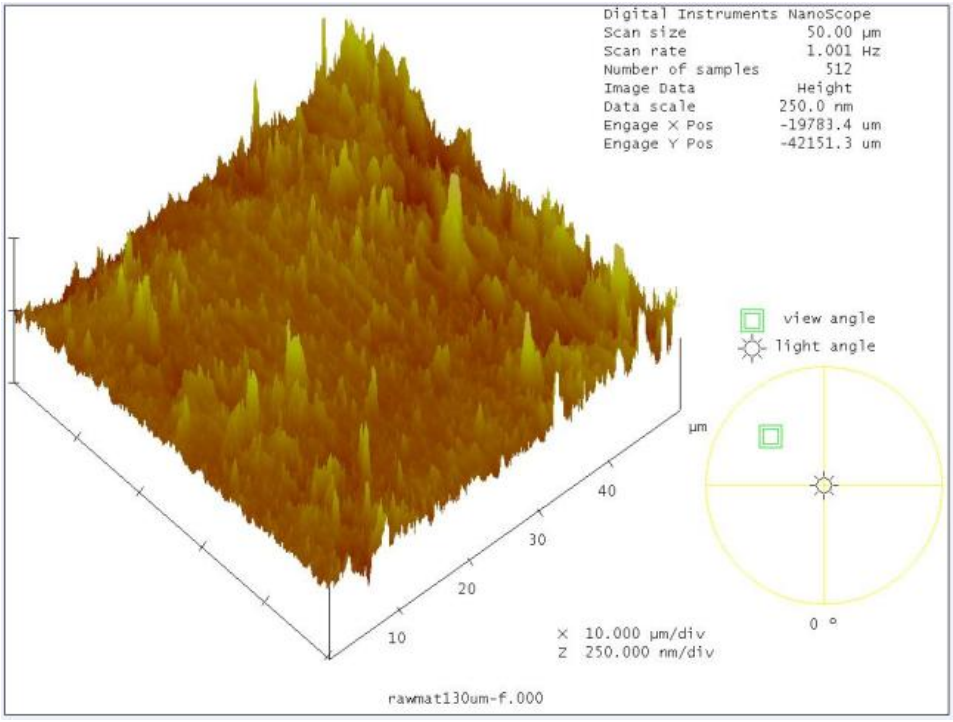

Fig. 3.13 Three dimensional surface profile of AA1235 specimen with thickness of 130 µm

Table 3.4 Ra, Rq, Sk, and K of Al foil of AA1235 determined by AFM

No.	Thickness, t (µm)	R_a (nm)	R_q (nm)	S_k (nm)	K (nm)
1	300	17.859	26.675	0.830	32.032
2	130	21.490	32.595	0.782	10.066
3	70	19.518	10.303	-0.742	12.826
4	41	36.088	58.635	-1.166	10.583
5	16	35.509	49.335	1.282	8.632

Three-dimensional surface profiles were measured with AFM for raw AA1235 material, with a scan size of 50 µm, as shown in Figs. 3.12 and 3.13, for a thickness of 300 and 130 µm. Different surface profiles emerged from the final rolling process. The S_k values for 70 and 41 µm thick materials had negative values of -0.742 and -

1.166 nm respectively, indicating that the roughness profile had some valleys. Skewness indicates an asymmetry value of the probability distribution of the height of the roughness profile [127]. Positive values for S_k on raw material that was 300, 130 and 16 μm thick indicated that the roughness profile had some peaks.

The Kurtosis values for the surfaces of materials that were 300, 130, 70, 41, and 16 μm thick were greater than 3, which indicated that the roughness profile had many high peaks and low valleys [128] [129]. The Kurtosis values were used to evaluate the sharpness of the probability distribution of the height of the profile [127]. A Gaussian distribution has a Kurtosis (K) value equal to 3. If $K < 3$ then the distribution has a few high peaks and low valleys and the surface is relatively flat, but if $K > 3$ then the distribution has many high peaks and low valleys and the surface is relatively rough [129].

The surface roughness of the materials and tools in the ARB process were measured by a Hommelwerk tester. A roughness profile of the results with the two-dimensional method is shown as an example of the roughness of the top surface of the die, with a diameter of 8.26 mm in the radial direction between the radii of 5.2 and 10 mm, as shown in Fig. 3.14.

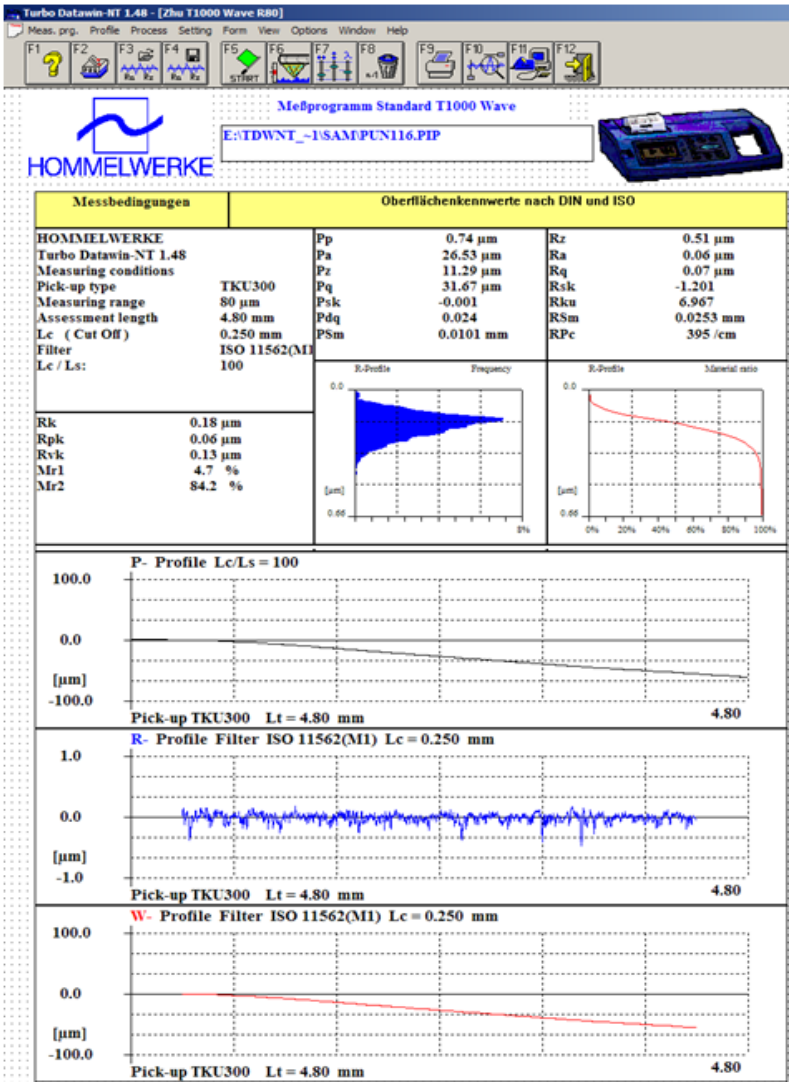

Fig. 3.14 Profile of surface roughness by a Hommelwerk tester

The surface roughness and Kurtosis of 4 cycles of ARB material, prior to and after rolling was performed in the rolling direction (RD) and the transverse direction (TD). These are shown in Figs. 3.14, 3.15 and Table 3.5.

Table 3.5 A value of the surface roughness and Kurtosis for ARB materials for 4 cycles

No.	Cycle(s)	Layers	Rolling							
			RD		TD		RD		TD	
			R_a (µm)				K			
			Before	After	Before	After	Before	After	Before	After
1	1st	9	1.22	0.11	1.08	0.19	3.92	0.40	3.13	0.59
2	2nd	18	1.04	0.23	1.09	0.40	3.09	0.48	3.47	0.89
3	3rd	36	1.06	0.19	1.10	0.23	3.19	0.63	3.19	0.73
4	4th	72	0.72	0.19	0.82	0.23	2.19	0.63	2.40	0.65

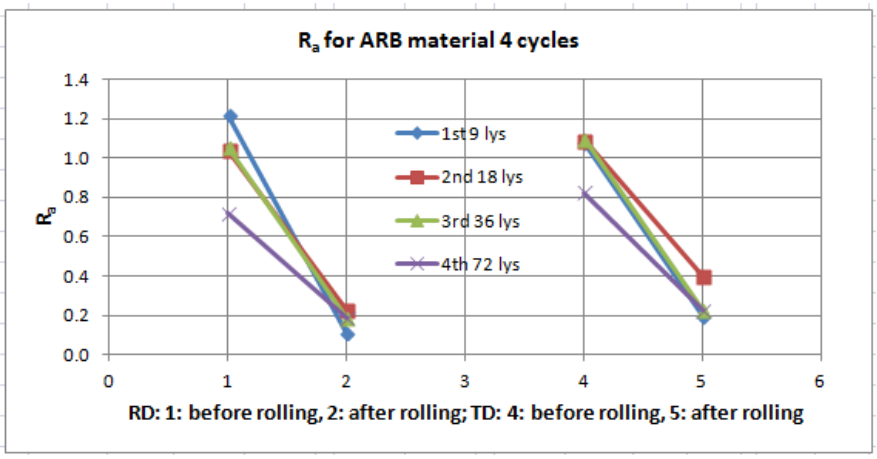

Fig. 3.15 R_a for ARB material for 4 cycles

The surface roughness of the material after the ARB process decreased, both in the RD and the TD. In the first rolling cycle the R_a decreased from 1.22 to 0.11 µm for RD and from 1.08 to 0.19 µm for the TD. The surface roughness on rolling in the first cycle had a greater reduction than with the subsequent second, third, and fourth cycles, due to the dominant effect of the work roll surface roughness, as shown in Fig. 3.15.

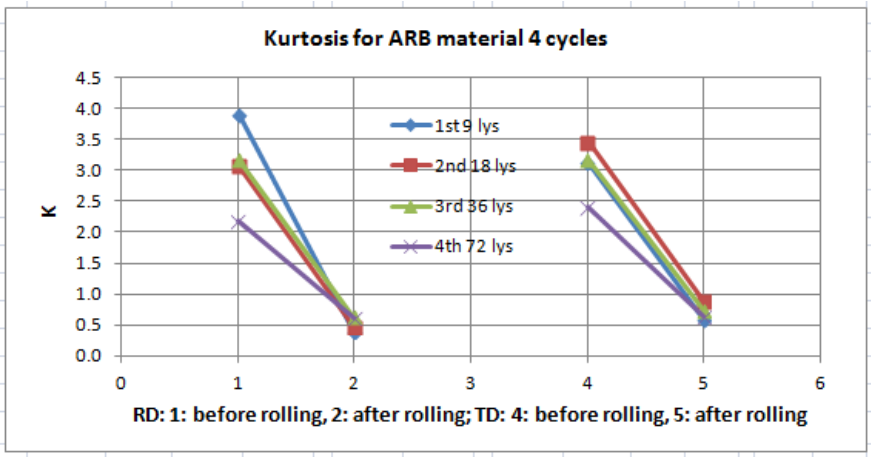

Fig. 3.16 Values of Kurtosis for ARB material for 4 cycles

The Kurtosis value for the material after the ARB process decreased, both in the RD and in the TD. At the first rolling, K decreased from 3.92 to 0.40 and from 3.13 in the RD to 0.59 in the TD. The K value in the first cycle had a greater reduction than the second, third, and fourth cycles for RD, but it was not the biggest drop for TD, as shown in Fig. 3.16.

The original K value was greater than 3, indicating that the surface was relatively rough. After experiencing the first rolling, its value decreased drastically to 0.4, which means that the surface condition changed from being relatively rough to being relatively flat due to the surface roughness of the work roll.

The most dominant parameter in surface roughness is Skewness (Sk). The more negative the parameter, the lower the friction that can be expected, although the average value of surface roughness is higher [130]. The skewness for 4 cycles of ARB materials decreased for the second cycle until it reached negative values. This occurred because the value of K had changed from a value greater than 3 to below 3, which indicated that the surface was relatively flat. Thus it can be said that friction has reduced, which is characterised by negative skewness values of -0.42, to become

-1.13 in RD, and 0.48 becoming -1.24 in TD, as shown in Table 3.6 and Fig. 3.17. The more negative the skewness parameter is, the lower the friction will be [130], because the surface has become flat and resistance has reduced.

Table 3.6 A value of the Skewness for ARB materials for 4 cycles

No.	Cycle(s)	Layers	Before rolling	After rolling	Before rolling	After rolling	t_{red} (%)
			RD		TD		
			R_{sk} (µm)	R_{sk} (µm)	R_{sk} (µm)	R_{sk} (µm)	
1	1st	9	0.26	0.41	0.44	1.38	63.78
2	2nd	18	-0.42	-1.13	0.48	-1.24	65.98
3	3rd	36	0.61	0.47	0.22	0.60	72.28
4	4th	72	0.44	0.05	-0.06	0.15	53.73

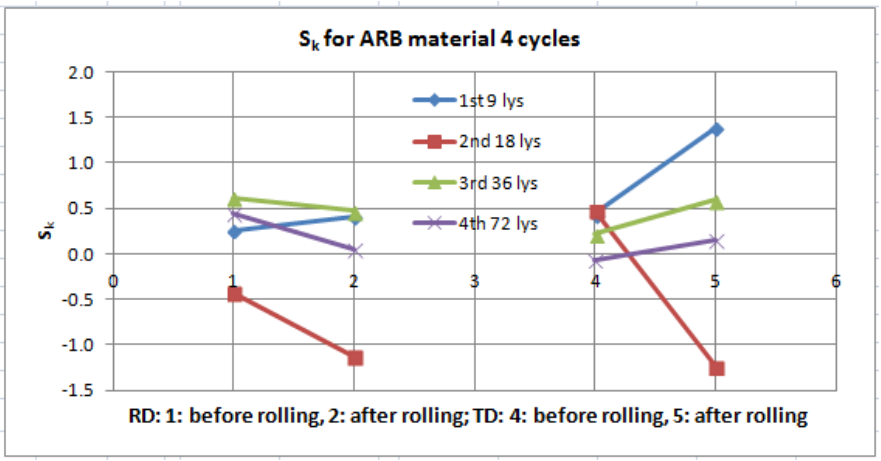

Fig. 3.17 A value of Skewness for ARB material for 4 cycles

The surface roughness (R_a, R_q, S_k and K) of tools is measured at the contact surface between the tool and the blank material. The roughness values for the cylindrical surface of the punch tip, the top surface of the die, the inside diameter of the die, and the bottom surface of the blank holder, are shown in Table 3.7.

Table 3.7 Values of the surface roughness of tools

No.	Surface	R_a (μm)	R_q (μm)	S_k	K
1	Cylindrical surface of punch	0.25	0.32	-0.49	3.97
2	Top surface of die	0.11	0.14	-0.77	6.23
3	Inner diameter of die	0.48	0.77	-1.39	14.13
4	Bottom surface of blank holder	0.11	0.16	-0.11	6.22

It can be concluded from surface roughness measurements on blank material, the material results of 4 cycles of ARB process, and from tools, that the surface of the tool is much smoother than the surface of the blank material. They are approximately the same as the material results for the ARB process. As a result of the ARB process, the R_a values for tools, blanks, and materials ranges from 0.11 to 0.48 μm (Table 3.7), from 17.86 to 36.09 μm (Table 3.4), and from 0.11 to 1.22 μm (Table 3.5).

The range of S_k values for tools, blanks, and materials, as a result of the ARB process, varied from -0.11 to -1.39 (Table 3.7), from -1.17 to 1.28 (Table 3.4), and from -1.13 to 1.38 (Table 3.5). This shows that the S_k values for blank materials were more negative than for the tools and materials after ARB processes. The K values for tools, blanks, and materials as a result of the ARB process, were from 3.97 to 14.13 (Table 3.7), from 8.63 to 32.03 (Table 3.4), and from 0.40 to 3.92 (Table 3.5). Most of the K values were greater than 3, so most of the surfaces of the three components were relatively rough.

3.3 Microstructure characterisation

3.3.1 Optical microscopy for micro structure of raw materials

The microstructure of AA1235 material was observed using an optical microscope. The raw materials were 16, 41, 70, 130, and 300 μm thick, and were cut and molded with a material made from copper powder, which made them conductive and easy to hold. A metallographic process commenced by cutting a sample, molding it with copper powder, mechanically grinding it with abrasive papers for a certain mesh, electro-polishing, observing the microstructure under a microscope, and taking pictures. The micro structural images were then analysed using VideoPro32 software previously installed in the optical microscope (Leica DMRM-DFC295), to determine the grain diameter. Determining the microstructure of the grain diameter was based on a standard [124].

The surface of the AA1235 specimen was polished with alumina powder. Mechanical grinding with SiC abrasive papers can embed abrasive particles into the soft surface, so water was used while grinding to flush the particles away. It is also recommended that grinding be carried out with low pressure on the specimen. Polishing was done using alumina powder (Al_2O_3) with grain diameters of 5, 1, and 0.5 μm. A very smooth, scratch free surface was achieved by electro-polishing (electro-chemical polishing) using Barker's reagent (5ml HBF_4 (48 %) + 200ml. H_2O) [131], with the time set to 120 seconds, 0.6 A, 16 ^oC, and 24 V.

An image of the microstructure of AA1235 at 300 μm thick is shown in Fig. 3.18.

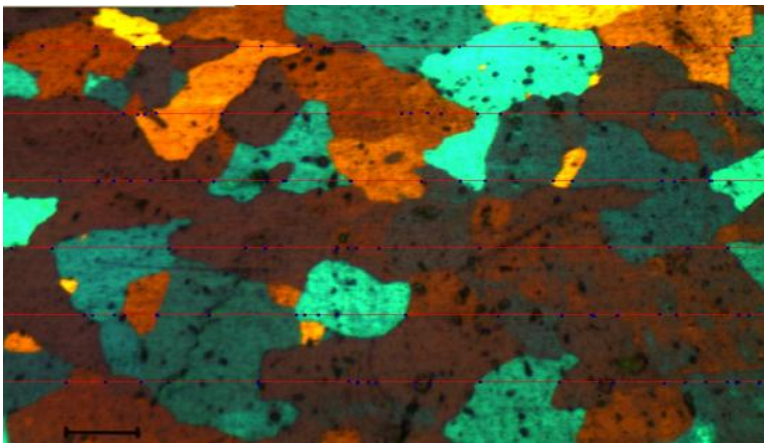

Fig. 3.18 Grain structure of AA1235 of thickness of 300 µm (scale bar: 75 µm)

3.3.2 EBSD

The grain size of AA1235 for the treatment of various conditions was observed by using a JEOL JSM-7100F SEM with the EBSD method. Seven surface specimens were prepared from the cross section, in line with the RD. EBSD specimens for AA1235 were materials with FA conditions; ARB with 2 cycles, and with 4 cycles; ARB with 4 cycles followed by AR for 1 cycle with a speed ratio of 1.3: 1, and 1.4:1; ARB with 4 cycles followed by stress relieving at 175 and 200 ^{o}C for 8 hours each. The results of scanning AA1235 with the EBSD method in the cross section in the RD are summarised in Table 3.8. The images of scanning with the EBSD on the cross section in the RD are shown in Fig. 3.19 to Fig. 3.25.

There was a difference between the measurements of the average grain size of the material AA1235 FA conditions. Those measurements obtained from an optical microscope were 40.9 µm (Table 3.2) while the results obtained by EBSD were smaller by 25.09 µm (Table 3.8) (38.66 %). These differences were possible because the low angle grain boundary cannot be clearly observed in the optical microscope, and the EBSD results do not depend on the process of etching and imaging techniques [132]. The difference for low carbon steel materials obtained by optical

image analysis (SIS imager analysis package) was 14.22 µm, and the value obtained from the EBSD method was smaller by 9.24 µm (35.02 %) [132]. The acquisition shows the difference percentage value is between 35.02 and 38.66 %.

Table 3.8 EBSD scanning results with AA1235 in the cross-sectional direction of the RD

No.	Treatment	Specimen code	t (µm)	t/layer (µm)	d (µm)	φ= t/d	d_{min} (µm)	d_{max} (µm)	N	TS (MPa)	ε (%)
1	Full annealed	FA	300	300	25.09	11.96	1.954	75.753	68	74.2	24
2	ARB2c, Hille100,18 lyrs	ARB2 (cut from D)	508	28.2	1.758	16.05	0.195	9.484	303	133	2.24
3	ARB4c, Hille100, 72 lyrs	ARB4 (cut from D)	276	3.83	1.744	2.20	0.113	7.145	565	130	2.09
4	ARB4c, Hille100, 72 lyrs + SR175	SR175 (cut from SR26)	278	3.86	1.773	2.18	0.195	9.198	535	33	0.5
5	ARB4c, Hille100, 72 lyrs + SR200	SR200 (cut from SR26)	278	3.86	2.146	1.80	0.195	7.288	274	37	13
6	ARB4c, Hille25, 72 lyrs + AR, Vr 1.3:1	AS1.3 (cut from code 5)	379	5.26	1.655	3.18	0.113	14.461	709	114	1.61
7	ARB4c, Hille25, 72 lyrs + AR, Vr 1.4:1	AS1.4 (cut from code 5)	379	5.26	1.633	3.22	0.113	14.990	652	105.2	1.54

Note: FA: full annealed at 450°C for 4 h, ARB were preheated at 200°C for 10 minutes, SR175 (SR200): stress relieving at 175°C (200 °C) for 8 h, AR: asymmetric rolling, Vr: speed ratio, Hille 25: type of rolling mill with roll diameter 120 mm, Hille 100: type of rolling mill with roll diameter 225 mm, and N: size of the data set.

The AA1235 specimens for examination in the SEM with the EBSD method were mounted with Polyfast (a thermosetting resin and Bakelite with a conductive carbon filler) [133].

Deformation through 4 cycles of the ARB process can reduce the original diameter of 25.09 µm grains to 1.773 µm, and further deformation through an AR can reduce the grain size to 1.655 µm for AR with a speed ratio of 1.3:1, and 1.633 µm for a speed ratio of 1.4:1. Although the grain size achieved was quite small, residual stress was still a problem in the deep drawing process. Stress relieving was carried out to improve the formability of the AA1235 material. After relieving the stress at 200 ^{o}C for 8 h, the grain size increased to 2.146 µm, and as a result the AA1235 material was successfully drawn into a good cup. There was also a low level of earing without wrinkles or tears.

The ratio between the thickness and grain diameter (φ = t/d), achieved by the ARB process AA1235 after 4 cycles (72 layers) and stress relieved at 200 ^{o}C for 8 hours was 1.80 (3.861/2.146) of the original material thickness of 278 µm, divided by 72 layers to 2.146 µm. The φ value obtained was greater than the φ value of 1.26 for a thickness of 16 µm (Table 3.2). It has been stated that the formability for micro-forming is worse when the ratio φ (=t/d) for a 26000 brass (1/2) hard (H02) was decreased [50]. However, this statement does not apply for the AA1235 material, because a blank of this material processed with 4 cycles of ARB, followed by stress relieving at 200 ^{o}C for 8 hours, can be drawn into a good cup with the ratio φ = 1.80. Even though the ratio φ = 2.18 was higher for a 4 cycle ARB processed blank, followed by stress relieving at 175 ^{o}C for 8 hours, a torn cup was produced because the material still had insufficient ductility for deep drawing, compounded by residual stress in the material. The material still had a higher hardness than the material that was stress relieved at 200 ^{o}C for 8 hours.

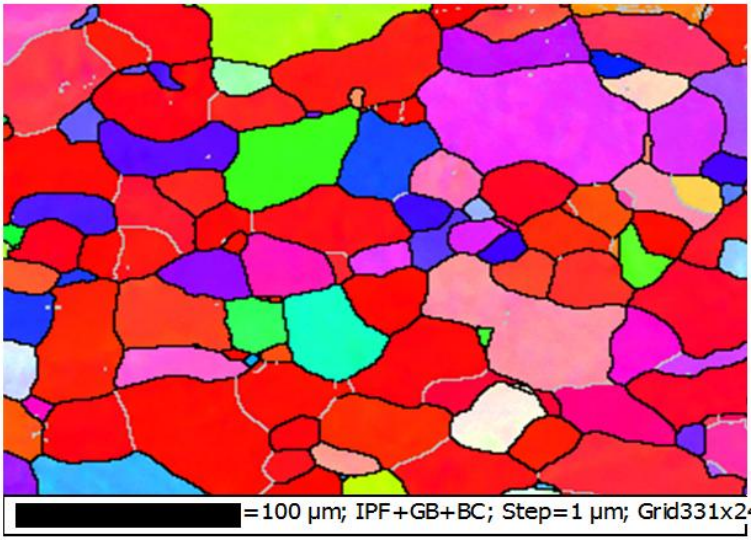

Fig. 3.19 EBSD image on the cross-section in the RD of FA material

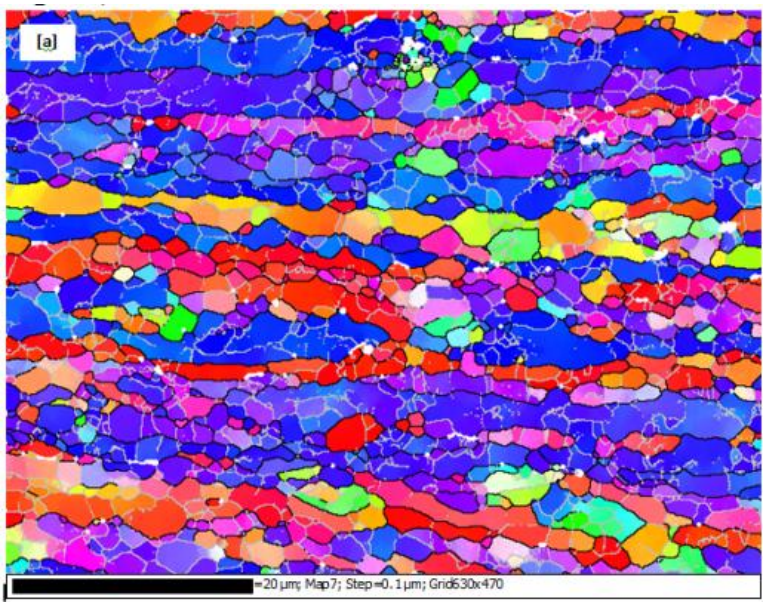

Fig. 3.20 EBSD image on the cross-section in the RD of ARB 2 cycles material

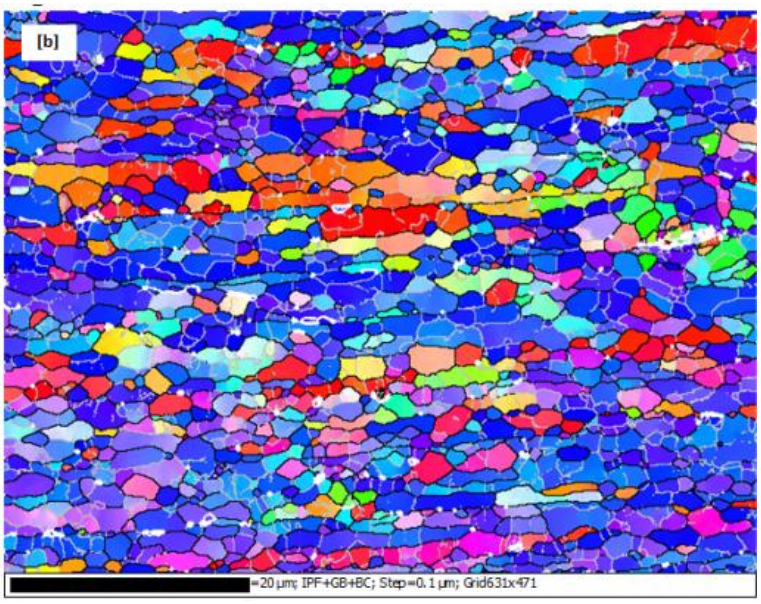

Fig. 3.21 EBSD image on the cross-section in the RD of ARB 4 cycles material

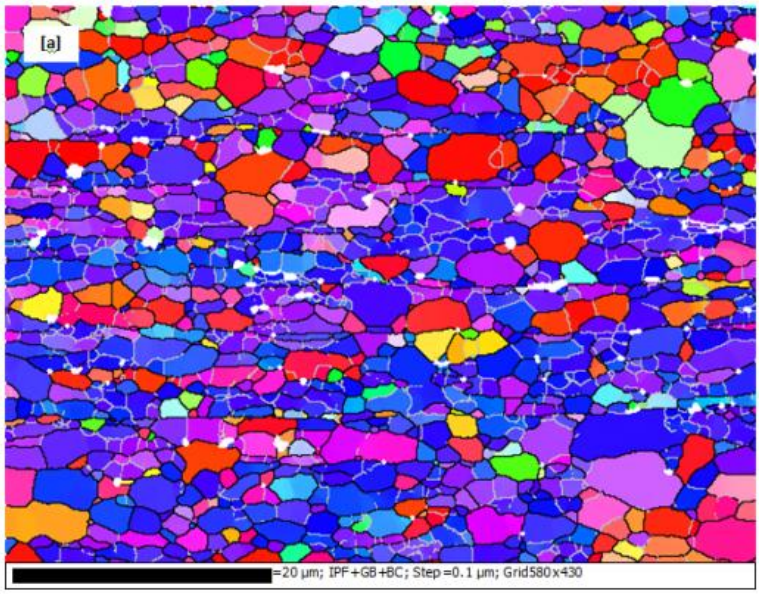

Fig. 3.22 EBSD image on the cross-section in the RD of ARB 4 cycles material subsequent stress relieved at 175 ^{o}C for 8 h

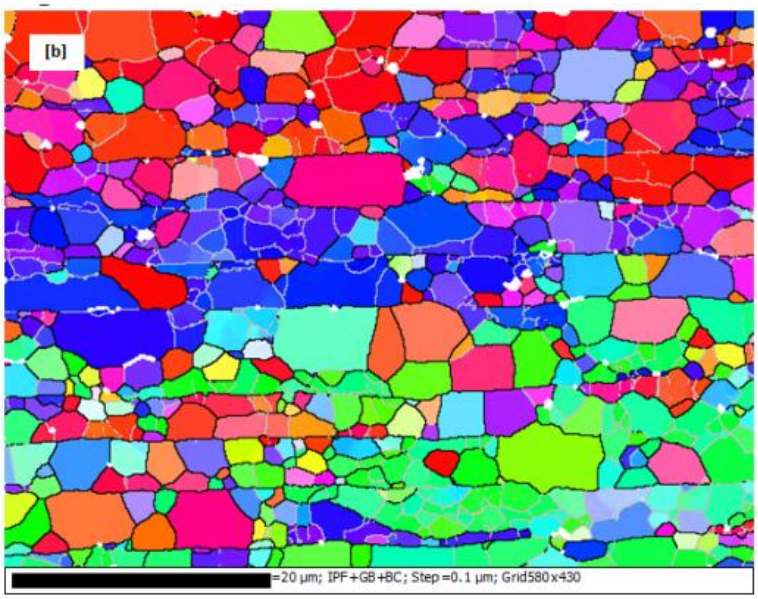

Fig. 3.23 EBSD image on the cross-section in the RD of ARB 4 cycles material subsequent stress relieved at 200 ^{o}C for 8 h

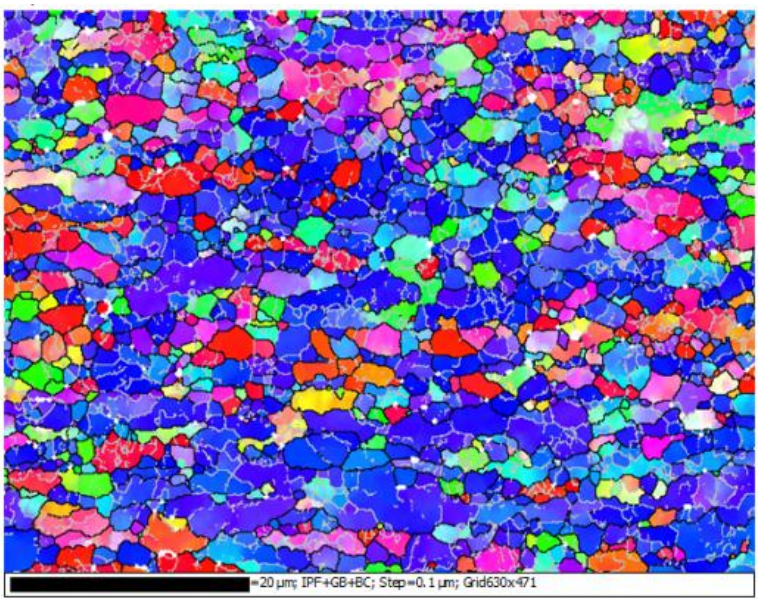

Fig. 3.24 EBSD image on the cross-section in the RD of ARB 4 cycles material subsequent AR at Vr=1.3:1

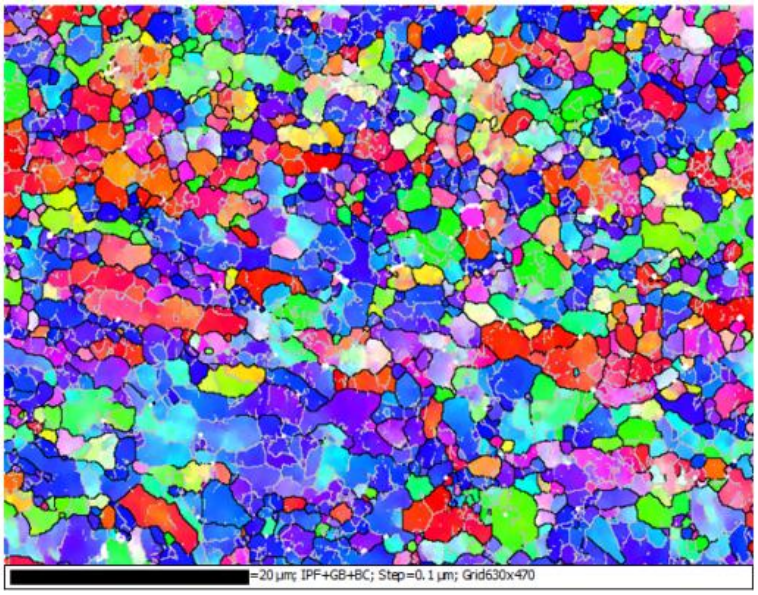

Fig. 3.25 EBSD image on the cross-section in the RD of ARB 4 cycles material subsequent AR at Vr=1.4:1

3.3.3 Transmission electron microscopy (TEM)

Images of the microstructure of AA1235 material were obtained by transmission electron microscopy (TEM). Equipment such as a Philips CM200 field emission gun/transmission electron microscope (FEG/TEM) equipped with a Bruker energy

dispersive X-ray (EDAX) spectroscopy system was operated at an accelerating voltage of 200 kV to observe details of the microstructure.

Fig. 3.26 shows the microstructure of a sample obtained by TEM. In Fig. 3.26 (a), the as-received material microstructure has a coarse grain which was refined during the rolling process. After the sixth cycle of ARB, followed by one and two AR processes, the grains were refined and rolled with a laminate structure, as shown in Fig. 3.26 (b-c). With further rolling, the grain structure of the laminated material turned into finer equi-axed shaped grains with an average grain size of 550 nm, as shown in Fig. 3.26 (d). This means the microstructure along the RD has been distributed equi-axed, which may increase the ductility and strength during the AR process [134].

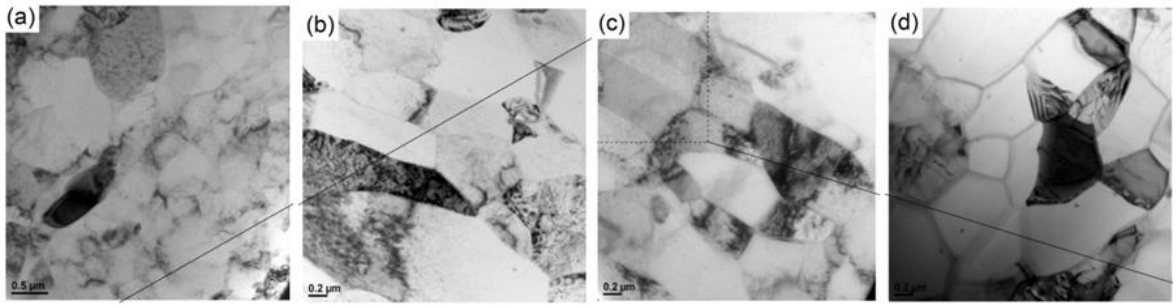

Fig. 3.26 TEM micro-structure of AA1235 samples: (a) as-received material, (b) after the first cycle of AR, (c) after the second cycle of AR, and (d) after the third cycle of the AR [135]

3.4 Diffraction pattern for deformed Aluminium foils

AA1235 material was pure Aluminium, with high levels of Al = 99.35 % and 0.65 % of other alloy elements such as Fe, Si, Ti, Zn, Ni, Mn, Cu, and others [122].

The diffraction pattern of AA1235 before and after deformation was obtained by X-ray diffraction. The diffracto-meter used for diffracting AA1235 specimens was a GBC MMA X-ray diffraction unit for thin films and phase analysis. Diffraction was carried out on these materials in the as-received (As-R) condition, with full annealing

at 450 ^{o}C for 4 hours (FA), an ARB 3 cycles (ARB3c), and ARB 3 cycles followed by 4 cycles of asymmetric rolling (ARB3cAR4c) with thicknesses of 303, 302, 434, and 44 µm, respectively. The specimen was circular, with a diameter of 14 mm.

For three cycles of the ARB process of AA1235 material, the total thickness reduction reached 77 %. Before the material was rolled with ARB it was preheated for 10 minutes to 200 ^{o}C. The four cycles of AR, and three cycles of ARB resulted in an 87 % reduction in thickness without any preheating.

Diffraction patterns before and after deformation are shown in Fig. 3.27 to Fig. 3.31.

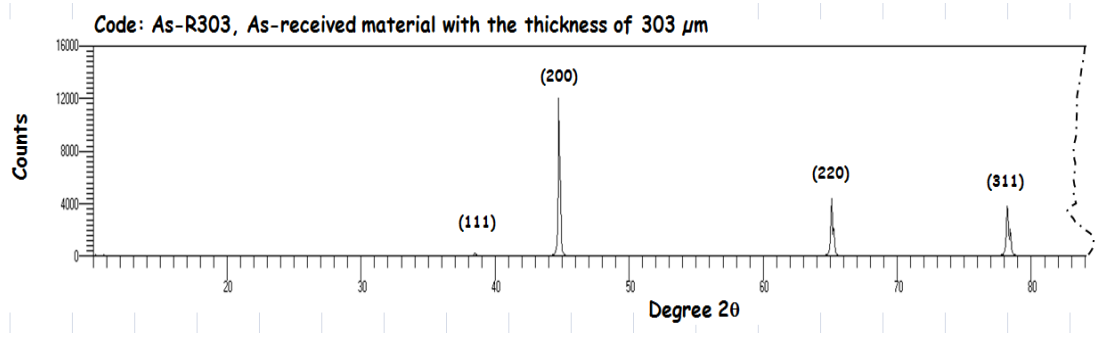

Fig. 3.27 Diffraction pattern of AA1235 in the as received condition, code: As-R303

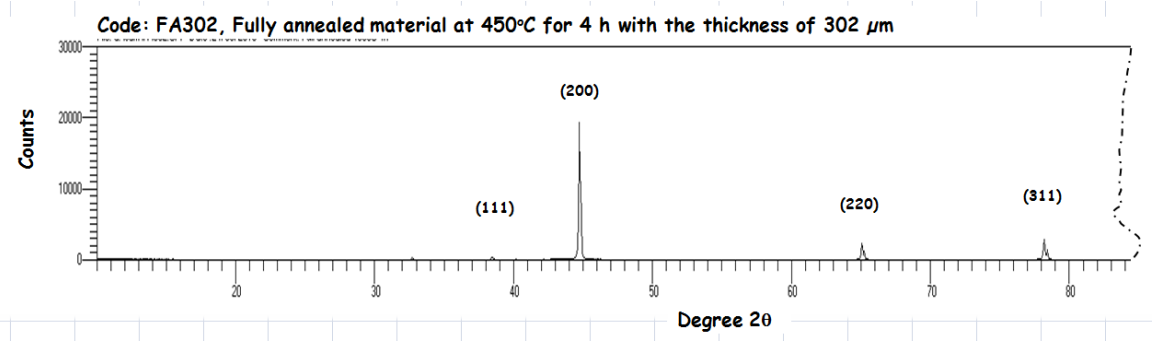

Fig. 3.28 Diffraction pattern of AA1235-FA condition at 450 ^{o}C for 4 h, code: FA302

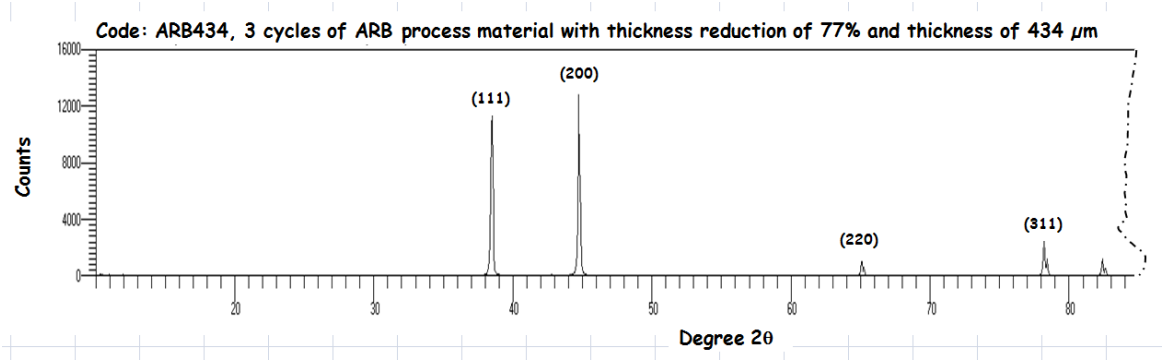

Fig. 3.29 Diffraction pattern of AA1235 on the condition of the ARB process 3 cycles with thickness reduction of 77 %, code: ARB434

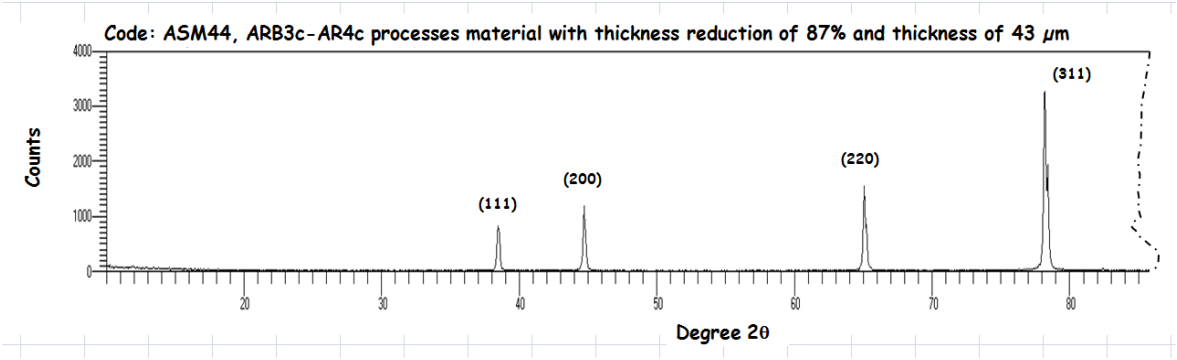

Fig. 3.30 Diffraction pattern of AA1235 on the condition of the ARB process 3 cycles followed by 4 cycles AR with thickness reduction of 87 %, code: ASM44

The results of the diffraction of the AA1235 material after treatment in the following conditions was: FA at 450 ^{o}C for 4 hours, As-R, while ARB3c and ARB3cAR4c were analysed using the software TRACES.

Aluminium has a face centered cubic (FCC) structure. The size of the lattice parameter of aluminium, according to [136] is 4.0406 Å. Aluminium has a melting point of 660 °C with a density of 2.70 g/cm^3 [137]. The lattice parameter of 4.0406 Å [137] (1 Å=0.1 nm) increased slightly to 4.0500 Å [138] (> 0.23 %) after the AA1235 material was deformed from the starting state of the as-received condition, processed in 3 cycles of ARB followed by 4 cycles of AR. The as-received thickness of 0.300 mm was reduced to 0.044 mm after ARB and AR. The peaks that appeared

are the crystal planes (111), (200), (220), and (311) at an angle of 2θ at ~38.5, ~45, ~65, and ~78.5^{o} after diffracted materials. Peaks on the crystal plane (111) rose when the material condition changed from the As-R to ARB3c. The crystal plane (311) had also grown from the material conditions of FA into ARB3cAR4c. This means that the preferred orientation became stronger on these crystal planes.

The AA1235 grain structure on conditions after ARB3cAR4c process was almost equi-axial, but it was not elongated like material usually is after being rolled. This is shown by the EBSD image with an average diameter of 1.655 μm, as shown in Fig. 3.24. Thus the X-ray diffraction results may indicate a change in the diffraction pattern for AA1235 material which was subjected to annealing heat treatment and deformation through an ARB and AR.

3.5 Summary

Rolling process can result in a strain hardened material that eventually leads to residual stress and reduced formability when deep drawing a cup. Residual stresses must be removed in an annealing process to improve formability, but their strength is then lower. This means that formability is a compromise between ductility and the tensile strength of a material. The selection of temperature and holding time for annealing is important because they can dictate the degree of stress relieving. The stress relieving temperature should be below the recrystallisation temperature.

Heating above the recrystallisation temperature can increase the grain size, and excessive grain growth should be avoided because the material produced by ARB is meant to reduce the diameter of the grain, so that thin material can still be formed with good results. The melting temperature of AA11235 was 660 ^{o}C, with a

recrystallisation temperature of around 200 ^{o}C. Full annealing at 450 ^{o}C, which is above the recrystallisation temperature, was considered to be enough to ensure that any residual stresses that may still exist can be eliminated by allowing the grain to grow to an optimum size in four hours. With a full annealing process, it would be expected there would be no more effect on residual stress, due to the previous process carried out by the manufacturer. Mechanical property tests were carried out to determine the mechanical properties of hardness, tensile strength, flow stress, normal anisotropy (R_{avg}), planar anisotropy (ΔR), surface roughness values, grain sizes, micro voids in structure, and the diffraction patterns for deformed materials. Equations of AA1235 material flow stress were obtained for different widths and thicknesses, and they showed a decreasing flow stress with reduced thickness, whereas the widths of the sample only had a small effect.

Anisotropy was considered in the occurrence of earing on a cup between materials that were stress relieved and those that were fully annealed. The LDR achieved was 2.003 for 0.3 mm thick AA1235 material after an annealing temperature of 450 ^{o}C for 4 hours, with respective normal and planar anisotropy values of 0.639 and 0.556. The results of the deep drawing of these materials produced a cup without wrinkles, but with high earing.

The normal anisotropy of 4 cycles of ARB, followed by asymmetric rolling with a speed ratio of 1:1.3, was 0.420, and the planar anisotropy was -0.040. The LDR achieved was 2.003 for 0.3 mm thick AA1235 material, from an ARB process with 4 cycles followed by asymmetric rolling. The results of deep drawing these materials produce a cup without wrinkles and with low earing.

The grain sizes obtained from scanning via SEM with the EBSD method were intended to determine the ratio between t/d (thickness and grain size) associated with the formability of a material. The greater the ratio of t/d of a material, the higher its formability will be.

TEM images of the results showed the effect of the large deformation of AA1235 material after an ARB process of up to 6 cycles followed by an AR of up to 3 cycles. The average grain size reached 550 nm, which is considered ultra-fine grain (UFG). The grain size achieved after an ARB process of up to 4 cycles followed by an asymmetric rolling was 1.633 μm (Table 3.8). The grain size for AA1235 material in an annealed condition was 25.09 μm, which meant it experienced a significant refinement of 15.36 times. A blank material can undergo a successful deep drawing process after ARB process, followed by a stress relieving at 200^{o}C for 8 hours. The results of the experiment indicate that the material has been successfully formed into a cup without wrinkles and with low earing, with a ratio φ (=t/d) of 1.86.

It can be concluded that the changes in the material properties of AA1235, with a mechanical or a heating process, generally improve formability. Increases in formability can be obtained with an increase in normal anisotropy and can refine the grain diameter. Refining the grain size can be obtained through ARB and asymmetric rolling. Reductions in the occurrence of earing can be achieved by reducing the value of the planar anisotropy because an increase in the value of a planar anisotropy means that a better cup can be formed.

Chapter 4 Rolling processes

4.1 Accumulative roll bonding process

4.1.1 Preparation of ARB samples

Accumulative roll bonding (ARB) is a rolling method aimed at obtaining finer grain diameters and bonding two or more sheets stacked together, and then repeating this process for the desired number of cycles.

The ARB process was carried out by using a Rolling Mill Hille 100, with 228 mm diameter top and bottom rolls, and a rolling speed of 10 rpm [88]. The material used was 140 mm long by 150 mm wide by 0.3 mm thick Aluminium AA1235. A strip of this material was cut into two halves, brushed, cleaned, stacked, and joined before rolling.

The sample was pre-heated in a Muffle furnace at 200 ^{o}C for 10 minutes before being rolled. The temperature was measured using a non-contact infrared thermometer, Model DT-8838, within the maximum distance of 1.5 m. The emissivity for Aluminum was 0.8.

Some results of this chapter have already been published:
Hadi, S., Tieu, A. K., Lu, C., Zhu, H.T., *A micro deep drawing of ARB processed aluminium foil AA1235.* International Journal of Materials and Product Technology, 2013. **47**(1/2/3/4): p. **175-187**.
Hadi, S., Tieu, A. K., Lu, C., Su, L.H., Yu, H.L, *Grain refinement in the formability of Aluminium thin cup.* Materials Science Forum, 2013. 773-774: p. **166-175**.

Pre-heating was also carried out on the ARB process for AA6016 material, at 230^{o}C for 4 minutes before rolling [139]. For AA1050 material in the ARB process, pre-heating was done at 250^{o}C for 3 minutes [140]. AA6014 material was pre-heated before the ARB process at 210^{o}C for 2.5 minutes [141].

4.1.2 Rolling of ARB samples of AA1235 for fourth cycles

Since Aluminium has a shiny surface the temperature readings would not be accurate, so the surface must be sprayed with black paint before pre-heating. There were 9 sheets for the first cycle, 18 layers after the second cycle, 36 layers after the third cycle, and 72 layers after the fourth cycle. The data from 4 cycles of the ARB process showed a reduction in thickness ranging between 62 and 66 %, as shown in Table 4.1.

Table 4.1 Data for a sample of the G code for 4 cycles of ARB process by Hille100 rolling mill

No.	Cycles	Layers	T (^{o}C)	Thickness (mm)						t_{red} (%)
				Before roll	After rolled					
				t	t_1	t_2	t_3	t_4	t_{av}	
1	1	9	150.2	9x0.3=2.7	1.010	1.042	1.032	1.000	1.021	62
2	2	18	156.0	1.021x2=2.042	0.818	0.744	0.703	0.803	0.767	62
3	3	36	153.2	0.767x2=1.534	0.583	0.576	0.547	0.530	0.559	64
4	4	72	152.6	0.559x2=1.118	0.410	0.383	0.363	0.370	0.382	66*

The interfaces of the 9 sheets of raw material were brushed and cleaned with Acetone, then stacked and welded into a single unit with tungsten inert gas (TIG). Brushing the interface of AA6061 can increase its hardness more than if not brushed in an ARB process [142]. The stacked sample was then sprayed with black paint so

that the pre-heating temperature could be measured. After pre-heating at 200 ^{o}C for 10 minutes, the sample was removed from the electric furnace, the temperature was measured, and then it was rolled.

The length of the sample in the rolling direction had increased to more than twice its original length, depending on the amount of reduction, and a small amount of edge cracking also occurred.

The Hille 100 rolling mill and associated equipment, Muffle furnace, and infrared thermometer are shown in Fig. 4.1.

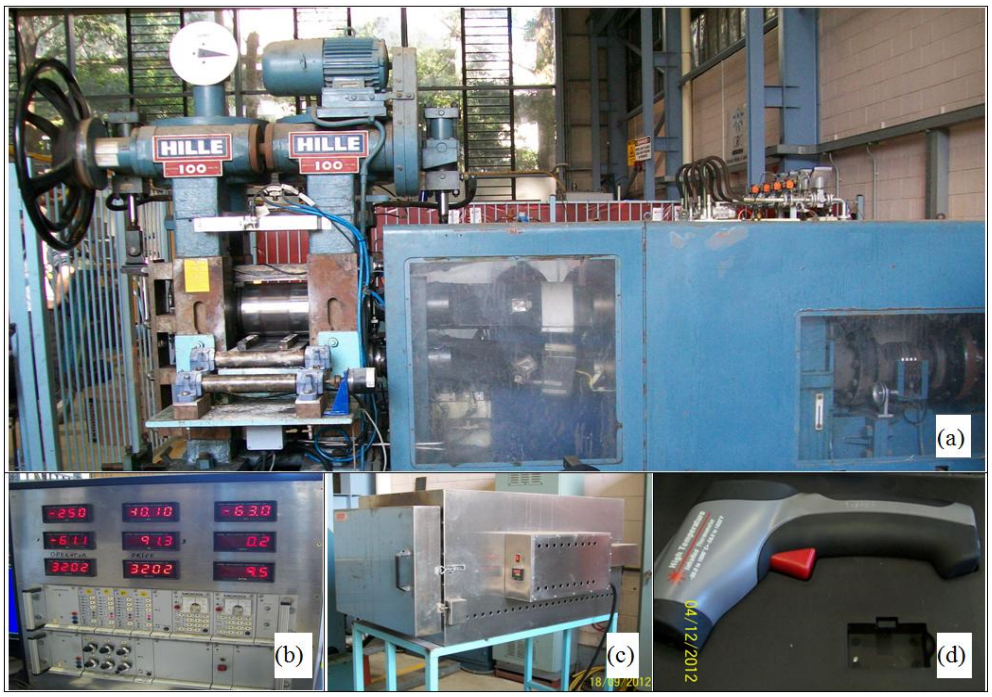

Fig. 4.1 (a) A Hille 100 rolling mill, (b) the control equipment of the Hille 100 rolling mill, (c) Muffle furnace, and (d) an infrared thermometer

The average temperature readings of the samples were slightly above 150 ^{o}C, as shown in Table 4.1. That means the temperature dropped by almost 50 ^{o}C from the time the furnace was opened and the samples were removed.

The main failure of the ARB process was edge cracks on both sides of the sample at high reduction. Reducing the rolling speed to 1 rpm can reduce edge cracks [143]. Edge cracks can be prevented by gradually reducing the thickness, as had been done in 1100 Aluminum material. This was done via tandem rolling, for a total reduction in thickness of 75 %, from 4 to 1 mm, in an ARB process with 4 stands rolls, and thickness reductions of 30 , 40 , 25 and 10 % [144].

4.1.3 Rolling of ARB samples of AA1235 for sixth cycles

The planned reduction in thickness of the first cycle of ARB process was 65 %, but adjusting the gap between the two rolls had to be repeated several times. A 62.8 % reduction in thickness in the first cycle and 60.0 % in second was considered to be enough to achieve a good bond. Reducing the thickness in the third, fourth, fifth and sixth cycles was set around 50 to 55 %, in order to reduce wasting material due to edge cracking.

Table 4.2 Data for 6 cycles of ARB process with Hille100 rolling mill

No.	Cycles	Layers	T (^{o}C)	Thickness, t (mm)		t_{red} (%)
				Before roll	After rolled	
1	1	13	137	3.900	1.452	62.76
2	2	26	154	2.905	1.162	60.00
3	3	52	151	2.324	1.116	51.99
4	4	104	155	2.231	1.064	52.30
5	5	208	150	2.129	1.023	51.96
6	6	416	145	2.045	0.942	53.92

4.1.4 Discussion

In the ARB process, if the strip was less than 0.5 mm thick, and a 50 % reduction in thickness was carried out, interface bonding was poor. A comparison of the reduced thickness for various ARB processed materials is shown in Table 4.3. In Table 4.3 the reduction in thickness by the ARB process for a 0.5 mm thick or more material was 50 %. The exceptions are multi-layers of Al (4 layers) and Cu (3 layers) that were stacked together the reduction in thickness was 43 % [74], and a sandwich of Cu/Zn/Al where the reduction in thickness was 57 % [80]. Only one type of material with a thickness of less than 0.5 mm was carried out at 65 % [9, 75] to obtain an adequate bonding.

Table 4.3 Thickness reduction for various materials processed by ARB

No.	Authors	Material	Cycles	t (mm)	t_{red} (%)
1	Saito et al. [68]	AA1100 Al-Mg(5083) IF steel	8 7 5	1 1 1	50
2	Tsuji et al. [70]	AA1100 & Ti-added IF steel	6	1	50
3	Huang et al. [76]	AA1100	8	1	50
4	Krallics & Lenard [71]	Low C steel (C=0.002 %)	5	2.5	50
5	Li et al. [67]	AA1100 Cu* 36 % Ni austenitic steel IF steel	6 6 6 6	1 1 1 1	50
6	Pirgazi et al. [77]	AA1100	10	0.5	50
7	Kwan et al. [57]	AA1100	8	1	50
8	Eizadjou et al. [74]	Multi-layers: AA1100 Cu	5 5	0.5 0.1	43#
9	Eizadjou et al. [74]	Pure Al	8	1	50
10	Tamimi et al. [69]	IF steel	10	2	50
11	Kwan and Wang [79]	Copper	7	1	50
12	Rezaei et al. [56]	AA6061	5	1	50
13	Bazzaz et al. [72]	AA1100	8	1	50
14	Roy et al. [59]	AA2219/AA5086	8	0.5	50
15	Mahdavian et al. [80]	Sandwich-Cu/Zn/Al	14	0.9/0.8/0.3	57
16	Milner [81]	Pure Ti (CP-Ti ASTM grd 2)	7	0.5	50
17	Su et al. [78]	AA1050/AA6061 composite	2	1.5	50
18	Su et al. [60]	AA1050/AA6061 composite	5	1.5	50
19	Hadi et al. [9]	AA1235	4	0.3	65
20	Hadi et al. [75]	AA1235	4	0.3	65
21	Utsunomiya et al. [144]	AA1100	4	4	75$
22	Lee et al. [142]	AA6061	8	1	50

Note:

*Oxide free high conductivity (OFHC) Cu.

#Thickness of multi-layered of 4 Al & 3 Cu layers with total thickness of 2.3 was reduced to 1 mm.

$ Using a tandem rolling by using 4 pairs of rolls stand.

Table 4.1 and Table 4.2 show that for AA1235 material (0.3 mm thick) processed by ARB, a 62 to 65 % reduction in thickness was enough for bonding. After a few cycles of the ARB process were carried out, an ultra-fine grain structured (sub-micron) material was formed and strengthened significantly [68].

With adequate bonding, the ARB can be produced by laminating various types of materials. The terms ‘multi-layers’, ‘composites’, ‘sandwich’, or ‘foils’ are already used for laminated materials processed by ARB, and have been achieved using, AA1100/Cu materials [74], AA2219/AA5086 [59], Cu/Zn/Al [80], AA1050/AA6061 [60, ‘79], Al/Ti [145], Al/Al_2O_3/TiC [146], Ti/Al/Nb [147], Al-4 wt.% Al_2O_3/B_4C [148], Al-SiC [149], Al-B_4C [150], Al/Ni/Cu [151], and Mg/Al [152]. Numerous laminated materials can be designed for specific purposes with a combination of different material properties. For example, a laminated material can be designed with an outer layer that is resistant to corrosion while the internal layers are fairly resilient, as long as adequate interface bonding is achieved.

Bonding tests have been carried out on laminated AA1200/AA3103 [153] by tensile testing the bond. This method is limited by the strength of the glue used. The glue can be used up to 40 MPa to investigate the bond strength of the ARB process to laminate materials from AA1200/AA3103 [153]. Roughing the interface can also be done by sand blasting, as was done on the sandwich Al/Cu composite (AA1100/Cu11000) [154].

It has been observed that in an ARB process of composite materials Cu/Ag, reductions of 33 and 48 % produced a low quality bonding, unlike when the thickness was reduced by more than 50 %, which had high quality bonding. This was carried out at values of 56, 57 and 62 % respectively [155].

Composite Al/Ni was produced through ARB using AA1060 and commercial Ni. In this process, necking and fractures occurred in the layer of nickel when the ARB cycles were increased. After six cycles of ARB, the layers of nickel in composite

Al/Ni were fragmented and distributed homogeneously in an aluminum matrix because Ni has a 3 % lower elongation than Al [156].

Sheets from an asymmetric accumulative roll bonding process showed that the inter-diffusion layer was thicker in the Al/Ti interface than similar materials processed by the ARB symmetrical method. This difference was more than 15 % [157].

Certain individual layers affect the mechanical properties and microstructure of different metal laminates. An AA1100/AA7075 material with the same thickness, but different individual layers, was successfully created with a hot ARB process [158].

4.1.5 Summary

It was concluded that an approximately 63 % reduction in thickness in the ARB process for 0.3 mm thick AA1235 material was enough to obtain bonding. Of course, all the interfaces had been brushed, cleaned with Acetone, and the sample had been pre-heated at 200 ^{o}C for 10 minutes. Edge cracks can be reduced by slowing the speed of the rolls in the rolling mill.

An ARB process can produce a variety of laminates, depending on the properties of the respective layers, i.e., layers with similar properties that are bonded can be manufactured into a new laminate with better properties. An ARB process does not depend on differences in the width of the sheets.

4.2 Asymmetric rolling process

4.2.1 Preparation of Asymmetric rolling samples

Asymmetric rolling (AR) involves using a pair of rollers with different angular velocity [84, 85]. This difference in the angular velocity can be obtained using a pair of rollers, (i) with different diameters rotating at the same angular speed, or (ii) with the same diameter but rotating at a different angular velocity. A multi-function rolling mill operating with two work rolls of the same size is shown in Fig. 4.2. In this figure, AR was carried out to vary the angular velocity of the top roller, while the angular velocity of the bottom roller was kept constant [84, ‘86].

Fig. 4.2 A multi-function rolling mill

Samples for AR were prepared by cutting an ARB processed sample whose minimum thickness of about 0.4 mm had been achieved on a Hille 100 rolling mill. The micro deep drawing process requires materials that are 300 μm thick, and thinner, and therefore further rolling with a special rolling mill, as shown in Fig. 4.2, is required.

4.2.2 Asymmetric rolling related to speed ratio

The speed ratio between a pair of rolls in a rolling mill can be controlled by a programmable logic controller (PLC) that has been assembled at the rolling mill. Given the difference in speeds between the two rolls, AR can produce a constant shear zone between the two neutral planes in the contact zone [85, '87, '88]. In conventional rolling (symmetric) there are only two slip zones in the friction force distribution, the forward slip zone and the backward slip zone, as shown in Fig. 4.3 [85] [159]. The speed ratios used were 1.1:1, 1.2:1, 1.3:1, and 1.4:1.

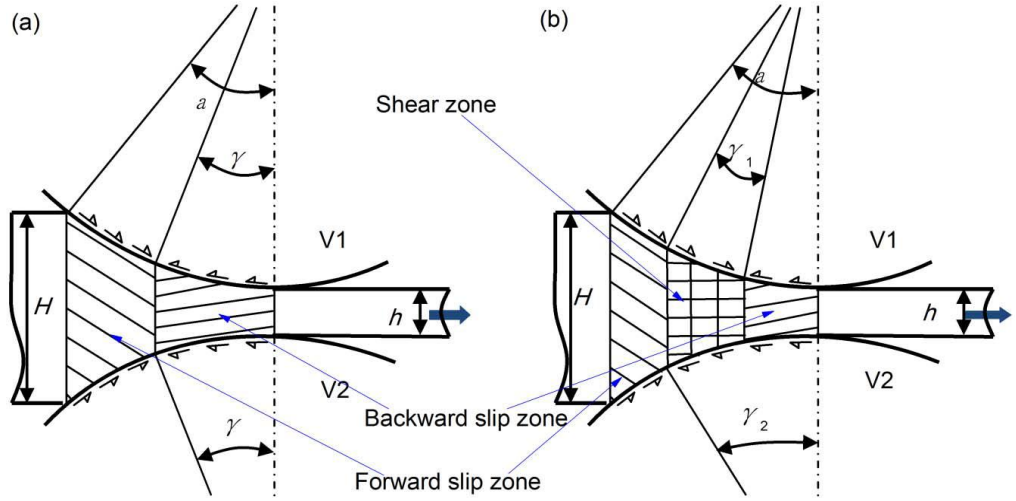

Fig. 4.3 A shear zone between the slip zones of a friction force distribution between the two rollers, (a) symmetric rolling, and (b) asymmetric rolling [85]

4.2.3 Asymmetric rolling of AA1235

A speed ratio of 1.3:1 was used for the AR process for AA1235 material, while other speed ratios were also used for the same material. The AR process could repair the surface of the material from the ARB process, by taking it from a state of having micro cracks on both surfaces into a smooth surface without micro-cracking, as shown in Fig. 4.4.

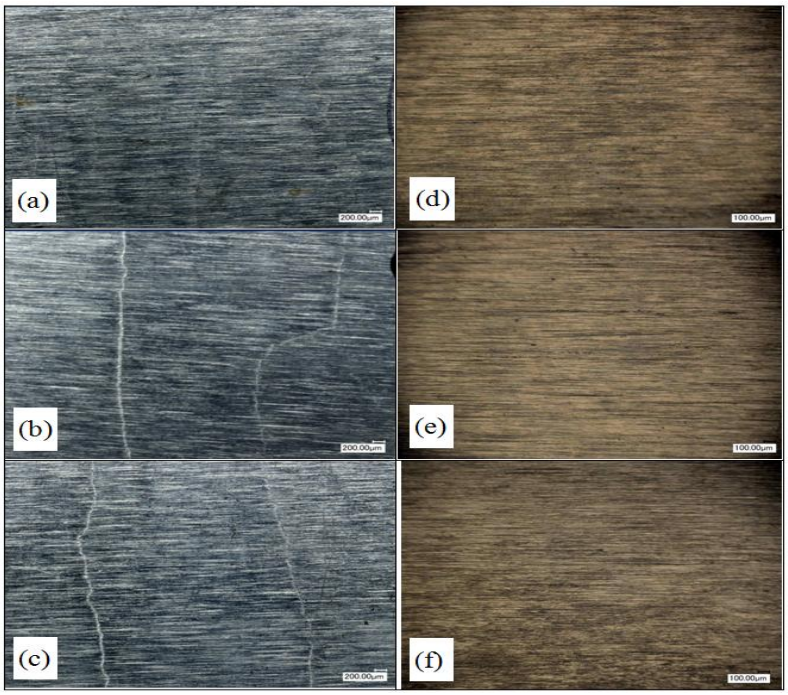

Fig. 4.4 A surface quality difference between the results of ARB and AR processes: (a) ARB1c, (b) ARB2c, (c) ARB3c, (d) AR1c, (e) AR2c, and (f) AR3c

A tensile test of the AR processed AA1235 material was carried out to determine the true stress/strain for a speed ratio of 1.2:1, as shown in Fig. 4.5.

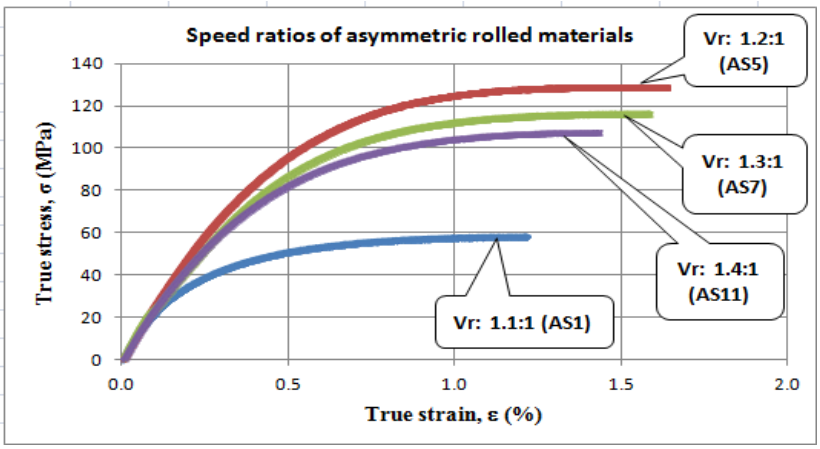

Fig. 4.5 Tensile tests of AA1235 material of asymmetric rolling results

4.2.3.1 Effect of AR on anisotropy values

The anisotropy values of AA1235 processed by ARB (4 cycles) and AR (1 cycle) were 0.42 for normal anisotropy (R_{avg}) and -0.04 for planar anisotropy (ΔR). These

values were better than those obtained for the AA1235 material from the ARB process before asymmetric rolling, which were 0.595 for normal anisotropy and 0.28 for planar anisotropy.

The best homogeneous state was obtained in AR when the sample of IF steel materials were rotated 180^{o} between cycles [86]. Experiments were also carried out for the same material using an idle roll, which improved the anisotropy if the sheet was rotated 180^{o} to the rolling direction between the cycles of AR [89]. An AR process carried out on the IF steel resulted in anisotropy values that were better than symmetric rolling [92].

4.2.3.2 Effect of speed ratio on grain size

The speed ratio affected the grain size of AA1235 material from the AR process performed on an ARB processed sheet consisting of 72 layers after 4 cycles. The EBSD results in Fig. 3.24 and Fig. 3.25 in Chapter 3 showed that an average grain size of 1.655 μm was produced with a speed ratio of 1.3:1 and a grain size of 1.633 μm for the speed ratio of 1.4:1 after 4 cycles of ARB.

The grain size from AR was smaller than the symmetric rolling results for AA1235. A grain size of 1.745 μm was obtained from EBSD for AA1235, as shown in Fig. 3.25. Similar findings were also indicated in reference [94] that the grain size for symmetric rolling of pure Mg (99.9 %) was higher than the results of AR. The best way to produce a metallic sheet is to use a certain speed ratio to obtain a uniform and severe plastic deformation. The use of a non-driven, 250 mm diameter upper roll, and a 500 mm diameter lower roll revolving at 1 rad/s was recommended because the total torque was minimal compared to 5 other cases [160].

4.2.3.3 Effect of thickness reduction on grain size of ARB and AR results

For AA1235 material, an initial thickness of 3.9 mm will be reduced by 72.7 % to 1.064 mm after four cycles of ARB (Table 4.4). The corresponding grain size of 25.09 µm before ARB became 1.744 µm after the fourth cycle, which was 14.39 times smaller. While the material thickness of the ARB after the fourth cycle was 1.064 mm, and after two cycles of rolling through the AR process with a total reduction in thickness of 99.6 % (Table 4.4), the grain size decreased from 1.744 µm (Table 3.8, in Chapter 3) to 0.550 µm. This means that the grain size of the material was about 3 times smaller (3.17). So grain refinement can be done more with ARB when the grain size is large, but refinement is smaller with small grains through the AR process. When the grain size of the ARB process in the second and fourth cycles, which were 1.758 µm and 1.744 µm respectively (Table 3.8) were compared, the diameter of grains had only reduced by 0.796 %. This means that the rate of grain refinement for the ARB and AR processes for AA1235 material was not linear and was becoming smaller for smaller grains. A comparison of the results of this grain size reduction is shown in Table 4.4.

Table 4.4 A comparison of the results of the grain size reduction between ARB4c and ARB4c+AR2c

Process	t (mm)	d (µm)	$t_{red.}$ (%)	$d_{red.\ from\ initial}$	$d_{red.\ from\ ARB4c}$
AA1235 initial	3.900	25.090			
ARB2c	1.116	1.758	71.38		
ARB4c	1.064	1.744	72.72	**14.39**	
ARB4c+AR2c	0.014	0.550	99.64		**3.17**

Note: $t_{red.}$: thickness reduction, and $d_{red.}$: grain size reduction.

4.2.4 TEM for asymmetric rolling

The average grain size from the annealed condition was 25.09 μm, but this was reduced to 0.550 μm after 6 cycles of ARB and 2 cycles of AR; the grain size decreased more than 45 times.

Fig. 4.6 shows the microstructure of a sample obtained by TEM. Fig. 4.6 (a) shows the as-received material with the microstructure in the form of coarse grains. After the sixth cycle of ARB, followed by an AR process, the grains were refined and rolled with a laminate structure, as shown in Fig. 4.6 (b). After further rolling, the layers of the laminate started to bond and merge together, as shown in Fig. 4.6 (c). Fig. 4.6 (e) shows a local zone of Fig.4.6 (c). In the image, the merging of four layers into a larger grain is clearly visible, although there are some cavities in the local zone in Fig. 4.6 (c). The nano-voids can initiate cracks in a material, and can coalesce into two or more voids. If these coalescing voids propagate, then eventually the material becomes torn and destroyed. It has been stated that material with a low ductility can cause faster crack propagation when the loading is perpendicular to the common axis of the voids [161]. With further rolling, the grain structure of the laminate turned into finer equi-axed grains, with an average grain size of 550 nm, as shown in Fig. 4.6 (d). It is an interesting phenomenon that the microstructure along RD was equi-axed, which may result in both increased ductility and strength during the AR process [134].

There was no evidence that elongated grains appeared in the rolled sample (either in a state of AR and SR) after a large number of cycles in silver materials [162]. The grain size of the silver material was between 200 and 300 nm when processed by ECAP, SR, and AR [162].

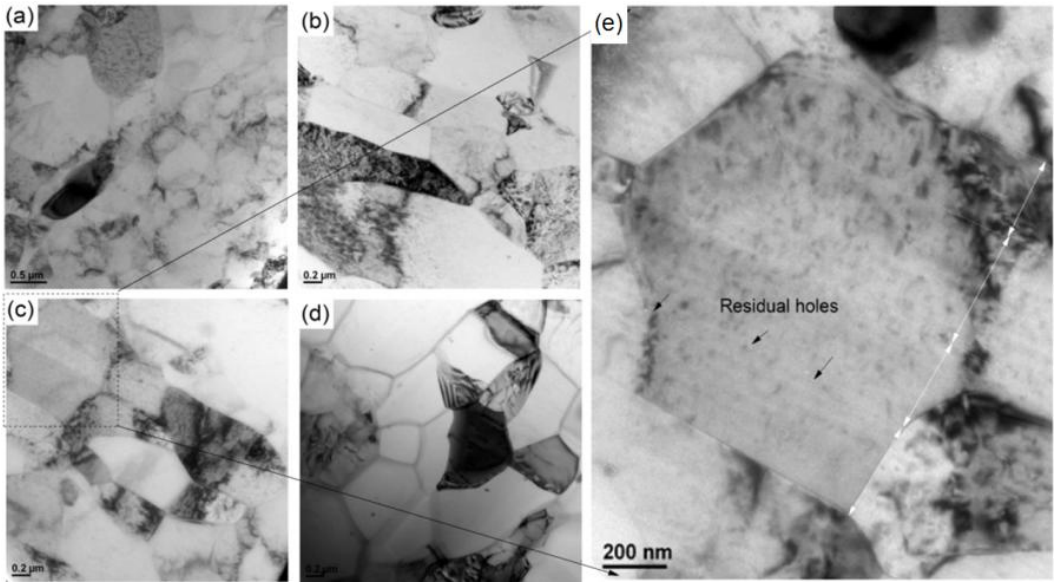

Fig. 4.6 TEM micro-structure of AA1235 samples: (a) the as-received material, (b) after the first cycle of AR, (c) after the second cycle of AR, (d) after the third cycle of AR, and (e) local zone in Fig. 4.6 (c) [135]

4.2.5 Discussion

An AR process can improve the surface quality of material produced by the ARB process. Initially the surface showed a micro crack, but after AR the surface became smooth and free of micro-cracks. Different speed ratios affected the tensile strength, strain, and grain diameter of AA1235 material. Fig. 4.5 shows the result of an AR process on AA1235 material with a 1.2:1 speed ratio and indicates the highest true strain and true stress, but the smallest grain was obtained with a speed ratio of 1.4:1, so the higher speed ratio in an AR did not always produce a high flow stress. This still requires further study.

A shear zone in the roll bite can smooth a surface and refine the grain, but reversing the direction of rolling between cycles of AR can turn the material into an almost homogeneous state.

The total reduction in thickness achieved while rolling some materials is shown in Table 4.5. The highest reduction in thickness of 99.9 in a rolling process, was achieved by the AA1235 material [135], followed by the AA1100 material [76] and

IF steel [68]. A reduction in thickness of almost 100 % indicates that an ultra-thin thickness without tears or damage can be achieved by thinning through ARB and AR rolling processes. A comparison of the material thickness before and after the rolling was carried out, and is shown in Fig. 4.7. The initial thickness of IF steel materials [68] reached 2 m, and the initial thickness of AA1100 [76] was more than 0.5 m.

Table 4.5 Total reduction of the material thickness by a rolling process

No.	Material	Process	$t_{initial}$ (mm)	Number of layers	Total thickness (mm)		$t_{red./cycle}$ (%)	Total $t_{red.}$ (%)	Remarks
					Initial	Final			
1	AA1235 [136]	ARB4c+AR2c*	0.3	416	124.8	0.014	52-62	**99.99**	* started by 13 layers
2	AA1100 [68]	ARB8c	1	256	256	0.5	50	99.80	
	Al-Mg(5083) [68]	ARB7c	1	128	128	0.5	50	99.61	
	IF steel [68]	ARB5c	1	32	32	0.5	50	98.44	
3	Low carbon steel [71]	ARB5c	2.5	32	80	1.25	50	98.44	
4	AA1100 [77]	ARB10c	0.5	1024	512	0.25	50	**99.95**	
5	IF steel [69]	ARB10c	2	1024	2048	1	50	**99.95**	
6	AA1050/AA6061 [79]	ARB2c	1.5	4	6	0.75	50	87.50	Composite
7	AA1235	ARB4c#	0.3	72	21.6	0.3	65	98.61	# started by 9 layers
8	IF steel [87]	AR6c	5.6	1	5.6	1.9	20-75	66.07	
9	Ti grade-2 [87]	AR15c+SyR4c	9	1	9	0.3	83 &80	96.67	AR by 83% and SyR by 80%
10	AA1050-AA6061 [85]	ARB1c+AR4c	1.5	2	3	0.04	43-95	98.67	
11	DSS 2205	AR7c	40	1	40	28	70	30.00	
12	IF steel [92]	SyR2c+AR3c +ARr2c	25.4	1	25.4	2	30-88	92.13	
13	Steel S355J2G3 [96]	AR5c	50	1	50	14	-	72.00	
14	6xxx [98]	SC+AR	6	1	6	2	30	66.67	
15	IF steel [90]	SyR6c-AR6c	16.67	1	16.67	2	88	88.00	

Note: AA: Aluminium alloy, ARB: accumulative roll bonding, c: cycle, IF: interstitial-free, AR: asymmetric rolling, SyR: symmetric rolling, SC: strip casting, m: monotonic (ARm: Asymmetric rolling monotonic), and r: reversal (180^o changed direction of rolling) (ARr: Asymmetric rolling reversal).

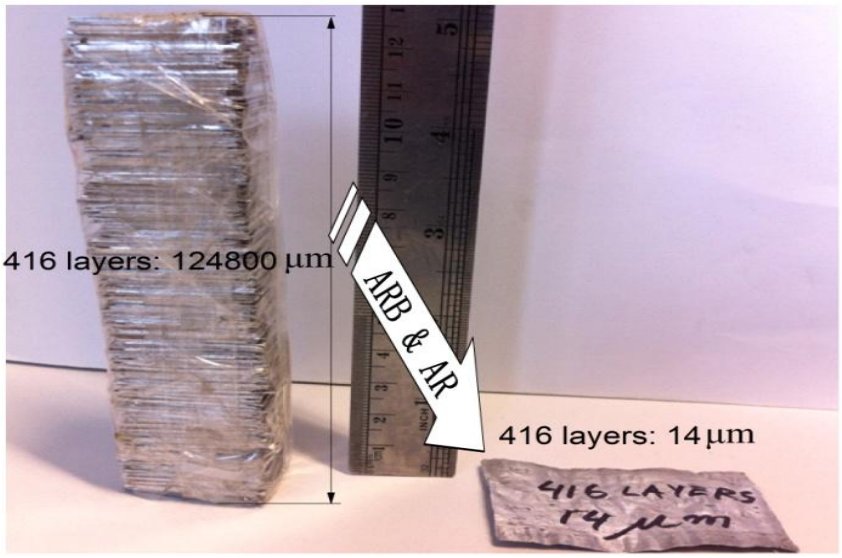

Fig. 4.7 A thickness comparison of 416 layers for AA1235 before and after rolling [135]

Table 4.5 shows the highest reduction in thickness of 99.99 % was achieved on AA1235 material after the material experienced four ARB process cycles followed by two cycles of AR, as shown in Fig. 4.7.

TEM observations have shown an average grain diameter of 0.550 µm for AA1235. This was 45 times smaller than the original size of the annealed condition after the material was processed through two types of rolling, 6 cycles of ARB and 2 cycles of AR. Cracks in the material could be initiated at the nano-voids.

4.2.6 Summary

Asymmetric rolling can improve the surface quality of material produced by ARB. Different speed ratios of asymmetric rolling (AR) affected the tensile strength, strain, and grain diameter on AA1235 material. The presence of a constant shear zone in AR can smooth the surface and refine the grain of a material. Reversing the direction of the sample between rolling cycles of AR can produce a more

homogeneous state. The rate of reduction of the grain diameter for the AA1235 material after ARB and AR processes slowed down considerably at fine grains.

The total reduction in thickness of AA1235 material in the ARB and AR rolling process was higher than the others.

Chapter 5 The deep drawing process

Deep drawing is a sheet metal forming process where a circular blank is drawn radially into a cup through a forming die with a punch force. This can also be achieved by redrawing the cup through a series of dies. The flange is the area where the sheet metal experiences a radial drawing stress and a compressive hoop stress. Hoop stresses can lead to wrinkles in the flange area if it is not held by a blank holder. A blank holder facilitates the flow of materials into the die radius.

The main components of deep drawing equipment that impress the blank material are a die, a punch, and a blank holder. A press tool was designed, manufactured and adapted to the operations of an Instron tensile-compression testing machine to directly record the force applied and the punch stroke.

5.1 Blanking a circular blank with a press tool

To obtain a circular blank of a certain size, a blanking punch and die block should be made. The blank allowed for pairs of 14, 15, and 16 mm several blanking punches and die blocks to be made. A press tool was specifically designed to for blanking and deep drawing processes. With a pair of blanking punches and die blocks for a particular diameter, the main shaft was equipped with a locking bolt to hold the blanking punch in place and a die block was placed on the base of a press tool.

Some results of this chapter have already been published:
Hadi, S., Tieu, A. K., Lu, C., Su, L.H., Yu, H.L, *Grain refinement in the formability of Aluminium thin cup.* Materials Science Forum, 2013. 773-774: p. **166-175**.
Hadi, S., Tieu, K., Lu, C., Yu, H.L., Caesarendra, W., Kusmoko, A., *The effect of bulged punch on wrinkles reduction in micro deep drawing.* Journal of Materials Processing Technology, 2014, **submitted**.

If a blank is to be cut, the blanking punch and die blocks are placed into a press tool, a blank sheet of material is placed on top of the die block, which is then given a compression force by the cross head of the Instron machine to form a circular blank.

The cutting edge of a blanking punch must be kept sharp and clean to produce a good blank. A punch and die suited for a particular thickness was mounted on a press tool to form a cup by deep drawing, as shown in Fig. 5.1. Data from the punch force and stroke are directly recorded by the Instron machine.

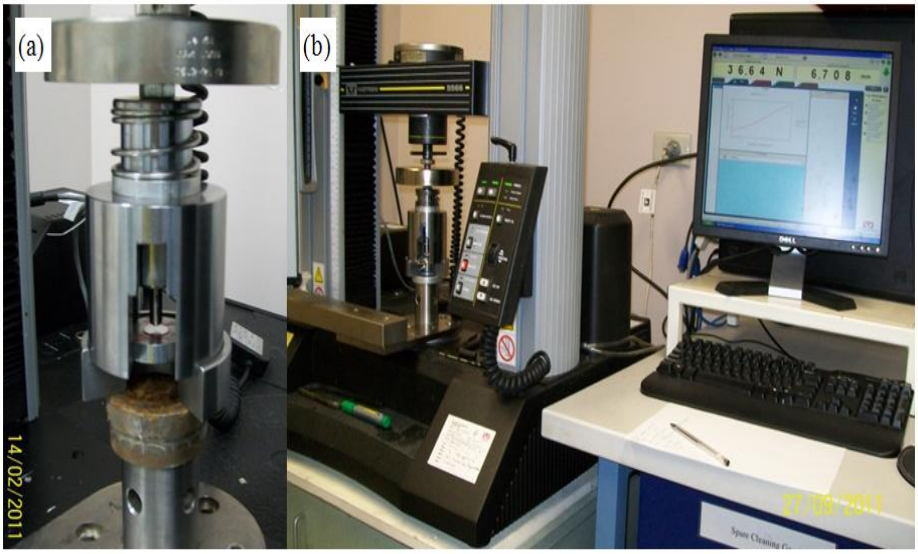

Fig. 5.1 A set of press tool: (a) a press tool for blanking and deep drawing processes, and (b) a press tool mounted on an Instron testing machine

5.2 Measuring the coefficient of friction

The friction force on the cup flange was considered in relation to the concept of open/closed lubricant pocket (O/CLP). Data from the friction force and the normal force were obtained for annealed AA1235 material. The friction shear strength formula used is given by [163]:

$$\tau = f\,\alpha_{RC}\,k \qquad (5.1)$$

where τ is the friction shear strength, f is the friction factor, α_{RC} is the real contact area fraction, and k is the yield stress.

The coefficient of friction (μ) was obtained by a strip drawing test [164] on the AA1235 material. In the strip drawing test the friction force (F) and normal force (N) on two contact areas on a sheet moving at a certain velocity were measured. The coefficient of friction was then calculated using the formula [164] [165]:

$$\mu=F/(2N) \tag{5.2}$$

where F is the friction force and N is the normal force.

A μ was obtained by a strip drawing test, as shown in Fig. 5.2, and the results are shown in Fig. 5.3. If a lubricant is trapped in pockets formed between the blank and the tool then a fraction of the normal force is transferred by the fluid pressure created by the lubricant [166]. So with a lubricant, the magnitude of the friction force will be reduced because a certain portion of normal force is supported by the lubricant.

The strip drawing test specimen was 10 mm wide x 100 mm long, while the contact area of the grips 14 x 14 mm. The effective displacement was 50 mm on an Instron 5566 tensile testing machine, as shown in Fig. 5.2. That part of the material in contact with the sheet was the same as that used for the die and the blank holder when drawing the cup. These materials were flame hardened to 762 VHN.

Fig. 5.2 Purpose designed equipment for strip drawing test on an Instron 5566 tensile testing machine

The calculation of μ on the flange was based on the lubricated contact between the blank and the tools, with the tool surfaces being the top surface of the die and the lower surface of the blank holder before the punch stroke begins to press a blank. The blank was AA1235 in the FA condition with a thickness of 300 μm.

A plot of the μ results is shown in Fig. 5.3. The average μ was 0.23 which was close to the 0.2 value used in the simulation in Chapter 6.

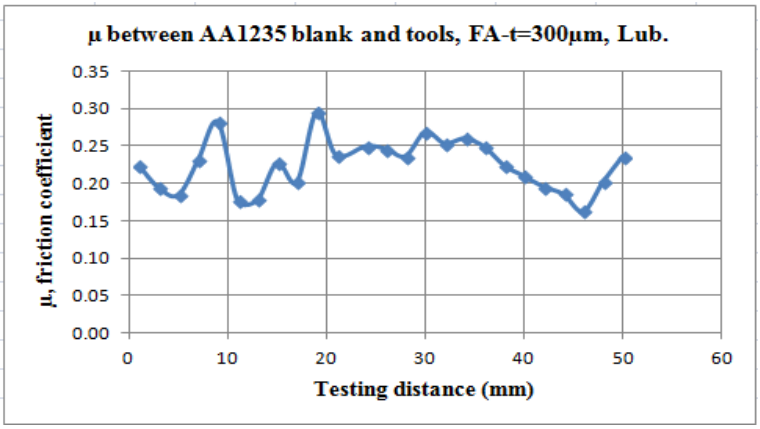

Fig. 5.3 A μ results for AA1235 sheet of FA condition, t = 300 μm, lubricated on both surfaces

5.3 Deep drawing of as received AA1235 material

The discrepancies of the rolling process and heat treatment on the raw materials of the blank can lead to differences in cup formability during deep drawing. As received AA1235 (As-R) material cannot be processed in deep drawing because it contains residual stress from the rolling process carried out at an earlier stage. The depth that could be achieved for the 14 mm diameter by 300 μm thick blank was about 2.1 mm or about 45 % of the full stroke of 4.7 mm. If the cup was drawn any further, it would tear at the corner, as shown in Fig. 5.4.

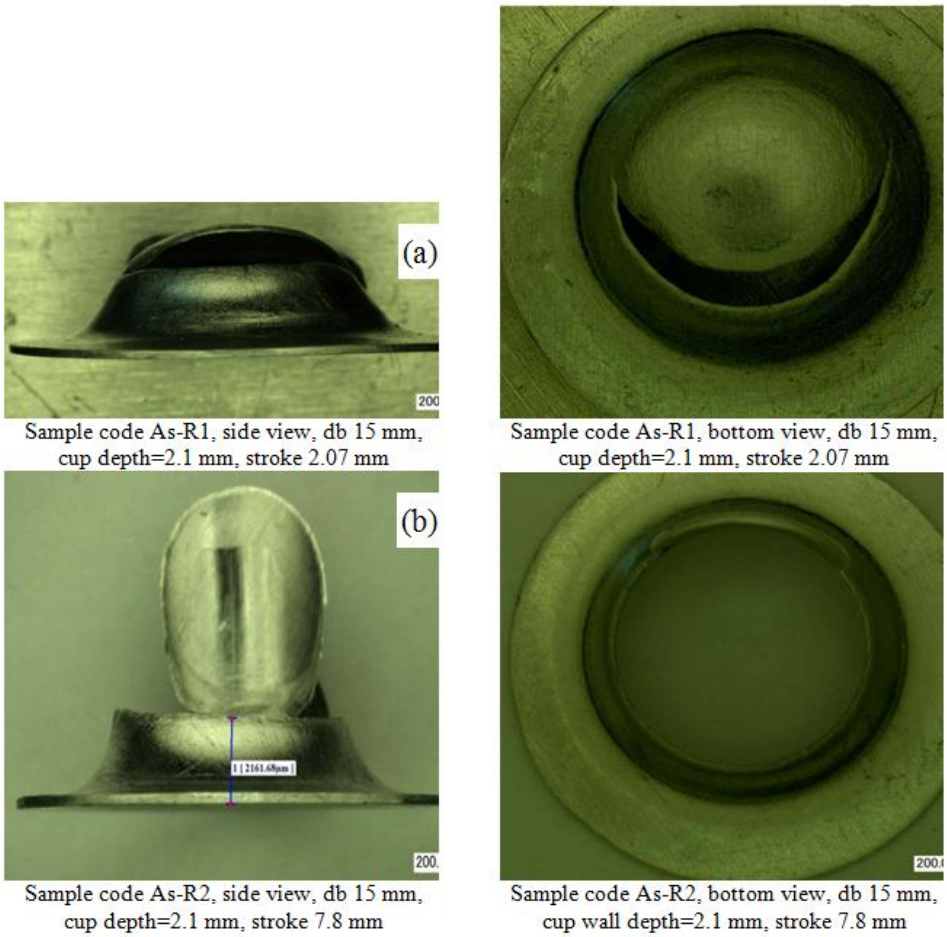

Fig. 5.4 Cup of an As-received of AA1235: (a) cup torn on a corner radius if the punch stroke is stopped, and (b) the bottom part of the cup torn continues to turn to the wall if the punch stroke is continued to full stroke

5.4 Drawing a cup from fully annealed material

For AA1235 material 300 µm thick in the FA condition at 450 ^{o}C for 4 hours, a good cup can be produced from a 14 mm diameter blank, but not from a 15 mm diameter blank. The LDR of the cup drawn from a 14 mm diameter blank was 1.87, with a punch force of 520 N and a punch stroke of 6 mm, as shown in Fig. 5.5 (a). Earing with four peak shapes formed on a cup from a 14 mm diameter blank. The depth of a cup drawn from a 15 mm diameter blank was about 1.6 mm, as shown in Fig. 5.5 (b).

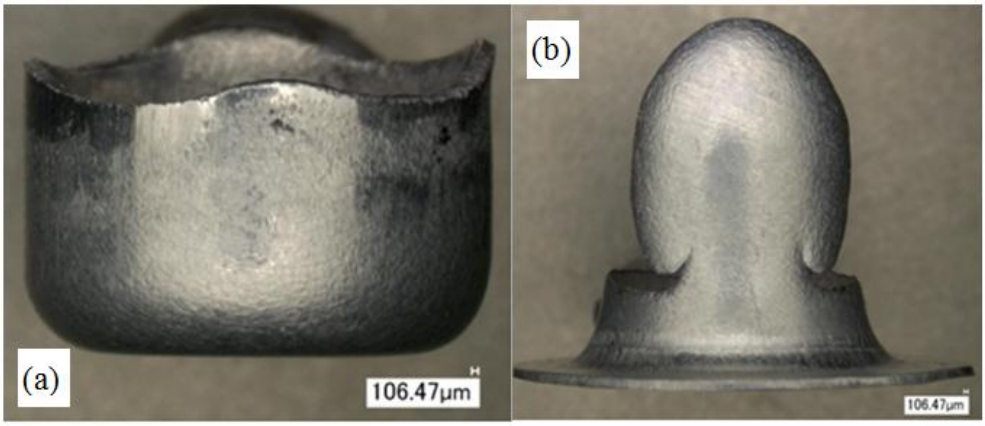

Fig. 5.5 Cups were obtained from AA1235 in FA condition: (a) a successful cup without any wrinkles to blank diameter of 14 mm and LDR 1.87 and (b) a failed cup to blank diameter of 15 mm [75]

5.5 Cup drawing of four cycles ARB material

For AA1235 material processed through 4 cycles of ARB, only 2.0 mm depth or 40 % of the full stroke could be achieved in deep drawing before failure, as shown in Fig. 5.6.

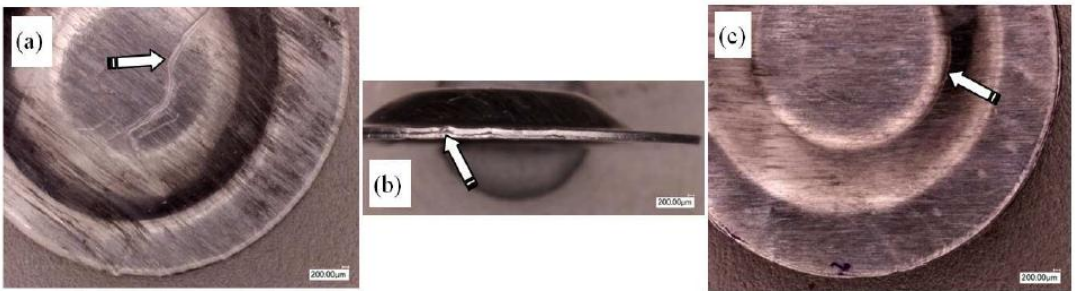

Fig. 5.6 Results of cup drawing from the ARB process materials: (a) crack in the outer layer is observed to occur at the cup bottom, (b) delaminating on the cup thickness in side view, and (c) the initial crack started from the cup corner [9]

The material processed from 4 cycles of ARB had 72 layers, and there were cracks in a few layers at the bottom of the cup which then spread to all the layers when the punch stroke was continued, as shown in Fig. 5.6 (a) and (c). The delaminating between the layers seen in Fig. 5.6 (b) can be attributed to residual stresses.

5.6 Drawing a cup from material after four cycles ARB and stress relieving

When AA1235 material processed by 4 cycles ARB was stress relieved at 200^{o}C for 8 hours, it could be drawn into a cup without any wrinkles and few earing from 14 and 15 mm diameter blanks, as shown in Fig. 5.7 [75]. The blanks used in the deep drawing were 340 μm thick at 1020 N punch force and a punch stroke of 12 mm.

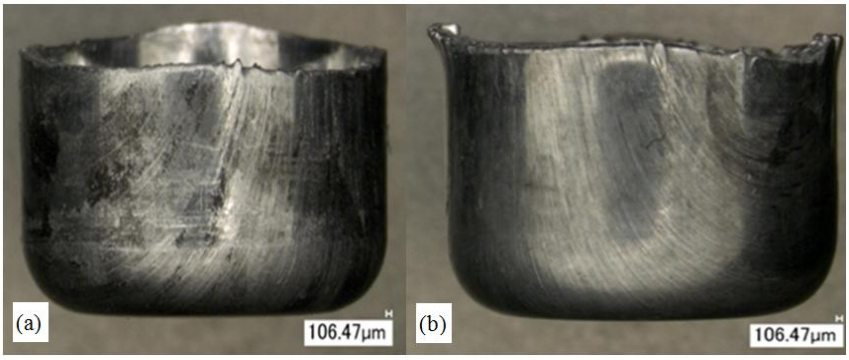

Fig. 5.7 Successful cups without wrinkles and lower earing in AA1235 material processed by 4 cycles ARB followed by stress relieving at 200 ^{o}C for 8 h: (a) DB =14 mm at 1.87 LDR, and (b) DB=15 mm with LDR 2.003 [75]

5.7 Cup drawing of ARB sixth cycles material

A blank (338 μm thick and 14 mm diameter) that resulted from 6 cycles of ARB can be formed into a cup with few wrinkles, is shown in Fig. 5.8 (b), but a blank from 4 cycles of ARB failed to produce a cup because it only reached a depth of about 2.0 mm. This means the blank processed by 6 cycles of ARB had better formability than the blank processed from 4 cycles of ARB. This was surprising because more ARB cycles normally produce material with a lower elongation.

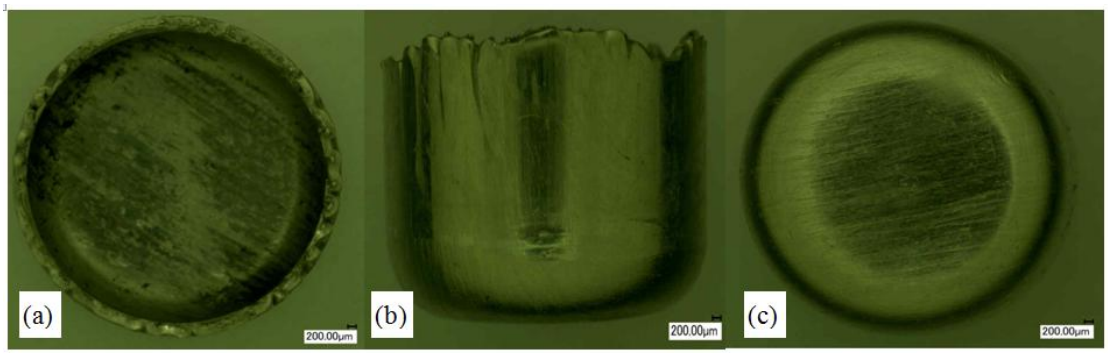

Fig. 5.8 A cup is formed of AA1235 material of an ARB process results in 6 cycles with blank thickness of 338 µm and diameter of 14 mm, code: R2, views of: (a) top, (b) side, and (c) bottom

5.8 Cup drawing of 6 cycles of ARB and 1 cycle of AR processes and SR

A cup was formed by deep drawing materials processed by 6 cycles of ARB followed by one cycle of AR, and then stress relieved (SR). The relevant parameters are a clearance of 0.114 mm, blank diameter/thickness 14 mm/303 µm, die/punch diameters 8.26/7.54 mm. For 14 mm diameter by 303 µm thick blank, the cup had wrinkles on the edge, as shown in Fig. 5.9.

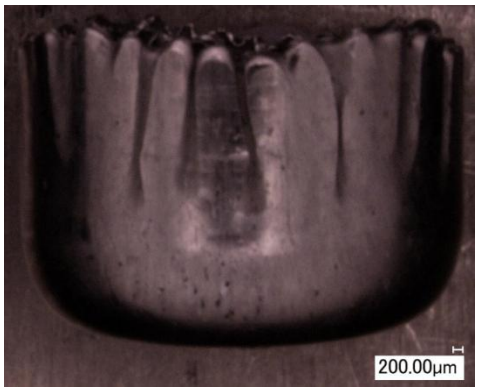

Fig. 5.9 Cup manufactured with the material processed by 6 cycles ARB followed by one cycle of AR and SR at 200^{o}C for 8 h, code: J3G

A free clearance of 0.114 mm between a pair of die and punch diameters is likely to produce a cup with wrinkles, but as long as the strength and ductility of a material is adequate for deep drawing then a minimum clearance is needed to produce a good

cup and reduce the wrinkles. The clearance relative to the thickness of the blank was (0.114)/0.303= 38 %. This was higher than for the case in [65] where a clearance of 15 % of the thickness produced a high LDR value.

Some micro cups with ARB and AR resulted from 45 μm (416 layers) thick blanks were produced, as shown in Fig. 5.10. The blank materials processed by ARB and AR show some earing, some wrinkles, but no tearing; this indicated that material that has not been stress relieved has a high ductility.

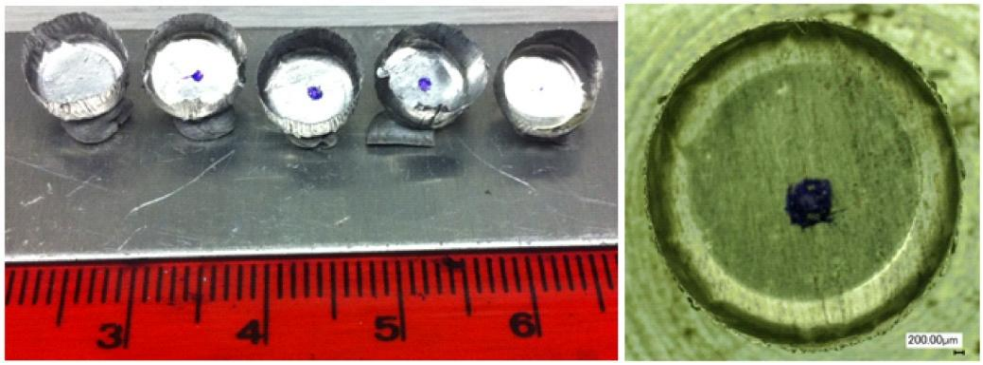

Fig. 5.10 Micro cups with blank thickness of 45 μm which has 416 layers after ARB of 6 cycles and the AR of 2 cycles

5.9 Progress of various conditions of AA1235 material for cup production

The progress of various conditions of the rolling process and heat treatment of AA1235 blank material for cup drawing is shown in Table 5.1.

The residual stresses that existed in the as-received material can be removed with an FA process at 450 ^{o}C for 4 hours. Under FA condition, the AA1235 material can be processed in deep drawing without a tear or wrinkles but earing still appeared along the edge of the cup. In a deep drawing, a die with a 1.2 mm corner radius was used previously and the resulting cup was always torn, but with a 2.0 mm corner radius a good cup was formed from 14 and 15 mm diameter blanks.

Table 5.1 Progress of various conditions of the rolling process and heat treatment of AA1235 blank material for cup production

No.	Process/heat treatment	Code	db (mm)	tb (µm)	LDR	Wrinkles	Torn	Earing	TS (MPa)	ε (%)	Grain size (µm)	Remarks
1	As-received	As-R	14	300	-	-	Yes	-	129	3	-	Depth =2.2mm
2	Full annealed 450°C-4h	R3	14	300	1.87	No	No	Yes	74.2	24	40.9	
		FA	15	300	2.003	No	No	Yes	74.2	24	40.9	rd=2.0mm
		FA3	15	300	2.003	No	No	Yes	74.2	24	40.9	rd=2.0mm, circular grid
3	ARB4c-SR175°C-8h	H1-H3	15	284	2.003	Yes	No	Low	33	0.5	1.773	rd=2.0mm, 72 layers
4	ARB4c-SR200°C-8h	H52-H53	15	284	2.003	No	No	Very low	37	13	2.146	rd=2.0mm, 72 layers
5	ARB6c-No heat treatment	R2	14	338	1.87	Few-partly	No	Low				rd=1.2mm, 416 layers
6	ARB6c-AR2c	-	14	45	1.87	Many						rd=1.2mm, 416 layers
7	ARB6c-AR1c-SR200°C-8h	3S1	14	141	1.87	Shallow: w_d 522 µm, w_h 1,221 µm	No	Low				Vr: 1.1:1, 416 layers
8	ARB6c-AR1c-SR200°C-8h	2S1	14	144	1.87	Few: w_d 1,775 µm, w_h 1,318 µm	No	Low				Vr: 1.2:1, 416 layers
9	ARB6c-AR1c-SR200°C-8h	1S1	14	147	1.87	Partly: w_d 563 µm, w_h 1,182 µm	No	Low				Vr: 1.3:1, 416 layers
10	ARB6c-AR1c-SR200°C-8h	4S1	14	134	1.87	Uniform: w_d 447 µm, w_h 2,223 µm	No	Low				Vr: 1.4:1, 416 layers

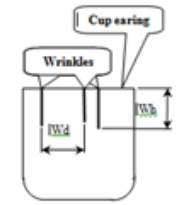

Note: db: blank diameter, tb: blank thickness, LDR: limiting drawing ratio, rd: die radii, ARB4c: ARB 4th cycles, SR: stress relieving, AR1c: asymmetric rolling 1st cycle, w_d: average wrinkles distance w_h: average wrinkles height, and Vr: speed ratio in AR process.

ARB was applied to thin AA1235 blanks for 4 and 6 cycles to produce finer grains and increased strength. They were then deep drawn to test the formability of ARBed materials, particularly with the bonding of multiple interfaces. With the ARB process, a smaller grain size is obtained with an increasing number of ARB cycles but the formability/elongation is reduced with higher strength, partly because of the remaining residual stress due to the ARB cycles. To eliminate residual stress by stress relieving was carried out in an electric furnace at 150, 175, and 200 ^{o}C for 8

hours. These temperatures are below the recrystallisation temperature of AA1235 material.

In an experiment [167], AA7150 material was heated to 480 ^{o}C for 1 hour followed by quenching in water and artificial ageing at 120 ^{o}C for 24 hours. The Vickers hardness measurement showed that the surface hardness was lower than at the centre, regardless of cooling in air or quenching in water. The volume fraction of recrystallised grains was higher in the surface layer than the central layers because the surface layer had experienced more severe deformation than the central layers during rolling. This means that when the material is heated to a temperature of recrystallisation, recrystallisation on the surface layer occurs faster than the central layer because the surface layer stores more energy for recrystallisation [167].

With the ARB process, the grain size was much smaller than the FA condition for AA1235 material, and as a result its strength increased, it became harder, and its formability was reduced. Therefore, an attempt was made to increase formability with a SR process at 150, 175, and 200 ^{o}C for 8 hours.

A cup resulting from blank material after an ARB process with 4 cycles followed by SR at 150 and 175 ^{o}C for 8 hours, and blank/die corner diameters of 14 mm/2 mm indicated a little earing, although the cup was torn when the blank was 15 mm in diameter. However, with a larger die corner radius of 2.0 mm, the blank material from the 4 cycles ARB process followed by SR at 175 ^{o}C produced a cup from a 15 mm diameter blank with low earing, as shown in Fig. 5.11.

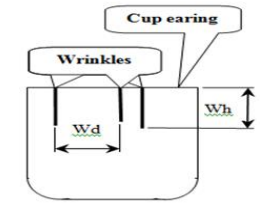

No.	W_d (μm)	No.	W_h (μm)
1	990.13	6	1777.98
2	862.37	7	415.22
3	915.67	8	1394.75
4	947.55	9	1341.64
5	1096.6	10	1192.64
		11	734.69

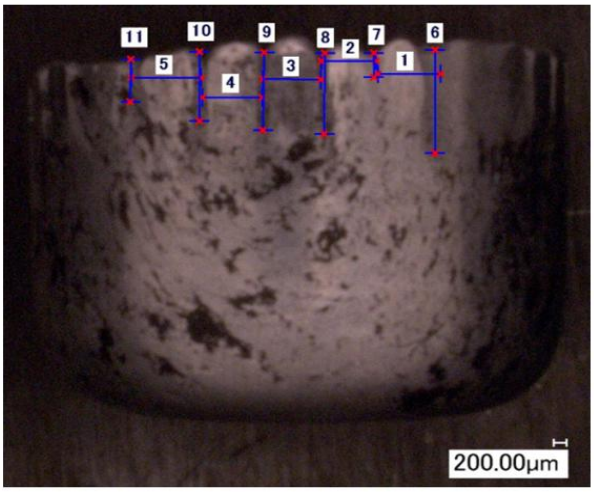

Fig. 5.11 A cup of 15 mm blank material from 4 cycles ARB process followed by SR at 175 ^{o}C for 8 h, case 3 of Table 5.1, code H1

An SR at 200 ^{o}C for 8 hours for blank material from the ARB process with 4 cycles (case 4 of Table 5.1) showed that a cup can be produced from a 14 mm diameter blank. During deep drawing the radius of the die corner was 1.2, as shown in Fig. 5.12.

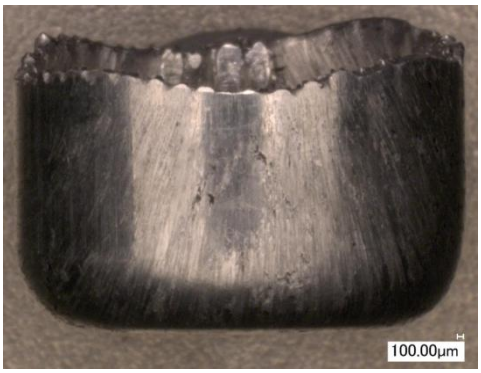

Fig. 5.12 A cup that can be formed from the blank material from the ARB process 4 cycles followed by SR at 200 ^{o}C for 8 h (case 4 of Table 5.1), code H53

Blank material processed by 6 cycles ARB followed by one cycle in AR with speed ratios Vr of 1.1, 1.2, 1.3, and 1.4:1 was drawn into a cup. All of the results (case 7-10 of Table 5.1) showed that wrinkles appeared on the edge of the cup edge

stemmed from the very thin blank material of AA1235. The blanks were between 134 and 147 µm thick.

5.10 Eliminating wrinkles using a bulged punch with 300 µm thick blanks

A normal deep drawing process can produce wrinkles and earing on the edge of the cup. The thinner the blank, the greater the chances are for wrinkles to occur. Various attempts have been made to abolish the wrinkles on the edge of the cup, these vary from reducing the clearance between the punch and the die, to controlling the blank holder pressure (BHP), but this method still left a flange in deep drawing process. Similarly, hydraulic pressure can be applied underneath the blank with a maximum stroke being limited to less than the full punch stroke [168], but the remaining flange must then be cut and discarded. Similarly, earing on the edge of the cup must be removed as waste by a trimming process.

In this thesis a deep drawing process was carried out using two blank holders in two stages. In the first stage the punch stroke was partly carried out using normal/flat blank holder, but in the second stage, a blank holder with the same thickness and a radius similar to the die corner radius was used. These attempts only reduced the occurrence of wrinkles it did not eliminate them all. In general, the blank at the edge of the cup was thicker than the original blank. Some cases of edge thickening are shown in Table 5.2.

A cup is thinner at the radius of the punch corner, and is prone to tear. When the thinning rate of the cup thickness exceeds 25 % [24], a work piece is not expected to form, but in another part of the cup, the flange thickened [24].

From the results of a multi-stage deep drawing process on thin low carbon steel with the initial blank thickness of 0.4 mm, the cup can be torn by excessive thinning [169]. An excessive reduction in thickness between 17 and 41.9 % on 0.4 mm strip produced torn cups. Simulations were used to modify the punch size to obtain a reduced thickness between 6.1 and 18.6 % [169], but a cup will not form if the reduction in thickness is more than 25 % [24].

The results from a finite element analysis showed that local deformation and wrinkling occurred along the major axis due to the non-uniform contact on a non-circular cross section between the blank and the tools [170]. One solution was to modify the size of the tools so the blank can always make contact with the tool by providing more deformation on the minor axis.

Maximum thinning on a two-point incremental forming (TPIF) was 30 %, which was more than a deep drawing process (25 %) [171]. TPIF is a group of asymmetric incremental sheet forming (AISF) that is a sequence of local plastic deformation caused by a simple tool that is controlled by a computerised numerical controlled (CNC) [171] machine. With this method, the thickness reduction of the cup was more than 25 % but the cup did not tear. TPIF is different from the normal deep drawing process.

According to Table 5.2, the percentage of thickening (%) of the edge of the cup in a deep drawing process for the Aluminium group (1000, 5000, and 6000 series) were worth 6.5 [33], 45 and 56 [8], 22 [16], 12 [172], 18.9 [173], 25.7 and 8.7 [Hadi et al.]. Thickening (%) of the edge of the cup for materials other than Aluminium were 36 [23], 5.2, 15, 35.7 [14], 11, 13.2 [27], 38.8 [24], 18 [29], 24 [28], 15 [174], and 10

[175]. Minimum thickening of the edge of the cup was 6.5 % for Aluminum [33] and 5.2 % for other materials [14].

Thickening at the edge of the cup or on the flange was due to the formation of a wrinkle which can be avoided by a smaller clearance, if the blank can withstand bulk deformation in the wall region. However, if the blank cannot withstand the tensile force provided by the punch, then other means must be applied.

Table 5.2 Difference between the blank thickness and the cup edge thickness in a deep drawing process

No.	Authors	Material	Blank thickness (mm)	Blank thickness at cup wall edge (mm)	Thickening (%)	Method applied	Remarks
1	Demirci et al. [33]	AA1050	2	2.13	6.5	BHF of 0.4, 1.5, 2, 4, 5, 7, 10 and 15MPa.	
2	Yoshihara et al. [23]	AZ31	0.5	0.68	36	Constant and variable BHF	
3	Brabie et al. [8]	AA1050	0.05, 0.10	0.078, 0.145	56 45	Simulation by DynaForm software, version 5.7.1	
4	Irthiea et al. [14]	SS304	0.10	0.1150 0.1357 0.1052	15 35.7 5.2	Simulation by Abaqus/Standard and experiment by using polyurethane die, 63 Shore A	RD (0°) DD (45°) TD (90°)
5	Colgan and Monaghan [27]	Mild steel EN10130 FeP01	1	1.132 1.11	13.2 11	Experimental and finite element analysis (FEA)	Experiment FEA predicted
6	Zhang et al. [24]	AZ31	0.8	1.11	38.75	Experiments and numerical simulation	Warm forming 105-170°C
7	Faraji et al. [29]	Brass (Cu63%-Zn37%)	0.6	0.71	18.33	Experiments and simulation by ABAQUS/explicit	
8	Grèze et al. [16]	AA5754	1	1.22	22	Experiments and simulation by Abaqus	25-200°C
9	Sezek et al. [28]	DC05 steel (DIN 10130-99)	1	1.24	24	Using different radius of blank holder (α)	α=0-15°
10	Khandeparkar and Liewald [174]	Low carbon steel (DC04)	0.8	0.92	15	Hydromechanical deep drawing	90° RD
11	Mayavan & Karthikeyan [175]	Deep draw steel	0.8	0.88	10	Experiments and simulation by Abaqus/Standard 6.10-1	
12	Ghosh et al. [172]	AA6016, AA6061	1.0	1.12	12	A deep drawing at RT and 250°C	
13	Modi & Digavalli [173]	AA5182	0.9	1.07	18.89	Experiments and simulation by DynaForm software	Hydroforming of square cups
14	Hadi et al.	AA1235	0.300	0.377 0.326	25.67 8.67	Experiments and simulation by LS Dyna	Normal punch Bulged-punch

Note: *: on the flange, RD: rolling direction, DD: diagonal direction, TD: transverse direction, RT: room temperature.

In hydro-forming, deep drawing pressure is applied onto the outer surface of the cup. The application of pressure from the inside is a difficulty in itself especially if the size of smaller punches limits the space available of the hydraulic equipment.

Preventing wrinkles on the edge of a cup in a micro deep drawing process can be carried out using a bulged punch which has not been used before. Details of the shape and size of a bulged punch are shown in Fig. 5.15. The cross section of a bulged punch shows a gradual curve joining a starting diameter of 7.59 mm to a final diameter 7.70 mm (Fig.5.13b). It was used with an 8.25 mm diameter die to draw on a blank that is 300 µm thick. The bulged punch size was determined by wrinkles location on the cup (Fig. 5.13a). The bulged punch diameter was designed to enlarge before appearance of the wrinkles. The transition region between the bulged diameter and the original diameter was reduced by turning.

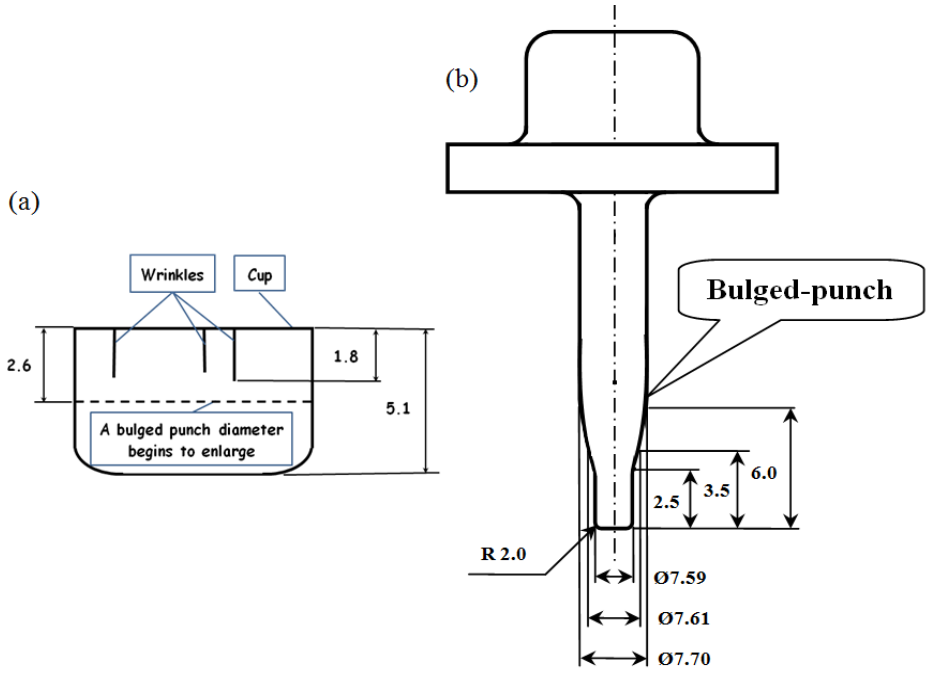

Fig. 5.13 Details of (a) depth of cup wrinkles, and (b) the shape and size of a bulged-punch for the blank thickness of 300 µm with die diameter of 8.25 mm

It can be seen in Fig. 5.14 (a) that an earing of 14.1% formed on an annealed AA1235 cup with a normal punch had the same diameter along the punch stem as a cup using a bulged punch (2.7 %) in Fig. 5.14 (b). The percentage of earing was calculated by [% earing = 2(hp-hv)/(hp+hv)] where hp was peak height of the cup

and hv was depth of the cup valley [20]. Thus it has been demonstrated that a bulged punch on a deep drawing process can produce a cup without any wrinkles. Moreover, it also reduced the extent of earing on the edge of the cup, as shown in Fig. 5.14.

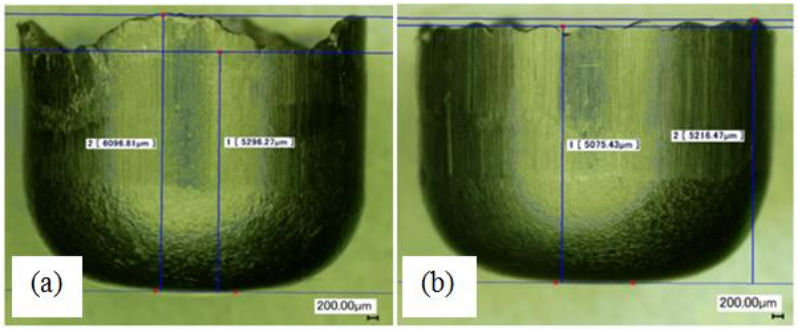

Fig. 5.14 Drawn cup (a) normal punch (14.1 % earing), and (b) bulged punch (2.7 % earing)

It is known that earing can be reduced by: (a) a modified non-circular shaped blank before a deep drawing process [44-46] [48] [107] [176], (b) carrying out an AR of the blank which is rotated 180^{o} between the cycles to reduce planar anisotropy [87], and (c) the SR process [9]. Furthermore, a bulged punch has also lessened earing in a cup. To prevent wrinkles from occurring after a certain depth of punch stroke, increasing the diameter of the bulged punch at that depth will iron the wall and produce a plastic flow that tends to reduce earing on the edge of the cup.

To obtain a clearer picture of this new idea, a comparison between the thickness of the blank and the wall of the cup using a normal punch and a bulged punch is shown in Fig. 5.15.

The thickness of the blank prior to a deep drawing process is shown in Fig. 5.15 (a). With a normal punch the thickness is less in the contact area at the radius of the punch corner, and it's thicker at the edge of the cup, as shown in Fig. 5.15 (b). In Fig. 5.15(c), a bulged punch produced a thicker corner radius and a thinner cup wall than a normal punch. The thickness with a normal punch and a bulged punch are shown

together in Fig. 5.16(d). The cup can be made thinner by increasing the diameter of the punch in the area where a wrinkle is likely to occur.

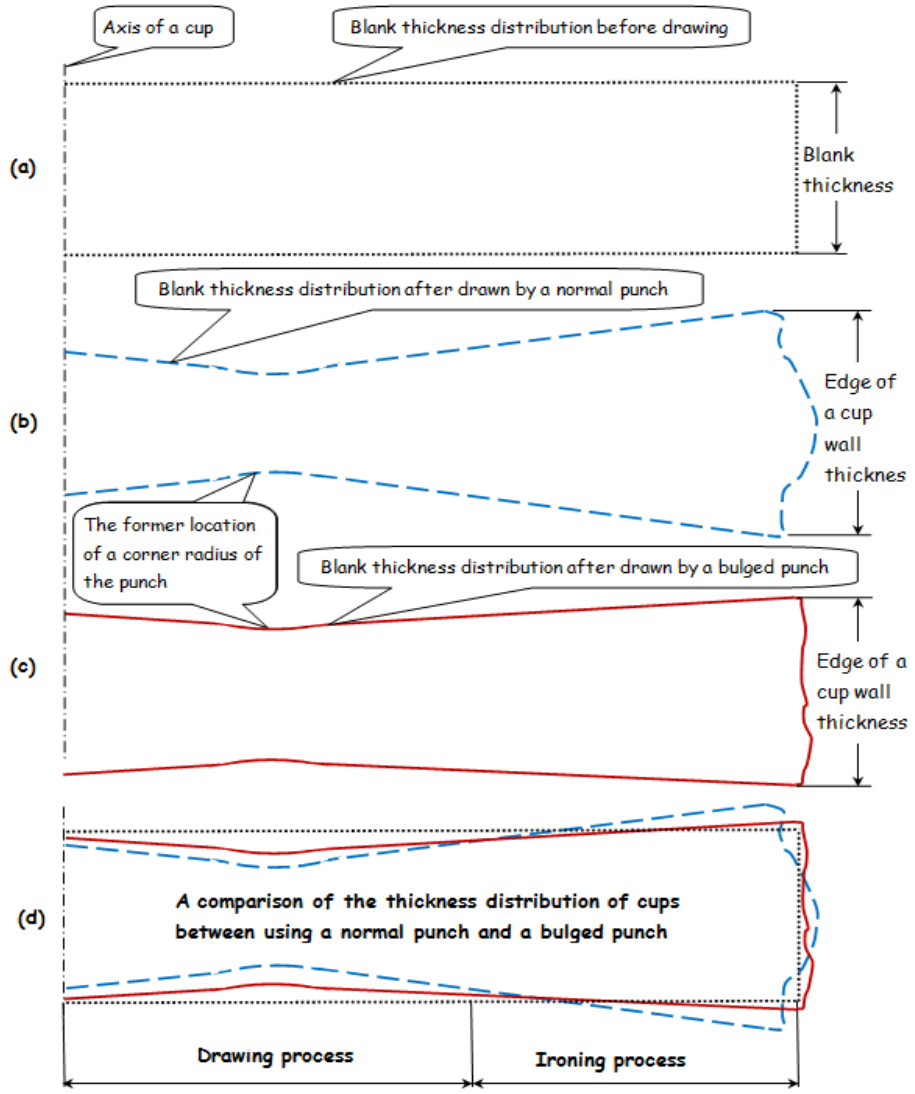

Fig. 5.15 A scheme of new ideas to avoid wrinkles by using a bulged-punch in a deep drawing and ironing processes in a single stroke. Thickness distribution of (a) a blank, (b) a cup if used a normal punch, (c) a cup if used a bulged-punch, and (d) a comparison between the two thickness distribution

This process can be categorised as an ironing process that creates a combined negative clearance to the cup wall. The wall of a cup can be reduced by an ironing die with a clearance that is less than the initial thickness of the wall [177]. At locations where wrinkles usually occur, the diameter of a punch is increased before wrinkles begin, so while the wrinkles of a deep drawing process are still developing,

and before expanding to the location of a certain wall thickness, the area is pressed by a punch that has been deliberately increased in size.

Initially, the aim was to eliminate or reduce wrinkles, but the bulged punch turned out to produce an even better outcome such as reducing the height of the earing. The earing height of a normal punch was 0.801 mm, but this was reduced to 0.141 mm or 5.6 times lower with the bulged punch.

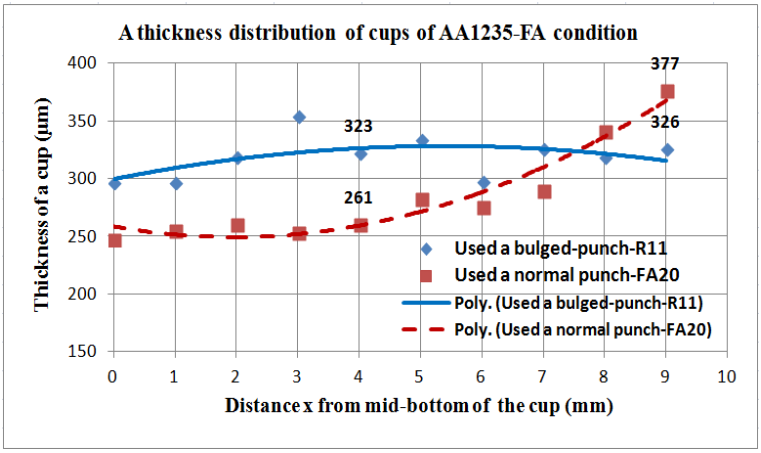

Fig. 5.16 A thickness distribution of cups of AA1235 from full annealed condition of blank diameter of 14 mm and thickness of 300 µm

Fig. 5.16 shows that the wall thickness with a normal punch has increased at the edge of the cup 7 to 9 mm from the axis of the cup. The bulged punch produced a thicker wall around the radius of the punch corner at 3 to 4 mm from the axis of the cup. This thickening was advantageous because a cup is generally torn at the radius the punch corner [178]. A reduction in the thickness of edge of the cup for a normal punch from 377 to 326 µm (or 13.5 % difference), was significant for the bulged punch because it made ejecting the cup easier.

The reduction in thickness due to ironing by a normal punch was 24 %, which was close to the 25 % reduction recommended by [35] and [36] to produce the best quality cup. Overall, the bulged punch does not produce a drastic thickening of the

material compared to a normal punch. If a normal punch is used, the material on the wall of the cup will experience tension due to the force of the punch at the bottom of the cup. According to the yield criteria, the radial pressure exerted by the bulged punch on the wall due to the radial interference between the punch and the inner wall can reduce the axial and circumferential stresses on the wall.

The force produced by the bulged punch was more than the normal punch and the ironing force was much more than the drawing force, as shown in Fig. 5.17a. Here the maximum ironing force reached 1640 N which was 181 % more than the maximum drawing force of 584 N. The results of the punch force from an experiment were still higher than the simulation results; they were not only caused by friction but by the cup being pressed onto the wall, especially in the ironing process, although the BHP was not considered in the simulation (Fig. 5.17b).

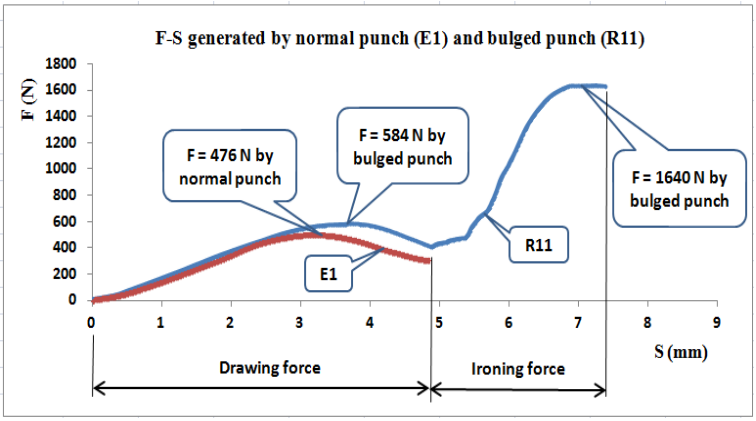

Fig. 5.17a Punch force produced by a normal punch (E1) and a bulged punch (R11) annealed AA1235 with a blank thickness 300 µm and a diameter 14 mm

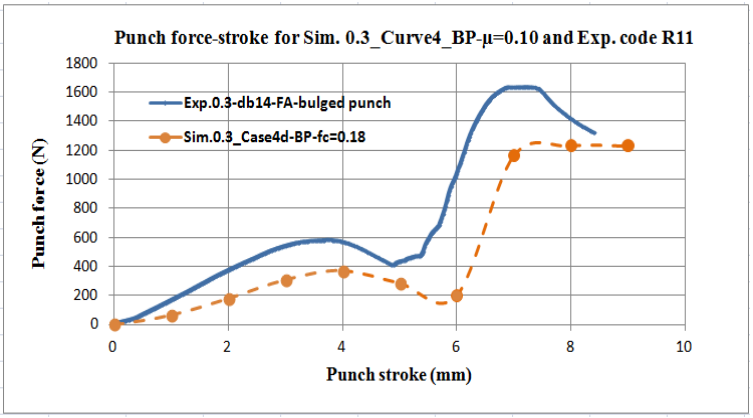

Fig. 5.17b A measured punch force compared to simulation result with a μ=0.18

The surface roughness of a cup a bulged punch is shown in Table 5.3. The average surface roughness (R_a) on the top surface was 24.8 and 23 μm on the bottom surface. The R_a of the cylindrical surface of the punch was 0.25 μm, the top surface of the die was 0.11 μm, the inside diameter of the die was 0.48 μm, and bottom surface of the blank holder was 0.11 μm.

The average roughness of the outer surface of the wall of the cup was less than the surface of the inner wall because there was more sliding contact and a higher friction between the blank and the die than between the blank and the punch. The roughness inside the base of the cup was small because the sliding contact between the bottom of the punch tip was small.

The roughness of both blank surfaces decreased significantly from an average of 23.9 μm ((24.8+23)/2) to 0.23 μm ((0.18+0.28)/2) for a normal punch, and to 4.47 μm ((3.95+4.99)/2) for a bulged punch. All the contact surfaces of the tools (punch, die and blank holder) had a surface roughness of less than 0.50 μm.

Table 5.3 Locations and values of the average surface roughness measured in a cup (a) outer surface, and (b) inner surface for normal punch (i) and bulged punch (ii)

(i) R_a (μm) for normal punch

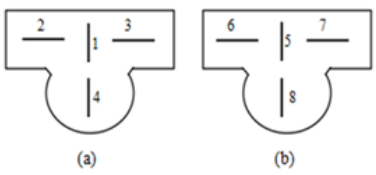

Location	(a) outer surface	Location	(b) inner surface
1	0.21	5	0.21
2	0.12	6	0.43
3	0.22	7	0.34
4	0.16	8	0.15
$R_{a\text{-average}}$	**0.18**		**0.28**

(ii) R_a (μm) for bulged punch

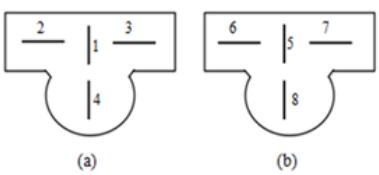

Location	(a) outer surface	Location	(b) inner surface
1	4.41	5	5.63
2	2.23	6	6.80
3	4.65	7	4.51
4	4.51	8	3.02
$R_{a\text{-average}}$	**3.95**		**4.99**

The average surface roughness of cup from a normal punch was smoother than the bulged punch because the wall from a bulged punch experienced a relative sliding during the ironing process.

5.11 Eliminating wrinkling with bulged punch and a 130 μm thick blank

A bulged punch has been proven to eliminate wrinkles and reduce earing. The thinner the blank the more likely wrinkles will appear in a cup. A normal punch still produced wrinkles in a 130 μm thick blank, but a bulged punch eliminated wrinkles from AA1235 for the FA material and also ARBSR material, as shown in Figs. 5.18 (a), (b), and (c) respectively. The top corner views of cups from a bulged punch for FA and ARBSR materials are shown in Figs. 5.18 (d) and (e).

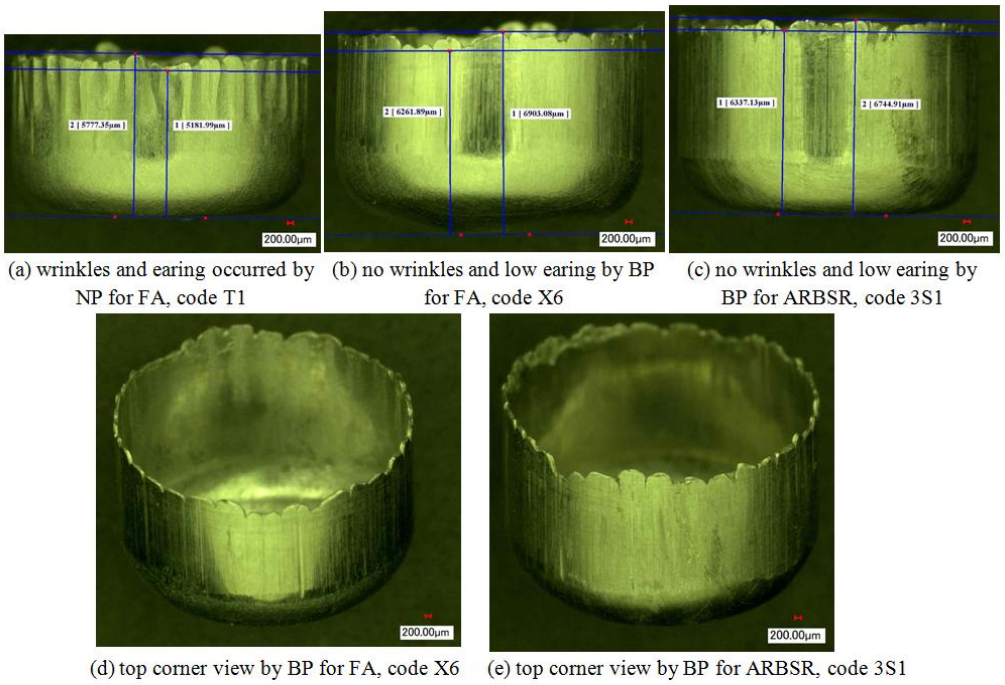

(a) wrinkles and earing occurred by NP for FA, code T1 (b) no wrinkles and low earing by BP for FA, code X6 (c) no wrinkles and low earing by BP for ARBSR, code 3S1

(d) top corner view by BP for FA, code X6 (e) top corner view by BP for ARBSR, code 3S1

Fig. 5.18 Cup with AA1235-FA and ARBSR materials resulted by NP and BP with TB of 130 µm

The earing that occurred when using FA material with a normal punch was 10.3 %, 9.3 % with a bulged punch, whereas earing for ARBSR material with a bulged punch was 6.0 %, so earing was reduced further in ARBSR material with a bulged punch than FA material with a normal punch.

The edge of a cup produced from 130 µm thick blank by a bulged punch shows a partial fracture for the ARBSR material and a solid edge for FA material, as shown in Figs. 5.18 (e) and (d).

Modifying the profile of a bulged punched created difficulties and failures; for instance, reducing the diameter of the punch by about 65 µm, resulted in a smaller diameter than it should have been, which meant the bulged punch did not work. With this experience, the diameter of the bulged punch was reduced by 20 µm, which resulted in obtaining a proper/good cup.

5.12 Ironing process

The cup drawn by an ironing die in Fig. 5.19a is shown in Fig. 5.19b. The ironing process used an 8.05 mm die, a 7.49 mm punch, a 300 µm thick blank, and a 6.2 mm punch stroke. The semi-die angle was 8^o which follows the recommended range of 5-15^o by [37]. The cup had less earing after ironing than normal drawing, and no wrinkles. The cup also had an average surface roughness (R_a) of 0.425 µm on the wall.

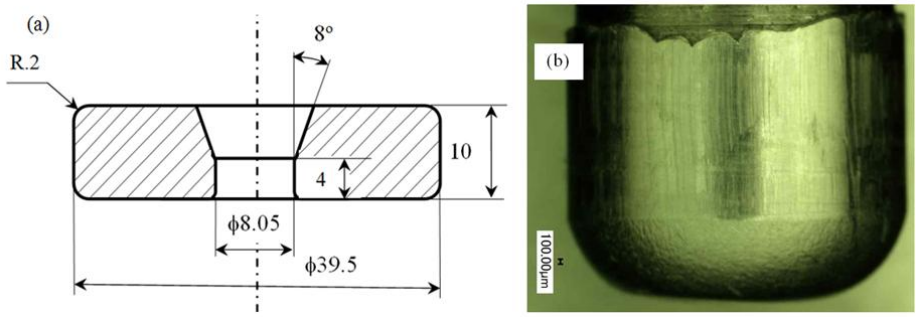

Fig. 5.19 Ironing die size (a) and a cup with no wrinkles from the ironing process (b)

5.13 Forming limit diagram (FLD) for cup forming

A forming limit diagram (FLD) was used to predict the forming behaviour of a cup based on the major and minor strains generated from a deep drawing process. FLD consists of three areas that generally include the tear area, the good cup (safe) area, and the wrinkled area. FLD has been carried out for 0.85 mm thick, non-coated IF steel sheet [105] and for 1.15 and 1.00 mm thick AA5182-O and AA5754-O materials, respectively, at room temperature [179]. Digital image correlation (DIC) analysis methods have also been used to measure the material strains for Al-Mg-Si alloy [180] more accurately.

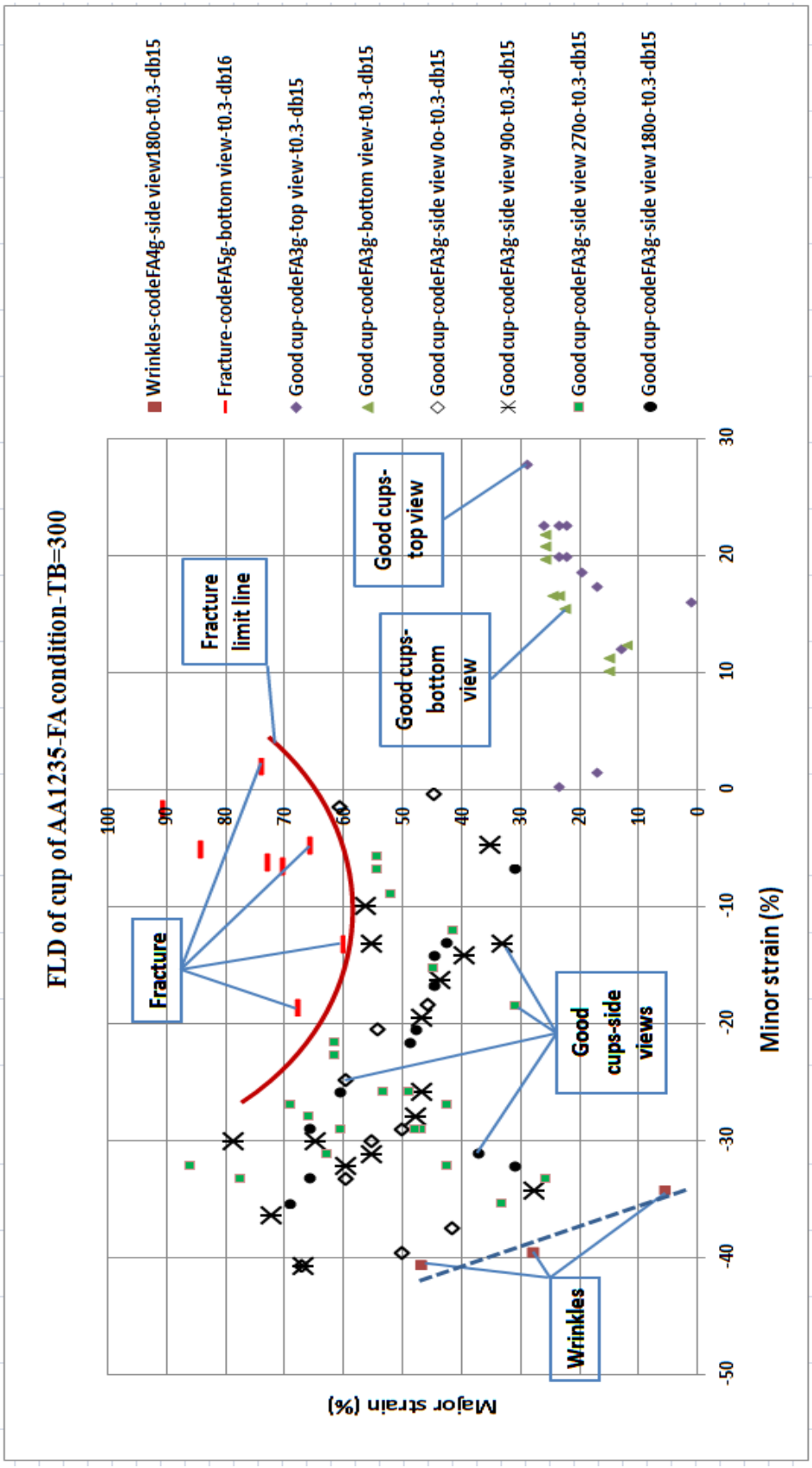

Fig. 5.20 FLD for AA1235-FA condition with TB of 300 µm and DB of 15 and 16 mm

Cups drawn from 15 and 16 mm thick FA blanks produced a distorted non-circular grid pattern on the surface, and they were measured and analysed to obtain the major and minor strains. The overall measurements and calculations for the major and minor strains in a FLD are plotted in Fig. 5.20.

Fig. 5.20 shows that strains in a deep drawing process occurred as the minor strains increased and the major strains decreased in wall of the cup, but positive strains occurred at the bottom of the cup from either the top or bottom views of the cup. When the major strain increased in the cup wall to a limit, it was followed by thinning, tearing, and then fractures. A good area in a deep drawing process is above the wrinkling limit and below the fracture limit.

5.14 Discussion

A deep drawing process is a process that forms cups from blanks that need special requirements to eliminate wrinkling, tearing, and minimum earing. A four cycle ARB process produced AA1235 with smaller grain size which was then deeply drawn. The ratio ($\varphi = t/d$) between the thickness of a blank and an average grain size was also obtained. The higher the value of φ, the better the formability of the material. A cup was formed from material resulting from 4 cycles ARB, as shown in Fig. 5.5 (a). The cup was made from 278 μm thick blanks with 72 layers, the average grain size was 2.146 μm, and the ratio $\varphi = 1.8$ is shown in Table 3.7 (Chapter 3). The material with a small grain size still did not produce a better formability because after the ARB process it still has a residual stress which must be removed by stress relieving.

It has been stated that formability is indicated by a cup without any defects such as wrinkles due to excessive compression and tear due to high local tensile stresses [181].

It has also been observed that 1.6 mm thick IF steel sheet is better suited to deep drawing because it has a larger gap between the forming limit line and the wrinkling limit line (WLD) of the FLD [105].

FLD for a drawing process is on the left and stretching is located to the right of the graph of minor-major strains in Fig. 5.21. Stretching was caused by the tensile stress exceeding the yield stress. If force is applied perpendicular to the sheet plane then biaxial stretching will occur.

The FLD for 0.6 mm thick IF steel sheet is shown in Fig. 5.22a [105]. The FLD is shown as a solid line, the fracture limit line is indicated by the dashed line, and the wrinkling limit line is shown with a dotted line [182].

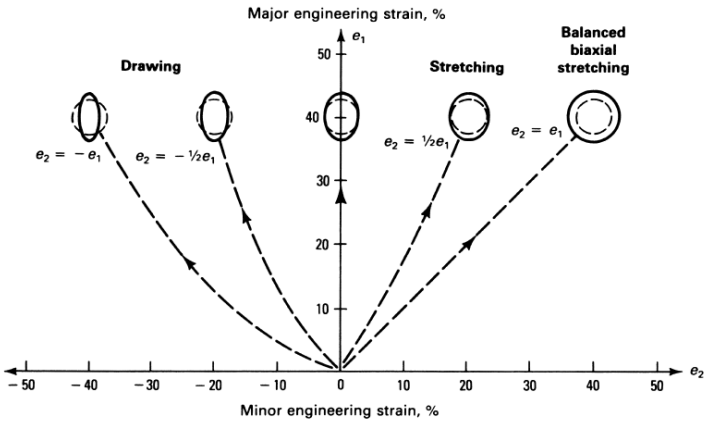

Fig. 5.21 FLD for a drawing and stretching processes in the minor-major strains graph [182]

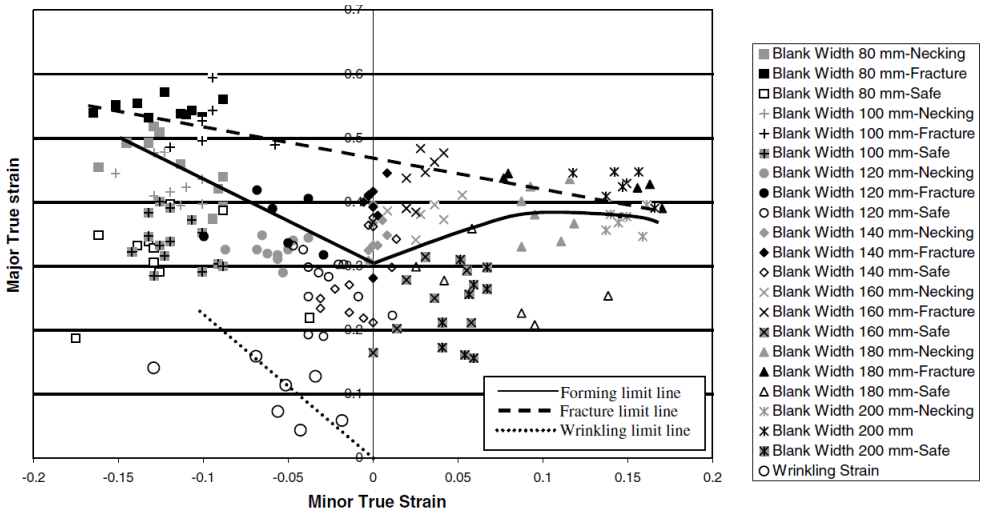

Fig. 5.22a FLD for IF steel sheet of 0.6 mm thick [105]

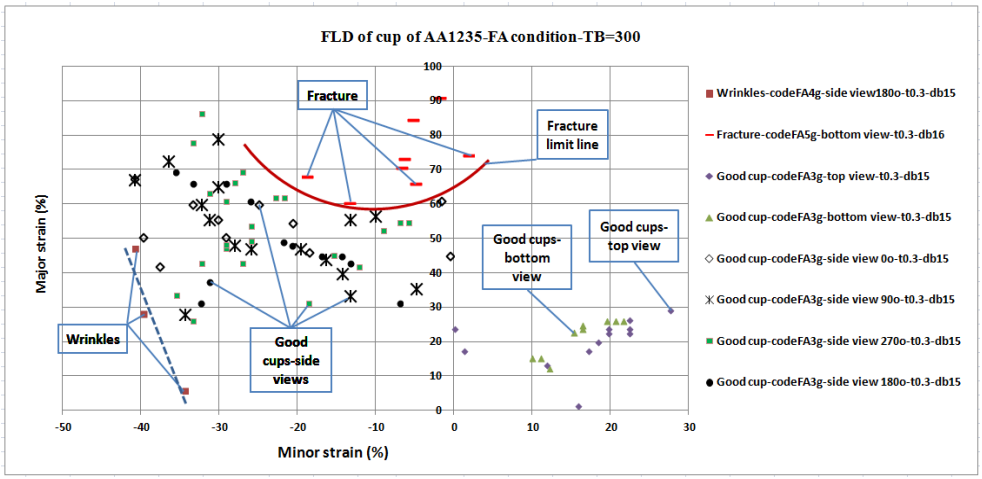

Fig. 5.22b FLD for AA1235 sheet of 0.3 mm thick (reproduced of Fig. 5.20)

Fig. 5.22a shows that the forming limit line for steel was under the fracture limit line and above the wrinkling limit line. Fig. 5.22b indicates there were 3 data (code FA4g) in the wrinkled area and 8 data (FA5g) from the fractured area (above the solid red line). In Fig. 5.22a the minor strains for IF steel are between -0.18 and 0.18 [105]. In Fig. 5.22b, the minor strain for AA1235 are between -0.48 and 0.28. The data range for AA1235 material was wider than IF steel so the formability of AA1235 is better than IF steel. Fig. 5.22b shows two groups of data seen from the bottom of the good cup and the view from the top of the good cup of AA1235

material that was stretched. The data from the views of four good cups showed that the major strain was more than the minor strains, and the data remained on the left side in the graph of the drawing process. Two data for the bottom of the cup were stretched and are plotted on the right side of the strain graph.

Although a cup can be formed, the occurrence of wrinkles on the wall is a problem that must be addressed. Various attempts have been made by many authors, but none have come up with a good solution. Hydro-forming still leaves flanges at the end of a deep drawing process [183], and even applying a controlled BHP will only prevent or eliminate wrinkles on the flange but not on the wall of the cup.

Wrinkles on thin sheets resulting from deep drawn parts will be generated when the die and punch are not aligned properly [184].

Wrinkling during deep drawing can be resisted better when the annealing temperature of an Aluminum is increased and furnace cooling is used instead of air cooling [185]. An annealing process for blank material can result in a cup with small wrinkles, but it still results in a large earing on the edge of the cup, which must then be removed as waste.

Low earing can be generated by planar anisotropy values that are almost zero. Attempts have been made to obtain these values by selecting materials that have a lower planar anisotropy value, if such choices are available. Another effort was made by modifying the shape of the blank to minimise earing. Reversing the direction of the AR between cycles can also improve the value of the planar anisotropy. The bulged punch can also eliminate wrinkles and reduce earing in a cup. The manufacture of a bulged punch was based on the experience gained from previous deep drawing of a blank and materials with specific treatment conditions.

The thickness of the wall of a cup is formed and thus distributed with a normal punch which results in a thinner wall around the radius of the punch corner and a thicker edge to the cup. A bulged punch resulted in a thickening of the walls around the radius of the punch corner, which is the opposite of a normal punch. This thickening is advantageous because cups generally begin to tear at the radius of the punch corner.

The wall region experiences tension due to force from a punch at the bottom of the cup if a normal punch is used, but if a bulged punch is used, the area of the cup wall will be ironed by a punch in the radial direction towards the inside diameter of the die.

One disadvantage of the bulged punch is the need for previous experience with a normal punch in order to modify its profile properly. A greater punch force is also required for the bulged punch.

5.15 Summary

Problems relating to wrinkles and earing from a deep drawing process are a common occurrence, but more so with thinner blanks. Earing that formed on a cup made from annealed material was higher with a normal punch than with a bulged punch because a bulged punch can eliminate wrinkles and reduce earing on the edge of the cup, thickening at the radius of the punch corner, and thinning at the edge of the cup, although its optimum profile depends on the experience gained from using a normal punch. The force required to drive a bulged punch was more than a normal punch because it is a combination of drawing and ironing. Moreover, the resulting

reduction in the thickness of the edge of the cup can facilitate its ejection from the punch and die.

Deep drawing can be carried out in a good cup (safe) region based on the established FLD for annealed AA1235. The average surface roughness of a cup by a normal punch was smoother than by a bulged punch.

Chapter 6 Simulation of deep drawing processes

6.1 Modelling a deep drawing process

A simulated deep drawing process of a cup was developed using the FEM software LS DYNA. The model consists of Aluminium AA1235, a die, a punch, and a blank holder. A model of the deep drawing assembly and the dimensions of the blank and tools are shown in Figs. 6.1 and 6.2.

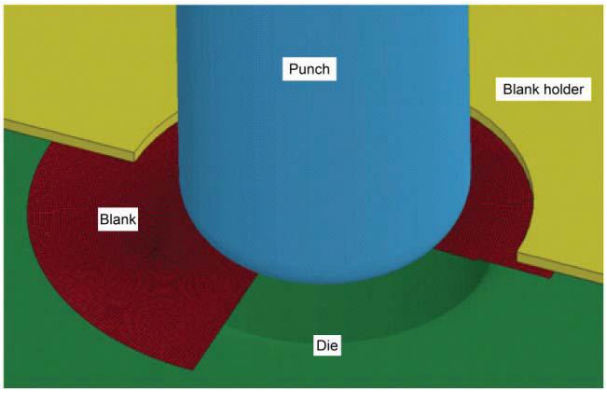

Fig. 6.1 A model of a configuration of the deep drawing tools assembly [10]

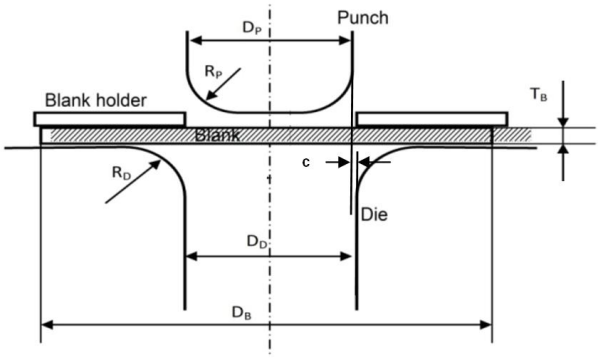

Fig. 6.2 Geometric dimensions of the blank and tools [10]

Some results of this chapter have already been published:
Hadi, S., Yu, H.L., Tieu, K., Lu, C., *Simulation of defects in micro-deep drawing of an aluminium alloy foil.* in The 11th International Conference on Numerical Methods in Industrial Forming Processes, AIP Conf. Proc. 1532, 298-303 (2013); doi: 10.1063/1.4806838, p. **298-303**.

A 3-D model of a deep drawing process for AA1235 aluminum foil was created in LS-DYNA using quadrilateral shell-shaped elements. The blank material was assumed to be isotropic. The anisotropy for AA5xxx in a simulation with LS-Dyna for a deep drawing process was not considered because its effect would be minimal [186].

The model for deep drawing a 14 mm diameter blank by 300 μm thick Aluminium AA1235 blank in a fully annealed condition contained 28561 elements and 34693 nodes. There were 28561 elements for the blank, die, punch, and blank holder, 10800 elements for the shell (blank), and 17761 elements for the die, punch, and blank holder. The punch speed was set at 100 mm/s for all simulations. The model of the deep drawing process is shown in Fig. 6.1, and its dimension is shown in Fig. 6.2. The Coulomb friction model was used with the coefficient of friction (μ) that varied between 0.1 and 0.30. In the models the punch, die, and blank holder were assumed to be rigid. The geometrical and material parameters are shown in Tables 6.1 and 6.2.

Table 6.1 Geometrical parameters in deep drawing in Figure 6.1

Parameters	Value
Diameter of blank (DB), mm	14 - 15
Thickness of blank (TB), mm	0.070, 0.130, 0.150, and 0.300
Diameter of drawing die (DD), mm	8.35
Radius at corner of die (RD), mm	1.21 and 1.40
Diameter of punch (DP), mm	7.54
Radius at corner of punch (RP), mm	1.21 and 2.50

Table 6.2 Material properties of blank

Parameters	Value
Density (ρ), kg/m^3	2700
Young's modulus (E), GPa	80
Yield stress (YS), MPa	74.18 - 106.8
Poisson's ratio (ν)	0.3

6.2 Validation of the simulation model to the experiment results

A model that simulates deep drawing a cup was developed in this chapter to understand how the stress/strain parameters of the cup would result in the cup having wrinkles and tearing. However, this model must be validated for accuracy against the experiments.

The results can be compared in terms of the punch force and thickness of the cup wall due to different RD/RP, DB, punch geometry, and μ. The positive and negative clearances between the die and punch diameter that can influence how the cup will form will also be considered.

A simulation can be used to estimate the parameters of experiments in a trial and error process in order to obtain better results with a reduced number of steps, and it can also explain the probable outcomes of the forming process such as tears, wall thickness, and wrinkles. Indeed, from the simulation, the results can be animated so that the forming process can be analysed. An analysis of the von Mises stress, strain, punch force, and punch strokes taken during deep drawing will increase our understanding of the process.

A comparison between a simulation and an experiment is shown in Fig. 6.3.

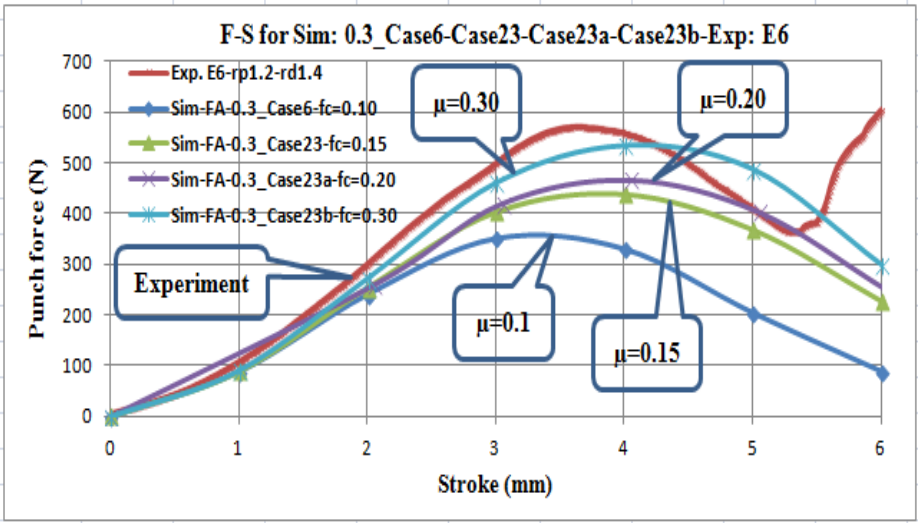

Fig. 6.3 Simulated punch force against experiment

For a punch stroke between 2 and 4 mm, the experimental punch force was higher than in the simulation due to wrinkles because the punch needs more force to iron out the wrinkles while forming the full cup. The simulation assumes that the blank material was isotropic, so any thickening of the cup wall due to wrinkles was ignored. The punch force must overcome the blank bending force at the corner radius of the die and punch, the friction force between the blank and the tools, and the flange friction force from the blank holder. Moreover, the bending force increases with the thickness of the blank, and the blank was thicker in the region of wrinkles.

6.2.1 Effect of the corner radius of die on a punch force

The difference in the use of a die corner radius to the punch force generated in the simulation shows that a larger corner radius would reduce the punch force by 4.6 %, as shown in Fig. 6.4.

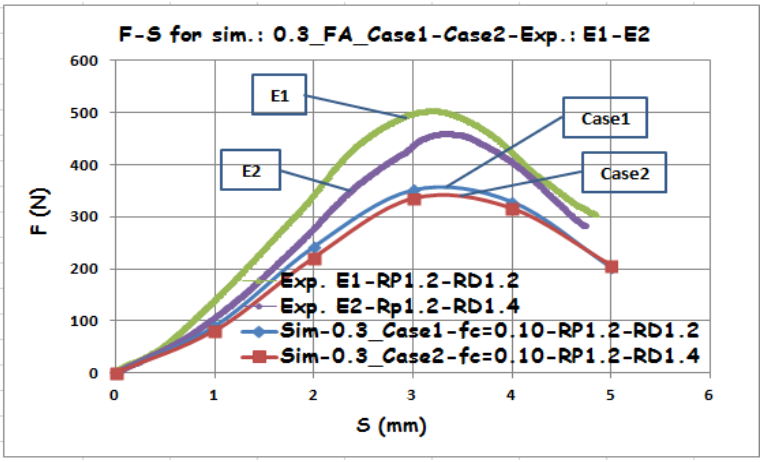

Fig. 6.4 Punch force with DB=14 mm and TB=300 µm from simulations with RD=1.2 mm (blue) and 1.4 mm (red), µ=0.1, and from experiments with RD=1.2 mm (green) and 1.4 mm (purple)

The experimental results shown in Fig. 6.4 indicated that a larger die corner radius reduced the maximum punch force when a 14 mm diameter by 300 µm thick blank was used. A die corner radius of 1.2 mm showed a maximum punch force of 506 N compared to 461 N with 1.4 mm die corner radius. The experiment has demonstrated that a larger die corner radius reduced the punch force by 8.9 %. The similarity between the trends of the simulation and experiments shown in Fig. 6.4 indicates the validity of the simulation model.

6.2.2 Effect of the punch corner radius

A difference in the punch corner radius to the punch force generated in the simulation showed that a larger corner radius on the punch would decrease the punch force by 2.7 %, as shown in Fig. 6.5.

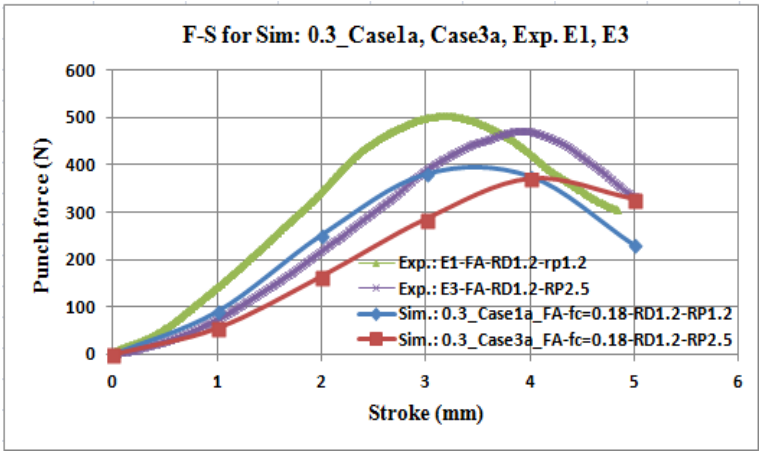

Fig. 6.5 Punch force with DB=14 mm and TB=300 µm from simulations with RP=1.2 mm (blue) and 2.5 mm (red), µ=0.1, and from experiments with RD=1.2 mm (green) and 2.5 mm (purple)

The experimental results in Fig. 6.5 show that a larger corner radius on the punch reduced the maximum punch force in deep drawing when a 14 mm diameter by 300 µm thick blank was used. A corner radius of 1.2 mm required a maximum punch force of 506 N compared with 474 N with 2.5 mm corner radius, a difference of 6.3 %. There was a similar trend between the simulation and experiments results, as shown in Fig. 6.5.

6.2.3 Effect of the coefficient of friction on the punch force

The coefficient of friction in a simulation can affect the punch force, so several values were tested and then an appropriate figure was selected when the simulated punch force stroke curve matched the experiment results. Fundamentally, when the coefficient of friction is increased there will be a corresponding increase in the punch force.

A number of friction coefficients were applied in the simulation, the results were compared with the experiment, and then an appropriate curve was selected when it came close to the experiment results, as shown in Fig. 6.6.

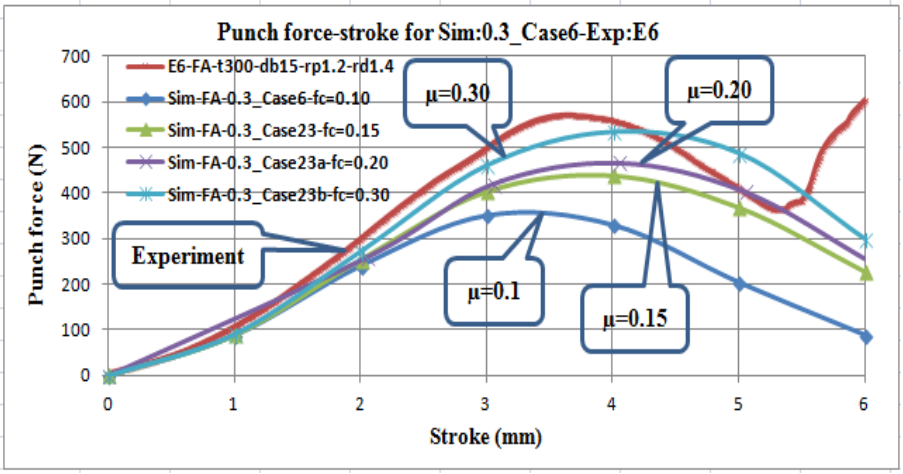

Fig. 6.6 Effect of friction coefficient in a deep drawing process

6.2.4 Effect of clearance to the wrinkles

In deep drawing, a clearance that is larger than a certain value results in a cup with wrinkles on the wall and vice versa, whereas less clearance will result in a cup without wrinkles on the wall.

A clearance of 0.46 mm (306 % of the thickness of the blank of 0.15 mm) in deep drawing with a 8.25 mm diameter die, and a 7.49 mm diameter punch, generated a wrinkled cup, as shown in Fig. 6.7a. However, when the clearance was reduce to 0.21 mm (70 % of the thickness of a blank) on an 8.35 mm diameter die, a 7.54 mm diameter punch, and an 0.3 mm thick blank produced a cup without wrinkles on the edge, as shown in Fig. 6.7b.

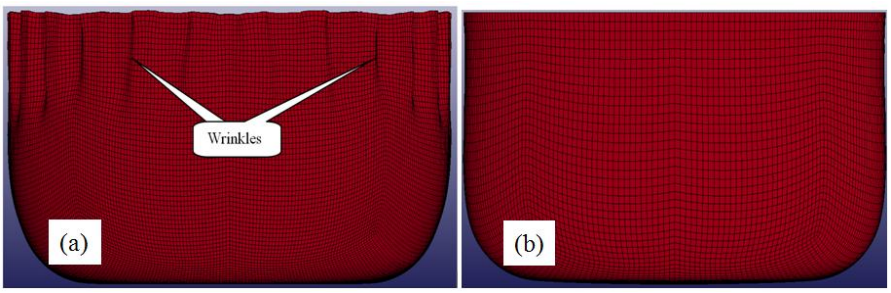

Fig. 6.7 Cups (a) with wrinkles on the cup edge with a clearance 3.06 times the 0.15 mm blank thickness, and (b) without wrinkles on the cup edge with a clearance of 70 % of the 0.3 mm blank thickness

The experiment therefore indicated that in deep drawing, a clearance of 0.5 mm (3.85 times the blank thickness) for an 8.25 mm diameter die, a 7.49 mm diameter punch, and a 0.13 mm thick blank resulted in a wrinkled cup, as shown in Fig. 6.8a, but when the clearance was 0.16 mm (53 % of a blank thickness of 0.3 mm) it resulted in a cup without wrinkles on the edge, as shown in Fig. 6.8b. However, the simulation cannot reproduce earings because the anisotropy was not included in the simulation, so when the clearance was increased, there would be more opportunity for wrinkles to occur on the edge of the cup, but when the clearance is reduced, there will be a cup without wrinkles. In fact, a clearance that is too small can result in the cup tearing before the punch stroke is completed. The results of the simulation models were quite consistent with the experimental results.

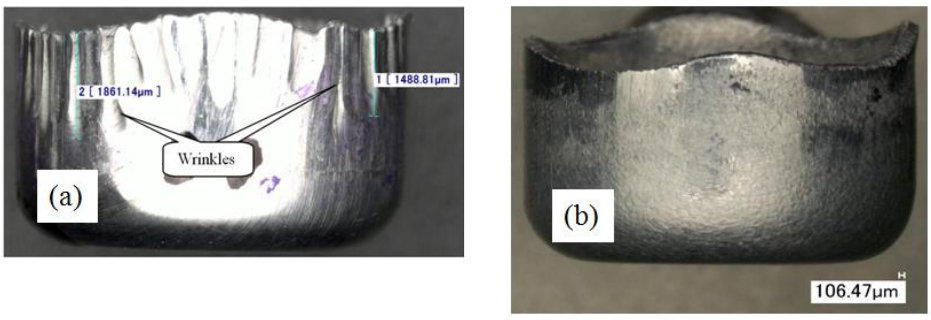

Fig. 6.8 Cup (a) with wrinkles with a clearance 3.85 times the 0.13 mm blank thickness, and (b) without wrinkles with a clearance 53 % of the blank thickness of 0.3 mm

6.2.5 Effect of the diameter of the blank to the punch stroke

The diameter of the blank governs the punch stroke in deep drawing, as shown in Fig. 6.9, such that the larger the diameter, the deeper the punch stroke will be, as shown in Figs. 6.9a and 6.9b. The experimental results indicated that the mean depth of the punch stroke was 4.93 and 5.69 mm respectively for 14 and 15 mm diameter blanks, as shown in Figs. 6.10a and 6.10b. The larger the diameter the blank, the

more punch stroke is required, as shown in Fig. 6.10. The simulation and experiment on different diameter blanks showed a reasonable match, within 3-6 %.

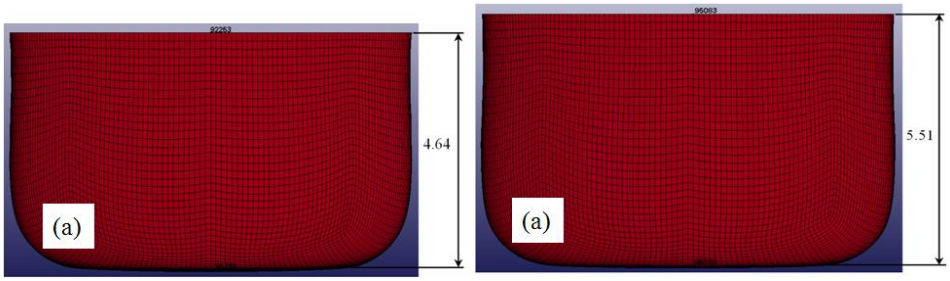

Fig. 6.9 Formed cup with stroke length of 4.64 mm (a) and 5.51 mm (b) respectively from the 14 and 15 mm diameter blanks

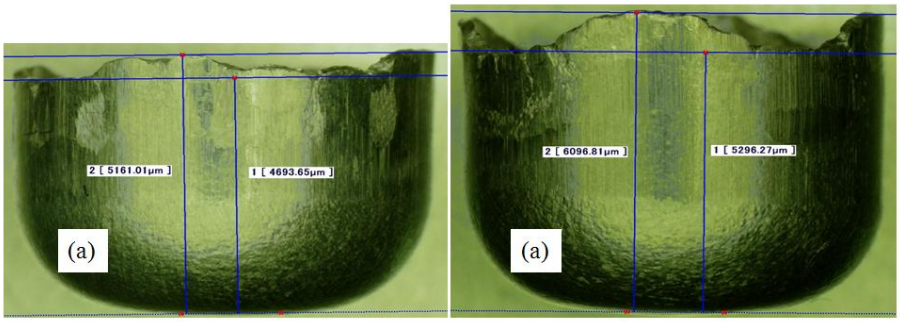

Fig. 6.10 A blank diameter of (a) 14 mm and (b) 15 mm have produced a drawn cup with mean punch stroke of 4.92 and 5.69 mm

The results so far have shown that a simulation model compared well with the experiment results while investigating the effect of the die corner radius, the coefficient of friction, clearance on the wrinkles, and punch stroke vs blank diameter. It can therefore be concluded that the simulation model is valid and can be used to investigate different aspects of the deep drawing process.

6.3 Some typical simulation results for AA1235

Simulations were carried out on Aluminium AA1235 in a fully annealed (FA) condition, as well as a combined ARB and stress relieving at 200 ^{o}C for 8 hours.

Variable parameters were the thickness and diameters of the blank, the corner radius of the punch and die, the coefficient of friction (μ), and the tensile strength. Some typical simulation results for some cases are shown in Table 6.3. The blanks 300, 130, and some cases 150 and 70 μm thick, and the blank diameters were 14 and 15 mm. The punch corner radii were 1.2 and 2.5 mm, and die corner radii were 1.2 and 1.4 mm. The μ were 0.10 for all FA and ARBSR (ARB followed by stress relieved) material for the first trial, and then 0.11 to 0.20, and 0.30 for further trial. The realistic values for μ were 0.18 and 0.20. The chosen tensile strengths were 74.18, and 76.19 MPa for FA materials and 104 and 106.8 MPa for ARBSR materials for blanks that were 300 and 130 μm thick, respectively.

The simulation of a deep drawing process by LS-DYNA software requires four files: (a) the main program, (b) a subroutine file for each case (each case has different input data sets) i.e.: the file of 0.3_Case2.dyn, (c) a file with extension k, i.e.: Micro-forming.k for a deep drawing process (a file with extension k is only valid for one set of input data which can be changed for the following parameters: TB, tensile strength, μ, and punch speed). The constant set of data for each case are tool geometry, DP, RP, DD, RD, and (d) a submission batch file DynaQsub.sh for submitting LS-DYNA job to the high performance computer (HPC)/cluster). All the simulation results are plotted from the files of d3plot. The results of all 62 simulation cases are shown in the Appendix. Every case corresponds to a specific combination of strength of material, DB, TB, DD, RD, DP, RP, and μ. Case 1 has been published in a paper. Fully annealed materials were used in cases 1, 2-19, 32-46, and 61-62. ARBSR materials applied to cases 20-31 and 47-60. Cases 1-61 used a normal punch whereas the bulged punch was considered in case 62 with different μ of 0.10, 0.12,

0.14, 0.16, 0.18, 0.20 and 0.30. In a simulation of the deep drawing process, the speed of the punch stroke (V_{Punch}) was 0.1 m/s.

Nine typical cases were selected from the above 62 cases and are presented here.

In the first case (0.3_Case1), a fully annealed (FA) 0.3 mm thick blank, DB of 14 mm, die corner radius 1.2 mm, and μ of 0.18 was considered, and resulted in a cup without wrinkles. The maximum punch force as a result from the experiment was 24.9 % higher than the simulation result. With a larger RD of 1.4 mm (0.3_Case 2), the maximum punch force of Case 1 was reduced by 4 N.

For ARBSR material in the second case (0.3_Case10), with a 0.3 mm thick by 14 mm diameter blank, and a μ of 0.18, the results showed a cup without wrinkles. The maximum punch force from the experiment was 7.7 % higher than the simulation result.

The third case was a cup simulated from FA material with a 0.3 mm thick by 15 mm diameter blank, and a μ of 0.18. This case also showed a cup without wrinkles, and the maximum punch force from the experiment was 22.9 % higher than the simulation result. With a larger punch corner radius of 2.5 mm, the maximum punch force was reduced by 11 N (0.3_Case5).

The fourth case (0.3_Case14) with ARBSR material also showed a cup without wrinkles, while the maximum punch force from the experiment was 22.17 % higher than the simulation result (Case22).

The fifth case (Microforming.15) was a cup simulated from FA material with an 0.15 mm thick by 14 mm diameter blank, and a μ of 0.10. The case showed a cup with wrinkles, while the border line (between the wrinkled and circular/smooth

areas) had a strain of 0.27. A strain of 0.39 and 0.90 were respectively the lowest in a valley and the maximum in a peak wrinkle area.

The sixth case (0.13_Case9) with FA material (0.13 mm thick by 14 mm diameter blank, and a μ of 0.15) showed a cup with wrinkles. The wrinkle border line had a strain 0.45 compared to the respective lowest and maximum strain of 0.61 and 1.1 in a valley/peak wrinkle area.

For ARBSR material in seventh case (0.13_Case8), the cup showed some wrinkles at the edge.

The eighth case (0.07_Case2) was a cup simulated from FA material with a 0.07 mm thick by 14 mm diameter blank, and a μ of 0.10. This case showed a cup with wrinkles, with a strain of 0.32 at the border line, compared to a minimum-maximum strain of 0.65 - 0.96 in the wrinkle area.

The ninth case (0.3_Curve4) was a cup simulated from FA material used a bulged punch with a 0.3 mm thick by 14 mm diameter blank, and μ of 0.10, 0.12, 0.14, 0.16, 0.18, 0.20 and 0.30. This case showed a cup without wrinkles. The maximum punch force from the experiment was 9 % lower than the simulation result, with a friction of 0.30. The experimental force was higher than the simulation result because the bulged punch needs more force on the thickened cup wall and to iron out the wrinkles in the ironing process. The simulation did not consider these results of the anisotropy properties of the material.

Table 6.3 Some typical simulation results for full set of simulations refer to Appendix

Table 6.3 Some typical simulation results for full set of simulations refer to Appendix

No.	TB (μm)	DB (mm)	Data of simulation/file	μ	Contours of Von Mises stress (MPa)	Punch force-stroke curve (strain)	$F_{max.}$ (N)	Remarks
1	300	14	0.3_Case1a_FA Material: FA TB=300μm DB=14 mm DP=7.54 mm RP=1.2 mm DD=8.35 mm RD=1.2 mm	- 0.10 0.18 0.10	0.3_Case1a_FA, μ=0.18 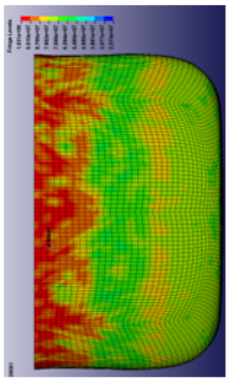 Time steps= 0.06 Min=22.73 (bottom) Max=103.15 (edge wall)	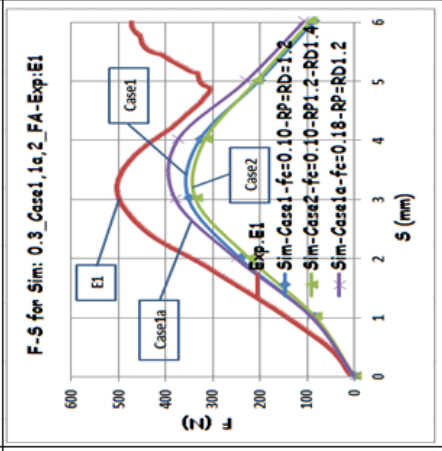	506 351 380 335	Exp. E1 0.3_Case1 0.3_Case1a 0.3_Case2 $F_{max.exp.}$ (E1) is 24.9% higher than $F_{max.sim.}$ (Case1a). With a larger RD of 1.4 mm (Case2), the $F_{max.sim}$ (Case1) is reduced by 4 N.
2	300	14	0.3_Case18_ARBSR Material: ARBSR TB=300μm DB=14 mm DP=7.54 mm RP=1.2 mm DD=8.35 mm RD=1.2 mm	- 0.10 0.18 0.30	0.3_Case18_ARBSR, μ=0.18 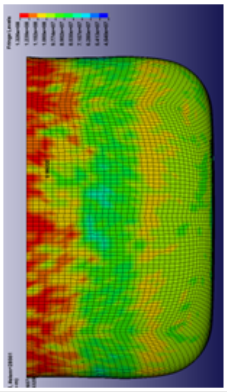 Time steps= 0.06 Min=45.40 (bottom) Max=132.64 (edge wall)	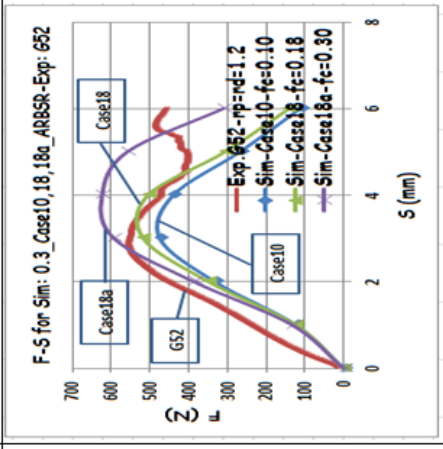	560 474 517 625	Exp. 0.3_Case10_ARBSR 0.3_Case18 0.3_Case18a With μ of 0.18, $F_{max.exp.}$ is 7.7% higher than $F_{max.sim.case18,}$ (more realistic), but with μ of 0.30, $F_{max.exp.}$ is 10.4% lower than $F_{max.sim.case18a.}$

Table 6.3 Some typical simulation results for full set of simulations refer to the Appendix (continued)

No.	TB (μm)	DB (mm)	Data of simulation/file	μ	Contours of Von Mises stress (MPa)	Punch force-stroke curve	$F_{max.}$ (N)	Remarks
3	300	15	0.3_Case5a_FA Material: FA TB=300μm DB= 15mm DP=7.54 mm RP=1.2 mm DD=8.35 mm RD=1.2 mm	- 0.10 0.14 0.18 0.10	0.3_Case5a_FA, μ=0.18 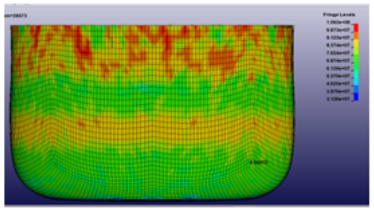 Time steps= 0.07 Min=31.26 (bottom) Max=106.3 (edge wall)	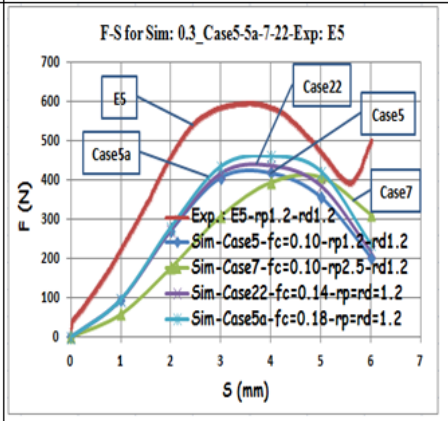	597 417 437 460 406	Exp. 0.3_Case5 0.3_Case22 0.3_Case5a 0.3_Case7 With μ of 0.18, $F_{max.exp.}$ (E5) is 22.9% higher than $F_{max.sim.}$ (Case5a). With a larger RP of 2.5 mm, $F_{max.sim}$ (Case7) is reduced by 11 N (Case5).
4	300	15	0.3_Case22_ARBSR Material: ARBSR TB=300μm DB=15 mm DP=7.54 mm RP=1.2 mm DD=8.35 mm RD=1.2 mm	- 0.10 0.18 0.30	0.3_Case22_ARBSR, μ=0.18 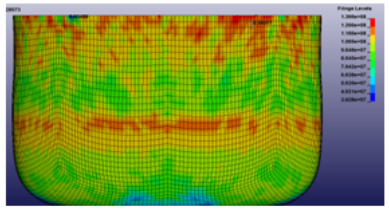 Time steps= 0.07 Min=36.28 (edge wall) Max=136.62 (edge wall)	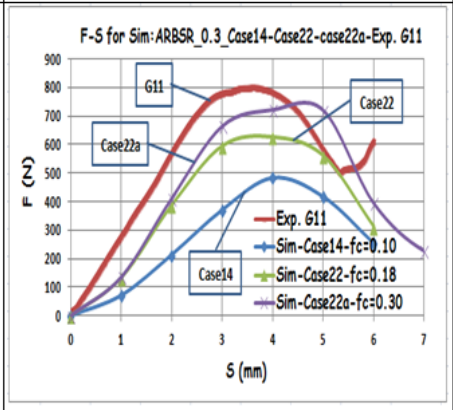	803 556 625 722	Exp. 0.3_Case14_ARBSR 0.3_Case22 0.3_Case22a $F_{max.exp.}$ (G11) is 22.17% higher than $F_{max.sim.}$ (Case22) with μ=0.18. $F_{max.exp.}$ (G11) is 10.1% higher than $F_{max.sim.}$ (Case22a) with μ=0.30.

Table 6.3 Some typical simulation results for full set of simulations refer to the Appendix (continued)

No.	TB (μm)	DB (mm)	Data of simulation/file	μ	Contours of Von Mises stress (MPa)	Punch force-stroke curve	$F_{max.}$ (N)	Remarks
5	150	14	Microforming_ .15 Material: FA TB=150μm DB=14 mm DP=7.49 mm RP=1.2 mm DD=8.25 mm RD=1.2 mm	0.10	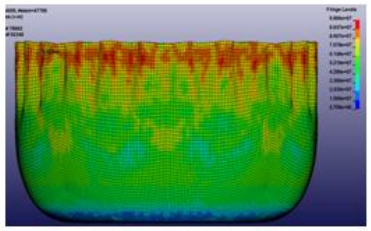 Time steps= 0.06 Min=5.71 (bottom) Max=98.66 (edge wall)	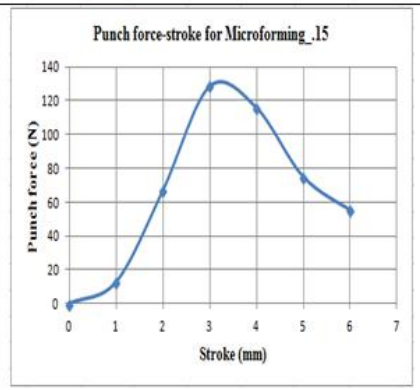	129	A conference paper in AIP Conf. Proc. 1532 *Simulation of defects in micro-deep drawing of an Aluminium alloy foil*, p. **298-303**.
					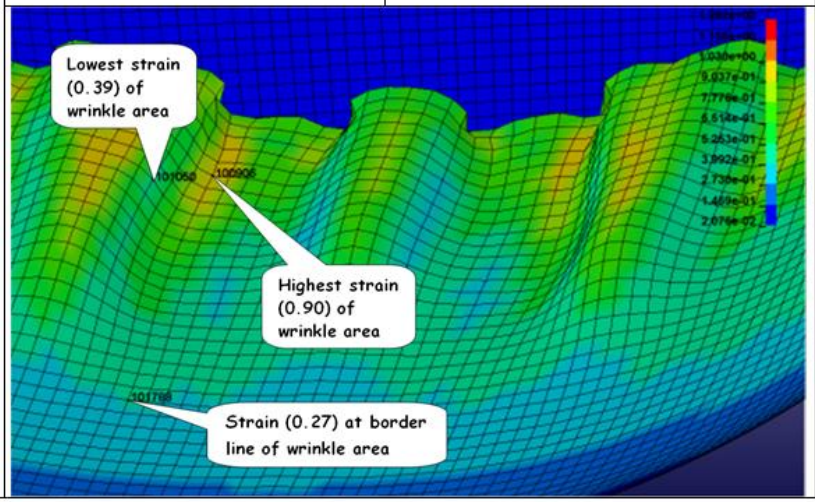			Strains on wrinkle area: (1) strain (0.27) at border line (between wrinkles area and circular/smooth area), (2) strain (0.39) as the lowest strain in a valley of wrinkle area, and (3) strain (0.90) as the highest strain in a peak of the wrinkle area.

Table 6.3 Some typical simulation results for full set of simulations refer to the Appendix (continued)

No.	TB (μm)	DB (mm)	Data of simulation/file	μ	Contours of Von Mises stress (MPa)	Punch force-stroke curve	$F_{max.}$ (N)	Remarks
6	130	14	0.13_Case9_FA Material: FA TB=130μm DB=14 mm DP=7.93 mm RP=1.2 mm DD=8.35 mm RD=1.2 mm	- 0.10 0.15	0.13_Case9_FA, μ=0.15 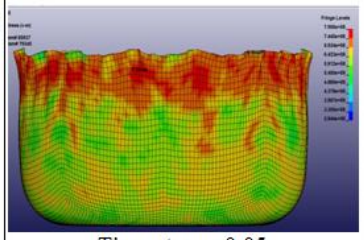 Time steps= 0.05 Min=28.44 (edge wall) Max=79.56 (edge wall)	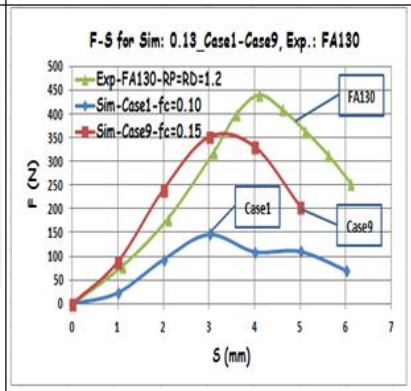	440 146 351	Exp. 0.13_Case1_FA 0.13_Case9-FA $F_{max.exp.}$ (FA130) is 20.23% higher than $F_{max.sim}$(Case9-FA) with μ=0.15.
					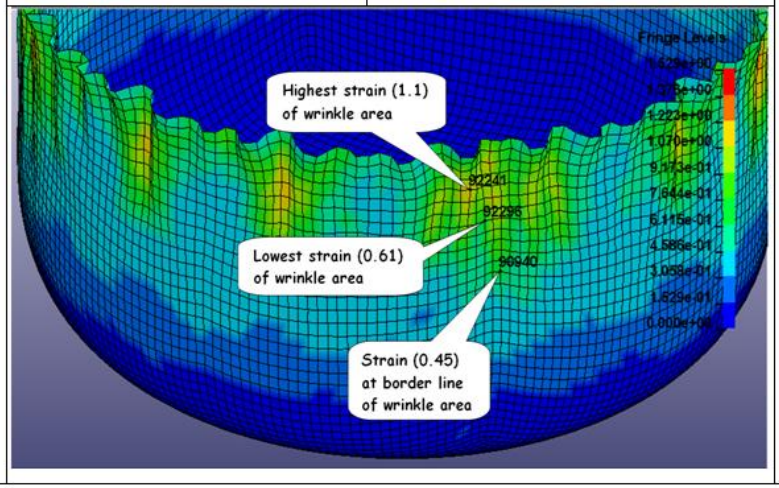			Strains on wrinkles area: (1) strain (0.45) at border line (between wrinkle area and circular/smooth area), (2) strain (0.61) as the lowest strain in a valley of the wrinkle area, and (3) strain (1.1) as the highest strain in a peak wrinkle area.

Table 6.3 Some typical simulation results for full set of simulations refer to the Appendix (continued)

No.	TB (μm)	DB (mm)	Data of simulation/file	μ	Contours of Von Mises stress (MPa)	Punch force-stroke curve	$F_{max.}$ (N)	Remarks
7	130	14	0.13_Case8_ARBSR Material: ARBSR TB=130μm DB=14 mm DP=7.93 mm RP=1.2 mm DD=8.35 mm RD=1.2 mm	0.10 0.15	0.13_Case8_ARBSR, μ=0.10 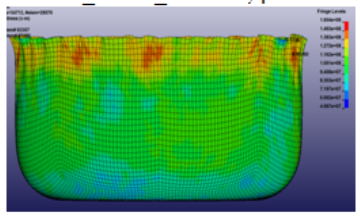 Time steps= 0.06 Min=49.87 (bottom) Max=160.4 (edge wall)	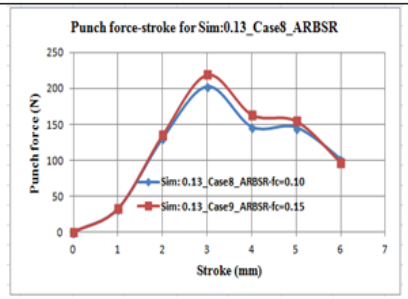	203 219	0.13_Case8_ARBSR 0.13_Case9_ARBSR $F_{max.sim.}$ with μ 0.10, 0.13_Case8_ARBSR is 7.3% lower than $F_{max.sim.}$ with μ 0.15, 0.13_Case9_ARBSR.
8	70	14	0.07_Case2_FA Material: FA TB=70μm DB=14 mm DP=8.08 mm RP=1.2 mm DD=8.35 mm RD=1.2 mm	0.10	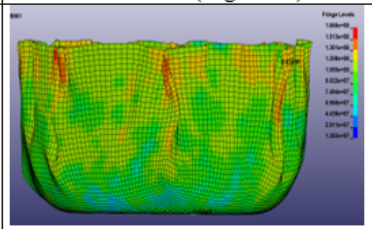 Time steps= 0.05 Min=13.83 (bottom) Max=166.6 (edge wall) 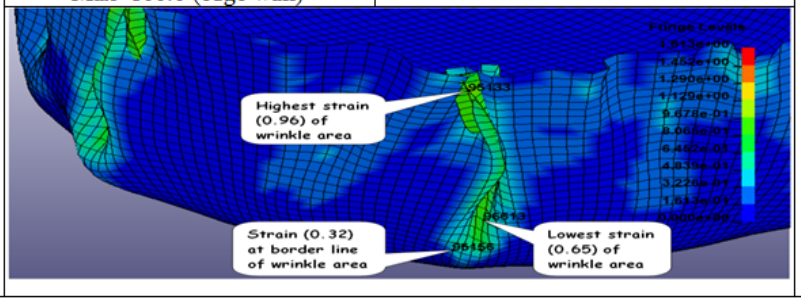	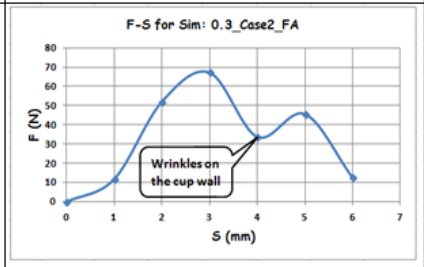	132	0.07_Case2_FA $F_{max.sim}$=67N, μ=0.10 Strains on wrinkle area: (1) strain (0.32) at border line (between wrinkle area and circular/smooth area), (2) strain (0.65) as the lowest strain in a valley wrinkle area, and (3) strain (0.96) as the highest strain in a peak wrinkle area.

Table 6.3 Some typical simulation results for full set of simulations refer to the Appendix (continued)

No.	TB (μm)	DB (mm)	Data of simulation/file	μ	Contours of Von Mises stress (MPa)	Punch force-stroke curve	$F_{max.}$ (N)	Remarks
1	2	3	4	5	6	7	8	9
9	300	14	0.3_Curve4_FA Material: FA TB=300μm DB=14 mm DP is shown in Fig. 5.14 in column of 7 RP=2 mm DD=8.35 mm RD=1.4 mm	0.10 0.12 0.14 0.16 0.18 0.18 0.20	0.07_Case2_FA, μ=0.10 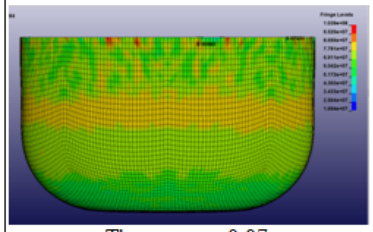 Time steps= 0.07 Min=16.94 (edge wall) Max=103.89 (edge wall)	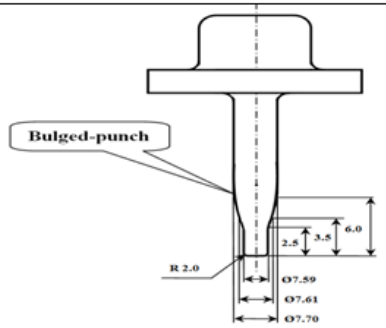 Fig. 5.15	751 859 979 1116 1262 1333	
					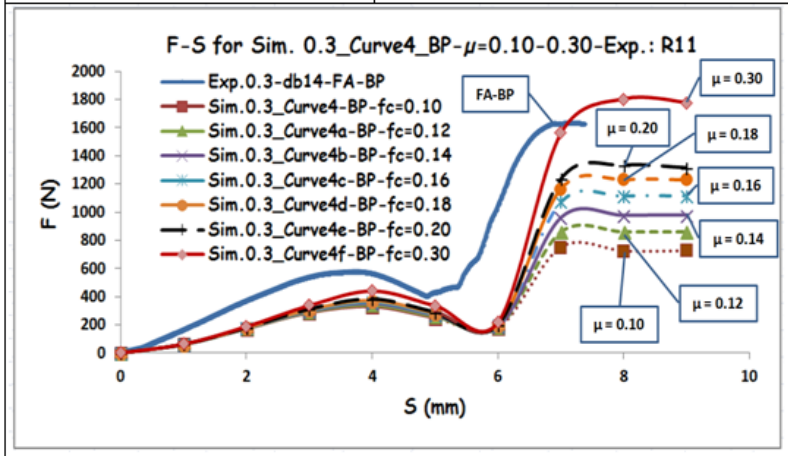		$F_{max.exp.}$ (FA-BP) = 1640 N is 23.03% higher than $F_{max.sim.}$(Curve4e) = 1333 N with μ=0.2. The experiment punch force is still higher than the simulation results is not only caused by friction, but also by ironing of the cup wall.

6.4 Simulation for deep drawing with fully annealed blank materials

6.4.1 Simulation for deep drawing FA blank materials with a TB=300 μm

The geometrical and physical parameters of deep drawing AA1235 blank material in an annealed condition are shown in Table 6.4. The parameters considered were the diameter of the blank, the corner radius of the punch and die, and the coefficient of friction. The simulated punch forces were compared to the experimental results, as shown in Fig. 6.11.

Table 6.4 Parameters of a deep drawing process for AA1235 blank material in the annealed condition and TB = 300 μm

No.	Geometrical parameter	Dimension (mm)							
		Case1	Case2	Case3	Case4	Case5	Case6	Case7	Case8
1	Diameter of blank (DB)	14	14	14	14	15	15	15	15
2	Corner radius of punch (RP)	1.2	1.2	2.5	2.5	1.2	1.2	2.5	2.5
3	Corner radius of die (RD)	1.2	1.4	1.2	1.4	1.2	1.4	1.2	1.4
	Physical parameter								
4	Friction coefficient (μ)	0.18	0.20	0.18	0.18	0.18	0.30	0.18	0.18
5	$F_{max.\ simulation}$, N	380	380	371	358	460	534	451	447
6	$F_{max.\ experiment}$, N	506	416	474	420	597	571	565	536
7	Sample code	E1	E2	E3	E4	E5	E6	E7	E8

Note: D_D = 8.35 mm, D_P = 7.54 mm, cl=(D_D-D_P)-2T_B = 0.16 mm, ρ = 2700 kg/m^3,
E = 80 GPa, YS = 74.18 MPa, ν = 0.3, V_{punch} = 100 mm/s.

For a TB of 300 μm, a simulation with DB of 14 and 15 mm was carried out. A RD and RP can be selected from the set of 1.2, 1.4, 1.2, and 2.5 mm.

6.4.1.1 Simulation for deep drawing FA materials with TB=300 μm, DB=14 mm

Case 1 to Case 8 simulations were carried out with an 8.35 diameter die and a 7.54 mm diameter punch.

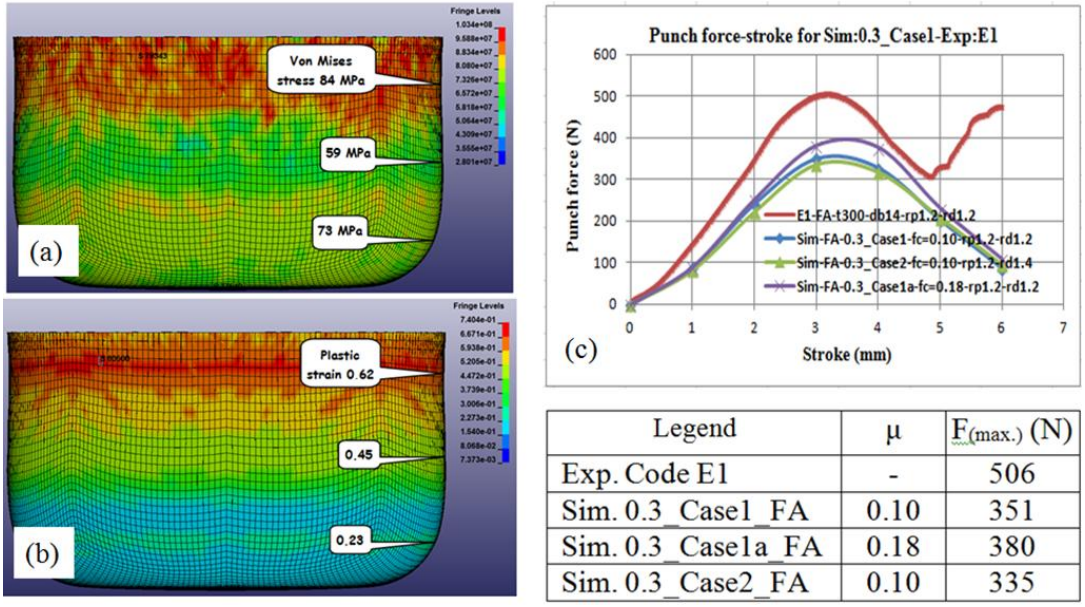

Legend	μ	$F_{(max.)}$ (N)
Exp. Code E1	-	506
Sim. 0.3_Case1_FA	0.10	351
Sim. 0.3_Case1a_FA	0.18	380
Sim. 0.3_Case2_FA	0.10	335

Fig. 6.11 Case 1 (a) Von Mises stress, (b) contours of effective plastic strain, and (c) simulated and experimental punch forces for different μ

In the Case 1 simulation, the corner radius of the punch and die was 1.2 mm. The values of Von Mises stress and strain results on the cup corner radius (73 MPa, 0.23), on the cup wall (59 MPa, 0.45), and on the cup edge (84 MPa, 0.62) are shown in Figs. 6.11a and 6.11b. The Von Mises stress respectively at the corner radius and on the cup edge were 23.7 and 42.4 % larger than the wall of the cup. The plastic strains of the cup corner radius were smaller than at the wall and the edge. The deformation on the cup corner radius was due to tension and on the edge of the cup, a compressive hoop stress, so the thickness on the cup corner radius experienced a reduction and on the edges of the cup, a thickening. The maximum simulated punch force (μ=0.18) was 24.9 % smaller than the measured value in Fig. 6.11c.

There was reduction in thickness in the cup corner radius for AA1235 material while deep drawing low carbon steel. The maximum Von Mises stress values in an experimental deep drawing process on low carbon steel with a blank diameter

between 90 and 114 mm resulted in a maximum reduction in blank thickness from 0.8 to 0.64 mm at the cup corner radius [193].

A μ of 0.10 and 0.18 was applied to 0.3_Case1_FA and the simulation results are shown in Fig. 6.11c. At μ = 0.10 a maximum punch force $F_{(max.sim.)}$ = 351 N was obtained, and it increased to 380 N (0.3_Case1a_FA) for μ = 0.18. They are still 24.9 % lower than the maximum punch force of 506 N from the experiment. A comparison of the simulation and experiment results for two die corner radii of 1.2 and 1.4 mm are shown in Fig. 6.11c, and indicate that with a larger die corner radius, the punch force required to form the cup will be reduced. These results were also in accordance with the simulation results for AA6061 which showed that the punch force required to form a cup would be reduced with a larger die corner radius [187].

The maximum punch force $F_{(max.sim)}$ = 351 N (0.3_Case1) was obtained for R_D = 1.2 mm compared with 335 N (0.3_Case2) with R_D = 1.4 mm. Both simulation results indicated that a larger die corner radius generates a lower punching force. A curve of the punch force-stroke of the experiment results showed a kick up in the force after a stroke 4.9 mm because the wrinkles were being ironed out.

For Case 2 (respective die and punch corner radius of 1.4 and 1.2 mm), the Von Mises stress and strain results are on the cup corner radius (73 MPa, 0.21), on the wall (66 MPa, 0.46), and on the edge (88 MPa, 0.60), as shown in Figs. 6.12a and 6.12b.

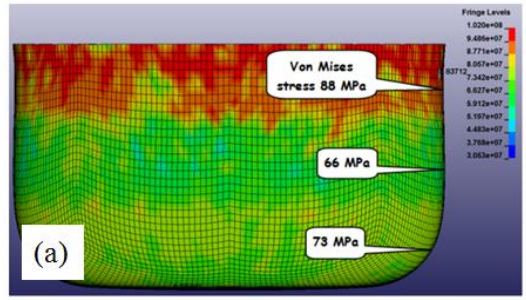

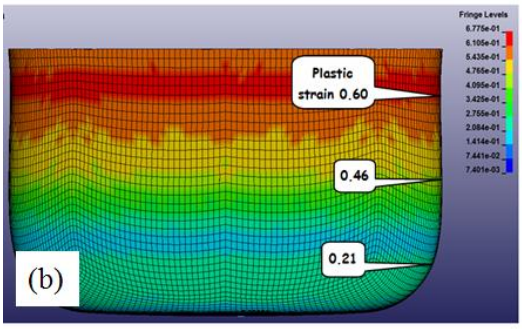

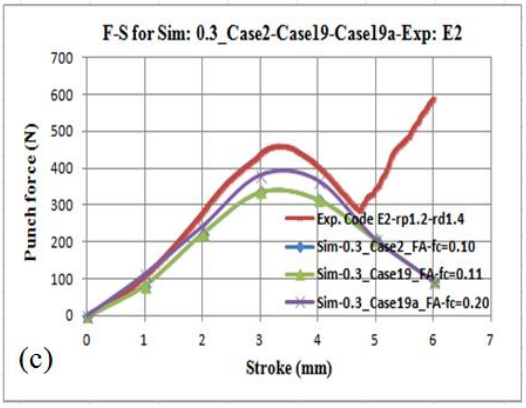

Legend	μ	$F_{(max.)}$ (N)
Exp. Code E2	-	461
Sim. 0.3_Case2_FA	0.10	335
Sim. 0.3_Case19_FA	0.11	335
Sim. 0.3_Case19a_FA	0.20	380

Fig. 6.12 Case 2 (a) Von Mises stress, (b) contours of effective plastic strain, and (c) simulated and experimental punch forces for different μ

The respective Von Mises stress at the corner radius and the edge of the cup were 33.3 and 10.6 % larger than at the wall. The maximum punch force with μ = 0.20 was 17.6 % smaller than the experiment, as shown in Fig. 6.12c.

The simulation results for a die corner radius of 1.2 mm and punch corner radius of 2.5 mm are shown in Figs. 6.13a and 6.13b. The Von Mises stress at the corner radius was 10.3 % larger than at the wall and 20.9 % larger at the edge than at the wall. The maximum punch force with μ = 0.18 was 13.8 % smaller than the experiment, as shown in Fig. 6.13c. Similar conclusions can also be made to the simulation results for a die corner radius of 1.4 mm and a punch corner radius of 2.5 mm, as shown in Figs. 6.14a and 6.14b.

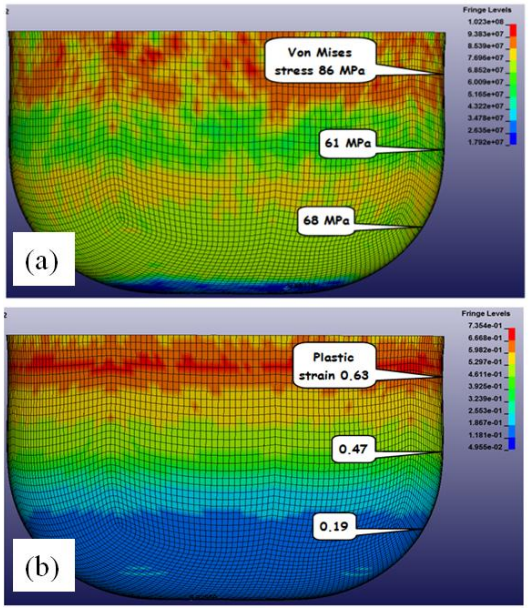

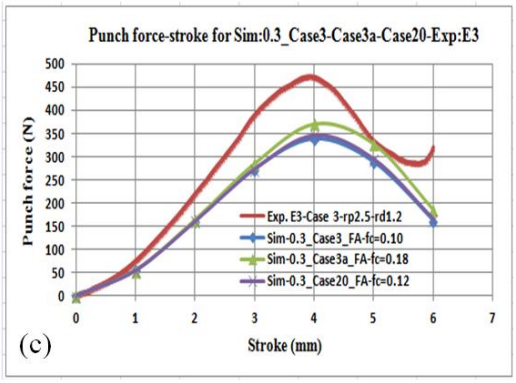

Legend	μ	$F_{(max.)}$ (N)
Exp. Code E3	-	474
Sim. 0.3_Case3_FA	0.10	338
Sim. 0.3_Case20_FA	0.12	347
Sim. 0.3_Case3a_FA	0.18	371

Fig. 6.13 Case 3 (a) Von Mises stress, (b) contours of effective plastic strain, and (c) simulated and experimental punch forces for different μ

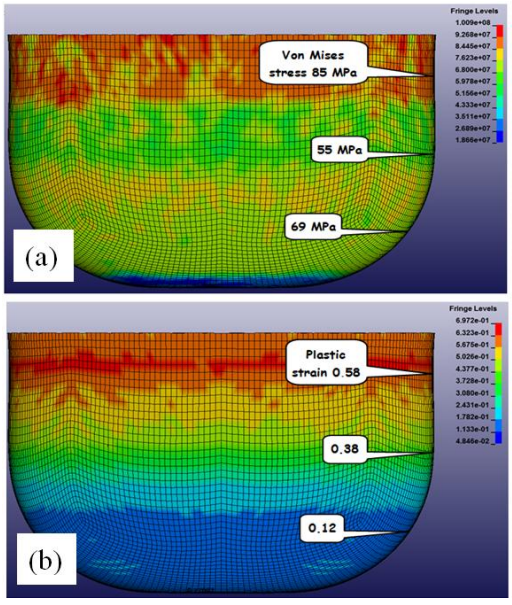

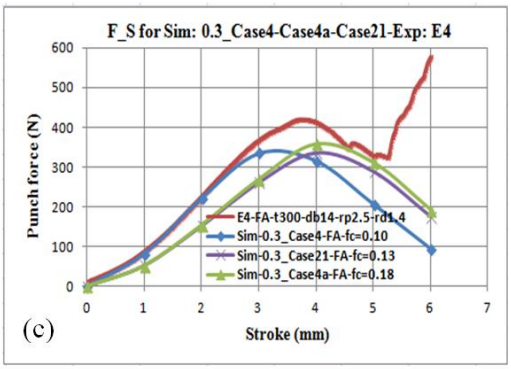

Legend	μ	$F_{(max.)}$ (N)
Exp. Code E4	-	420
Sim. 0.3_Case4_FA	0.10	325
Sim. 0.3_Case21_FA	0.13	336
Sim. 0.3_Case4a_FA	0.18	358

Fig. 6.14 Case 4 (a) Von Mises stress, (b) contours of effective plastic strain, and (c) simulated and experimental punch forces for different μ

6.4.1.2 Simulation for deep drawing FA materials with TB =300 μm, DB=15 mm

In the Case 5 simulation the punch and die corner radii were both 1.2 mm. The Von Mises stress and strain results on the corner radius of the cup (76 MPa, 0.18), on

the wall (63 MPa, 0.53), and on the edge (84 MPa, 0.69) are shown in Figs. 6.15a and 6.15b. The respective Von Mises stress at the corner radius and edges of the cup were 17.1 and 25.0 % larger than at the wall. The maximum simulated punch force with μ = 0.18 was 22.9 % smaller than the experiment, as shown in Fig. 6.15c.

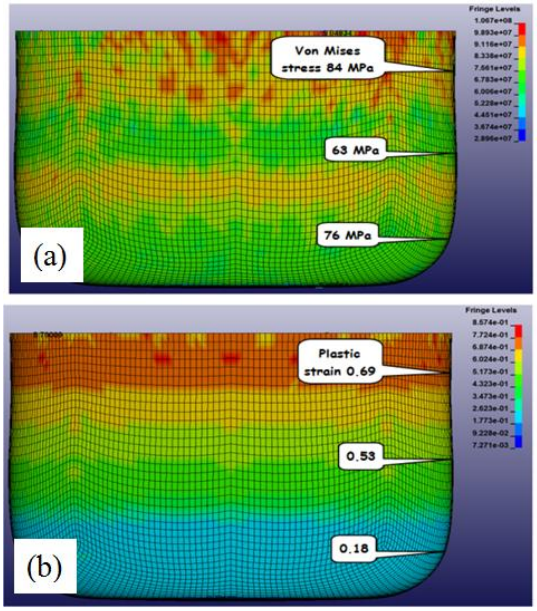

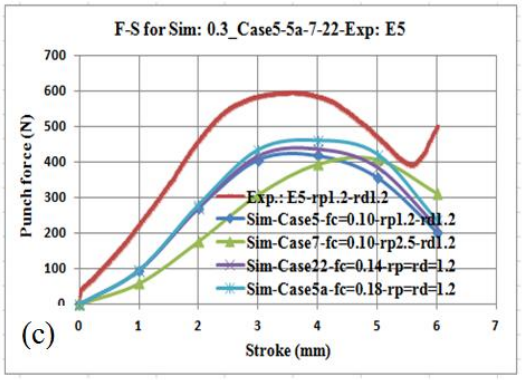

Legend	μ	$F_{(max.)}$ (N)
Exp. Code E5	-	597
Sim. 0.3_Case5_FA	0.10	352
Sim. 0.3_Case22_FA	0.14	437
Sim. 0.3_Case5a_FA	0.18	460

Fig. 6.15 Case 5 (a) Von Mises stress, (b) contours of effective plastic strain, and (c) simulated and experimental punch forces for different μ

Pure aluminium foil with a thickness of 20 μm and an LDR of 1.7 was simulated, and the results compared very well with the experiment when a friction coefficient of 0.17 was used [188]. The change in the corner radius of the punch and die by 10 % produced a small change between 0.41 and 1.44 % in the punch force, compared to the change in the clearance and diameter of the punch [188]. That assumption will be verified with further simulation.

The simulation results for a die corner radius of 1.4 mm and a punch corner radius of 1.2 mm are shown in Figs. 6.16a and 6.16b.

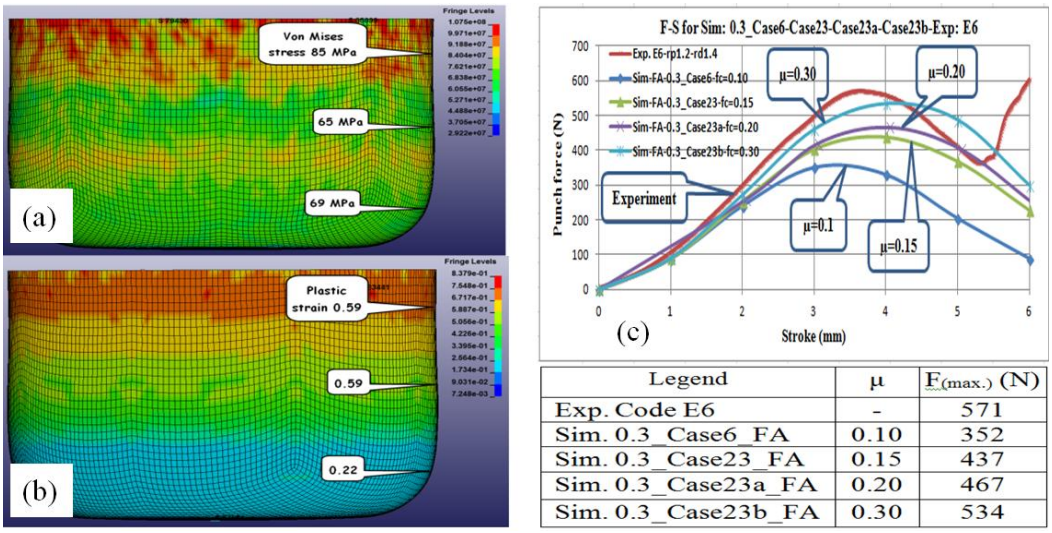

Legend	μ	$F_{(max.)}$ (N)
Exp. Code E6	-	571
Sim. 0.3_Case6_FA	0.10	352
Sim. 0.3_Case23_FA	0.15	437
Sim. 0.3_Case23a_FA	0.20	467
Sim. 0.3_Case23b_FA	0.30	534

Fig. 6.16 Case 6 (a) Von Mises stress, (b) contours of effective plastic strain, and (c) simulated and experimental punch forces for different μ

The simulated punch force with different friction values 0.10, 0.15, 0.20, and 0.30 (0.3_Case6_FA) are shown in Fig. 6.16. The experimental punch force $F_{(max.exp.)}$ = 571 N was 6.5 % higher than the simulated punch force at a μ of 0.3. The simulated punch forces were compared with the measured results, as shown in Fig. 6.16. The coefficient of friction μ = 0.30 (Case23b) showed the best match between simulation and experiment, but in this thesis, μ = 0.30 was high for a lubricated condition. However, an un-lubricated deep drawing was carried out on low carbon steel foil (thickness 0.2 mm) with a semi-active control of BHF to prevent wrinkles and cracking, the appropriate coefficient of friction was μ = 0.4 [189].

The results of a simulation of fully annealed AA1235 with a 15 mm diameter blank, RD = 1.2 mm and RP = 2.5 mm are shown in Figs. 6.17a and 6.17b.

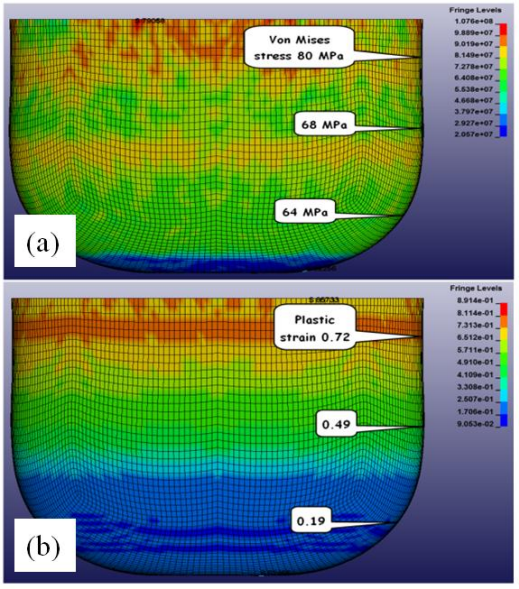

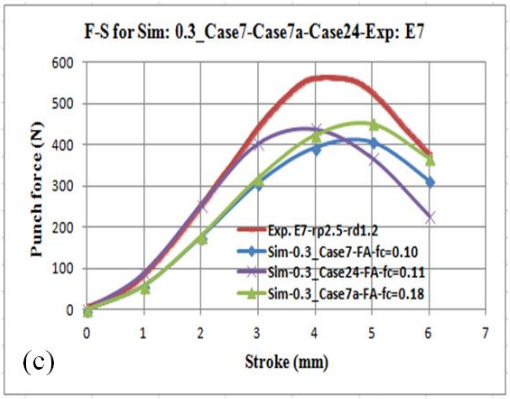

Legend	μ	$F_{(max.)}$ (N)
Exp. Code E7	-	565
Sim. 0.3_Case7_FA	0.10	352
Sim. 0.3_Case24_FA	0.11	437
Sim. 0.3_Case7a_FA	0.18	451

Fig. 6.17 Case 7 (a) Von Mises stress, (b) contours of effective plastic strain, and (c) simulated and experimental punch forces for different μ

A μ of 0.10, 0.11 and 0.18 were applied in the simulation on 0.3_Case7_FA, as shown in Fig. 6.17. For μ = 0.18 $F_{(max.sim.)}$ is 451 N (0.3_Case7a_FA). In this case the measured punch force $F_{(max.exp.)}$ = 565 N (Code E7) was 25.3 % lower. The punch force from the simulation and experiment are shown in Fig. 6.17c.

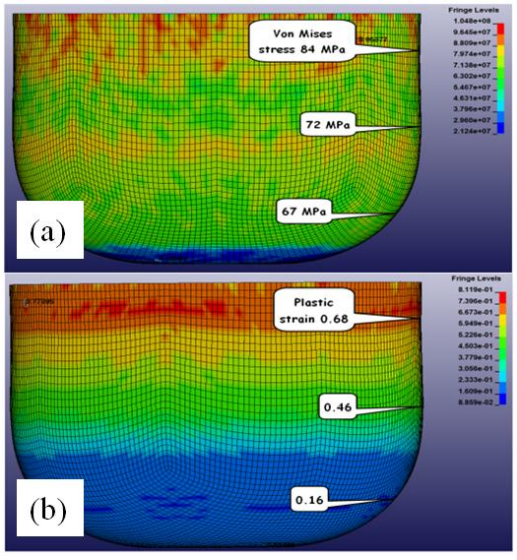

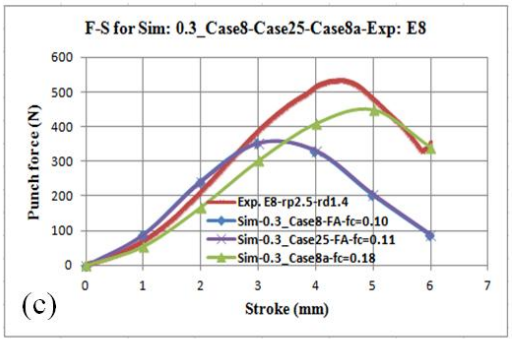

Legend	μ	$F_{(max.)}$ (N)
Exp. Code E8	-	536
Sim. 0.3_Case8_FA	0.10	352
Sim. 0.3_Case25_FA	0.11	352
Sim. 0.3_Case8a_FA	0.18	447

Fig. 6.18 Case 8 (a) Von Mises stress, (b) contours of effective plastic strain, and (c) simulated and experimental punch forces for different μ

The simulation with an RD = 1.4 and RP = 2.5 mm are shown in Figs. 6.18a and 6.18b.

In Fig. 6.18, the μ = 0.18 brings a closer agreement to the measurement. There was almost no difference in the force for μ = 0.10 and 0.11. The maximum punch force, $F_{(max.exp.)}$ = 536 N (Code E8) was 16.6 % higher than $F_{(max.sim.)}$. The effects of μ, RP, RD parameters in a deep drawing process are shown in Table 6.5.

Table 6.5 Effect of μ, RP, RD parameters in a deep drawing process for TB = 300 μm to the punch force

No.	Parameter	Dimension (mm)							
		Case1	Case2	Case3	Case4	Case5	Case6	Case7	Case8
1	Diameter of blank (DB)	14	14	14	14	15	15	15	15
2	Corner radius of punch (RP)	1.2	1.2	2.5	2.5	1.2	1.2	2.5	2.5
3	Corner radius of die (RD)	1.2	1.4	1.2	1.4	1.2	1.4	1.2	1.4
4	Friction coefficient (μ)	0.18	0.20	0.18	0.18	0.18	0.30	0.18	0.18
5	$F_{max.\ simulation}$, N	380	380	371	358	460	534	451	447
6	$F_{max.\ experiment}$, N	506	416	474	420	597	571	565	536
7	Ratio of $F_{max.}$ exp./sim.	1.3	1.1	1.3	1.2	1.3	1.1	1.3	1.2
8	Sample code	E1	E2	E3	E4	E5	E6	E7	E8

All measured punch forces were higher than the simulation results due to wrinkles on the wall of the cup. The punch needed more force to press out the wrinkles while forming a full cup. In the simulation it was assumed that the blank material was isotropic and the wall thickening due to wrinkles was ignored.

A comparison of the wall thickness from the simulation and measurements for an initial TB of 300 μm from the centre point at the bottom of the cup to the edge is shown as Fig. 6.19.

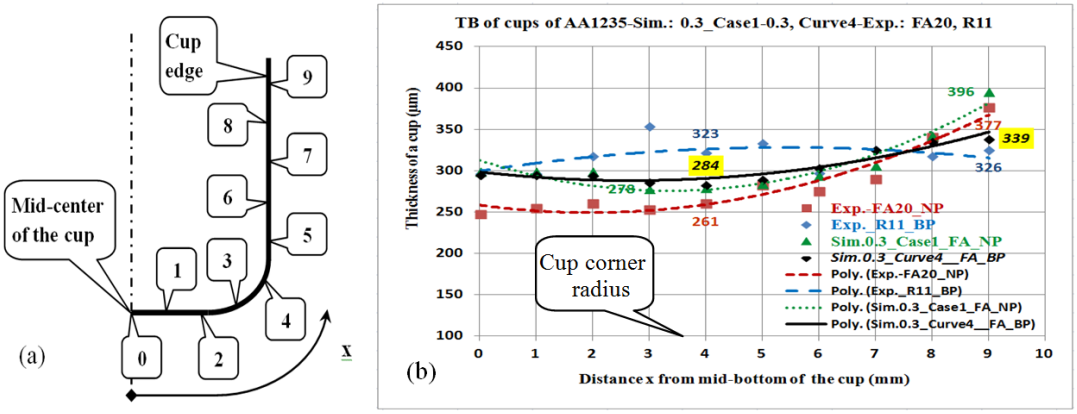

Fig. 6.19 (a) Cup thickness locations, and (b) thickness distribution from simulation and experiment

It can be seen that the wall of the simulated cup was thicker than those measured from the bottom, but they agreed with those on the wall. The maximum wall thickness of 394 µm was compared to the measured value of 377 µm. Both these results were higher than the edge thickness of 326 µm that resulted from a bulged punch.

At the corner radius located between 3 and 5 mm from the axis of the cup, there was a difference in the thickness of the wall. The simulation and experiment show a reduction in thickness in the wall, and while a bulged punch resulted in a thicker wall, there was less chance of the cup tearing at the corner radius than when a normal punch was used.

6.4.2 Simulation for deep drawing with FA blank materials with TB=130 µm

In this section a simulation were carried out for a 130 µm thick blank. The geometrical and physical parameters are shown in Table 6.6. The simulated results are shown in Figs. 6.20a and 6.20b. Around the edge of the cup there was a wrinkled and partly distorted edge at element 82140, as shown in Fig. 6.20a. The difference between the measured punch force and the simulated results was due to an

excessively large plastic strain at the edge of the cup, and the FEM model with simple elements and mesh size could not simulate the real case. The choices of element and mesh size were moderated by the significant computational time required for each case.

A μ of 0.10 and 0.15 were used in the simulation on 0.13_Case1_FA, and the results are shown in Fig. 6.20c. For a μ = 0.15, the maximum punch force $F_{(max.sim.)}$ of 351 N (0.13_Case9_FA) was 20.2 % lower than the measured force. In Fig. 6.20c it appears that the curve with μ = 0.10 does not form a smooth curve, which probably indicates there was a wrinkle on the wall of the cup. There was also a wrinkle in a simulation with LS-DYNA on an Aluminium alloy foils that were 0.15 and 0.10 mm thick, respectively [10].

Table 6.6 Geometrical and physical parameters for AA1235 material in FA-condition

No.	Geometrical parameter	Dimension (mm)	Physical parameter	Value
1	Thickness of blank (TB)	130	ρ, kg/m^3	2700
2	Diameter of blank (DB)	14	E, GPa	80
3	Diameter of die (DD)	8.35	YS, MPa	74.18
4	Diameter of punch (DP)	7.93	ν	0.3
5	Punch Corner radius (RP)	1.2	Punch speed, mm/s	100
6	Die corner radius (RD)	1.2	μ	0.10, 0.15
7	Radial clearance, cl=(DD-DP)-2TB	0.21	$F_{max.\ simulations}$, N	146, 351
8	Sample code	FA-130	$F_{max.\ experiment}$, N	440

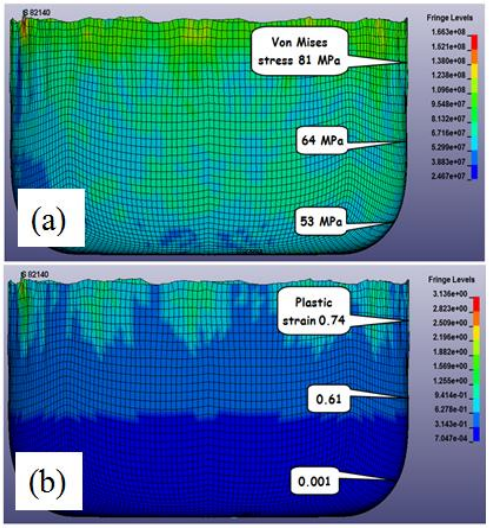

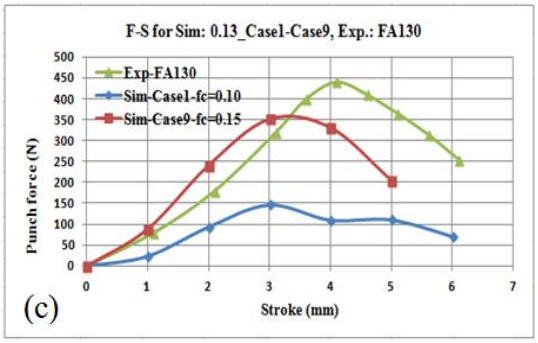

Legend	μ	$F_{(max.)}$ (N)
Exp. Code FA-130	-	440
Sim. 0.13_Case1_FA	0.10	146
Sim. 0.13_Case9_FA	0.15	351

Fig. 6.20 Von Mises stress in AA1235 with FA-conditions for TB = 130 μm and DB = 14 mm (0.13_Case1_FA)

6.4.3 Effect of the stress, strain, and coefficient of friction on the wrinkles

The formation of wrinkles is correlated to the stress, strain, and μ as shown in Table 6.7. The parameters used were DB of 14 and 15 mm, RP and RD of 1.2 mm, and μ of 0.1

Table 6.7 Effects of stress and strain against the formation of cup wrinkles in a deep drawing process

No.	Condition	TB (μm)	DB (mm)	Case files	μ	c	Maximum stress (MPa)	Maximum strain	Wrinkles	
1	FA	300	14	0.3_Case1_FA	0.1	0.21	103.43	0.740		N
2	ARBSR	300	14	0.3_Case10_ARBSR	0.1	0.21	132.96	0.725		N
3	FA	150	14	Microforming_.15	0.1	0.46	98.66	1.282	Y	
4	FA	130	14	0.13_Case1_FA	0.1	0.16	166.3	3.136	Y	
5	ARBSR	130	14	0.13_Case8_ARBSR	0.1	0.16	160.40	1.478	Y	
6	FA	70	14	0.07_Case2_FA	0.1	0.13	169.01	1.613	Y	
7	FA	300	15	0.3_Case5_FA	0.1	0.21	106.7	0.857		N
8	ARBSR	300	15	0.3_Case14_ARBSR	0.1	0.21	137.57	0.894		N
9	FA	130	15	0.13_Case3_FA	0.1	0.16	110.1	2.128	Y	
10	ARBSR	130	15	0.13_Case6_ARBSR	0.1	0.16	151.14	1.147	Y	
11	FA	300	14	0.3_Case18_FA	0.11	0.21	103.52	0.741		N
12	ARBSR	300	14	0.3_Case18_ARBSR	0.18	0.21	132.64	0.729		N
13	FA	130	14	0.13_Case9_FA	0.15	0.16	79.56	1.529	Y	
14	ARBSR	130	14	0.13_Case9_ARBSR	0.15	0.16	157.21	1.574	Y	

Note: *N: no wrinkles on any cup wall, Y: wrinkles on the cup wall.

Table 6.7 shows that all the cups that were 300 μm thick did not have wrinkles in the wall, but when the thicknesses of 150, 130, and 70 μm were used, wrinkles

formed on all the walls because the cups experienced a strain greater than 0.7. A more detailed observation of the 150 µm thick blank (case of Microforming_.15) is shown in Fig. 6.21. A strain of 0.27 was obtained where the wrinkles began in Fig. 6.21. The lowest strain on the wrinkles area was 0.39 and the highest was 0.90.

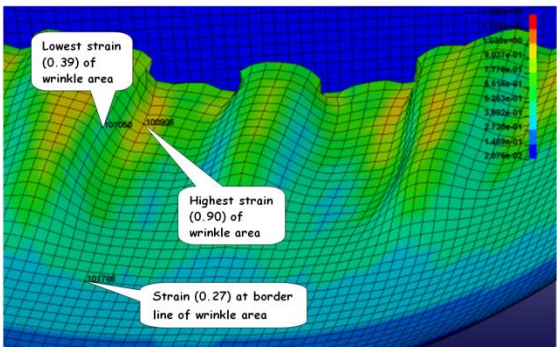

Fig. 6.21 Wrinkles occur in the cup wall on a blank thickness of 150 µm (case of Microforming_.15)

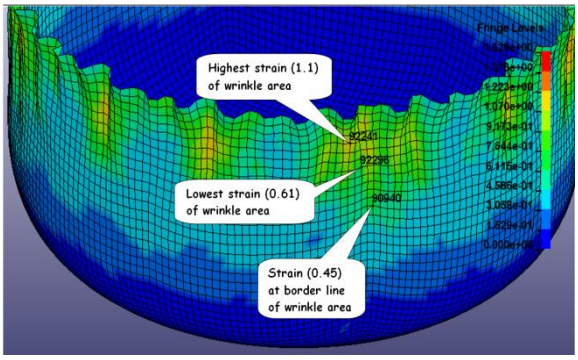

Fig. 6.22 Wrinkles occur in the cup wall on a blank thickness of 130 µm (case of 0.13_Case9_FA)

Wrinkles on 130 µm thick blanks (case of 0.13_Case9_FA) are shown in Fig. 6.22.

The mid-wall position where the wrinkles began had a strain of 0.45. The lowest strain on the wrinkles area was 0.61 and the highest was 1.10. A wrinkle on the 70 µm thick blanks (case of 0.07_Case2_FA) is shown in Fig. 6.23. The range of strain was 0.65-0.96.

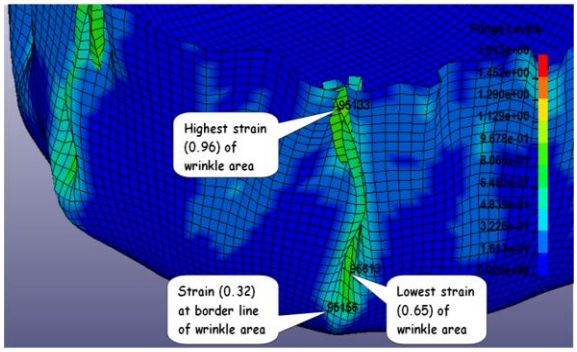

Fig. 6.23 Wrinkles occur in the cup wall, on a blank thickness of 70 µm (case of 0.07_Case2_FA)

Blanks that were 130 and 150 µm thick experienced wrinkles on the edge of the cup, but blank that were 70 µm thick experienced wrinkles over the entire wall.

There was no observed relationship between µ and stress, but at the highest µ of 0.18, as shown in Table 6.7 for the case (0.3_Case18_ARBSR), the maximum stress was 132.64 MPa. The highest stress of 169 MPa was achieved by a µ of 0.1, as in the case (0.07_Case2_FA). At a minimum strain of about 0.4, wrinkles began to occur on a wall of a blank that was 150 µm thick, with a clearance of 0.46 mm (case of Microforming_.15); at a minimum strain of about 0.6, wrinkles begin to occur on a wall of a blank that was 130 µm thick, with a clearance of 0.16 mm (case of 0.13_Case9_FA); and at a minimum strain of about 0.65, wrinkles occurred on a wall of a blank 70 µm thick, with a clearance of 0.13 mm (case of 0.07_Case2_FA). The wrinkles were caused not only by the minimum strains but also by the given clearance value.

The degree to which selected parameters affected the behaviour of the circular cup drawing for AA6061 material was influenced by an RD of approximately 67 %, a BHF of approximately 29 %, and an RP of about 9 % [190].

Seven parameters were considered for deep drawing steel (CR1) with blank size (DB) of ø72.28 mm and thickness of 0.9 mm. They were the punch corner radius, the die corner radius, the BHP, the punch force, punch speed, type of lubricant, and the lubrication positions of both sides, from the side of the die and punch. The optimal level of deep drawing on AA6061 was achieved by a punch corner radius of 4 mm, a die corner radius of 6 mm, a BHF of 80 kN, Poly Ethylene (PE) lubricants and lubrication positions of both sides of the blank [190].

The BHP was strongly influenced by the thickness of the blank and μ, such that the wrinkle problem can be improved as the thickness of the blank is reduced. The LDR can be reduced when the blank thickness is reduced, but when a blank is very thin, the LDR is strongly influenced by μ [117].

6.5 Deep drawing simulation with ARB and subsequent SR blank materials

6.5.1 Deep drawing simulation with ARBSR materials with TB=300 μm

The geometrical and physical parameters of deep drawing for AA1235 material processed by accumulated roll bonding followed by stress relieving (ARBSR) is shown in Table 6.8.

Table 6.8 Geometrical and physical parameters of a deep drawing process for AA1235 blank material in the ARBSR condition and TB = 300 µm

No.	Geometrical parameter	Dimension (mm)							
		Case10	Case11	Case12	Case13	Case14	Case15	Case16	Case17
1	DB	14	14	14	14	15	15	15	15
2	RP	1.2	1.2	2.5	2.5	1.2	1.2	2.5	2.5
3	RD	1.2	1.4	1.2	1.4	1.2	1.4	1.2	1.4
	Physical parameter								
4	µ	0.10, 0.18, 0.30	0.10, 0.18	0.10, 0.18	0.10, 0.18	0.10, 0.18, 0.30	0.10, 0.18	0.10, 0.18	0.10, 0.18
5	$F_{max.\ simulation}$, N	474, 517, 625	452, 498	456, 502	439, 484	550, 625, 722	550, 615	536, 611	530, 572
6	$F_{max.\ experiment}$, N	560				803			
7	Sample code	G52				G11			

Note: DD = 8.35 mm, DP = 7.54 mm, cl=(DD-DP)-2TB = 0.16 mm, ρ = 2700 kg/m^3, E = 80 GPa, YS = 104 MPa, ν = 0.3, V_{punch} = 100 mm/s.

6.5.1.1 Deep drawing simulation of ARBSR-materials with TB=300µm, DB=14mm

A simulation for AA1235 material on ARBSR condition with an RD and RP of 1.2 mm. The simulation results are shown in Figs. 6.24a and 6.24b.

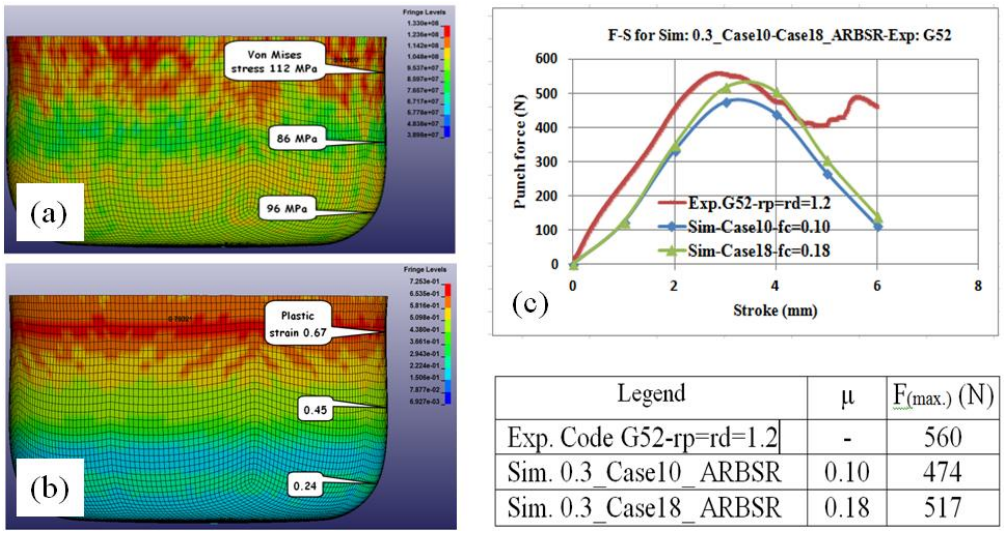

Legend	µ	$F_{(max.)}$ (N)
Exp. Code G52-rp=rd=1.2	-	560
Sim. 0.3_Case10_ARBSR	0.10	474
Sim. 0.3_Case18_ARBSR	0.18	517

Fig. 6.24 Case 10 (a) Von Mises stress, (b) contours of effective plastic strain, and (c) simulated and experimental punch forces for different µ

Fig. 6.24 shows the results obtained with a μ of 0.10 and 0.18. Where μ = 0.18 the maximum punch force $F_{(max.sim.)}$ was 517 N (0.3_Case18_ARBSR) which was 7.7 % lower than the measured punch force of 560 N. The punch force from the simulation and experiment are shown in Fig. 6.24c.

A simulation with RP of 1.2 and RD of 1.4 mm is shown in Figs. 6.25a and 6.25b.

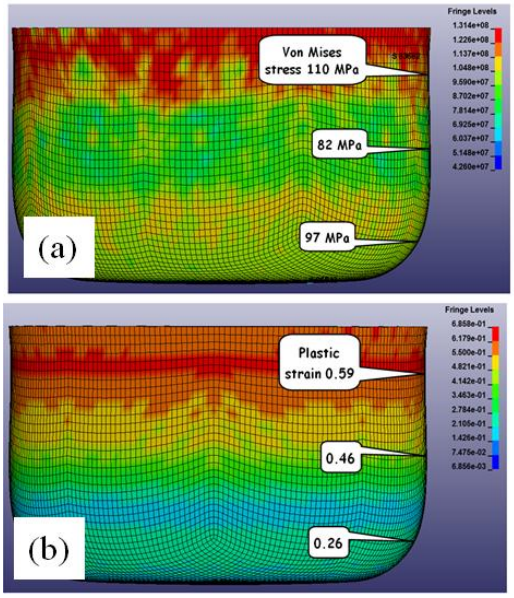

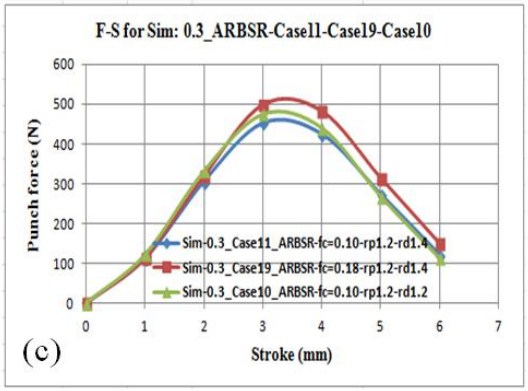

Legend	μ	$F_{(max.)}$ (N)
Sim. 0.3_Case11_ARBSR-RP1.2-RD1.4	0.10	452
Sim. 0.3_Case10_ARBSR-RP1.2-RD1.2	0.10	474
Sim. 0.3_Case19_ARBSR-RP1.2-RD1.4	0.18	517

Fig. 6.25 Case 11_ARBSR (a) Von Mises stress, (b) contours of effective plastic strain, and (c) simulated and experimental punch forces for different μ

The simulation results for the 0.3_Case11_ARBSR with a μ of 0.10 and 0.18 are shown in Fig. 6.25. Where μ = 0.10, the maximum punch force of 452 N for Case11_ARBSR with RP = 1.2 and RD = 1.4 mm was lower than $F_{(max.sim.)}$ = 474 N of Case10_ARBSR with R_P and R_D of 1.2 mm. As Fig. 6.25c shows, it appears that by increasing the RD, the required maximum punch force was lower, and when an RD of 1.2 was increased to 1.4 mm, the maximum punch force required was reduced by 22 N or 4.6 %. For a higher friction μ = 0.18 for Case19_ARBSR the maximum punch force, $F_{(max.sim.)}$ = 517 N was obtained.

A simulation was carried out for deep drawing with an RP of 2.5 and an RD of 1.2 mm. The simulation results are shown in Figs. 6.26a and 6.26b. The results for an RD of 1.4 mm from Fig. 6.27 do not differ much from those from Fig. 6.26 with RD of 1.2 mm. In Fig. 6.27 for Case13_ARBSR with RP = 2.5 and RD = 1.4 mm, a maximum punch force F of 439 N was obtained with μ = 0.10, and 484 N for μ = 0.18, a 9.3 % increase.

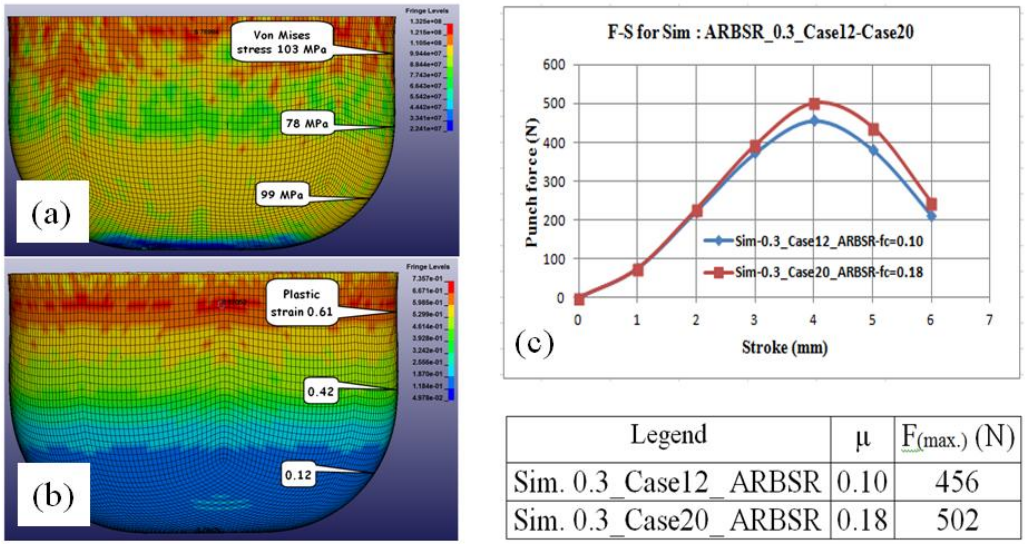

Legend	μ	$F_{(max.)}$ (N)
Sim. 0.3_Case12_ARBSR	0.10	456
Sim. 0.3_Case20_ARBSR	0.18	502

Fig. 6.26 Case 12_ARBSR (a) Von Mises stress, (b) contours of effective plastic strain, and (c) simulated and experimental punch forces for different μ

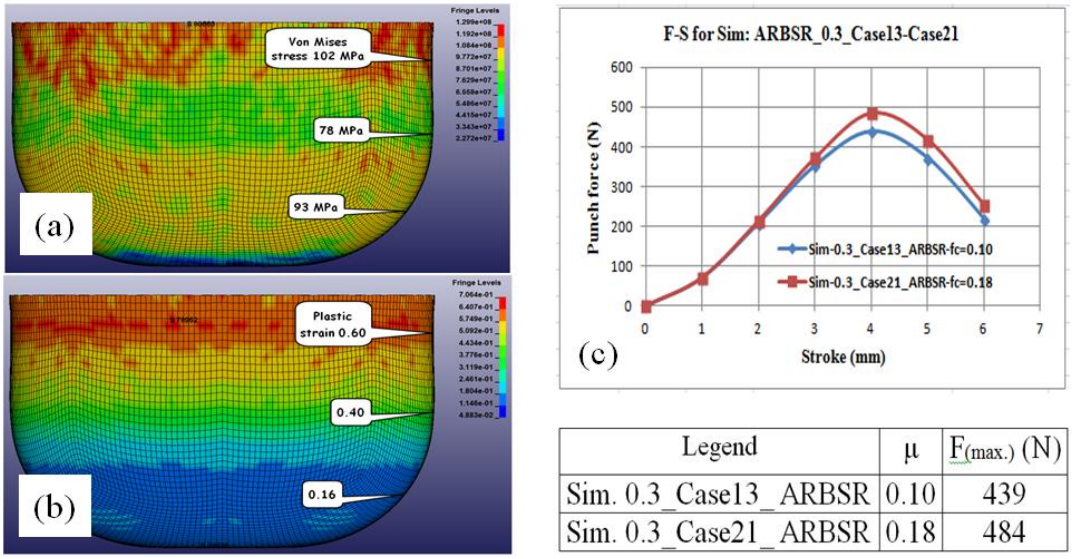

Legend	μ	$F_{(max.)}$ (N)
Sim. 0.3_Case13_ARBSR	0.10	439
Sim. 0.3_Case21_ARBSR	0.18	484

Fig. 6.27 Case 13_ARBSR (a) Von Mises stress, (b) contours of effective plastic strain, and (c) simulated and experimental punch forces for different μ

6.5.1.2 Deep drawing simulation with ARBSR materials, TB=300μm, DB=15mm

The simulation results for AA1235 material processed under ARBSR conditions with an RP and RD of 1.2 mm are shown in Figs. 6.28a and 6.28b.

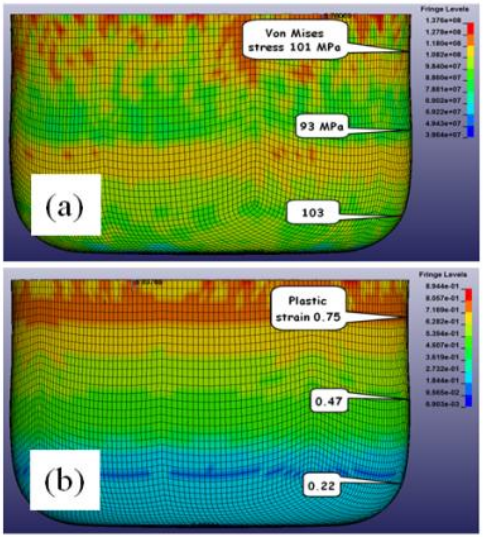

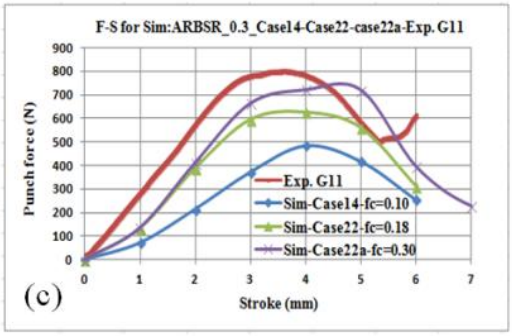

Legend	μ	$F_{(max.)}$ (N)
Sim. 0.3_Case14_ARBSR	0.10	556
Sim. 0.3_Case22_ARBSR	0.18	625
Sim. 0.3_Case22a_ARBSR	0.30	722

Fig. 6.28 Case 14_ARBSR (a) Von Mises stress, (b) contours of effective plastic strain, and (c) simulated and experimental punch forces for different μ

When the μ changed from 0.10 to 0.18, the maximum punch force increased by 11 %, Fig. 6.28c. Where μ = 0.30 in Case22a_ARBSR, the measured punch force was 10.1 % higher than the corresponding simulated value.

The simulation results for the respective RP and RD of 1.2 and 1.4 mm are shown in Figs. 6.29a and 6.29b. The results of the stress, strain, and punch force differed little from those in Fig. 6.29. The maximum punch force increased by 10.6 % when μ changed from 0.10 to 0.18.

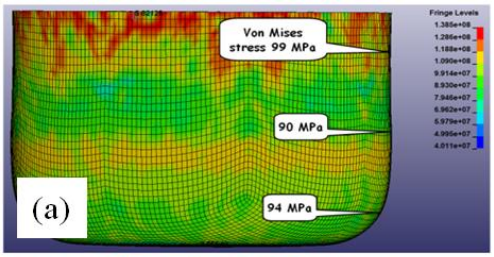

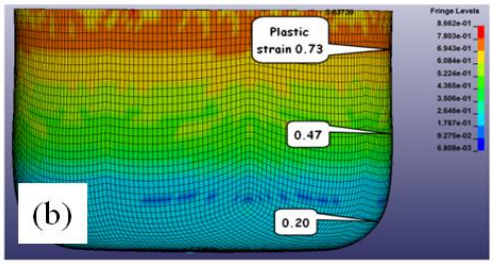

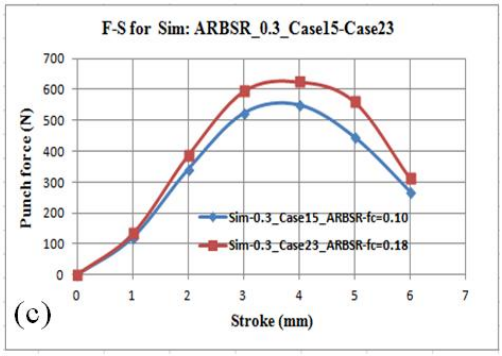

Legend	μ	$F_{(max.)}$ (N)
Sim. 0.3_Case15_ARBSR	0.10	550
Sim. 0.3_Case23_ARBSR	0.18	615

Fig. 6.29 Case 15_ARBSR (a) Von Mises stress, (b) contours of effective plastic strain, and (c) simulated and experimental punch forces for different μ

A simulation of deep drawing with AA1235 material on ARBSR condition used an RP of 2.5 and an RD of 1.2 mm. The simulation results are shown in Figs. 6.30a and 6.30b. The strain at the corner radius region was smaller with a larger RP of 2.5mm compared to an RD of 1.2 mm. With μ increased from 0.10 to 0.18, the required maximum punch force was 12.3 % higher, as shown in Fig. 6.30.

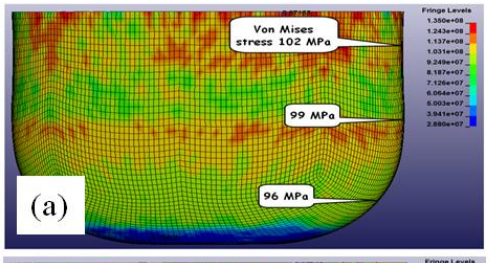

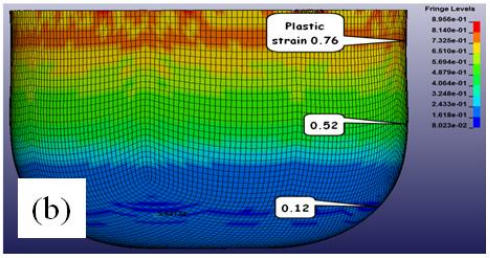

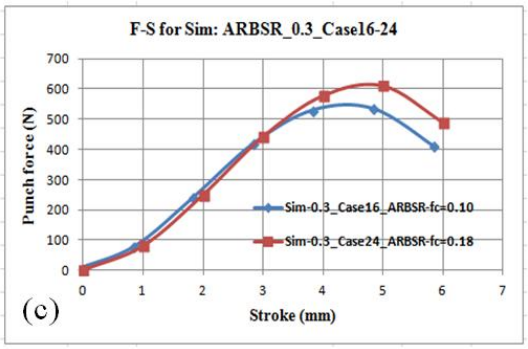

Legend	μ	$F_{(max.)}$ (N)
Sim. 0.3_Case16_ARBSR	0.10	536
Sim. 0.3_Case24_ARBSR	0.18	611

Fig. 6.30 Case 16_ARBSR (a) Von Mises stress, (b) contours of effective plastic strain, and (c) simulated and experimental punch forces for different μ

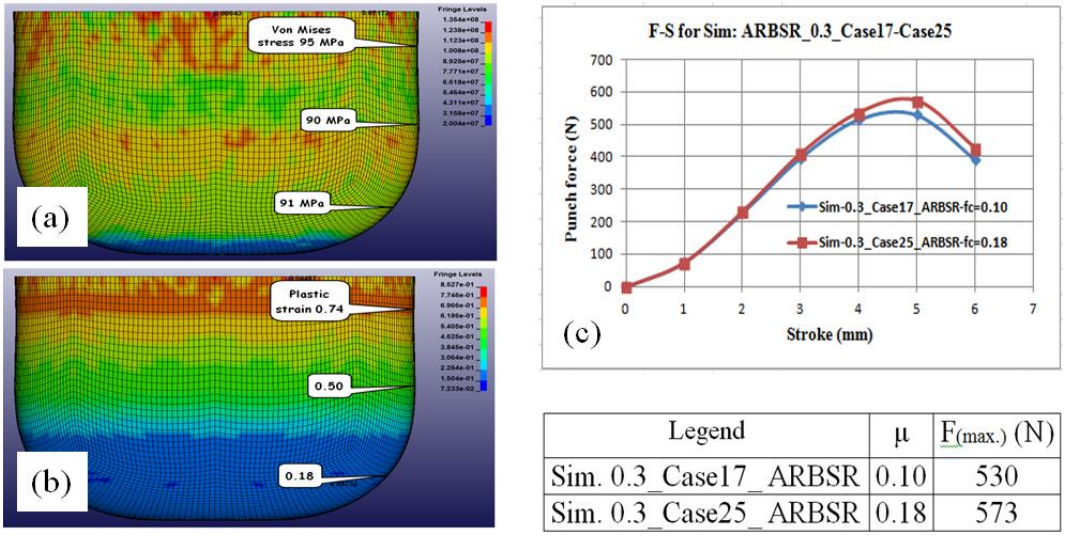

Legend	μ	$F_{(max.)}$ (N)
Sim. 0.3_Case17_ARBSR	0.10	530
Sim. 0.3_Case25_ARBSR	0.18	573

Fig. 6.31 Case 17_ARBSR (a) Von Mises stress, (b) contours of effective plastic strain, and (c) simulated and experimental punch forces for different μ

The simulation results for an RP of 2.5 and an RD of 1.4 mm are shown in Figs. 6.31a and 6.31b. The maximum punch force was only 7.3 % higher when μ increased from 0.10 to 0.18, as shown in Fig. 6.31c.

6.5.2 Deep drawing simulation with ARBSR blank thickness of 130 μm

Simulations for AA1235 material in an ARBSR condition with 130 μm thick blanks were carried out for two cases because the simulation showed wrinkles on the edge of the cup. The geometrical and physical parameters for AA1235 material in an ARBSR condition with a TB=130 μm are shown in Table 6.9.

Table 6.9 Geometrical and physical parameters for AA1235 in the ARBSR condition and TB = 130 µm

No.	**Geometrical parameter**	**Dimension (mm)**	**Physical parameter**	Values
1	TB	130	ρ, kg/m^3	2700
2	DB	14	E, GPa	80
3	DD	8.35	YS, MPa	74.18
4	DP	7.93	ν	0.3
5	RP	1.2	Punch speed, mm/s	100
6	RD	1.2	µ	0.10, 0.15
7	Radial clearance, c=(DD-DP)-2TB	0.21	$F_{max.\ simulations}$, N	146, 351
8	Sample code	FA-130	$F_{max.\ experiment}$, N	440

Figs. 6.32a and 6.32b show the simulation results carried out for deep drawing with AA1235 material processed by ARB and stress relieved, with a DB of 14 and a TB of 130 µm, while using an RD of 1.2 and an RP of 1.2 mm. When µ increased from 0.10 to 0.15, the required maximum punch force increased by 7.3 %, as shown in Fig. 6.32c, although there was little difference between the punch force curves. Fig. 6.32c shows a change in the slope of the punch force curves at a punch stroke of 4 mm where wrinkles have begun to form on the walls of the cup.

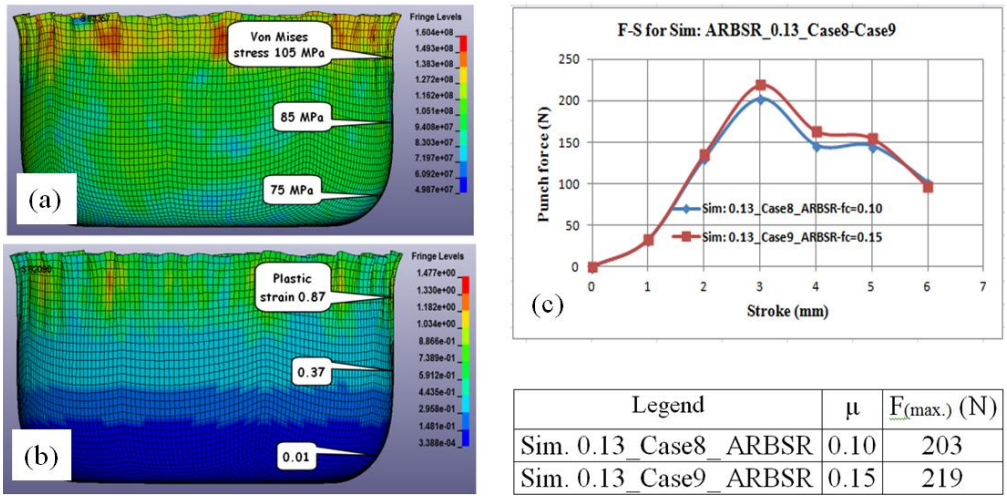

Legend	µ	$F_{(max.)}$ (N)
Sim. 0.13_Case8_ARBSR	0.10	203
Sim. 0.13_Case9_ARBSR	0.15	219

Fig. 6.32 Case 8_ARBSR (a) Von Mises stress, (b) contours of effective plastic strain, and (c) simulated and experimental punch forces for different µ

6.6 Deep drawing simulation using a bulged punch with FA blank and TB = 300 µm

A model (20084 elements and 25337 nodes) was built to simulate deep drawing using a bulged punch for AA1235 in a fully annealed condition, and with a DB of 14 mm, a TB of 300 µm, and an RD and RP of 1.2 and 1.4 mm, respectively. The geometrical and physical parameters for simulating deep drawing are shown in Table 6.10. The results using a µ of 0.12 are shown in Figs. 6.33a and 6.33b.

Table 6.10 Geometrical and physical parameters of a deep drawing process using a bulged punch for AA1235 blank in FA condition and TB = 300 µm

No.	Geometrical parameter	Dimension (mm)
		Curve4
1	DB	14
2	RP	1.2
3	RD	1.4
	Physical parameter	
4	Friction coefficient, µ	0.10, 0.12, 0.14, 0.16, 0.18, 0.20
5	$F_{max.\ simulation}$, N	1333 for µ=0.20
6	$F_{max.\ experiment}$, N	1640
7	Sample code	R11

Note: DD = 8.35 mm, DP as Fig. 5.13 (Chapter 5), cl=(DD-DP)-2TB=0.005mm, ρ=2700 kg/m^3, E= 0 GPa, YS=74.18 MPa, ν=0.3, V_{punch}=100 mm/s.

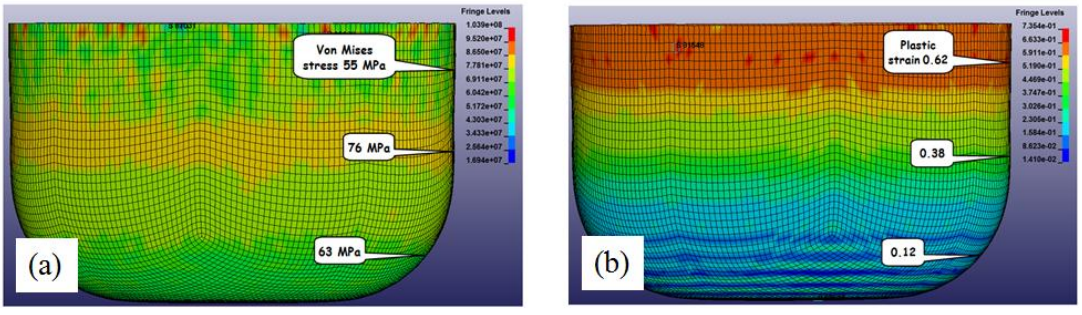

Fig. 6.33 Case 0.3_Curve4_FA used a bulged punch with:(a) Von Mises stress, and (b) contours of effective plastic strain

A μ of 0.10, 0.12, 0.14, 0.16, 0.18, 0.20, and 0.30 were used for the 0.3_Curve4_FA simulation and the results are shown in Fig. 6.34. The corresponding maximum punch force were $F_{max.sim.(0.10)}$ = 724 N; $F_{max.sim.(0.12)}$ = 859 N; $F_{max.sim.(0.14)}$ = 978 N; $F_{max.sim.(0.16)}$ 1116 N; $F_{max.sim.(0.18)}$ = 1163 N; $F_{max.sim.(0.20)}$ = 1333 N, and $F_{max.sim.(0.30)}$ = 1803 N. However in the experiment, the measured maximum punch force was 1640 N, which was 9 % lower than the simulated value. This discrepancy was due not only to friction, but also to radial pressure being applied to the wall during the ironing stage.

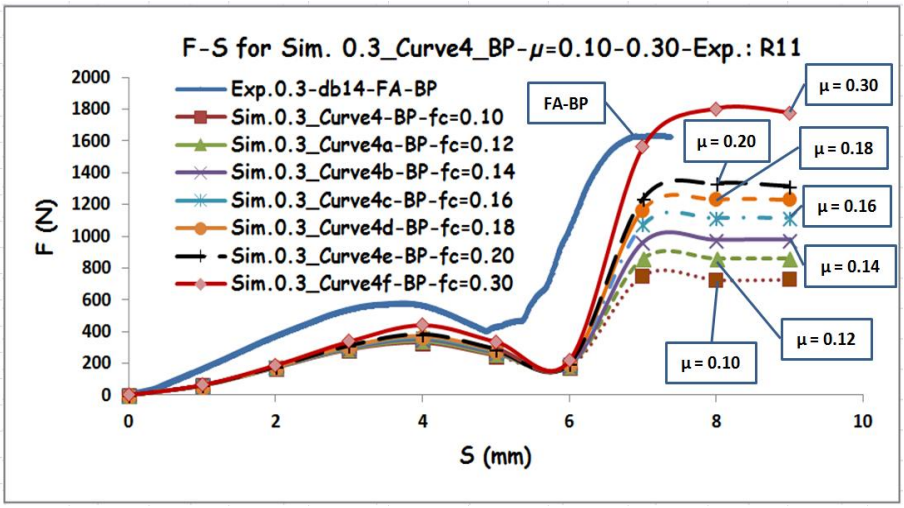

Fig. 6.34 The coefficient of friction was tried at 0.10-0.30 for simulations on 0.3_Curve4_FA

6.7 Discussion

Simulations were performed for AA1235 material in fully annealed conditions, as well as being processed by ARB and stress relieved at 200 ^{o}C for 8 hours. The parameters in this simulation were the thickness and diameter of the blank, the corner radius of the die and the punch, the coefficient of friction, and the yield strength. The simulation results indicated that the thinner blank had more wrinkles on the wall, but

when the blanks were 300 μm thick, the resulting cups were good, without tears or wrinkles.

The thinner the blank, the more chance there will be for wrinkles to occur in the wall. A larger diameter blank results in a larger punch stroke and produces a deeper cup. When the corner radius of the die and punch are larger, the punch force is reduced, but with a higher coefficient of friction, the maximum punch force also increased.

The coefficient of friction can be estimated by matching the drawing force with the experiment results, but this is not easy because deep drawing is a fairly complex process where various parts of a blank experience tension, compression, and bending by the corner radius of the punch, and die corner radius, and the blank holder presses onto the flange area. As the clearance between diameters of a punch and a die increased, there is more chance of wrinkles forming on the wall. Simulation models have been validated by a good agreement between the simulation and experimental results, but in the simulation the influence of the anisotropy of a material was not considered.

The thickness of the cup wall shows that a normal punch produced a similar shape between the simulation and experimental results, but when these results are compared to those where a bulged punch were used, there were two differences. With a normal punch, the corner radius becomes thinner, whereas with a bulged punch the wall becomes thicker. Second, when a normal punch was used, the edge of the cup experienced maximal thickening of the simulation and experiment results, but when a bulged punch was used, the edge of the cup was closer to the initial thickness of the blank. This is an advantage of the thickness distribution with a

bulged punch, moreover, evidence has shown that deep drawing with a bulged punch can prevent the formation of wrinkles and reduce earing.

It has been proven that the forming limit in deep drawing can be improved and the occurrence of defects can be prevented by using a flexible powder cavity as a substitute for a die [191], and an ARB process followed by stress relieving can also increase the formability and lower earing on AA1235 material.

The corner radius of the punch was identified as an important factor in improving the formability of deep drawing a cylindrical cup [192], such that a smaller corner radius will facilitate tearing in this area during deep drawing. A maximum thinning of the wall and minimum punch corner radius was taken criteria for evaluating formability [173], and therefore formability is limited by the critical thickness on the corner radius without causing a cup to tear.

The forming limit of a cup-shaped box was increased in height by a larger die corner radius and punch corner radius [193], therefore the height of the cup-shaped box can be increased by increasing the corner radius of a die and/or punch.

When the radius of a die corner was increased for deep drawing AA1100 material, the strain limit also increased [194]. The extent of the behaviour of cup drawing for AA6061 material influenced by the die corner radius was estimated to be 65 %, the BHP was 27 %, and the punch corner radius was 8 % [190].

There were seven factors involved when deep drawing a steel blank with a diameter of ø72.28 mm and thickness of 0.9 mm. Those factors were (i) the punch corner radius, (ii) the die corner radius, (iii) the BHP, (iv) the punch force, (v) punch speed, (vi) type of lubricant, (vii) lubrication positions of both sides, and from the side of the die and punch. The optimal conditions for deep drawing were achieved by

a 4 mm punch corner radius, a 6 mm die corner radius, a BHF of 80 kN, PE lubricants, and lubrication positions of both sides of the blank [195].

Wrinkles that occurred while deep drawing metal increased rapidly when the thickness of the blank decreased. The BHP was strongly influenced by the thickness of the blank and the coefficient of friction, and the LDR decreased when the thickness was reduced, and it decreased rapidly [117]. When the blank was very thin the LDR was strongly influenced by the coefficient of friction.

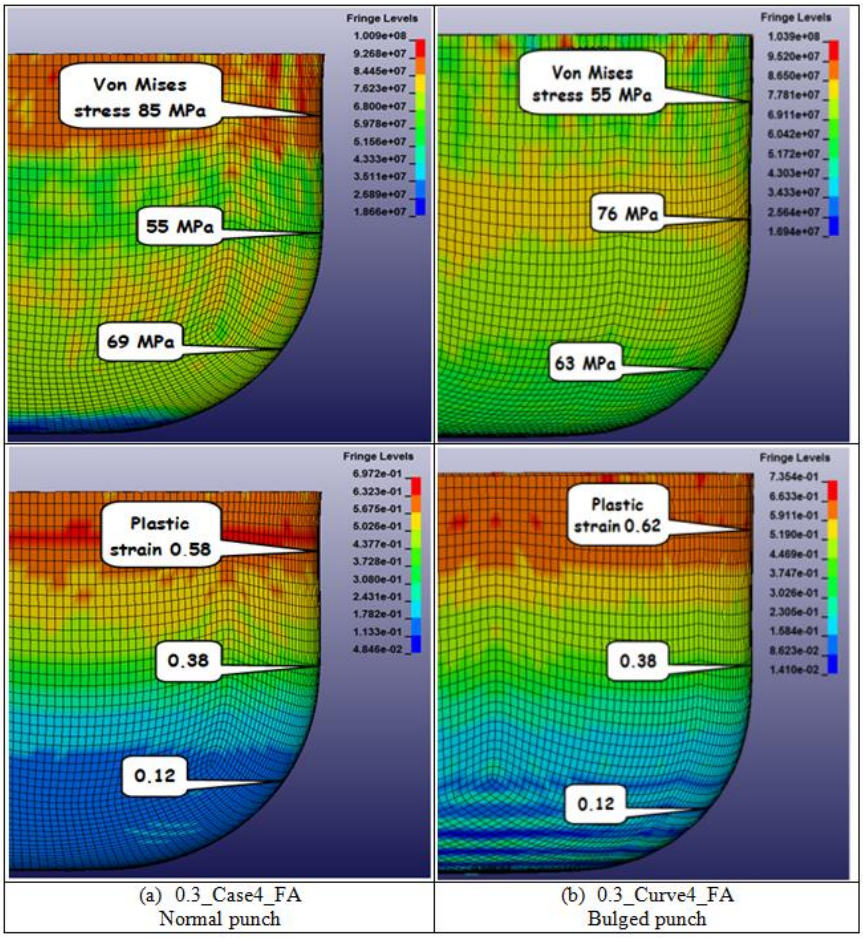

Fig. 6.35 Von Mises stress and plastic strain on AA1235 with FA-conditions for TB = 300 µm, and DB = 14 mm (a) normal punch and (b) bulged punch

The maximum stress for a normal punch and a bulged punch were quite different; the maximum stress on the corner radius of a normal punch was 69 MPa (Fig. 6.35a)

compared to 63 MPa for the bulged punch (Fig 6.35b). This means that the stress experienced by the cup being formed by a bulged punch was lower, so the possibility of tearing was also lower. The edge of a cup for a normal punch showed an average Von Mises stress of 85 MPa (Fig. 6.35a), and only 55 MPa (Fig. 6.35b) for a bulged punch. This means that the Von Mises stress experienced by the cup being formed by a bulged punch was lower, and the edge of the cup was not becoming thicker at the end of the punching stroke. A normal punch always resulted in the edge of the cup being thicker. Plastic strain on the edge of the when a bulged punch was used was higher (0.62) than for a normal punch (0.58) which means the edge experienced more deformation with a bulged punch than a normal punch.

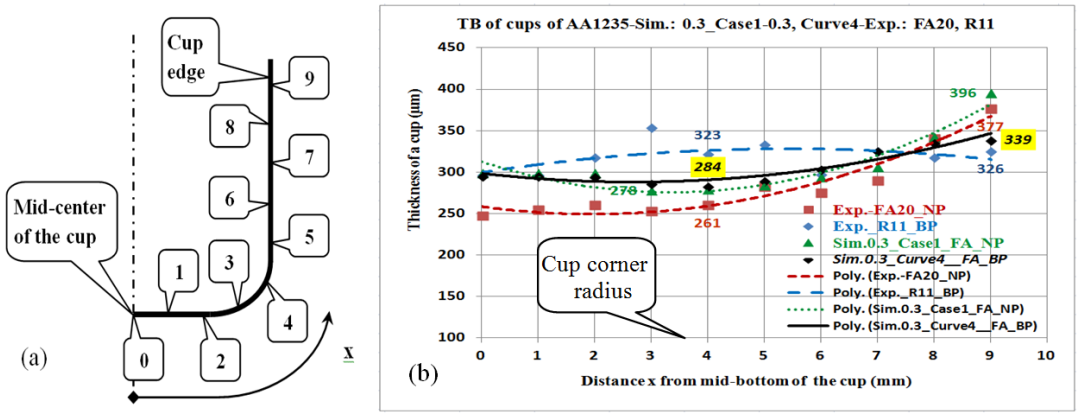

Fig. 6.36 A comparison of the distribution of the cup wall thickness of the experiment and the simulation results for the use of normal punch and bulged punch

A comparison of the thickness of the wall of the cup between the experiment and simulation is shown in Fig. 6.36. The thickness of the cup from the experiment was obtained from AA1235 material in an FA condition, with a TB of 300 µm, and a DB of 14 mm, and when a normal punch (Exp.FA_20_NP) and a bulged punch was used (Exp.R11_BP). A simulation with a normal punch (Sim.0.3_Case1_FA_NP) and a bulged punch (Sim.0.3_Curve4_FA_BP) was carried out.

The thickness near the radius of the cup corner using a normal punch was 261 μm and 323 μm using a bulged punch; this indicated a significant thickening of 62 μm (23.8 %). Thickening in this region is an advantage because it can reduce the possibility of tearing which is common here. The thickness at the edge of the cup using a normal punch was 377 μm and 326 μm with a bulged punch; this indicated a significant reduction in thickness of 51 μm (13.5 %), which would help the cup to eject from the punch and die.

The reduction in thickness at the edge of the cup is also an advantage because it was always thicker when a normal punch was used; both of these advantages can be obtained with a bulged punch, and it can reduce earing on the edge.

Thus the simulation model in this chapter demonstrated that it can be used to:

(a) estimate the drawing force,

(b) predict the occurrence of wrinkles,

(c) check the clearance between the die and punch diameters for a given blank thickness, and

(d) complete a stress/strain analysis of the whole cup which can predict the maximum allowable stress that will cause a cup to tear during deep drawing.

6.8 Summary

The simulation showed that the thinner the blank, the more chance there will be of wrinkles forming on a thin wall. When 300 μm blanks were used, all the cups had no tears or wrinkles. When a larger corner radius for the die and punch were used, the punching force was reduced, but it increased with a higher coefficient of friction.

Different coefficients of friction were used in the simulation to estimate the average coefficient of friction by matching them with the experimental drawing

force. When a larger clearance (gap between the punch and die diameters) was given, the chance of a wrinkle in the cup wall increased. A simulation model was validated after several parameters from the simulation and experiment showed qualitative and quantitative agreements. The thickness of the cup walls showed that a normal punch produced similar results between the simulation and the experiment.

When a bulged punch was used for annealed AA1235 compared to a normal punch there were four improvements:

(a) The wrinkles on the wall of the cup can be prevented,

(b) The earing on the edge of the cup can be reduced,

(c) The thickness of the wall at the punch corner radius was increased, and

(d) The edge of the cup was close to the initial thickness of the blank.

Chapter 7 Conclusions and recommendations

7.1 Conclusions

7.1.1 Experiment

The objectives in Chapter 1 have been fully achieved as conclusions for the experimental results of AA1235 for thicknesses of 130 μm to 300 μm are as follows:

1) Equations of the flow stress of AA1235 related to grain size and the thickness of the specimen were obtained to account for the effect of size. The tensile strength of annealed AA1235 increased as the specimen increased in thickness from 16 μm to 70 μm, but the tensile strength decreased as the specimen decreased in thickness from 70 μm to 300 μm. The width of the specimen did not significantly affect the tensile strength.
2) A reduction of 63 % in the thickness of AA1235 in the ARB process, whose initial thickness was 300 μm, provided a good interface bonding suitable for micro deep drawing. An asymmetric rolling (AR) process produced a finer grain diameter than ARB symmetric rolling, and AR improved the surface quality of material produced by the ARB process. The different in the speed ratio affected the tensile strength, strain, and grain size.
3) For AA1235 300 μm thick, that was produced by a combination of ARB and stress relieving at 200^{o}C for 8 hours, the following improvements were observed:
   (a) The strength increased by 14 % and grain refinement by 93 %.
   (b) Normal anisotropy (R_{avg}) increased by 1.9 %.

(c) The LDR, an indicator of cup formability, can be increased by 6.5 % from 1.87 to 2.00.

(d) The planar anisotropy (ΔR) decreased by 96 % from 0.556 to -0.022, which reduced earing in the edge of the cup.

4) A safe region for micro deep drawing has been mapped out, based on the forming limit diagram (FLD). This is the area above the wrinkled area and below the fracture limit line.

5) The occurrence of wrinkles increased as the thickness of the blank decreased. The bulged-punch can remove wrinkles by ironing in the latter part of the stroke by applying an internal radial pressure on the cup wall (negative clearance or interference) just before wrinkles begin to occur. This proposed bulged punch can produce a good cup without wrinkles, which is not possible with a normal punch. Other benefits of the new method compared to a normal punch are, (i) thickening of the cup corner radius which reduces tearing at the corner, (ii) thinning of the cup edge which makes it easier to eject the part, and (iii) reduced earing.

6) Earing can be reduced by stress relieving the blank material prior to deep drawing. Under annealed conditions, using the bulged punch on the 300 μm thick blank may decrease earing on the cup, but the force on the bulged punch was 181 % higher than on a normal punch, due to a combination of drawing and ironing processes.

7) The thickness at a corner radius of the cup region became thinner with a normal punch, but it thickened when a bulged punch was used. The edge of the cup became thicker when a normal punch was used, but it decreased almost to the

thickness of the blank when the bulged punch was used. The 13.5 % iron reduction in the thickness of the edge of the cup when the bulged punch was used was quite significant because it helped to eject the cup from the punch and die.

7.1.2 Simulation

Conclusions drawn from the simulation results are as follows:

1) A fully validated simulation model with a range of five parameters demonstrated: (i) the corner radius of the die, (ii) the corner radius of the punch, (iii) the coefficient of friction, (iv) the clearance between the die and the punch diameters, and (v) the diameter of the blank. The results of the simulation agreed well with the experiment. The wall thickness distribution of the cup after a normal punch was used in the experiment agreed with the simulation results.
2) The coefficient of friction in the micro deep drawing process can be estimated by matching the drawing force between the theories and the experiment; they ranged between 0.18 and 0.23. A higher coefficient of friction will increase the maximum punch force.
3) For an annealed blank of AA1235 at 300 μm thick, all the resulting cups were perfect, without tears or wrinkles, however, at a thickness of 150 μm or thinner, the wall of a cup showed a greater tendency towards wrinkling. A larger corner radius of the die or punch will reduce the punch force, and more clearance between the punch and die increases the chance of a wrinkle in the cup wall.

7.2 Recommendations

Suggestions for improving the research results are as follows:

1) Further refine the bulged punch for foil thinner than 130 μm to avoid wrinkles in the cup wall, tears in the corner, and reduce earing at the edge of the cup.
2) Incorporate anisotropy when simulating the deep drawing process to quantify the effects of relevant parameters on earing at the edge of the cup.
3) Use a die with a smaller diameter (i.e. < 7 mm), and a thinner blank (i.e. <70 μm).
4) Implementing asymmetric rolling is recommended to produce a better product, by changing the rolling direction of the strip by 180^{o} to the direction between asymmetric rolling cycles.
5) In accordance with predicting the occurrence of tearing, the data for a forming limit diagram (FLD) should be used when simulating micro deep drawing.
6) The effect of size related to the ratio of the thickness of a blank to its average grain size for micro deep drawing a cup needs to be simulated.

7.3 Thesis contributions

The thesis contributions to the body of existing knowledge are as follow:

1) The flow stress of fully annealed AA1235 increased when the thickness was reduced from 300 to 71 μm and decreased sharply when the thickness was reduced further to 16 μm. These thicknesses were still in the micro forming region (< 300 μm),

2) Good cups without wrinkles and low earing can be produced with a normal punch and the materials pre-processed from 4 cycles ARB and then subsequently stress relieved at 200^{o}C for 8 hours,
3) The bulged punch can produce good cups with the following features: without wrinkles, reduced earing, thicker cup wall at the punch corner radius, and thinner cup wall at the top edge of cup, and
4) The simulated results compared well with the experiment. It can be used to optimize the design of pair of the punch and the die through the calculated stress and strain to produce a good cup.

References

1. Fu, M.W., Chan, W. L., *A review on the state-of-the-art microforming technologies.* The International Journal of Advanced Manufacturing Technology, 2012. **67**(9-12): p. 2411-2437.
2. Tajally, M., Emadoddin, E., *Mechanical and anisotropic behaviors of 7075 aluminum alloy sheets.* Materials & Design, 2011. **32**(3): p. 1594-1599.
3. Wifi, A.S., Abdelmaguid, T.F., El-Ghandour, A.I. *A review of the optimization techniques applied to the deep drawing process*. in *37th International Conference on Computers and Industrial Engineering*. 2007. Alexandria, Egypt.
4. Oluwole, O.O., Anyaeche, C.O., Faola, O.V., *Effect of draw ratio and sheet thickness on earing and drawability of Al 1200 cups.* Jounal of Materials & Materials Characterization & Engineering, 2010. **9**(2010): p. 461-470.
5. Geiger, M., Kleiner, M., Eckstein, R., Tiesler, N., Engel, U., *Microforming.* CIRP Annals - Manufacturing Technology, 2001. **50**(2): p. 445-462.
6. Hirt, G., Justinger, H., Witulski, N., *Analysis of size effects in micro sheet forming.* 1st Colloqium Processscaling, Bremen, 2003.
7. Vollertsen, F., Hu, Z., Niehoff, H.S., Theiler, C., *State of the art in micro forming and investigations into micro deep drawing.* Journal of Materials Processing Technology, 2004. **151**(1-3): p. 70-79.
8. Brabie, G., Costache, E. M., Nanu, N., Chirita, B., *Prediction and minimisation of sheet thickness variation during deep drawing of micro/milli parts.* International Journal of Mechanical Sciences, 2013. **68**: p. 277-290.
9. Hadi, S., Tieu, A. K., Lu, C., Su, L.H., Yu, H.L, *Grain refinement in the formability of Aluminium thin cup.* Materials Science Forum, 2013. **773-774**: p. 166-175.
10. Hadi, S., Yu, H.L., Tieu, K., Lu, C., *Simulation of defects in micro-deep drawing of an aluminium alloy foil.* 2013: p. 298-303.
11. Molotnikov, A., Lapovok, R., Gu, C. F., Davies, C. H. J., Estrin, Y., *Size effects in micro cup drawing.* Materials Science and Engineering: A, 2012. **550**: p. 312-319.
12. Vollertsen, F., Niehoff, H.S. and Z. Hu, *State of the art in micro forming.* International Journal of Machine Tools and Manufacture, 2006. **46**(11): p. 1172-1179.
13. Gau, J.T., Teegala, S., Huang, K.M., Hsiao, T.J., Lin, B.T., *Using micro deep drawing with ironing stages to form stainless steel 304 micro cups.* Journal of Manufacturing Processes, 2013. **15**(2): p. 298-305.
14. Irthiea, I., Green, G., Hashim, S., Kriama, A., *Experimental and numerical investigation on micro deep drawing process of stainless steel 304 foil using flexible tools.* International Journal of Machine Tools and Manufacture, 2014. **76**: p. 21-33.
15. Kadkhodayan, M., Pourhasan, R, *Finite element simulation of process and springback of friction aided deep drawing using tapered blank holder divided into eight segments.* 2010.
16. Grèze, R., Manach, P. Y., Laurent, H., Thuillier, S., Menezes, L. F., *Influence of the temperature on residual stresses and springback effect in an aluminium alloy.* International Journal of Mechanical Sciences, 2010. **52**(9): p. 1094-1100.
17. Li, D., Ghosh, A.K., *Biaxial warm forming behavior of aluminum sheet alloys.* Journal of Materials Processing Technology, 2004. **145**(3): p. 281-293.

18. Moshksar, M.M., Zamanian, A., *Optimization of the tool geometry in the deep drawing of Aluminium.* Journal of in Materials Processing Technology, 1997. **72**(1997): p. 363-370.
19. Demirci, H.I., Yaşar, M., Demiray, K., Karalı, M., *The theoretical and experimental investigation of blank holder forces plate effect in deep drawing process of AL 1050 material.* Materials & Design, 2008a. **29**(2): p. 526-532.
20. Mahmudi, R., Alaiha, M.M., *Control of earing in deep drawing of roll-cast AA3003 Aluminium sheets.* Materials Science Forum, 2006. **519-521**: p. 1545-1550.
21. Chang, Q.F., Li, D.Y., Peng, Y.H., Zeng, X.Q., *Experimental and numerical study of warm deep drawing of AZ31 magnesium alloy sheet.* International Journal of Machine Tools and Manufacture, 2007. **47**(3-4): p. 436-443.
22. Mori, K., Tsuji, H., *Cold deep drawing of commercial Magnesium alloy sheets.* CIRP Annals - Manufacturing Technology, 2007. **56**(1): p. 285-288.
23. Yoshihara, S., Manabe, K., Nishimura, H., *Effect of blank holder force control in deep-drawing process of magnesium alloy sheet.* Journal of Materials Processing Technology, 2005. **170**(3): p. 579-585.
24. Zhang, S.H., Zhang, K., Xu, Y. C., Wang, Z. T., Xu, Y., Wang, Z. G., *Deep-drawing of magnesium alloy sheets at warm temperatures.* Journal of Materials Processing Technology, 2007. **185**(1-3): p. 147-151.
25. Watiti, V.B., Labeas, G.N., *Finite element optimization of deep drawing process forming parameters for Magnesium alloys.* International Journal of Material Forming, 2010. **3**(S1): p. 97-100.
26. Kim, S.H., Kim, Seung H., Huh, H., *Tool design in a multi-stage drawing and ironing process of a rectangular cup with a large aspect ratio using FEA.* International Journal of Machine Tools and Manufacture, 2002. **42**(2002): p. 863-875.
27. Colgan, M., Monaghan, J., *Deep drawing process: analysis and experiment.* Journal of Materials Processing Technology, 2003. **132**: p. 35-41.
28. Sezek, S., Savas, V., Aksakal, B., *Effect of die radius on blank holder force and drawing ratio: a model and experimental investigation.* Materials and Manufacturing Processes, 2010. **25**(7): p. 557-564.
29. Faraji, G., Mashhadi, M.M., Hashemi, R., *Using the finite element method for achieving an extra high limiting drawing ratio (LDR) of 9 for cylindrical components.* CIRP Journal of Manufacturing Science and Technology, 2010. **3**: p. 262-267.
30. Atrian, A., Fereshteh-Saniee, F., *Deep drawing process of steel/brass laminated sheets.* Composites Part B: Engineering, 2013. **47**: p. 75-81.
31. Yagami, T., Manabe, K., Yamauchi, Y., *Effect of alternating blank holder motion of drawing and wrinkle elimination on deep-drawability.* Journal of Materials Processing Technology, 2007. **187-188**: p. 187-191.
32. Agrawal, A., Reddy, N.V., Dixit, P. M., *Determination of optimum process parameters for wrinkle free products in deep drawing process.* Journal of Materials Processing Technology, 2007. **191**(1-3): p. 51-54.
33. Demirci, H.İ., Esner, C., Yasar, M., *Effect of the blank holder force on drawing of aluminum alloy square cup: Theoretical and experimental investigation.* Journal of Materials Processing Technology, 2008b. **206**(1-3): p. 152-160.
34. Zhang, S.H., Jensen, M.R., Nielsen, K.B., Danckert, J., Lang, L.H., Kang, D.C., *Effect of anisotropy and prebulging on hydromechanical deep drawing of mild steel cups.* Journal of Materials Processing Technology, 2003. **142**(2): p. 544-550.

35. Singh, S.K., Gupta, A.K., Mahesh, K., *A study on the extent of ironing of EDD steel at elevated temperature.* CIRP Journal of Manufacturing Science and Technology, 2010. **3**(1): p. 73-79.
36. Singh, S.K., Gupta, A.K., *Comparison of ironing in warm and hydromechanical deep drawing of low carbon steel.* Materials Science Forum, 2013. **773-774**: p. 203-210.
37. Danckert, J., *Ironing of thin walled cans.* CIRP Annals - Manufacturing Technology, 2001. **50**(1): p. 165-168.
38. Simões, V.M., Coër, J., Laurent, H., Oliveira, M.C., Alves, J.L., Manach, P.Y., Menezes, L.F., *Sensitivity analysis of process parameters in the drawing and ironing processes.* Key Engineering Materials, 2013. **554-557**: p. 2256-2265.
39. Kotani, Y., Watanabe, A., Watari, H., *Effect of tool shape on increases in sheet thickness during drawing and ironing.* Advanced Materials Research, 2011. **320**: p. 462-467.
40. Xu, W.J., Zhai, C.H., Li, W.H., *Optimization on deep drawing and ironing process of compressed natural gas containers.* Applied Mechanics and Materials, 2013. **401-403**: p. 867-870.
41. Folle, L.F., Netto, S.E.S, Schaeffer, L., *Analysis of the manufacturing process of beverage cans using aluminum alloy.* Journal of Materials Processing Technology, 2008. **205**(1-3): p. 347-352.
42. Gavas, M., Izciler, M., *Effect of blank holder gap on deep drawing of square cups.* Materials & Design, 2007. **28**(5): p. 1641-1646.
43. Kalpakjian, S., Schmid, S.R., *Manufacturing processes for engineering materials.* Pearson Education, 2009. **6**: p. 49-09-410.
44. Zaky, A.M., Nassr, A.B., El-Sebaie, M.G., *Optimum blank shape of cylindrical cups in deep drawing of anisotropic sheet metals.* 1998.
45. Kishor, N.K., D.R., *Optimization of initial blank shape for minimize earing in deep drawing using FEM.* Journal of Materials Processing Technology, 2002. **130-131**(2002): p. 20-30.
46. Desai, S.G., Pardeshi, R.H., Date, P.P., *Study of various initial blank shapes to minimize the earing in the different shaped formed parts using finite element analysis.* American Institute of Physics, 2005. **A, Numisheet 2005**: p. 855-860.
47. Turkoz, M., Dilmec, M., Halkaci, H.S., *Investigation on earing behavior of AA2024-T4 and AA5754-O aluminum alloys.* Advance Material Research, International Conference on Advances in Materials and Processing Technologies, AMPT 2009, 2008. **264-265**: p. 12-17.
48. Paunoiu, V., Teodor, V., *Blank shape optimization in deep drawing with combined restraint.* Applied Mechanics and Materials, 2013. **371**: p. 178-182.
49. Pegada, V., Chun, Y., Santhaman, S., *An algorithm for determining the optimal blank shape for the deep drawing of Al cups.* Journal of Materials Processing Technology, 2002. **125-126**: p. 743-750.
50. Lai, X., Peng, L., Hu, P., Lan, S., Ni, J., *Material behavior modelling in micro/meso-scale forming process with considering size/scale effects.* Computational Materials Science, 2008. **43**(4): p. 1003-1009.
51. Yeh, F.H., Li, C.L., Lu, Y.H., *Study of thickness and grain size effects on material behavior in micro-forming.* Journal of Materials Processing Technology, 2008. **201**(1-3): p. 237-241.

52. Yun, W., Peilong, D., Zhenying, X., Hua, Y., Jiangping, W., Jingjing, W, *A constitutive model for thin sheet metal in micro-forming considering first order size effects.* Materials & Design, 2010. **31**(2): p. 1010-1014.
53. Gau, J.T., Principe, C., Wang, J, *An experimental study on size effects on flow stress and formability of aluminm and brass for microforming.* Journal of Materials Processing Technology, 2007. **184**(1-3): p. 42-46.
54. Peng, L., Lai, X., Lee, H.J., Song, J.H., Ni, J., *Friction behavior modeling and analysis in micro/meso scale metal forming process.* Materials & Design, 2010. **31**(4): p. 1953-1961.
55. Gong, F., Guo, B., Wang, C., Shan, D., *Size effect on friction of C3602 in cylinder compression.* Tribology Transactions, 2010. **53**(2): p. 244-248.
56. Rezaei, M.R., Toroghinejad, M. R., Ashrafizadeh, F., *Effects of ARB and ageing processes on mechanical properties and microstructure of 6061 aluminum alloy.* Journal of Materials Processing Technology, 2011. **211**(6): p. 1184-1190.
57. Kwan, C., Wang, Z., Kang, S.B., *Mechanical behavior and microstructural evolution upon annealing of the accumulative roll-bonding (ARB) processed Al alloy 1100.* Materials Science and Engineering: A, 2008. **480**(1-2): p. 148-159.
58. Jamaati, R., Toroghinejad, M.R., *Effect of friction, annealing conditions and hardness on the bond strength of Al/Al strips produced by cold roll bonding process.* Materials & Design, 2010. **31**(9): p. 4508-4513.
59. Roy, S., Nataraj, B. R., Suwas, S., Kumar, S., Chattopadhyay, K., *Accumulative roll bonding of aluminum alloys 2219/5086 laminates: Microstructural evolution and tensile properties.* Materials & Design, 2012. **36**: p. 529-539.
60. Su, L.H., Lu, C., Tieu, K., Deng, G., *Annealing behavior of accumulative roll bonding processed Aluminium composites.* Steel Reasearch International, 2013. **84**(12): p. 1241-1245.
61. Tanner, D.A., Robinson, J. S., *Reducing residual stress in 2014 Auminium alloy die forgings.* Materials & Design, 2008. **29**(7): p. 1489-1496.
62. Engel, U., *Tribology in microforming.* Wear, 2006. **260**(3): p. 265-273.
63. Yang, T.S., *Finite element analysis of elliptic cup deep drawing of magnesium alloy sheet.* Journal of Achievement in Materials and Manufacturing Engineering, 2008. **27**(2008): p. 139-142.
64. Huang, Y.M., Chen, J.W., *Influence of the tool clearance in the cylindrical cup drawing process.* Journal of Materials Processing Technology, 1996. **57**: p. 4-13.
65. Tommerup, S., Endelt, B., *Experimental verification of a deep drawing tool system for adaptive blank holder pressure distribution.* Journal of Materials Processing Technology, 2012. **212**(11): p. 2529-2540.
66. Diehl, A., Engel, U., geiger, M., *Influence of microstructure on the mechanical properties and the forming behaviour of very thin metal foils.* Manufacturing Technology, University of Erlangen-Nuremberg Egerlandstr. 11, D-91058 Erlangen-Germany, 2006.
67. Li, B.L., Tsuji, N., Kamikawa, N., *Microstructure homogeneity in various metallic materials heavily deformed by accumulative roll-bonding.* Materials Science and Engineering: A, 2006. **423**(1-2): p. 331-342.
68. Saito, Y., Utsonomiya, H., Tsuji, N., Sakai, T., *Novel ultra-high straining process for bulk materials-development of the accumulative roll-bonding (ARB) process.* Acta Mater., 1999. **47**: p. 579-583.

69. Tamimi, S., Ketabchi, M., Parvin, N., *Microstructural evolution and mechanical properties of accumulative roll bonded interstitial free steel.* Materials & Design, 2009. **30**(7): p. 2556-2562.
70. Tsuji, N., Ito, Y., Saito, Y., Minamoto, Y., *Strength and ductility of ultrafine grained aluminum and iron produced by ARB and annealing.* 2002.
71. Krallics, G., Lenard, J. G., *An examination of the accumulative roll-bonding process.* Journal of Materials Processing Technology, 2004. **152**(2): p. 154-161.
72. Bazzaz, A.R., Ahmadian, S., Reihani, H., *Modeling of microstructure and mechanical behavior of ultra fine grained aluminum produced by accumulative roll-bonding.* Materials & Design, 2011. **32**(8-9): p. 4580-4585.
73. Eizadjou, M., Kazemitalachi, A., Daneshmanesh, H., Shakurshahabi, H., Janghorban, K., *Investigation of structure and mechanical properties of multi-layered Al/Cu composite produced by accumulative roll bonding (ARB) process.* Composites Science and Technology, 2008. **68**(9): p. 2003-2009.
74. Eizadjou, M., Manesh, H.D., Janghorban, K., *Microstructure and mechanical properties of ultra-fine grains (UFGs) aluminum strips produced by ARB process.* Journal of Alloys and Compounds, 2009. **474**(1-2): p. 406-415.
75. Hadi, S., Tieu, A. K., Lu, C., Zhu, H.T., *A micro deep drawing of ARB processed aluminium foil AA1235.* Int. J. Materials and Product Technology, 2013. **47**(1/2/3/4): p. 175-187.
76. Huang, X., Tsuji, N., Hansen, N., Minamoto, Y., *Microstructural evolution during accumulative roll-bonding of commercial purity aluminum.* Materials Science and Engineering A, 2003. **340**: p. 265-271.
77. Pirgazi, H., Akbarzadeh, A., Petrov, R., Kestens, L., *Microstructure evolution and mechanical properties of AA1100 aluminum sheet processed by accumulative roll bonding.* Materials Science and Engineering: A, 2008. **497**(1-2): p. 132-138.
78. Su, L., Lu, C., Deng, G. Tieu, K., Sun, X., *Microstructure and mechanical properties of 1050-6061 laminated composite processed by accumulative roll bonding.* 2013.
79. Kwan, C.C.F., Wang, Z., *Cyclic deformation behavior of ultra-fine grained copper processed by accumulative roll-bonding.* Procedia Engineering, 2010. **2**(1): p. 101-110.
80. Mahdavian, M.M., Ghalandari, L., Reihanian, M., *Accumulative roll bonding of multilayered Cu/Zn/Al: An evaluation of microstructure and mechanical properties.* Materials Science and Engineering: A, 2013. **579**: p. 99-107.
81. Milner, J.L., Bunget, C., Farha, A.F., Kurfess, T., Hammond, V.H., *Modeling tensile strength of materials processed by accumulative roll bonding.* Journal of Manufacturing Processes, 2013. **15**(2): p. 219-226.
82. Alawode, A.J., Adeyemi, M. B., *Effects of degrees of deformation and stress-relief temperatures on the mechanical properties and residual stresses of cold drawn mild steel rods.* Journal of Materials Processing Technology, 2005. **160**(2): p. 112-118.
83. Hallberg, H., *Influence of process parameters on grain refinement in AA1050 aluminum during cold rolling.* International Journal of Mechanical Sciences, 2013. **66**: p. 260-272.
84. Yu, H.L., Lu, C., Tieu, A.K., Godbole, A., Su, L.H., Sun, Y., Liu, M., Tang, D., Kong, C., *Fabrication of ultra-thin nanostructured bimetallic foils by accumulative roll bonding and asymmetric rolling.* Scientific Reports, 2013. **3**: p. 1-9.

85. Xie, H.B., Manabe, K., Jiang, Z. Y., *A novel approach to investigate surface roughness evolution in asymmetric rolling based on three dimensional real surface.* Finite Elements in Analysis and Design, 2013. **74**: p. 1-8.
86. Lapovok, R., Orlov, D., Timokhina, I.B., Pougis, A., Toth, L.S., Hodgson, P.D., Haldar, A., Bhattacharjee, D., *Asymmetric rolling of Interstitial-free steel using one idle roll.* Metallurgical and Materials Transactions A, 2011. **43**(4): p. 1328-1340.
87. Li, Z., Fu, L., Fu, B., Shan, A., *Effects of annealing on microstructure and mechanical properties of nano-grained titanium produced by combination of asymmetric and symmetric rolling.* Materials Science and Engineering: A, 2012. **558**: p. 309-318.
88. Jiang, Z.Y., Xie, H.B., Yang, L.M., Zhu, H.T., Wei, D.B., Tieu, A.K., *Mechanics of asymmetric rolling of thin strip with effect of work roll edge contact.* Materials Science Forum, 2007. **561-565**: p. 115-118.
89. Orlov, D., Lapovok, R., Toth, L.S., Timokhina, I.B., Hodgson, P.D., Haldar, A., Bhattacharjee, D., *Asymmetric rolling of interstitial-free steel using differential roll diameters. Part II: microstructure and annealing effects.* Metallurgical and Materials Transactions A, 2014. **45**(1): p. 447-454.
90. Mapelli, C., Barella, S., Mombelli, D., Baldizzone, C., Gruttadauria, A., *Comparison between symmetric and asymmetric hot rolling techniques performed on duplex stainless steel 2205.* International Journal of Material Forming, 2012. **6**(3): p. 327-339.
91. Orlov, D., Pougis, A., Lapovok, R., Toth, L.S., Timokhina, I.B., Hodgson, P.D., Haldar, A., and D. Bhattacharjee, *Asymmetric rolling of interstitial-free steel using differential roll diameters. Part I: mechanical properties and deformation textures.* Metallurgical and Materials Transactions A, 2013. **44**(9): p. 4346-4359.
92. Tóth, L.S., Beausir, B., Orlov, D., Lapovok, R., Haldar, A., *Analysis of texture and R value variations in asymmetric rolling of IF steel.* Journal of Materials Processing Technology, 2012. **212**(2): p. 509-515.
93. Beausir, B., Biswas, S., Kim, D.I., Tóth, L.S., Suwas, S., *Analysis of microstructure and texture evolution in pure magnesium during symmetric and asymmetric rolling.* Acta Materialia, 2009. **57**(17): p. 5061-5077.
94. Biswas, S., Kim, D.I., Suwas, S., *Asymmetric and symmetric rolling of magnesium: Evolution of microstructure, texture and mechanical properties.* Materials Science and Engineering: A, 2012. **550**: p. 19-30.
95. Kawałek, A.M., Dyja, H.S., Knapiński, M.J., Kwapisz, M.A., Laber, K.B., *Influence of rolling reduction, strip shape and asymmetry factor on the strip curvature.* Solid State Phenomena, 2013. **199**: p. 436-441.
96. Liang, H., Hong-shuang, D., Dian-yao, G., *Analysis of sheet curvature in asymmetrical cold rolling.* Journal of Iron and Steel Research, International, 2013. **20**(5): p. 34-37.
97. Yang, H.P., Sha, Y.H., Zhang, F., Pei, W., Zuo, L., *Through-thickness shear strain in Silicon steel under asymmetric rolling.* Materials Science Forum, 2012. **702-703**: p. 762-765.
98. Kim, H.K., Kim, H.W., Cho, J.H., Lee, J.C., *High-formability Al alloy sheet produced by asymmetric rolling of strip-cast sheet.* Materials Science and Engineering: A, 2013. **574**: p. 31-36.
99. Zhou, J., Shan, D.B., Guo, B., Ma, D.L., *Experimental study on specimen and grain size effects in uniaxial tension test of Al foil.* key Engineering Materials, 2007. **344**(2007): p. 777-782.

100. Peng, L., Liu, F., Ni, J., Lai, X., *Size effects in thin sheet metal forming and its elastic–plastic constitutive model.* Materials & Design, 2007. **28**(5): p. 1731-1736.
101. Michel, J.F., Picart, P., *Size effects on the constitutive behaviour for brass in sheet metal forming.* Journal of Materials Processing Technology, 2003. **141**(3): p. 439-446.
102. Raulea, L.V., Goijaerts, A.M., Govaert, L.E., Baaijens, F.P.T., *Size effects in the processing of thin metal sheets.* Journal of Materials Processing Technology, 2001. **115**(2001): p. 44-48.
103. Goh, T.N., Shang, H.M., *Effects of shape and size of tensile specimens on the stress-strain relationship of sheet metal.* Journal of Mechanical Working Technology, 1982. **7**: p. 23-37.
104. Hong, S., Hoffmann, H., *Study of scaling effect on mechanical properties for milli-forming of sheet metal-Tensile test of a very thin sheet*, in *1st Colloqium Processcaling*. 2003: Bremen.
105. Narayanasamy, R., Narayanan, C.S. , *Forming, fracture and wrinkling limit diagram for if steel sheets of different thickness.* Materials & Design, 2008. **29**(7): p. 1467-1475.
106. Hoffmann, H., Hong, S., *Tensile test of very thin sheet metal and determination of flow stress considering the scaling effect.* CIRP Annals - Manufacturing Technology, 2006. **55**(1): p. 263-266.
107. Salehinia, I., Shahani, A. R., *Effect of sheet anisotropy on the wear in deep-drawing process of a cylindrical cup.* International Journal of Mechanical Sciences, 2009. **51**(11-12): p. 856-868.
108. Shimizu, T., Ogawa, M., Yang, M., Manabe, K.I., *Plastic anisotropy of ultra-thin rolled phosphor bronze foils and its thickness strain evolution in micro-deep drawing.* Materials & Design, 2014. **56**: p. 604-612.
109. Padmanabhan, R., Oliveira, M.C., Baptista, A.J., Alves, J.L., Menezes, L.F., *Numerical study on the influence of initial anisotropy on optimal blank shape.* Finite Elements in Analysis and Design, 2009. **45**(2): p. 71-80.
110. Chung, K., Kim, D., Park, T., *Analytical derivation of earing in circular cup drawing based on simple tension properties.* European Journal of Mechanics - A/Solids, 2011. **30**(3): p. 275-280.
111. Yang, F., Li, J.C.M., *Deformation behavior of tin and some tin alloys.* Journal of Materials Science: Materials in Electronics, 2006. **18**(1-3): p. 191-210.
112. Chamanfar, A., Mahmudi, R., *Ti sheet-the effect of gage length and width measurement on plastic strain ratio.* Journal of Modeling, Simulation, and Characterization, 2004: p. 49-52.
113. Wifi, A., Mosallam, A., *Some aspects of blank-holder force schemes in deep drawing process.* Journal of Achievement in Materials and Manufacturing Engineering, 2007. **24**(2007): p. 315-323.
114. Fan, J.P., Tang, C.Y., Tsui, C.P., Chan, L.C., Lee, T.C., *3D finite element simulation of deep drawing with damage development.* International Journal of Machine Tools and Manufacture, 2006. **46**(9): p. 1035-1044.
115. Peng, L., Lai, X., Lee, H.J., Song, J.H., Ni, J. , *Analysis of micro/mesoscale sheet forming process with uniform size dependent material constitutive model.* Materials Science and Engineering: A, 2009. **526**(1-2): p. 93-99.
116. Ehlers, S., *Strain and stress relation until fracture for finite element simulations of a thin circular plate.* Thin-Walled Structures, 2010. **48**(1): p. 1-8.

117. Marumo, Y., Saiki, H., Ruan, L., *Effect of sheet thickness on deep drawing of metal foils.* Journal of Achievement in Materials and Manufacturing Engineering, 2007. **20**(2007): p. 479-482.
118. Wang, C., Guo, B., Shan, D., *Effect of die cavity dimension on micro U deep drawing behaviour with T2 foil.* Trans. Nonferrous Met. Soc. China, 2009. **19**(2009): p. 790-794.
119. Venkateswarlu, G., Davidson, M.J., Tagore, G.R.N., *Finite element simulation of deep drawing of al alloy sheets at elevated temperature.* ARPN journal of Engineering and APplied Sciences, 2010. **5**(2010): p. 93-98.
120. Chan, W.L., Fu, M. W., Yang, B., *Study of size effect in micro-extrusion process of pure copper.* Materials & Design, 2011. **32**(7): p. 3772-3782.
121. Zwick, R., *Indentec hardness tester with CCD camera and LCD line display.* Zwick-Roel AG, Germany.
122. Ruimin, C., *Mill Certificate of AA1235-H14-lot of MX 08441-size 0.3x1035 mm.* Fujian China 350015, 2010.
123. AS-1391, *Metallic materials-tensile testing at ambient temperature.* 2007.
124. AS-1733, *Methods for determination grain size on metals.* 1976.
125. Leu, D.K., Wu, J.Y., *A simplified approach to estimate limiting drawing ratio and maximum drawing load in cup drawing.* Journal of Engineering Materials and Technology, 2004. **126**(1): p. 116.
126. Narayanasamy, R., Ponalagusamy, R., Raghuraman, S., *The effect of strain rate sensitivity on theoretical prediction of limiting draw ratio for cylindrical cup drawing process.* Materials & Design, 2008. **29**(4): p. 884-890.
127. D'Andrea, A., Tozzo, C., Boschetto, A., Bottini, L., *Interface roughness parameters and shear strength.* Modern Applied Science, 2013. **7**(10).
128. Thomas, T.R., *Characterization of surface roughness.* Precision Engineering, 1981. **0140**: p. 97-104.
129. Ma, B., Tieu, A.K., Lu, C., Jiang, Z., *An experimental investigation of steel surface characteristic transfer by cold rolling.* Materials Processing Technology, 2002. **125-126**: p. 657-663.
130. Sedlaček, M., Podgornik, B., Vižintin, J., *Correlation between standard roughness parameters skewness and kurtosis and tribological behaviour of contact surfaces.* Tribology International, 2012. **48**: p. 102-112.
131. Cerri, E., Evangelista, E., *Metallography of Aluminium alloys.* TALAT-Training in Aluminium Appliation Technologies, EAA-European Aluminium Assosiacion, 1999.
132. Gao, N., Wang, S.C., Ubhi, H.S., Starink, M.J. , *A comparison of grain size determination by light microscopy and EBSD analysis.* Jounal of Materials Science Letters, 2005b. **40**: p. 4971-4974.
133. Struers, *Hot mounting.* A complete range of resins for high preparation quality, uniform size and shape of specimens, and short process times, 2010.
134. Yoshida, Y., Arai, K., Itoh, S., Kamado, S., Kojima, Y., *Realization of high strength and high ductility for AZ61 magnesium alloy by severe warm working.* Science and Technology of Advanced Materials, 2005. **6**(2): p. 185-194.
135. Yu, H.L., Hadi, S., Tieu, A.K., Lu, C., Godbole, A., Kong, C., *High strength and ductility of ultrathin laminate foils by accumulative roll boning and asymmetric rolling.* Acta Materialia, 2014. **Submitted**.
136. Davey, *XRD pdf standard card for Al-00-001-1176, Data on Chem. for Cer. Use, Natl. Res. Council Bull. 107.* Phys. Rev., 1925. **25**: p. 753.

137. Hanawalt, et, al., *XRD pdf standard card for Al-00-001-1180, Data on Chem. for Cer. use, Natl. Res. Council Bull. 107, .* Anal. Chem, 1938. **10**(475).
138. Hull, *XRD pdf standard card for Al-00-001-1179, Data on Chem. for Cer. Use, Natl. Res. Councill Bull, 107.* Phys. Rev., 1917. **10**: p. 661.
139. Topic, I., Höppel, H.W., Göken, M., *Deformation behaviour of accumulative roll bonded and friction stir welded Aluminium alloys.* Materials Science Forum, 2008. **584-586**: p. 833-839.
140. Cheng, K.Y., Tieu, K., Lu, C., Zhu, H., Pei, L., *Effect of pre-heating on the microstructural evolution and super-plasticity of Al deformed by accumulative roll bonding.* Steel Research International, 2013. **84**(12): p. 1209-1215.
141. Ruppert, M., Höppel, H.W., Göken, M., *Influence of cross-rolling on the mechanical properties of an accumulative roll bonded aluminum alloy AA6014.* Materials Science and Engineering: A, 2014. **597**: p. 122-127.
142. Lee, S.H., Saito, Y., Sakai, T., Utsunomiya, H., *Microstructures and mechanical properties of 6061 aluminum alloy processed by accumulative roll-bonding.* Materials Science and Engineering A, 2002. **325**: p. 228-235.
143. McNeice, T., *Manufacture of high strength metal through severe plastic deformation by accumulative roll bonding.* Undergraduate thesis in Mechanical Engineering, Faculty of Engineering, University of Wollongong, Australia, 2008: p. 1-90.
144. Utsunomiya, H., Souba, R., Sakai, T., Saito, Y., *Ultra grain refinement of 1100 Aluminium strip by tandem rolling.* Materials Science Forum, 2003. **426-432**: p. 2681-2686.
145. Yang, D., Hodgson, P., Wen, C., *The kinetics of two-stage formation of TiAl3 in multilayered Ti/Al foils prepared by accumulative roll bonding.* Intermetallics, 2009. **17**(9): p. 727-732.
146. Dehkordi, H.F., Toroghinejad, M.R., Raeissi, K., *Fabrication of Al/Al2O3/TiC hybrid composite by anodizing and accumulative roll bonding processes and investigation of its microstructure and mechanical properties.* Materials Science and Engineering: A, 2013. **585**: p. 460-467.
147. Zhang, R., Acoff, V.L., *Processing sheet materials by accumulative roll bonding and reaction annealing from Ti/Al/Nb elemental foils.* Materials Science and Engineering: A, 2007. **463**(1-2): p. 67-73.
148. Alizadeh, M., Beni, H.A., Ghaffari, M., Amini, R., *Properties of high specific strength Al–4wt.% Al2O3/B4C nano-composite produced by accumulative roll bonding process.* Materials & Design, 2013a. **50**: p. 427-432.
149. Darmiani, E., Danaee, I., Golozar, M.A., Toroghinejad, M.R., *Corrosion investigation of Al–SiC nano-composite fabricated by accumulative roll bonding (ARB) process.* Journal of Alloys and Compounds, 2013. **552**: p. 31-39.
150. Alizadeh, M., Paydar, M.H., Jazi, F.S., *Structural evaluation and mechanical properties of nanostructured Al/B4C composite fabricated by ARB process.* Composites Part B: Engineering, 2013b. **44**(1): p. 339-343.
151. Shabani, A., Toroghinejad, M.R., Shafyei, A., *Fabrication of Al/Ni/Cu composite by accumulative roll bonding and electroplating processes and investigation of its microstructure and mechanical properties.* Materials Science and Engineering: A, 2012. **558**: p. 386-393.
152. Wu, K., Chang, H., Maawad, E., Gan, W.M., Brokmeier, H.G., Zheng, M.Y., *Microstructure and mechanical properties of the Mg/Al laminated composite*

fabricated by accumulative roll bonding (ARB). Materials Science and Engineering: A, 2010. **527**(13-14): p. 3073-3078.
153. Govindaraj, N.V., Lauvdal, S., Holmedal, B., *Tensile bond strength of cold roll bonded aluminium sheets.* Journal of Materials Processing Technology, 2013. **213**(6): p. 955-960.
154. Hsieh, C.C., Shi, M.S., Wu, W., *Growth of intermetallic phases in Al/Cu composites at various annealing temperatures during the ARB process.* Metals and Materials International, 2012. **18**(1): p. 1-6.
155. Ghalandari, L., Moshksar, M.M., *High-strength and high-conductive Cu/Ag multilayer produced by ARB.* Journal of Alloys and Compounds, 2010. **506**(1): p. 172-178.
156. Mozaffari, A., Manesh, H.D., Janghorban, K., *Evaluation of mechanical properties and structure of multilayered Al/Ni composites produced by accumulative roll bonding (ARB) process.* Journal of Alloys and Compounds, 2010. **489**(1): p. 103-109.
157. Ng, H.P., Przybilla, T., Schmidt, C., Lapovok, R., Orlov, D., Höppel, H.W., Göken, M., *Asymmetric accumulative roll bonding of aluminium–titanium composite sheets.* Materials Science and Engineering: A, 2013. **576**: p. 306-315.
158. Chen, Z., Wu, X., Hu, H., Chen, Q., Liu, Q., *Effect of individual layer shape on the mechanical properties of dissimilar Al alloys laminated metal composite sheets.* Journal of Materials Engineering and Performance, 2013. **23**(3): p. 990-1001.
159. Yu, H.L., Lu, C., Tieu, A.K., Liu, X., Sun, Y., Yu, Q., Kong, C., *Asymmetric cryorolling for fabrication of nanostructural aluminum sheets.* Scientific Reports, 2012. **2**.
160. Ji, Y.H., Park, J.J., *Development of severe plastic deformation by various asymmetric rolling processes.* Materials Science and Engineering: A, 2009. **499**(1-2): p. 14-17.
161. Benzerga, A.A., Besson, J., Pineau, A, *Coalescence-controlled anisotropic ductile fracture.* Journal of Engineering Materials and Technology, 1999. **121**(April): p. 221-229.
162. Angella, G., Jahromi, B.E., Vedani, M., *A comparison between equal channel angular pressing and asymmetric rolling of silver in the severe plastic deformation regime.* Materials Science and Engineering: A, 2013. **559**: p. 742-750.
163. Wanheim, T., Bay, N., Petersen, A.S., *A theoretically determined model for friction in metal working processes.* Wear, 1974. **28**: p. 251-258.
164. Guo, B., Gong, F., Wang, C., Shan, D., *Size effect on friction in scaled down strip drawing.* J Mater Sci, 2010. **45**(2010): p. 4067-4072.
165. Severo, V., Vilhena, L., Silva, P.N., Dias, J.P., Becker, D., Wagner, S., Cavaleiro, A., *Tribological behaviour of W–Ti–N coatings in semi-industrial strip-drawing tests.* Journal of Materials Processing Technology, 2009. **209**(10): p. 4662-4667.
166. Vollertsen, F., *Size effects in micro forming.* Key Engineering Materials, 2011. **473**: p. 3-12.
167. Zhang, Y., Bettles, C., Rometsch, P. A., *Effect of recrystallisation on Al3Zr dispersoid behaviour in thick plates of aluminium alloy AA7150.* Journal of Materials Science, 2013. **49**(4): p. 1709-1715.
168. Kandil, A., *An experiment study of hydroforming deep drawing.* Jounal of Materials Processing Technology, 2003. **134**: p. 70-80.
169. Kang, B.S., Song, W.J., Ku, T.W., *Study on process parameters and its analytic application for nonaxisymmetric rectangular cup of multistage deep drawing*

process using low carbon thin steel sheet. The International Journal of Advanced Manufacturing Technology, 2009. **49**(9-12): p. 925-940.
170. Ku, T.W., Kim, Y., Kang, B.S., *Design and modification of tool to manufacture rectangular cup of Ni-MH battery for hybrid cars.* Journal of Materials Processing Technology, 2007. **187-188**: p. 197-201.
171. Araghi, B.T., Bambach, M., Hirt, G., *Comparison of some final part geometrical characteristics of cylindrical cups manufactured by deep-drawing and two-point incremental sheet forming.* Key Engineering Materials, 2009. **410-411**: p. 355-363.
172. Ghosh, M., Miroux, A., Werkhoven, R.J., Bolt, P.J., Kestens, L.A.I., *Warm deep-drawing and post drawing analysis of two Al–Mg–Si alloys.* Journal of Materials Processing Technology, 2014. **214**(4): p. 756-766.
173. Modi, B., Digavalli, R.K., *Effect of friction and lubrication on formability of AA5182 alloy in hydroforming of square cups.* Materials Science Forum, 2013. **762**: p. 621-626.
174. Khandeparkar, T., Liewald, M., *Hydromechanical deep drawing of cups with stepped geometries.* Journal of Materials Processing Technology, 2008. **202**(1-3): p. 246-254.
175. Mayavan, T., Karthikeyan, L., *Experimental and finite element studies on formability of low carbon steel sheets using deep drawing.* International Journal of Engineering and Technology, 2013. **5**(1): p. 166-174.
176. Liu, P., Ku, T.W., Kang, B.S., *A study on initial blank design to minimize earing in multi-stage deep drawing process for rectangular cup using high strength steel material.* Advanced Materials Research, 2013. **652-654**: p. 1971-1975.
177. Anggono, A.D., Siswanto, W.A., *Simulation of ironing process for earring reduction in sheet metal forming.* Applied Mechanics and Materials, 2013. **465-466**: p. 91-95.
178. Costache, E.M., Nanu, N., Chirita, B., Brabie, G., *Prediction and prevention of material cracking in the case of micro or milli drawn parts made from aluminium foils.* International Journal of Mechanical Sciences, 2013. **69**: p. 125-140.
179. Hsu, E., Carsley, J.E., Verma, R., *Development of forming limit diagrams of Aluminum and Magnesium sheet alloys at elevated temperatures.* Journal of Materials Engineering and Performance, 2008. **17**(3): p. 288-296.
180. Wang, K., Carsley, J.E., He, B., Li, J., Zhang, L., *Measuring forming limit strains with digital image correlation analysis.* Journal of Materials Processing Technology, 2014. **214**(5): p. 1120-1130.
181. Maier, C., Paunoiu, V., Marinescu, V., *Developments in deep-drawing process control review.* The Annals of Bunarea de jos University of Galati, 2013: p. 25-30.
182. Miles, M., *Formability testing of sheet metals.* ASM Handbook, Sheet Forming, 2006. **14B**: p. 673-696.
183. Wang, H., Gao, L., Chen, M., *Hydrodynamic deep drawing process assisted by radial pressure with inward flowing liquid.* International Journal of Mechanical Sciences, 2011. **53**(9): p. 793-799.
184. Prakash, S., Kumar, D., *Investigation and analysis for the wrinkling behaviour of deep drawn die sheet metal component by using fast form.* Proceeding of the Natioanl Conference on Trends and Advances in Mechanical Engineering, 2012(Oct 19-20).
185. Loganathan, C., Narayanasamy, R., Sathiyanarayanan, S., *Effect of annealing on the wrinkling behaviour of the commercial pure aluminium grades when drawn through a conical die.* Materials & Design, 2006. **27**(10): p. 1163-1168.

186. Winklhofer, J., Tratting, G., Lind, C., Sommitsch, C., Feuerhuber, H., *Process simulation of Aluminium sheet metal deep drawing at elevated temperature.* NUMIFORM, Proceeding of the 10th International Conference, American Institute of Physics, 2010: p. 927-934.
187. Gowtham, K., Srikanth, K.V.N.S., Murty, K.L.N., *Simulation of the effect of die radius on deep drawing process.* International Journal of Applied Research in Mechanical Engineering, 2012. **2**(1): p. 12-17.
188. Behrens, G., Vollertsen, F., *Influence of tool geometry variation on the punch force in micro deep drawing.* Key Engineering Materials, 2013. **554-557**: p. 1306-1311.
189. Candra, S., Batan, I.M.L., Berata, W., Pramono, A.S., *Simulation of semi-active the blank holder force control to prevent wrinkling and cracking in deep drawing process.* Applied Mechanics and Materials, 2014. **493**: p. 473-479.
190. Raju, S., Ganesan, G., Karthikeyan, R., *Influence of variables in deep drawing of AA 6061 sheet.* Transactions of Nonferrous Metals Society of China, 2010. **20**(10): p. 1856-1862.
191. Yongfei, G., Qianying, H., Cunjie, F., Junting, L., *Numerical simulation for cup shell deep drawn by powder flexible cavity.* Applied Mechanics and Materials, 2012. **217-219**: p. 1397-1402.
192. Nguyen, D.T., Dinh, D.K., Nguyen, H.M.T., Banh, T.L., Kim, Y.S., *Formability improvement and blank shape definition for deep drawing of cylindrical cup with complex curve profile from SPCC sheets using FEM.* Journal of Central South University, 2014. **21**(1): p. 27-34.
193. Chen, K., Peng, C.Y., Li, B.B., Liu, H., *Effect of die radius and BHF on formability of the corner of box-shaped parts in deep drawing processes.* Advanced Materials Research, 2012. **490-495**: p. 2071-2075.
194. Reddy, P.V.R.R., Reddy, G.C.M., Reddy, T.A.J., *Studies on the effect of die corner radius and blank holding force on limit strains in deep drawing process.* Indian Journal of Engineering & Materials Sciences, 2012. **19**: p. 24-30.
195. Browne, M.T., Hillery, M. T., *Optimising the variables when deep-drawing C.R.1 cups.* Journal of Materials Processing Technology, 2003. **136**(1-3): p. 64-71.

Appendix: Simulation and experimental results of deep drawing for AA1235 material with FA-ARBSR treatments for the thicknesses of 300, 130 and 70 µm

Note:

1) The Appendix was separated as a different file, due to they have larger size as A3 rather than standard size of A4 for this thesis).
2) The Appendix has 62 files of simulation results in 17 pages.